U.S. Department of the Interior
U.S. Geological Survey

Modeling Discharge, Temperature, and Water Quality in the Tualatin River, Oregon

By Stewart A. Rounds, Tamara M. Wood, and Dennis D. Lynch

Open-File Report 98–186

Prepared in cooperation with
the Unified Sewerage Agency of Washington County, Oregon

Portland, Oregon: 1998

U.S. DEPARTMENT OF THE INTERIOR
BRUCE BABBITT, Secretary

U.S. GEOLOGICAL SURVEY
Thomas J. Casadevall, Director

For additional information write to:

District Chief
U.S. Geological Survey
10615 S.E. Cherry Blossom Drive
Portland, Oregon 97216-3159
E-mail: info-or@usgs.gov

Copies of this report can be purchased from:

U.S. Geological Survey
Branch of Information Services
Box 25286
Denver, CO 80225-0286
Telephone: (303) 202-4210

CONTENTS

FIGURES

TABLES

CONVERSION FACTORS

Multiply	By	To obtain
acre	4,047	square meter (m^2)
acre-foot (acre-ft)	1,233	cubic meter (m^3)
cubic foot per second (ft^3/s)	0.02832	cubic meter per second (m^3/s)
inch	25.4	millimeter (mm)
foot (ft)	0.3048	meter (m)
mile (mi)	1.609	kilometer (km)
square mile (mi^2)	2.590	square kilometer (km^2)
cubic yard (yd^3)	0.7646	cubic meter (m^3)
cubic foot per second (ft^3/s)	0.02832	cubic meter per second (m^3/s)

Temperature in degrees Celsius (°C) as follows:

$$°C = (°F-32)/1.8.$$

Sea level: In this report "sea level" refers to the National Geodetic Vertical Datum of 1929 (NGVD of 1929)—a geodetic datum derived from a general adjustment of the first-order level nets of both the United States and Canada, called Mean Sea Level of 1929.

Modeling Discharge, Temperature, and Water Quality in the Tualatin River, Oregon

By Stewart A. Rounds, Tamara M. Wood, *and* Dennis D. Lynch

Abstract

A laterally averaged, two-dimensional model was used to simulate discharge, temperature, and water quality in the Tualatin River during the summers (May–October) of 1991, 1992, and 1993. During low-flow periods, the lower main stem of the Tualatin River (river miles 38.4 to 3.4) is characteristic of a long, slow-moving lake. Water-quality problems encountered during the summer include intermittent violations of the State of Oregon minimum dissolved oxygen and maximum pH standards, exceedances of the action level for nuisance phytoplankton growth, and impairment of several of its designated beneficial uses (aesthetics, aquatic life, and water-contact recreation). This river was modeled with a modified version of CE-QUAL-W2, a U.S. Army Corps of Engineers reservoir model that is appropriate for use on the lower main stem of the Tualatin River. Eighteen water-quality constituents were simulated: chloride, suspended solids, dissolved solids, dissolved organic matter, phytoplankton, detritus, soluble orthophosphate, ammonia, nitrate, dissolved oxygen, bottom sediment, total inorganic carbon, carbonate alkalinity, pH, carbon dioxide, bicarbonate, carbonate, and zooplankton; total phosphorus and carbonaceous biochemical oxygen demand were simulated by using a combination of these constituents.

The model was calibrated for 18 months of data: May through October in each of 1991, 1992, and 1993. Only six calibration parameters were used for the water-quality routines in the model; of these, the model was most sensitive to the maximum algal growth rate and the zooplankton mortality rate. Values for most of the parameters required by the model were either independently measured or taken from the available literature. The maximum algal growth rate was varied over the summer in accordance with observed patterns in measured primary productivity rates. The zooplankton mortality rate was kept constant throughout each summer but was calibrated to different values for each year due to differences in observed zooplankton population levels. The calibration process resulted in a model that performed very well; it captured the dynamics of the most important water-quality processes in the lower main-stem Tualatin River during each of three hydrologically distinct summers. Accuracy in day-to-day fluctuations was sacrificed somewhat in order to more accurately simulate the overall cycle of algal growth for these 18 months while varying the calibration parameters only as absolutely necessary. This level of accuracy was sufficient to simulate the interactions among nitrogen, phosphorus, phytoplankton, zooplankton, and dissolved oxygen, but was insufficient to accurately simulate pH during every algal bloom. The ability to extrapolate beyond the calibrated conditions of the model, however, was determined to be more important than accurately simulating the pH during the shorter time scales of individual algal blooms; therefore, this calibration philosophy was retained, and the further calibration of pH was not pursued.

Using the model as a diagnostic tool, a number of general conclusions were made during the calibration process:

(1) Water quality in the lower main-stem Tualatin River is dominated by three physical

constraints and conditions—residence time, air temperature, and solar insolation. Given ample nutrients in conjunction with the long travel time, warm climate, and sunny days frequently encountered during the summer low-flow period, phytoplankton blooms of sufficient size to have an important influence on water quality will develop.

(2) Carbonaceous biochemical oxygen demand (CBOD) and sediment oxygen demand (SOD) are the most important oxygen consumption processes. Instream nitrification was negligible most of the time due to the low concentrations of ammonia found in the river during these summers. Reaeration is a slow process in the modeled reach; the slow reaeration rates are important in determining instream dissolved oxygen concentrations.

(3) The pH in the lower main stem cannot be modeled well unless the algal dynamics are simulated accurately during each algal bloom. That level of short-term accuracy was not required to model other constituents well and was somewhat incompatible with the goal of modeling trends and water-quality changes on longer time scales.

(4) During most of the modeled time period, algal growth was limited only by light conditions. Only during large algal blooms and near the surface of the river was phosphorus found to limit algal growth. Data to substantiate the existence of such a transitory phosphorus limitation to algal growth in the Tualatin River, however, was not available. The model indicates that phosphorus can limit the peak size of algal blooms and, therefore, can be used to limit the number and frequency of violations of the State of Oregon maximum pH standard.

(5) With respect to the State of Oregon minimum dissolved oxygen standard, the phytoplankton were found to be important both in their presence and their absence. Violations of the standard in midsummer were usually associated with the crash of a large algal bloom; such violations were normally of short duration although the minimum dissolved oxygen concentration associated with a large crash may be less than 4 mg/L. Violations of the standard during September and October, on the other hand, were normally associated with small populations of phytoplankton. The CBOD and SOD consumed more oxygen during those periods than the small populations of phytoplankton were able to produce via photosynthesis. This period was often characterized by dissolved oxygen concentrations near or below the standard for extended periods of time.

(6) The model confirmed that a large nonpoint source of phosphorus from ground water and small, ungaged tributaries is present within the lower main-stem reach of the Tualatin River. The phosphorus and water budgets cannot be balanced without it.

Once calibrated, the model of the lower main-stem Tualatin River was used to evaluate the effectiveness of several potential management strategies. Simulations that were used to explore their effects on water quality included tributary phosphorus reductions, flow augmentation, tributary phosphorus reductions with flow augmentation, Oswego diversion dam (the low-head diversion dam at RM 3.4) modifications, water temperature reductions, optimal wastewater-treatment-plant removal of ammonia and phosphorus, nitrogen removal in the wastewater-treatment plants, SOD reduction, and wastewater-treatment-plant operations prior to nutrient removal. Several general conclusions were obtained from these simulations:

(1) Few of the scenarios tested for this report have significant effects upon dissolved oxygen conditions in the main stem.

(2) During September and October, the most significant improvements in dissolved oxygen (as much as 1 mg/L) were obtained only through a large amount of flow augmentation (minimum flow of 200 cubic feet per second at river mile 38.4) or through a lesser amount of flow augmentation (minimum flow of 150 cubic feet per second at river

mile 38.4) combined with a reduction in the loads of CBOD from the boundaries.

(3) For the period May through August, several scenarios showed some ability to limit algal growth during large blooms. When these scenarios failed to reduce the impact of the background oxygen demands (SOD, CBOD), however, dissolved oxygen concentrations between algal blooms still showed a tendency to decrease to near-problem levels.

(4) Phosphorus reduction scenarios showed that if the total phosphorus total maximum daily load (TMDL) is achieved at the boundaries to the main-stem Tualatin River and the wastewater-treatment plants are efficiently removing phosphorus from their effluent and meeting their wasteload allocations, then the main-stem river will be in compliance with the TMDL. Even if the TMDL is achieved, however, the predicted effect on dissolved oxygen concentrations is unclear. If particulate and organic phosphorus is removed rather than soluble orthophosphate, then dissolved oxygen conditions will improve, especially in October, primarily because CBOD will be removed. If soluble phosphorus is removed instead, then dissolved oxygen conditions may actually worsen because of reduced photosynthetic production of oxygen without the loss of CBOD at the boundaries.

(5) The most promising scenarios, in terms of providing the most improvement in dissolved oxygen conditions, most likely will include both a decrease in residence time via flow augmentation and a decrease in the background oxygen demands (CBOD and SOD).

This modeling study has contributed to the current understanding of the interactions between nutrients, phytoplankton, and dissolved oxygen in the Tualatin River as well as the potential changes in water quality that might be caused by variations in the management of that system. The tools produced during this study should be useful to the managers of this important resource.

INTRODUCTION

Background

The Tualatin River drains a 712-square-mile basin on the west side of the Portland metropolitan area in northwestern Oregon (fig. 1). The basin supports a growing population of more than 320,000 people and a wide range of urban, agricultural, and forest-related activities. The urban area is served by four wastewater-treatment plants (WWTPs), all of which are operated by the Unified Sewerage Agency (USA) of Washington County. Historically, these plants discharged high concentrations of ammonia (> 20 mg/L) and phosphorus (> 2 mg/L) into the main stem of the Tualatin River. The high ammonia concentrations often caused significant instream nitrification during the summer, resulting in a high oxygen demand and low dissolved oxygen (DO) concentrations downstream of the plants. In addition, large populations of phytoplankton thrived in the lower reaches of the main stem during the summer; the algal blooms and subsequent population crashes contributed to violations of the State of Oregon minimum DO standard (6.0 mg/L, pre-1996) and the maximum pH standard of 8.5. Several sites on the main stem also exceeded the 15 µg/L chlorophyll-a action level for nuisance phytoplankton growth.

In response to the Federal Clean Water Act of 1972, the Oregon Department of Environmental Quality listed the Tualatin River as a "water-quality limited" stream. The term "water-quality limited" is used in the Federal Clean Water Act of 1972 to define stream reaches that do not meet established water-quality standards even after the implementation of standard technology to control the point sources. In 1984 and 1986, the Oregon Department of Environmental Quality again listed the Tualatin River as water-quality limited because of low DO concentrations and nuisance levels of phytoplankton. One of the designated beneficial uses of the river, aesthetics, was listed as impaired by algal blooms. Once a river has been designated as water-quality limited, the Federal Clean Water Act of 1972 requires that total maximum daily loads (TMDLs) be developed for that water body in order to meet the established water-quality standards. In December of 1986, the Northwest Environmental Defense Center filed suit against the U.S. Environmental Protection Agency to require that TMDLs be established for the Tualatin River.

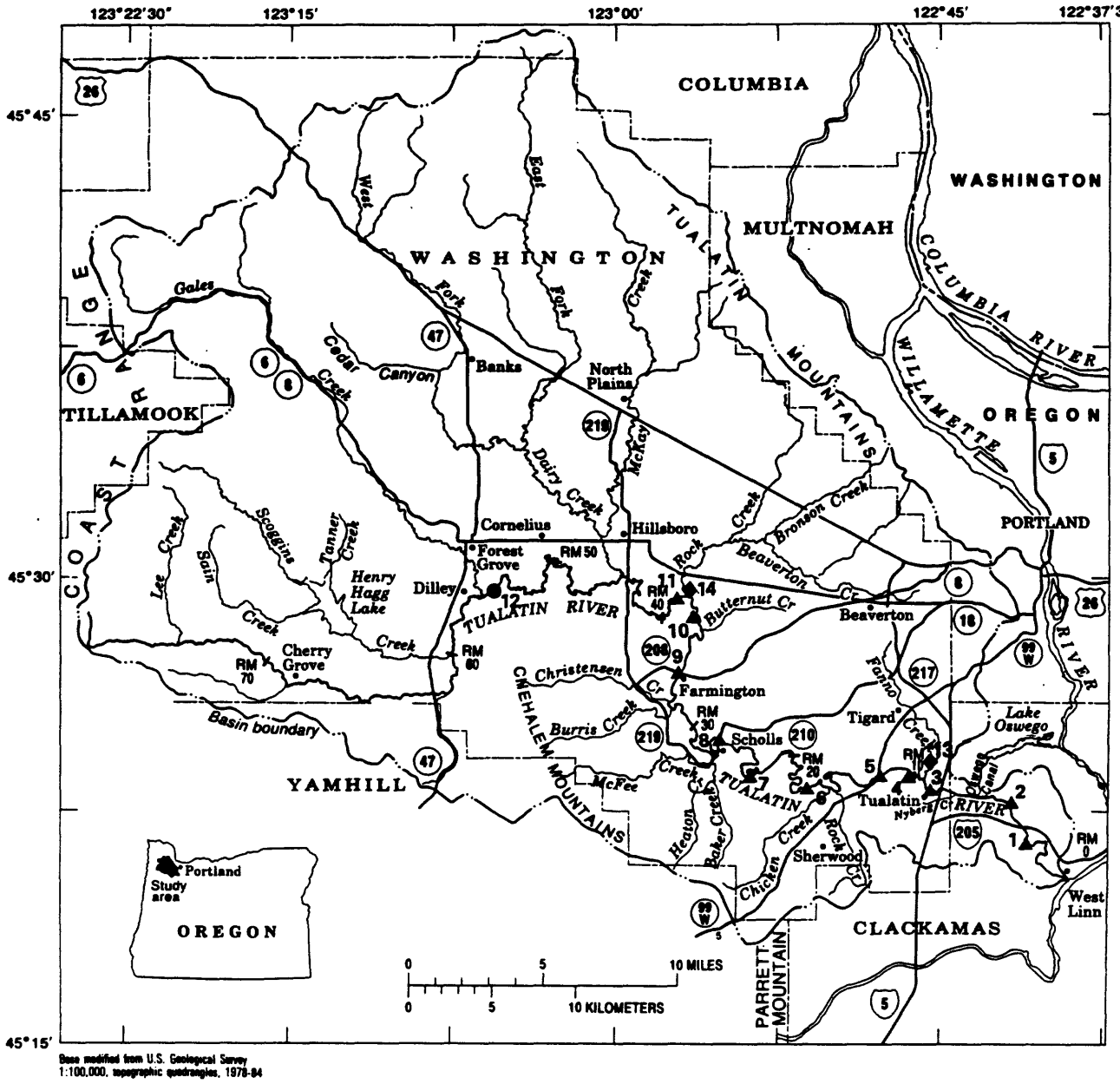

EXPLANATION

2▲ River site

1 Tualatin River at Oswego diversion dam at RM 3.4

2 Tualatin River at Stafford Road near Lake Oswego, Oregon (RM 5.5)

3 Tualatin River at Boones Ferry Road at Tualatin, Oregon (RM 8.7)

4 Tualatin River at Cook Park near Tigard, Oregon (RM 10.0)

5 Tualatin River near Highway 99W bridge near King City, Oregon (RM 11.7)

6 Tualatin River at Elsner Road near Sherwood, Oregon (RM 16.2)

7 Tualatin River near Scholls, Oregon (RM 23.2)

8 Tualatin River at Highway 210 bridge near Scholls, Oregon (RM 26.9)

9 Tualatin River at Farmington, Oregon (RM 33.3)

10 Tualatin River at Meriwether irrigation pump near Hillsboro, Oregon (RM 36.8)

11 Tualatin River at Rood Bridge at Hillsboro, Oregon (RM 38.4)

12● Withdrawal site

12 Springhill Pumping Plant on Tualatin River at RM 56.1

14◆ Discharge site

13 Durham Wastewater Treatment Plant near Durham, Oregon (RM 9.3)

14 Rock Creek Wastewater Treatment Plant at Hillsboro, Oregon (RM 38.1)

RM 10/ River mile

Figure 1. The Tualatin River and its major tributaries. (RM, river mile)

In September of 1988, the Oregon Department of Environmental Quality established TMDLs for both ammonia-nitrogen and total phosphorus for the main-stem Tualatin River and its largest tributaries (Oregon Department of Environmental Quality, 1997). The ammonia TMDL was designed to decrease instream nitrification and its associated oxygen demand; the phosphorus TMDL was designed to limit algal growth and thereby restore the designated beneficial uses and minimize the number of violations of the dissolved oxygen and pH standards.

The establishment of TMDLs in the Tualatin River Basin prompted the various designated management agencies (USA, many of the cities and counties in the basin, and the Oregon Departments of Forestry and Agriculture) to take action to meet their wasteload and load allocations for phosphorus and ammonia set by the TMDLs. USA's two largest tertiary-treatment plants were upgraded with the addition of biological nutrient removal to reduce ammonia and total phosphorus concentrations. Two-stage alum treatment was added to further reduce total phosphorus to levels below the wasteload allocation. The Oregon Department of Agriculture helped control phosphorus releases from many dairy and nursery operations. The Oregon Department of Forestry utilized the Forest Practices Act to comply with the TMDL. As of June, 1993, the Tualatin River was generally in compliance with the ammonia-nitrogen TMDL, and an extended implementation and compliance schedule had been developed and approved for the total phosphorus TMDL.

Basin Characteristics and Hydrology

The main stem of the Tualatin River is about 80 miles long and flows generally from west to east, starting in the forested Coast Range and discharging to the Willamette River near West Linn, Oregon (fig. 1). The characteristics of the river change dramatically from its headwaters to its mouth. The headwater reach, from river mile (RM) 79.4 to 55.3, is narrow (about 15 feet wide) and has an average slope of 74 feet per mile, including several waterfalls. Once the river reaches the valley floor, the slope decreases and the river begins to meander. This meandering reach (RM 55.3–33.3) has an average slope of 1.3 feet per mile, a width of about 50 feet, and nearly complete riparian shading. Downstream of the meandering reach, the river flows into a backwater reach (RM 33.3–3.4) with an estimated slope of only 0.08 feet per mile. The backwater characteristics are caused both by the low slope and the presence of a low-head diversion dam at RM 3.4 (Oswego diversion dam). In this reach, the river continues to meander and widens to roughly 150 feet, thus exposing much of the river surface to direct solar insolation. From the Oswego diversion dam to the mouth (RM 3.4–0.0), the Tualatin River is characterized by small pools and riffles and has an average slope of 13 feet per mile. These physical characteristics are important factors in determining the river's water quality because they affect the river's reaeration potential, the time required for a parcel of water to traverse the system, and the amount of solar energy that can reach the water surface.

The discharge of the Tualatin River reflects the seasonal rainfall. Most of the annual precipitation falls between November and June, and the effect of snowmelt is minimal. Seasonal streamflow is typically highest from December through April and lowest from July through October (fig. 2). The low-flow summer period is defined as May 1 through October 31. Since January of 1975, Tualatin River streamflow has been augmented during this low-flow period with water releases from Henry Hagg Lake, a man-made reservoir on Scoggins Creek (fig. 1). Most of the water in this reservoir is used for irrigation, but 12,618 acre-feet of stored water are available to USA for summertime flow augmentation (Unified Sewerage Agency, 1997). River discharge is managed in an attempt to maintain some minimum flow, generally 150 ft^3/s (cubic feet per second), at RM 33.3; the available augmentation water may or may not be sufficient to meet that goal during a particularly dry summer. Before Henry Hagg Lake was constructed, summer flows often dropped well below 50 ft^3/s (fig. 3).

In addition to Scoggins Creek, the Tualatin River has four other major tributaries and numerous minor tributaries. None of these receive appreciable flow augmentation; therefore, their discharges typically decrease as the summer low-flow period progresses. Gales Creek flows through a predominantly forested landscape, whereas the Dairy Creek subbasin is predominantly agricultural. Rock Creek has both agricultural and urban influences, and Fanno Creek flows almost exclusively through urban areas. The USA operates four WWTPs in the basin, but the two smaller plants generally do not discharge into the Tualatin River during the May 1 to October 31 period.

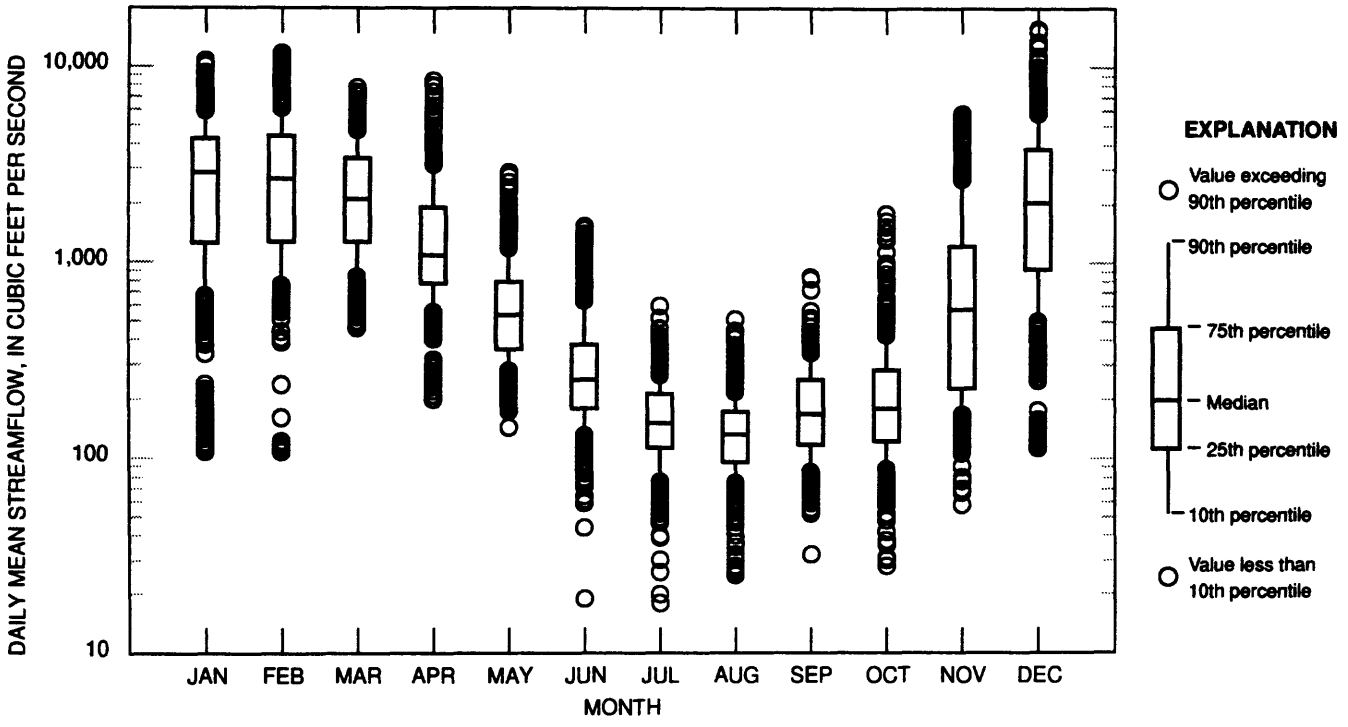

Figure 2. Monthly distribution of daily mean streamflow in the Tualatin River at river mile 1.8 (West Linn) for the years 1975 through 1994.

In 1994, the largest two plants (Rock Creek WWTP at RM 38.1 and Durham WWTP at RM 9.3) each discharged approximately 23 ft^3/s (15 million gallons per day) of treated effluent into the river under dry, summer conditions. The daily variation in discharge ranged from approximately 20 ft^3/s in the early morning to 35 ft^3/s in the middle of the day.

Water withdrawals are made from the Tualatin River for public water supply, irrigation and power generation. The Joint Water Commission and the Tualatin Valley Irrigation District jointly operate the Spring Hill Pumping Plant at RM 56.1. The Joint Water Commission supplies municipal water to several of the cities in the basin, and the Tualatin Valley Irrigation District operates a pressure pipeline that delivers irrigation water to about 10,000 acres of cropland. This pumping plant typically draws between 25 and 125 ft^3/s of water from the river during the summer months, depending on irrigation needs. Additional irrigation withdrawals are taken directly from the river by the end users. A canal at RM 6.7 diverts an average of 60 ft^3/s of water from the Tualatin River for the purpose of power generation at a small hydropower plant owned by the Lake Oswego Corporation. The people who live in the Tualatin River Basin depend on the Tualatin River for drinking water, irrigation water, recreation, and dilution and transport of wastes. The economic prosperity currently enjoyed within the basin is dependent upon the proper management of this surface-water resource and the maintenance of its quality.

Purpose and Scope

In 1990, the U.S. Geological Survey (USGS) entered into a cooperative agreement with the USA to assess the water-quality conditions of the Tualatin River. The objectives of that project were:

(1) to identify the major sources of nutrients (nitrogen and phosphorus) to the main-stem Tualatin River,

(2) to assess the transport and fate of those nutrients in the main stem,

(3) to quantify processes that affect dissolved oxygen concentrations in the main stem, and

(4) to construct and use a mechanistically based, process-oriented model of nutrients and dissolved oxygen for the main stem.

Each of these objectives was limited to the low-flow, high-temperature, summer period defined as May 1 through October 31. This report describes the results of the modeling work performed for the USGS-USA cooperative project. The specific objectives of the modeling work were:

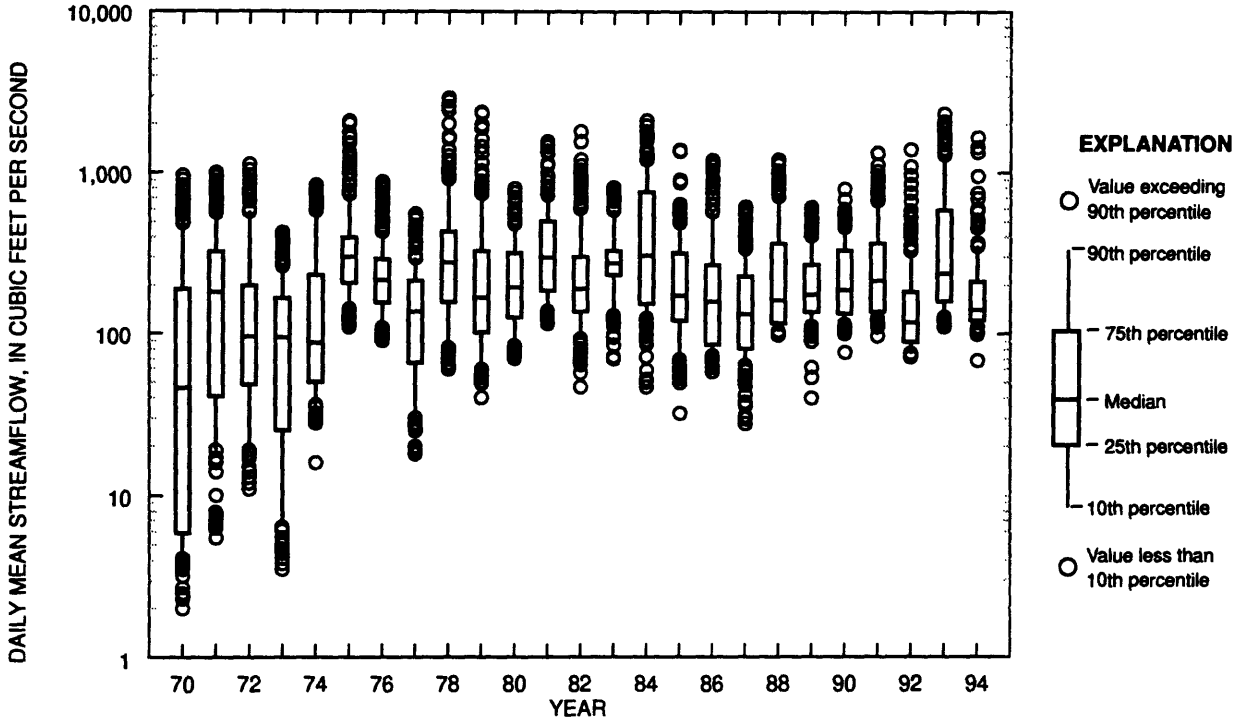

Figure 3. Distribution of daily mean summer streamflow (May–October) in the Tualatin River at river mile 1.8 (West Linn) for the years 1970 through 1994.

(1) to develop and test a computer model of the main-stem Tualatin River from RM 38.4 to 3.4 that integrates the pertinent physical, chemical, and biological processes,

(2) to better understand nutrient and dissolved oxygen dynamics, fate, and transport, and to assess the relative importance of various interdisciplinary processes by using the model as a diagnostic tool, and

(3) to create a tool that can be used to evaluate the relative water-quality benefits of various management alternatives for the Tualatin River.

This report describes the model used in this study and how it was modified for use in the Tualatin River. The simulated processes are described and their relative importance is discussed. The philosophy and results of the model calibration are described, and, finally, various management options for improving the water quality of the Tualatin River are evaluated with the calibrated model. Throughout this report, all references to algae refer only to phytoplankton.

Acknowledgments

The authors received information, insight, and assistance in this work from many people and organizations. We thank everyone who provided that help. For cooperative funding, information, insight, and data, we thank the Unified Sewerage Agency of Washington County, especially John Jackson, Gary Krahmer, William Gaffi, Janice Miller, Tom VanderPlaat, Jan Wilson, Carlo Spani, and all of the crew at the USA Water Quality Laboratory. For assistance with the numerical model, we thank Tom Cole of the U.S. Army Corps of Engineers. Wesley Jarrell and Tim Mayer of the Oregon Graduate Institute of Science & Technology gave valuable assistance and information regarding soils and the forms and sorption characteristics of phosphorus. For assistance in designing hypothetical management options for the model to evaluate, we thank Bob Baumgartner and Michael Wiltsey of the Oregon Department of Environmental Quality. We thank Jerry Rodgers of the Oregon Water Resources Department for water-use information, and Chuck Schaefer of the Lake Oswego Corporation for providing information regarding the time-varying configuration of the Oswego diversion dam. For providing additional subroutines that were important to the model, we thank Scott Wells and Chris Berger of Portland State University. Finally, we thank Ralph Vaga, formerly of the U.S. Geological Survey, for his many valuable insights into algal dynamics and the relations between phytoplankton, zooplankton, and nutrients.

MODEL DESCRIPTION

The model used in this study to simulate the discharge, temperature, and water quality (see constituent list in table 1) of the Tualatin River is called CE-QUAL-W2. It is a two-dimensional, laterally averaged, hydrodynamic and water-quality model developed and maintained by the U.S. Army Corps of Engineers (USACE). The hydrodynamic component of CE-QUAL-W2 was taken originally from a model named GLVHT (Generalized Longitudinal-Vertical Hydrodynamics and Transport Model), which in turn was based on the model LARM (Laterally Averaged Reservoir Model, Edinger and Buchak, 1975). Since its creation in 1986, CE-QUAL-W2 has been updated frequently to incorporate new algorithms and improve its efficiency. Such changes are essential in the fast-changing field of water-quality modeling, but those changes quickly make the documentation obsolete. This study was performed using a modification of version 2.0 of CE-QUAL-W2, for which a user manual is available (Cole and Buchak, 1995). In this section, the general capabilities, limitations, and algorithms of this modified version of CE-QUAL-W2 are discussed.

Capabilities

CE-QUAL-W2 simulates the hydrodynamics, water temperature, and water quality of a water body in two dimensions. Unlike two-dimensional estuarine models that often are depth-averaged, this model is laterally averaged; the simulated dimensions are longitudinal (along the length of the water body) and vertical. CE-QUAL-W2 is best applied, therefore, to a body of water whose quality has distinct variations with length and depth and few differences from side to side. Such is often the case for relatively narrow lakes or rivers that have a tendency to thermally stratify. A few reaches of the Tualatin River thermally and chemically stratify during periods of warm, sunny weather in the summer. This model, therefore, can capture some of the important water-quality impacts of that stratification. The CE-QUAL-W2 grid incorporates variable spacing so that the river bathymetry can be well described.

CE-QUAL-W2 is a dynamic model rather than a steady-state model. The water quality of the Tualatin River is dependent upon the dynamics of fundamental physical conditions such as discharge and meteorology. A dynamic model, therefore, is required to capture the accompanying changes in water quality. CE-QUAL-W2 accepts time-dependent boundary conditions and simulates discharge, water-surface elevations, horizontal and vertical velocities, water temperature, density, and water quality in a dynamic manner. Hydrodynamics and constituent transport are simulated in CE-QUAL-W2 through its implementation of six fundamental fluid-flow equations for laterally averaged systems: (1) the horizontal momentum equation, (2) the constituent transport equation, (3) the free-water-surface elevation equation, (4) the hydrostatic pressure equation, (5) the continuity equation, and (6) the equation of state. The details of these equations and their numerical solution are discussed in the user manual (Cole and Buchak, 1995).

CE-QUAL-W2 contains a fairly simple set of algorithms to simulate heat flow. The algorithms are simple and do not incorporate all of the details used by other temperature models. For example, a variable shading algorithm that depends upon river orientation, solar angle, riparian height and vegetative density is not included, primarily because CE-QUAL-W2 was developed for reservoirs and estuaries for which such shading is not critical. All of the most important components of the heat budget for this application, however, are present. These are short-wave solar insolation, long-wave atmospheric radiation, water-surface back radiation, evaporation, and conduction. A simple shading capability was added as a modification. The heat-flow algorithms are discussed in more detail in the *Algorithms* section of this report.

A complex set of water-quality algorithms are implemented in CE-QUAL-W2. These algorithms focus on carbon and nutrient cycling, phytoplankton and zooplankton dynamics, dissolved oxygen production and consumption, and pH. Some of these algorithms were modified, either slightly or drastically, as part of this effort to simulate the important instream processes of the Tualatin River. These modifications, and the simulated instream processes, are discussed in the *Algorithms* section. CE-QUAL-W2 keeps track of 22 water-quality constituents (table 1), 18 of which were included in parts of this application. The water-quality routines include most of the instream processes that are important in the Tualatin River, and were easily modified when different algorithms were required.

Some of the capabilities of CE-QUAL-W2 relate more to the *implementation* of the transport and reaction equations rather than the choice or inclusion of those equations. For example, this model has a

Table 1. Names and descriptions of the water-quality constituents simulated by CE-QUAL-W2

[mg/L, milligrams per liter; †, constituent not used in this study; P, phosphorus; N, nitrogen; O, oxygen; g/m^2, grams per square meter; C, carbon; Ca, calcium; H, hydrogen; Fe, iron; CBOD, carbonaceous biochemical oxygen demand]

Constituent name	Units	Description / Remarks
Nonreactive tracer	relative	A conservative constituent. Used to simulate the transport of nonreactive species such as chloride or a dye tracer.
Inorganic suspended solids	mg/L	Suspended solids that affect light penetration and water density.
Coliform bacteria †	mg/L	A generic bacterial compartment.
Total dissolved solids	mg/L	A conservative constituent that affects water density.
Labile organic matter	mg/L	Dissolved organic matter that decomposes rapidly.
Refractory organic matter †	mg/L	Dissolved organic matter that decomposes slowly.
Algae	mg/L	Total phytoplanktonic biomass, regardless of species.
Detritus	mg/L	Particulate organic matter that settles and decomposes.
Soluble orthophosphate	mg/L as P	Bioavailable phosphorus.
Ammonium	mg/L as N	Ammonia and ammonium. A nitrogen source for algae.
Nitrate and nitrite	mg/L as N	Oxidized nitrogen. A nitrogen source for algae.
Dissolved oxygen	mg/L	Dissolved oxygen: O_2.
Sediment	g/m^2	Bed sediment organic matter, decomposes on the river bottom.
Total inorganic carbon	mg/L as C	Sum of dissolved CO_2, HCO_3^-, and CO_3^{2-}.
Carbonate alkalinity	mg/L as $CaCO_3$	A measure of the acid neutralizing capacity.
pH	—	A measure of the H^+ concentration.
Carbon dioxide	mg/L as C	Dissolved CO_2 and H_2CO_3.
Bicarbonate	mg/L as C	Bicarbonate ion: HCO_3^-.
Carbonate	mg/L as C	Carbonate ion: CO_3^{2-}.
Total iron †	mg/L as Fe	Dissolved and suspended iron(II) and iron(III).
CBOD †	mg/L	Ultimate carbonaceous biochemical oxygen demand.
Zooplankton	mg/L	Total biomass of zooplankton, regardless of species.

variable time-step algorithm that is designed to ensure the mathematical stability of the numerical methods. In addition, an advanced solution technique (Leonard, 1979) is used to reduce numerical dispersion. CE-QUAL-W2 also has a wide variety of capabilities that were *not* used in the Tualatin River simulations. Although the Tualatin simulations required only one continuous river reach, the model is designed to handle a network of branched streams or lakes. The ice-cover algorithms are extensive. The user manual (Cole and Buchak, 1995) contains more details on these and other related topics.

Limitations

CE-QUAL-W2 was written for lakes, reservoirs, estuaries, and low-gradient streams. Strictly, it cannot simulate a river reach in which the water-surface elevation at the downstream boundary is lower than the elevation of the river bottom at any point in the grid. In its present form, this two-dimensional model can be used only to simulate the slow-moving, reservoir-like reach of the Tualatin River (RM 30 to RM 3.4). In higher gradient areas above and below this reach (see *Basin Characteristics and Hydrology* on page 5), a one-dimensional model would be more appropriate. In this study, the modeled reach was extended upstream from the reservoir reach and into a more one-dimensional reach so that the upstream boundary (at RM 38.4) would fall at a point with measured discharge and water-quality characteristics. This extension did not violate any model constraints.

Lateral differences in velocity, temperature, and water quality are averaged in CE-QUAL-W2. In some rivers or reservoirs, this lateral averaging might present a serious limitation and prevent the application of this model. In the case of the Tualatin River, however, the width of the river is small relative to its length. Although it is true that some lateral differences in water quality or temperature might be expected due to uneven shading of the river surface, such differences are insignificant compared with observed differences in the vertical and longitudinal dimensions.

Some limitations of CE-QUAL-W2 can be avoided through prudent modifications of the source code. The USACE version of the model restricts the geometry of the grid such that each segment, or vertical column, in the two-dimensional grid must contain at least two *active* layers. In other words, the river must be deep enough so that at least two layers are transporting water in every segment; each segment must be *two dimensional*. The computer code was modified to remove this limitation. The Tualatin River has several shallow spots (< 6 feet during low flow) in its reservoir-like reach that are sometimes important in controlling its flow and in breaking up thermal stratification. One particular part of the river is especially shallow (< 4 feet during low flow) and is best modeled using only one active layer. Above the reservoir-like reach, the river is relatively shallow and gains some elevation. To extend the grid upstream to a location that is well suited to be an upstream boundary (RM 38.4), many segments with only one active layer had to be included. In the version of CE-QUAL-W2 used in this study, the code supports the existence of such one-dimensional segments.

The vertical momentum equation is not included in the mathematical formulation used by CE-QUAL-W2. The absence of this equation may result in errors where a significant amount of vertical acceleration is encountered; for example, significant vertical velocities can be generated in deep grid segments that are bordered by shallow segments. This can generate an undue amount of advective vertical mixing near abrupt changes in river depth. This problem, however, is limited to a few segments of the grid and does not affect results in this application farther than a short distance downstream of those segments.

The heat-flow algorithms implemented in this version of CE-QUAL-W2 are adequate for this study, despite the fact that one particular process that might have improved the simulation of vertical stratification is absent. That process is the conduction of heat across the sediment/water interface. A later USACE version of the model includes a simple sediment heat-exchange algorithm that might have improved the simulated hypolimnetic water temperatures in this application. The lack of such an algorithm in the USGS version of the model is a very small limitation; it did not significantly affect the results of the simulations.

The water-quality algorithms in CE-QUAL-W2 include many important processes that control nutrient cycling, algal dynamics, and the production and consumption of dissolved oxygen. The mathematical descriptions of chemical and biological reactions used in this model, however, contain many simplified generalizations and assumptions. For example, all organic matter, whether it is dissolved, particulate, planktonic, or deposited in the sediment, is assumed to have the same, constant, ratio of carbon to nitrogen to phosphorus. Although this is convenient, it is not altogether accurate. In addition, only one algal compartment is available; all algal species are combined and simulated with one set of growth and death parameters and one carbon to chlorophyll ratio. CE-QUAL-W2 does not simulate the growth of benthic algae, but algal growth and primary production in the Tualatin River are dominated by phytoplankton in the water column; therefore, the lack of a benthic algae constituent is not a limitation for this application.

Most of the rate constants and growth parameters used in CE-QUAL-W2 are assumed to be constant. No seasonal variation in the phytoplankton growth rate is incorporated in the USACE version, other than the dependence of reaction rates upon the seasonally varying water temperature. This limitation makes it difficult for the model to simulate variations in, for example, algal growth as a response to seasonal changes in light and other conditions. In this version, the model was modified to allow seasonal changes in both the algal growth rate and the shading of the river surface. The biological food web is cut off at the level of zooplankton; the zooplankton mortality rate must account for a variety of different death processes.

The sediment compartment in CE-QUAL-W2 is not designed to simulate long-term (decades) changes in the loading of organic matter or nutrients in response to long-term changes in the amount of organic matter entering the system. In this application, the absence of this sort of long-term predictive capability is not a serious problem, as the scenarios are tested over periods of only 6 months rather than 10 to 20 years. Nevertheless, this shortcoming will be addressed in future versions.

Many of the simplifications in the water-quality algorithms were made by the authors of CE-QUAL-W2 in an attempt to balance the need to accurately simulate the dominant instream processes against a need to restrict the number of difficult-to-measure parameters. Despite its limitations, this version of CE-QUAL-W2 is able to simulate the *general* characteristics and dynamics of water quality in the Tualatin River, thereby enabling a better understanding of the processes that control water quality in this system and how that water quality would be affected by possible management options.

Code Modifications

Many important changes to the USACE version of CE-QUAL-W2 were made during this study. The starting point for this work was version 2.0 (May, 1989), obtained from Dr. Scott Wells of Portland State University. Dr. Wells' research group made some important modifications to the code, such as adding an algorithm that calculates the discharge over the Oswego diversion dam using a calculated water-surface elevation at the dam and a set of hydraulic and physical parameters. The discharge at the downstream boundary (Oswego diversion dam), therefore, is calculated internally rather than imposed externally. This change allows the model to be responsive to changes in the management of the river flow or the dam dimensions. Other code modifications were made by the USGS modeling team. For example, changes were made to the reaeration algorithm, many of the reaction-rate temperature-dependence functions, the algal light-limitation function, the sediment oxygen demand (SOD) algorithm, and the distributed tributaries (nonpoint source) code. Several new algorithms were added that allow the model to shade part of the water surface, seasonally vary that shading and the algal growth rate, and make ammonia the preferred source of nitrogen for the phytoplankton. Most of the modifications to the USACE version are described in the *Algorithms* section of this report. Some might be considered major modifications, changing the basic algorithms used by the model, while others would be considered minor modifications that have little effect on the model. Each change was tested to make sure that it had only the intended effect. The major modifications to the code are listed in Appendix A.

Algorithms

The mathematical expressions within CE-QUAL-W2 dictate exactly how the sources, sinks, and transport of water, heat, and constituents are simulated. Because they embody the fundamental concepts used by the model, an examination of these expressions is perhaps the best way to reveal the model's conceptual framework. This section details some of the most important algorithms used in CE-QUAL-W2. This is not meant to be a complete description of the hydraulics and water-quality processes; much of that is readily available in the user manual (Cole and Buchak, 1995). Rather, this section is meant to provide an overview of the algorithms that are fundamentally important to this application and to describe several that are new to this version of CE-QUAL-W2. Several parameters used in these equations are also quantified in this section; the balance of the input parameter values are listed in the *Boundary Conditions, Reaction Rates, and Forcing Functions* section.

Hydraulics and the Water Budget

The water budget of CE-QUAL-W2 includes upstream inflows, tributary or point inflows, nonpoint source inflows including ground water (called *distributed tributaries*), precipitation, diversions, irrigation withdrawals, evaporation, and a downstream outflow. In the Tualatin River application, the only two components of the water budget that are not explicitly specified as time-varying boundary conditions are the evaporation function and the downstream outflow. Evaporation is calculated as a function of the water temperature at the surface of the river, the dew-point temperature, the wind speed, and the surface area of the river. The resulting evaporation rate is (Cole and Buchak, 1995):

$$Q_{evap} = \frac{f(W)\,(e_s - e_a)\,A}{H_{vap}\rho} \quad , \qquad (1)$$

where $f(W)$ is the evaporative wind-speed function, e_s is the saturation vapor pressure of water at the temperature of the surface water, e_a is the vapor pressure of water at the air temperature, A is the river surface area of a segment, H_{vap} is the latent heat of vaporization of water, and ρ is the density of water.

The discharge of the river at the downstream boundary can be specified explicitly as a time-varying boundary condition in CE-QUAL-W2. In this application, however, the flow over the Oswego diversion dam was calculated internally. The code that calculates this discharge was an addition to the model made by Dr. Scott Wells and his research group at Portland State University. Water can flow past the Oswego diversion dam via three separate paths: over a broad, flat-crested, cement weir; through a fish ladder; or through a submerged pipe near the fish ladder. The flow past the dam, therefore, is simply the sum of the flows over or through the three structures:

$$Q_{dam} = Q_{cw} + Q_{fl} + Q_{pipe}, \qquad (2)$$

where Q_{dam} is the flow past the dam, Q_{cw} is the flow over the cement weir, Q_{fl} is the flow through the fish

ladder, and Q_{pipe} is the flow through the submerged pipe.

The flows over the cement weir and through the fish ladder are quantified using the basic weir equation (Streeter and Wylie, 1985):

$$Q = Cbh^{3/2}, \quad (3)$$

where Q is the flow through the weir, C is a weir coefficient, b is the effective width of the weir, and h is the height of the water surface above the weir crest. The weir coefficient depends upon the shape of the weir. For sharp-crested weirs, the weir coefficient is:

$$C = \frac{2}{3} C_d \sqrt{2g}, \quad (4)$$

where C_d is a dimensionless discharge coefficient and g is the gravitational constant. The fish ladder may be modeled as a sharp-crested weir. The wide, cement weir of Oswego diversion dam is not sharp crested. For a broad-crested weir such as this, the weir coefficient may be approximated as:

$$C = 0.385 C_d \sqrt{2g}, \quad (5)$$

The discharge coefficient varies, depending upon the amount of debris that accumulates on the weir. These equations are approximate, and the Oswego diversion dam is not composed of perfect, well-calibrated weirs. The discharge coefficients of these weirs, therefore, are considered to be calibration parameters in this application (see the *Boundary Conditions, Reaction Rates, and Forcing Functions* section). Once the dimensions and discharge coefficients are set, the flow through and over these structures can be calculated as a function of the upstream water-surface elevation.

The flow through the submerged pipe at the Oswego diversion dam can also be calculated as a function of the upstream water-surface elevation. An energy balance for the submerged pipe results in an equation that can be solved iteratively for the pipe discharge (Streeter and Wylie, 1985). That equation is:

$$\frac{8(1+K_e)}{g\pi^2 D^4} Q_{pipe}^2 + \frac{RL}{C_{hw}^{1.852} D^{4.8704}} Q_{pipe}^{1.852} + h_2 - h_1 = 0, \quad (6)$$

where K_e is an energy-loss coefficient for the entrance of the pipe, D is the diameter of the pipe, R is a constant, L is the length of the pipe, C_{hw} is a Hazen-Williams frictional coefficient, h_2 is the tailwater elevation, and h_1 is the upstream water-surface elevation. Once the dimensions and hydraulic characteristics of the pipe are set, the flow through the pipe can be calculated knowing only the value of h_1, as h_2 does not vary significantly during the low-flow summer period.

Nonpoint sources of water to the river are included in CE-QUAL-W2 through the use of a *distributed tributary* algorithm. A distributed tributary is simply a source of water, heat, and constituents that is added to the model reach along its entire length rather than as a point source. Time-varying boundary conditions of flow, temperature, and constituent concentrations are required, just as if all of the water were coming from a tributary, but the flow, heat content, and constituent loads from that source are *distributed* across the entire model reach. In the USACE version, these inputs are distributed along the model reach according to the water-surface area of each segment, and the entire amount is discharged to the top of the water column. Normalizing the nonpoint source input to the water-surface area, which is similar to the sediment-surface area, allows this input to simulate either precipitation or ground-water discharge. In the Tualatin River application, the distributed tributary is composed of many ungaged, point sources such as tile drains, small tributaries, and seeps as well as ground water. Many of these sources are probably best normalized to bank length rather than water-surface or sediment-surface area. In addition, the presence of a ground-water source suggests that the input should be distributed throughout the water column rather than placed only at the top. Therefore, the model code was changed to normalize the distributed tributary input to bank length and to distribute that input over the entire water column.

The five hydraulic variables in the model—longitudinal velocity, vertical velocity, surface elevation, pressure, and density—are found with five laterally averaged equations of fluid motion, all of which are described in detail in the USACE user manual (Cole and Buchak, 1995). The only hydraulic algorithm implemented in this version of CE-QUAL-W2 that is not discussed in the user manual is the one used to describe the shear stress at the edges of the channel. The USACE version of the model uses Chezy's equation to simulate this shear stress; the version used in this study was modified to use Manning's equation.

While Manning's equation is based upon the same principles as Chezy's, the parameters of the former are more intuitive, easier to quantify, and less dependent upon channel geometry. The model code was simply modified to make use of the relation (SI units):

$$C_z = \frac{R_h^{1/6}}{n}, \quad (7)$$

where C_z is the Chezy coefficient, R_h is the hydraulic radius (cross-sectional area divided by the wetted perimeter), and n is a roughness coefficient. Values for "Manning's n" have been tabulated for a wide variety of channel characteristics (Barnes, 1967; Arcement and Schneider, 1989).

Heat Flow

The heat budget used by CE-QUAL-W2 accounts for all of the most important heat-flow processes. Short-wave solar insolation, long-wave atmospheric radiation, water-surface back radiation, evaporation, and air/water conduction are all included (fig. 4). A fraction of the solar insolation may be blocked, shading a part of the river surface. Solar insolation is extinguished and converted to heat as it travels downward into the water column. Any solar insolation that reaches the river bottom is assumed to transfer its heat to the water at the sediment/water interface. The river bottom is assumed to be neither a heat source nor a heat sink. Heat is advected and dispersed with all of the other water-quality constituents.

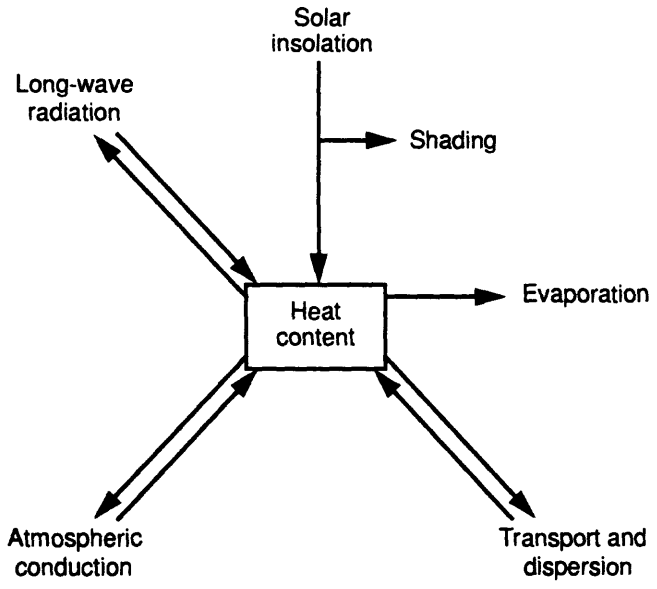

Figure 4. The major heat-flow processes implemented in CE-QUAL-W2.

The USGS version of CE-QUAL-W2 applies a linearized formulation of the heat-transfer equations and the *equilibrium temperature* concept to calculate the net heat flux across the air/water interface. This approach combines all of the heat-transfer processes into two easily calculated parameters: a heat-exchange coefficient and the equilibrium temperature. The resulting heat-transfer equation is:

$$H_n = -K_{aw}(T_w - T_e), \quad (8)$$

where H_n is the net heat flux into the water body (Watts per square meter, W/m^2), K_{aw} is the coefficient of surface heat exchange ($W/m^2/°C$), T_w is the water-surface temperature (degrees Celsius, °C), and T_e is the equilibrium temperature (°C). The equilibrium temperature is defined as the water-surface temperature that, for a given set of meteorological conditions, results in a net heat flux of zero. It is calculated by balancing the back radiation, evaporation, and conduction losses against the radiation inputs.

The heat-transfer algorithm was modified in this version of CE-QUAL-W2 to allow a part of the water surface to be shaded by streambank vegetation. Shading can be an important process for rivers that are narrow enough for the riparian vegetation to cast a significant shadow over the water surface. The shading algorithm added to the model is simple. Each segment, or vertical column in the two-dimensional grid, is assigned a shading factor, calculated from the surface width of that segment, that represents the fraction of the river surface area that is shaded from solar radiation. The shading factors do not vary with the time of day and are not dependent upon the orientation of the segment; such complexity was not merited due to the dearth of riparian height and density data at the time of this study. A simple seasonal dependence is included to simulate the growth of leaves in the spring and the disappearance of leaves in the fall. This seasonality is implemented by multiplying the assigned shading factor by a function that varies from 0 to 1 and back to 0 as the seasons pass. In mathematical terms, the seasonally dependent shading factor is:

$$f_S = f_S' \left(\frac{k_1 F_1}{1 + k_1 (F_1 - 1)} \right) \left(\frac{k_4 F_2}{1 + k_4 (F_2 - 1)} \right), \quad (9)$$

where f_S' is the unmodified shading factor, and the F values are given by:

$$F_1 = \left(\frac{k_2 (1 - k_1)}{k_1 (1 - k_2)} \right)^{\frac{\eta - \eta_1}{\eta_2 - \eta_1}} \text{ and}$$

$$F_2 = \left(\frac{k_3 (1-k_4)}{k_4 (1-k_3)} \right)^{\frac{\eta_4 - \eta}{\eta_4 - \eta_3}}. \quad (10)$$

These functions were adapted from those that the USACE version uses to modify reaction rates as a function of temperature (Thornton and Lessem, 1978). The desired seasonal dependence in the shading factor is achieved by using 0.1 for k_1 and k_3, 0.98 for k_2 and k_4, and the values 75, 120, 275, and 305 for η_1 through η_4, respectively (fig. 5).

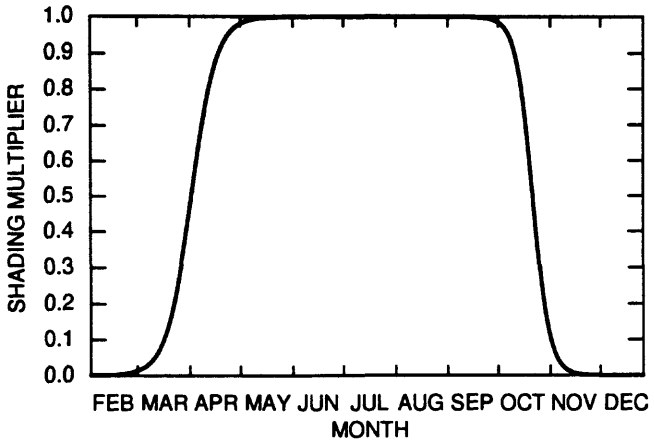

Figure 5. Seasonal variation of the shading multiplier as implemented in the U.S. Geological Survey version of CE-QUAL-W2.

Light extinction is modeled with Beer's Law:

$$I_z = (1-\beta)(1-f_S) I_0 e^{-\alpha_{tot} z}, \quad (11)$$

where I_z is the light intensity at depth z, I_0 is the incident light intensity, β is the fraction of incident light absorbed at the water surface, and α_{tot} is the extinction coefficient. The extinction coefficient is a function of the suspended solids and phytoplankton concentrations and is modeled as:

$$\alpha_{tot} = \alpha_{ss}\Phi_{ss} + \alpha_a \Phi_a + \alpha_w, \quad (12)$$

where α_{ss}, α_a, and α_w are the extinction coefficients for suspended solids, phytoplankton, and water, respectively. The concentrations of suspended solids and phytoplankton (algae) are represented by Φ_{ss} and Φ_a. The extinction coefficient for water accounts for light absorption by dissolved organic compounds, colloids, and small particles. Equation 12 represents a small departure from the USACE version of the model, in which the influence of detrital matter is explicitly included in the calculation of α_{tot}. Because no reliable measurements of detrital matter were available for use in estimating these extinction coefficients, the detrital contribution to light extinction in this application was included in the value of α_w.

Water-Quality Constituents

Twelve of the 22 water-quality constituents included in table 1 were used in all aspects of this study: suspended solids, dissolved solids, orthophosphate, nitrate-plus-nitrite, ammonia, phytoplankton biomass, zooplankton biomass, labile dissolved organic matter, detritus, dissolved oxygen, a conservative tracer (chloride), and organic matter in bottom sediment. Six others (total inorganic carbon, carbonate alkalinity, pH, carbon dioxide, bicarbonate, and carbonate) were used only in an exploratory fashion. The unused constituents were not considered crucial to the primary goals of understanding the cycling of nutrients in the Tualatin River and the role played by primary production in determining water quality. Inorganic carbon species are not important in determining primary production unless carbon is a limiting nutrient, and such a limitation has not been substantiated for the Tualatin River system. The accurate calculation of inorganic carbon is crucial to an accurate calculation of the pH in the system, but insufficient boundary and calibration data make this an unrealistic goal for the current study. The carbonaceous biochemical oxygen demand (CBOD) constituent was not used because it would have been redundant with the oxygen demand provided by the other dissolved organic-matter constituents specified at the boundaries. Refractory organic matter was not included due to insufficient boundary and calibration data, but this organic compartment is not thought to play an important role in the Tualatin River. Iron may be important to the cycling of phosphorus. Recent work in the Tualatin River indicates that phosphorus adsorption to iron colloids may constitute a significant reservoir of phosphorus in the water column, although the evidence suggests that the colloids are formed by a coprecipitation process that is not well represented by the linear adsorption formulation used by CE-QUAL-W2 (Mayer, 1995). At this time, however, reasonable estimates of boundary conditions and adsorption data are unavailable; therefore, this constituent was also omitted. The 12 constituents that are included in the simulations are sufficient to provide a reasonable simulation of the cycling of nutrients and the growth and decline of algal populations in the Tualatin River.

A discussion of the rate equation for each constituent follows. Each equation is applied to every cell in the model grid, and is vertically and longitudinally averaged over the depth and length of the cell. The kinetic source/sink terms take a consistent general form for all of the constituents: $K \times \delta \times \gamma \times \Phi$ where K is a rate constant, δ is a stoichiometric coefficient (omitted if equal to 1), γ is a rate modifier based on ambient water temperature, and Φ is a constituent concentration. The term may include rate modifiers in addition to that for temperature. The rate constant K in this expression is a model input parameter and is referenced to 20°C. The stoichiometric coefficient δ is also an input parameter when it is not equal to one. The temperature rate modifier takes the form of the van't Hoff equation (e.g., McCutcheon and French, 1989), such that:

$$\gamma = Q_{10}^{\frac{(T-20)}{10}} = \theta^{(T-20)}, \qquad (13)$$

where T is the water temperature and θ is an input parameter. The code maintained by the USACE employs a temperature rate modifier with both a rising and a falling limb for most reactions, thus simulating the decline in the rate of biological processes that occurs at inhibitory high temperatures. This type of formulation requires the specification of an optimum range in temperature for the reaction, as well as inhibitory high and low temperatures to properly characterize the function. In this version of the model, all temperature rate modifiers were replaced with an unbounded exponential (eq. 13). This function probably is more accurate for the (May–October) temperature range found in the Tualatin River, where it is unlikely that temperatures high enough to inhibit biological processes are ever reached. Equation 13 has the additional advantage of requiring only one input parameter.

In addition to kinetic source and sink terms, several of the constituents are transported vertically through settling. The settling term takes the general form $\omega (\Delta\Phi / \Delta z)$, where ω is the settling velocity, $\Delta\Phi$ is the difference in constituent concentration between the current cell and the cell above, and Δz is the depth of the current cell. The settling velocity for each type of particle (algal, detrital, inorganic suspended solid) is an input parameter, and is referenced to 20°C.

Carbon

Carbon in this model is partitioned among several compartments: water-column biomass (phytoplankton and zooplankton), other water-column organic matter (detritus and dissolved labile organic matter), total inorganic carbon, and bottom sediments (fig. 6). Equations are presented only for the organic-matter compartments. Inorganic carbon is not part of the model solution in this application; therefore, that compartment acts like an unlimited reservoir that does not affect the cycling of carbon among the organic-matter compartments.

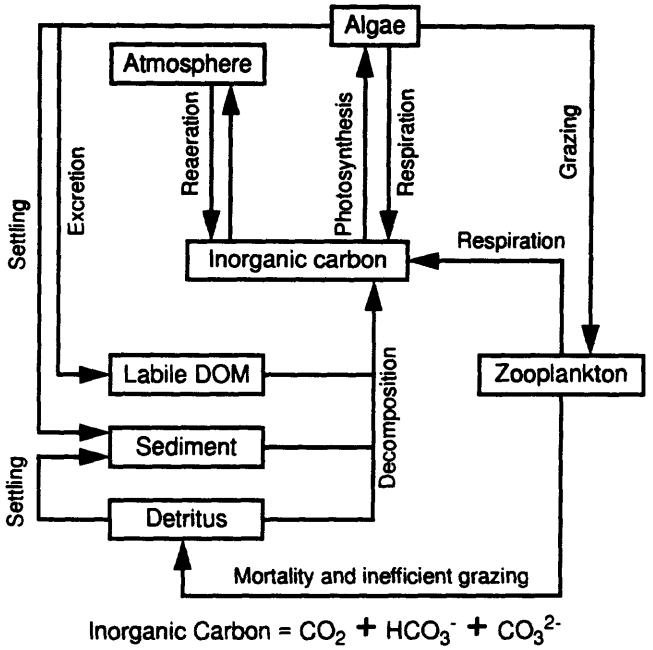

Figure 6. The model compartments that contain carbon, and the processes that cause carbon to move among those compartments in the U.S. Geological Survey version of CE-QUAL-W2. (DOM, dissolved organic matter)

Algal biomass increases through photosynthesis and decreases through the combined processes of respiration, excretion, and predatory and nonpredatory mortality. Suspended algal cells also are transported vertically through the water column by settling. The resulting rate equation for the algal biomass is:

$$\frac{d\Phi_a}{dt} = (K_{ag}\lambda_{ag} - K_{ar} - K_{ae}\lambda_{ae} - K_{am})\gamma_a\Phi_a - K_{zg}f_{zg}\lambda_{zg}\gamma_z\Phi_z - \omega_a\frac{\Delta\Phi_a}{\Delta z} \qquad (14)$$

where Φ_a and Φ_z are the biomass concentrations of phytoplankton and zooplankton, ω_a is the settling velocity of algal cells, $\Delta\Phi_a$ is the difference in the concentration of phytoplankton between the current cell and the cell above, and Δz is the depth of the current cell.

The rate constants K_{ag}, K_{ar}, K_{ae}, and K_{am} are the maximum rates of algal growth, respiration, excretion, and nonpredatory mortality, respectively, at 20°C; K_{zg} is the maximum grazing rate of zooplankton, also at 20°C. The temperature rate modifier γ_a applies to all the algal processes and γ_z applies to grazing by zooplankton.

The growth-rate modifier in CE-QUAL-W2, λ_{ag}, is set equal to the minimum of a phosphorus, nitrogen, and light-limitation factor. The nutrient limitation factors use a Michaelis-Menten formulation, which requires specification of the half-saturation concentrations. The USACE version of the model utilizes a light-limitation factor that is based on describing the light-saturation curve with an exponential function (Steele, 1962):

$$P^B = \alpha I_z e^{\left(\frac{\alpha I_z}{P_m^B e}\right)}, \qquad (15)$$

where α is the initial slope of the light-saturation curve, P_m^B is the rate of primary production at optimal light intensity, I_z is the light intensity at depth z, P^B is the rate of primary production at depth z, and $e \approx 2.71828$. In this version of the model, the light limitation was changed and is based on depicting the light-saturation curve with a hyperbolic tangent function (Jassby and Platt, 1976):

$$P^B = P_m^B \tanh\left(\frac{\alpha I_z}{P_m^B}\right). \qquad (16)$$

Equation 15 allows for photoinhibition and equation 16 does not. At intensities less than saturation, light limitation based on equation 15 exceeds that based on equation 16, and the difference can be as much as 10 percent. Photoinhibition is not of major importance in the Tualatin River (due to the partial shading and the large light-extinction coefficient), and because equation 16 was found to be a better descriptor of experimental light-saturation curves (Jassby and Platt, 1976), it was used. The light limitation is the ratio P^B / P_m^B. The rate modifier λ_{ag}, therefore, is given by:

$$\lambda_{ag} = \min\left\{\frac{\Phi_P}{h_P + \Phi_P}, \frac{\Phi_N}{h_N + \Phi_N}, \overline{\tanh\left(\frac{eI_z}{I_s}\right)}\right\}, \qquad (17)$$

where Φ_P is the concentration of orthophosphate phosphorus, Φ_N is the sum of ammonia-nitrogen and nitrate-plus-nitrite nitrogen concentrations, h_P and h_N are the Michaelis-Menten half-saturation concentrations for phosphorus and nitrogen, I_S is the saturation light intensity equal to eP_m^B / α, and the overbar on the depth-specific light limitation notation indicates that it is vertically averaged over the cell depth. Light intensity varies continuously with depth as determined with Beer's Law, the incident light intensity, the reduction in incident light at the surface by shading and absorption in the surface microlayer, and the light-extinction coefficient. Beer's Law and the ancillary algorithms required to use it are discussed under *Heat Flow* in this section. Algal excretion is also modified by a light-dependent factor:

$$\lambda_{ae} = 1 - \overline{\tanh\left(\frac{eI_z}{I_s}\right)}, \qquad (18)$$

which maximizes the excretion rate where algal growth is most light limited.

The loss of algal biomass due to zooplankton grazing is modified by two factors in addition to the temperature rate modifier. The first of these, f_{zg}, represents the relative preference of the zooplankton for algae as food and requires the selection of two preference factors p_a, and p_{dt}, for algae and detritus, in the range 0–1 (values listed in the *Boundary Conditions, Reaction Rates, and Forcing Functions* section):

$$f_{zg} = \frac{p_a \Phi_a}{p_a \Phi_a + p_{dt} \Phi_{dt}}. \qquad (19)$$

The second, λ_{zg}, further reduces the zooplankton grazing rate at low food concentrations with a modified Michaelis-Menten factor, requiring the selection of a half-saturation food concentration h_{zg} and a threshold food concentration μ_z below which no grazing occurs:

$$\lambda_{zg} = \frac{p_a \Phi_a + p_{dt} \Phi_{dt} - \mu_z}{h_{zg} + p_a \Phi_a + p_{dt} \Phi_{dt}}. \qquad (20)$$

Zooplankton biomass is increased through grazing and decreased through respiration and mortality. Because the zooplankton compartment represents the top of the food chain in this model, the zooplankton mortality rate must include predatory as well as nonpredatory mortality. The rate equation is:

$$\frac{d\Phi_z}{dt} = (K_{zg} \lambda_{zg} e_{zg} - K_{zr} - K_{zm}) \gamma_z \Phi_z, \qquad (21)$$

where Φ_z is the concentration of zooplankton biomass. The rate constants K_{zg}, K_{zr}, and K_{zm} are the maximum possible rates of zooplankton grazing, respiration, and mortality at 20°C. All of the zooplankton processes share the same temperature modifier, γ_z. The efficiency of the grazing process is represented by an efficiency factor e_{zg} selected in the range 0–1. The fraction of ingested food $1 - e_{zg}$ that does not contribute to an increase in zooplankton biomass appears instead as a contribution to the detritus compartment.

Detrital organic matter also constitutes a food source for zooplankton; therefore, the flow of nutrients between the zooplankton and detritus compartments goes in both directions during grazing. Direct grazing by zooplankton depletes the detritus compartment while simultaneously the inefficiency of grazing sends some of the organic matter ingested to the detritus compartment. Mortality of phytoplankton and zooplankton also contributes to this compartment. Detritus is depleted by bacterially mediated decay. Each layer receives settling detritus from the layer above, and where the layer is in contact with the bed sediments, settling removes detritus from the water column. For this application it was useful to distinguish between two types of detritus: the allochthonous detritus that enters the system through the tributaries and upstream boundary, and the autochthonous detritus that is created when algal cells die or pass through zooplankton during inefficient grazing. The allochthonous detritus consists of small particles in suspension that settle slowly; the larger particles making up the autochthonous detritus retain the settling velocity of algal cells. The total detrital organic matter, Φ_{dt}, is the sum of the detrital organic matter that enters at the boundaries, Φ_{bdt}, and the detrital organic matter that originates as live algal cells, Φ_{adt}. The resulting equation for the rate of change in the detritus concentration is:

$$\frac{d\Phi_{dt}}{dt} = P_{am}K_{am}\gamma_a\Phi_a - K_{zg}[(1-f_{zg}) - (1-e_{zg})]\lambda_{zg}\gamma_z\Phi_z + K_{zm}\gamma_z\Phi_z - K_{dt}\gamma_{dt}\Phi_{dt} - \omega_{dt}\frac{\Delta\Phi_{bdt}}{\Delta z} - \omega_a\frac{\Delta\Phi_{adt}}{\Delta z}, \quad (22)$$

where $\Delta\Phi_{bdt}$ and $\Delta\Phi_{adt}$ are the differences in concentration between the current cell and the cell above. The factor P_{am} determines the fraction of dead algae that becomes detrital organic matter, with the balance becoming labile organic matter.

The labile organic matter compartment is increased through algal excretion and algal mortality. Organic matter entering this compartment is rapidly recycled as nutrients through a fast decay rate, K_{lom}. The equation describing the effect of these processes on the concentration of labile organic matter is:

$$\frac{d\Phi_{lom}}{dt} = K_{ae}\lambda_{ae}\gamma_a\Phi_a + (1-P_{am})K_{am}\gamma_a\Phi_a - K_{lom}\gamma_{lom}\Phi_{lom}, \quad (23)$$

where Φ_{lom} is the concentration of labile organic matter, and γ_{lom} is the temperature rate modifier for its decay.

Organic matter builds up in the bottom sediment when settling detrital and algal particles reach the river bottom. Organic matter in this compartment undergoes aerobic decomposition that releases nutrients back into the water column and creates a:

$$\frac{d\varphi_s}{dt} = \omega_{dt}\Phi_{bdt} + \omega_a(\Phi_a + \Phi_{adt}) - K_s\gamma_s\varphi_s, \quad (24)$$

where φ_s is the concentration of organic matter (OM) in the sediment, K_s is the rate of the aerobic decomposition, and γ_s is the temperature-dependent rate modifier. The sediment organic matter is normalized to the area of each cell that has contact with the bottom sediments and has units of g OM/m^2. In contrast, in the previous USACE version of the code, the sediment organic matter was normalized to the volume of the cell and had units of g OM/m^3. The current USACE version has been updated to reflect this surface-area normalization. This change makes the application of mass-balance constraints in the model more computationally straightforward, and sediment concentrations expressed in this way are more physically intuitive.

Dissolved Oxygen

Photosynthesis is the sole biochemical producer of dissolved oxygen. Oxygen is consumed by several biochemical processes: respiration of algae and zooplankton, nitrification, and the decay of three organic-matter compartments: water-column detritus, labile dissolved organic matter, and bottom sediments (fig. 7).

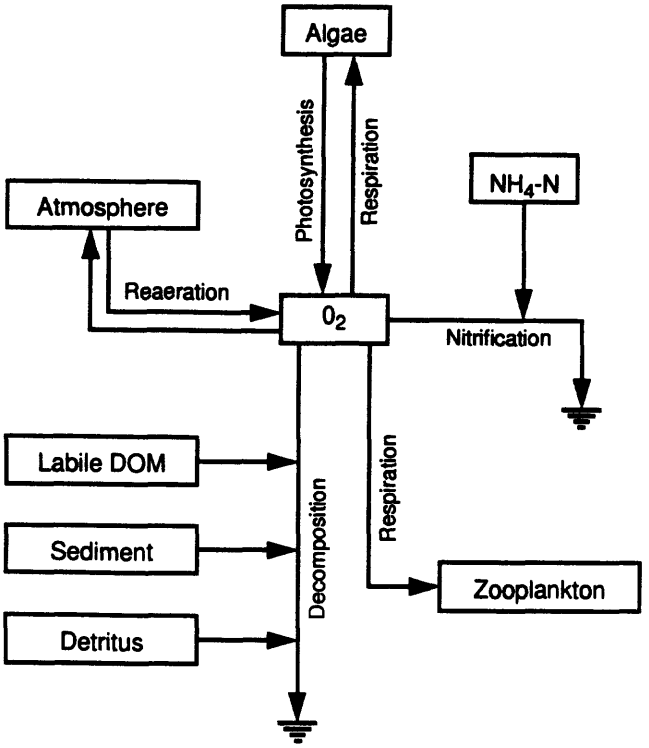

Figure 7. The model compartments and processes that influence the dissolved oxygen concentration in the U.S. Geological Survey version of CE-QUAL-W2. (DOM, dissolved organic matter)

Reaeration is a physical process that transfers oxygen across the air/water interface such that the concentration of dissolved oxygen in the water approaches saturation. The rate of change of the dissolved oxygen concentration is expressed mathematically as:

$$\frac{d\Phi_{DO}}{dt} = (K_{ag}\lambda_{ag}\delta_{ag} - K_{ar}\delta_{ar})\gamma_a\Phi_a$$
$$- K_{NH_3}\delta_{NH_3}\gamma_{NH_3}\Phi_{NH_3}$$
$$- K_{dt}\delta_{dt}\gamma_{dt}\Phi_{dt} - K_s\delta_s\gamma_s f_b\frac{\varphi_s}{\Delta z}$$
$$- K_{lom}\delta_{lom}\gamma_{lom}\Phi_{lom}$$
$$- K_{zr}\delta_{zr}\gamma_z\Phi_z + E_{DO}(\Phi'_{DO} - \Phi_{DO}) \quad , \quad (25)$$

where Φ_{DO} is the concentration of dissolved oxygen, Φ'_{DO} is the concentration at saturation, K_{NH_3} is the nitrification rate, and δ_{ag}, δ_{ar}, δ_{zr}, δ_{NH_3}, δ_{dt}, δ_s, and δ_{lom} are the stoichiometric coefficients defining, respectively, the amount of oxygen produced when organic matter is synthesized, consumed by the respiration of algae and zooplankton, consumed by nitrification, and consumed by the decay of detrital, sediment, or labile organic matter. The factor f_b is the fraction of the cell width that is in contact with the sediments. The reaeration coefficient E_{DO} was modified from that in the USACE version of the code to use water velocity rather than wind speed, making the expression more appropriate to a river system:

$$E_{DO,20°} = \frac{5.58U^{0.607}}{D^{1.689}}, \quad (26)$$

where U is the downstream velocity in m/s averaged over the water column, D is the average depth of the water column in m, and $E_{DO,20°}$ is the reaeration coefficient at 20°C (Bennett and Rathbun, 1972). This coefficient is corrected for temperature according to the method reported by McCutcheon and French (1989):

$$E_{DO} = E_{DO,20°}(1.0241)^{(T-20)}. \quad (27)$$

Phosphorus

CE-QUAL-W2 solves for the concentration of bioavailable phosphorus in the form of orthophosphate. The model's algorithms assume that orthophosphate is consumed during photosynthesis and released by respiration and the decay of organic material (fig. 8).

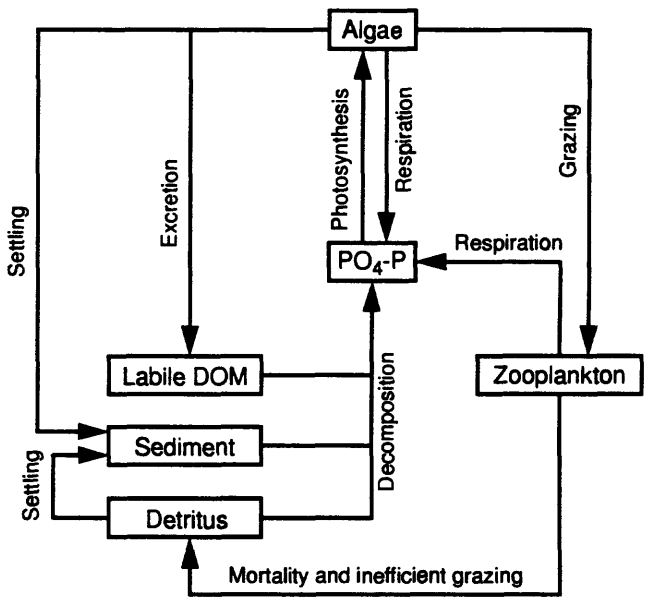

Figure 8. The model compartments that contain phosphorus and the processes that cause phosphorus to move among those compartments in the U.S. Geological Survey version of CE-QUAL-W2. (DOM, dissolved organic matter)

Orthophosphate adsorbed onto inorganic particles settles and is removed from the water column when those particles reach the river bottom. The rate of change of orthophosphate is expressed mathematically as:

$$\frac{d\Phi_P}{dt} = (K_{ar} - K_{ag}\lambda_{ag})\,\delta_P\gamma_a\Phi_a + K_{zr}\delta_P\gamma_z\Phi_z + K_{lom}\delta_P\gamma_{lom}\Phi_{lom} + K_{dt}\delta_P\gamma_{dt}\Phi_{dt} + K_s(1-f_P)\,\delta_P\gamma_s\Phi_s - K_P\frac{\Delta(\Phi_P(\omega_{ss}\Phi_{ss} + \omega_{Fe}\Phi_{Fe}))}{\Delta z}, \quad (28)$$

where Φ_P is the concentration of orthophosphate-P, δ_P is the stoichiometric coefficient of phosphorus in organic matter, K_P is a linear adsorption coefficient, and the last term represents the change in orthophosphate concentration due to the settling of suspended solids and particulate iron that have adsorbed phosphorus. The solution for the total iron concentration Φ_{Fe} is not included in this application due to insufficient boundary data; nonetheless, adsorption onto iron oxyhydroxides may be important in the Tualatin River (Mayer, 1995). The inclusion of iron in the calculations and the adsorption of phosphorus onto iron oxyhydroxides is probably an important refinement to consider for future modeling efforts in this river, but adsorption is not considered in this application, and K_P is set to zero.

The USGS version of the model was modified by the addition of the factor $(1-f_P)$ to the bottom-sediment decay term. The parameter f_P is the fraction of phosphorus in sediment organic matter that is *not* released to the water column when that organic matter decays. Calibration of the model indicated that this factor was needed. Several mechanistic reasons for this factor are reasonable. One probable explanation is that orthophosphate is adsorbed onto iron oxyhydroxides in the surface layer of sediment. For this mechanism to be effective at retaining phosphorus in the sediments, a large Fe:P ratio is required (Jensen and others, 1992). The factor f_P could also be interpreted to compensate for organic matter in the sediments that has aged and has a higher C:P ratio than organic matter in the water column (recall that δ_P, unfortunately, is the same for all types of organic matter in this model).

Nitrogen

Inorganic nitrogen in CE-QUAL-W2 is treated explicitly as either ammonia or nitrate-plus-nitrite nitrogen (fig. 9).

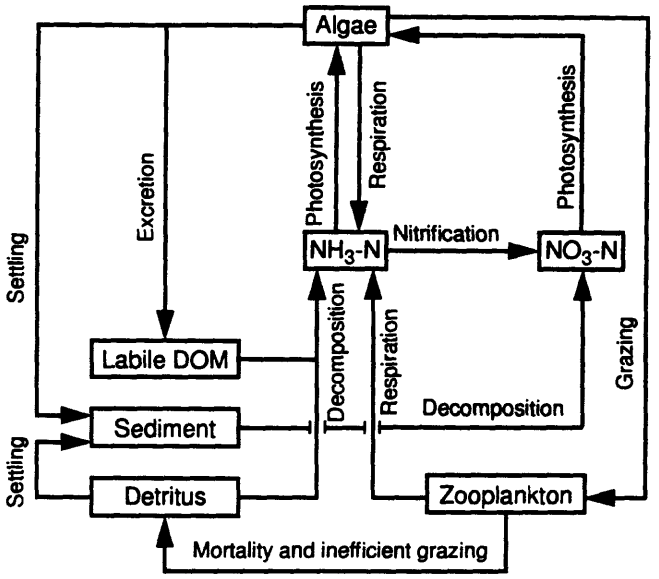

Figure 9. The model compartments that contain nitrogen and the processes that cause nitrogen to move among those compartments in the U.S. Geological Survey version of CE-QUAL-W2. (DOM, dissolved organic matter)

The ammonia pool is depleted by algal photosynthesis and nitrification. Processes which recycle nitrogen to the ammonia pool are respiration by algae and zooplankton, and the decay of each of the water-column organic-matter constituents. The resulting rate equation for ammonia is:

$$\frac{d\Phi_{NH_3}}{dt} = -\left(K_{ag}\lambda_{ag}f_{NH_3} - K_r\right)\delta_N\gamma_a\Phi_a + K_{zr}\delta_N\gamma_z\Phi_z + K_{lom}\delta_N\gamma_{lom}\Phi_{lom} + K_{dt}\delta_N\gamma_{dt}\Phi_{dt} - K_{NH_3}\gamma_{NH_3}\Phi_{NH_3}, \quad (29)$$

where Φ_{NH_3} is the concentration of ammonia-nitrogen, K_{NH_3} is the rate of nitrification at 20°C, γ_{NH_3} is the temperature rate modifier for nitrification, and δ_N is the stoichiometric coefficient of nitrogen in organic matter. Phytoplankton use ammonia or nitrate nitrogen for growth; however, they show a marked preference for ammonia-N when it is plentiful (Ambrose and others, 1988). The factor f_{NH_3} indicates the relative intensity of this preference, which is based on water-column concentrations of both quantities.

The factor $f_{NH_3} = \Phi_{NH_3}/(\Phi_{NH_3} + \Phi_{NO_3})$ in the USACE code has the algae consume ammonia in proportion to the contribution of ammonia to the total bioavailable nitrogen in the water column. This factor was replaced with an algorithm used in the model WASP4 (Ambrose and others, 1988):

$$f_{NH_3} = \left(\frac{\Phi_{NH_3}}{\Phi_{NH_3} + h_N}\right)\left(\frac{\Phi_{NO_3}}{\Phi_{NO_3} + h_N}\right) + \left(\frac{\Phi_{NH_3}}{\Phi_{NH_3} + \Phi_{NO_3}}\right)\left(\frac{h_N}{h_N + \Phi_{NO_3}}\right), \quad (30)$$

where h_N is the same half-saturation concentration that is used to determine the nitrogen limitation to algal growth. This algorithm hconcentration of nitrate-plus-nitrite is much greater than the concentration of ammonia.

The nitrate-plus-nitrite pool is depleted by photosynthetic uptake and replenished by nitrification. Nitrogen is also recycled to this compartment through the decay of bottom sediments. This represents a change in the nitrogen cycle from the USACE version of the code, in which nitrogen released from the sediments is put into the ammonia compartment. Early attempts at calibration of the model showed that this change was necessary to avoid building up too much ammonia in the water column. The need to change the cycling of the nitrogen in this way is indirect evidence that nitrification is occurring within the microbe-rich bottom sediments, and is supported by the literature (Bowie and others, 1985). The rate equation for the change in nitrate-plus-nitrite concentration is:

$$\frac{d\Phi_{NO_3}}{dt} = K_{NH_3}\gamma_{NH_3}\Phi_{NH_3} + K_s\delta_N\gamma_s\Phi_s - K_{ag}\lambda_{ag}\left(1 - f_{NH_3}\right)\delta_N\gamma_a\Phi_a, \quad (31)$$

where Φ_{NO_3} is the concentration of nitrate-plus-nitrite nitrogen.

Total dissolved solids and total suspended solids

Total dissolved solids are treated as a conservative quantity in CE-QUAL-W2 and, therefore, require no kinetic rate equation. They are included in this application primarily for their role as a tracer of wastewater from the treatment plants, which tends to have a high dissolved solids concentration. They are also used in the calculation of water density and ionic strength.

The suspended solids compartment of the model refers only to *inorganic* suspended solids because organic suspended solids are included as detrital or algal particles. This constituent is included because it affects the attenuation of light with depth in the water column. These solids are chemically conservative, but they settle through the water column and are removed when they reach the river bottom. The rate equation for this constituent is:

$$\frac{d\Phi_{ss}}{dt} = -\omega_{ss}\frac{\Delta\Phi_{ss}}{\Delta z}, \quad (32)$$

where Φ_{ss} is the concentration of inorganic suspended solids, ω_{ss} is the settling velocity of those solids, and $\Delta\Phi_{ss}$ is the difference in suspended solids concentration between the current cell and the cell above.

pH

CE-QUAL-W2 simulates the pH of a water body using standard chemical-equilibrium relations and the assumption that the pH is controlled by the chemistry of carbonate. The effects of phosphates, silicates, iron, aluminosilicates, and other constituents on pH are not included; however, these species generally do not affect the pH in a carbonate system because they typically are present in low concentrations or have dissociation constants that are outside the relevant range. Assuming that carbonate equilibria are dominant, the pH is easily calculated from two quantities: the total inorganic-carbon concentration (C_T) and the alkalinity (*Alk*).

The relations used to calculate pH from C_T and *Alk* are discussed in the user manual (Cole and Buchak, 1995) and also can be found in standard aquatic chemistry texts (Stumm and Morgan, 1981; Pankow, 1991). Nonetheless, a short review is useful. Carbonate alkalinity (equivalents/L) is defined as:

$$Alk = [HCO_3^-] + 2[CO_3^{2-}] + [OH^-] - [H^+], \quad (33)$$

where [X] represents the concentration of species X (moles/L). The total inorganic-carbon concentration (moles/L) is:

$$C_T = [H_2CO_3^*] + [HCO_3^-] + [CO_3^{2-}], \quad (34)$$

where

$$[H_2CO_3^*] = [H_2CO_3] + [CO_2]. \quad (35)$$

Using equations 33 and 34, the alkalinity can be represented solely as a function of C_T and the hydrogen ion activity $\{H^+\}$:

$$Alk = \left(\frac{K_1' \{H^+\} + 2K_1'K_2'}{\{H^+\}^2 + K_1' \{H^+\} + K_1'K_2'} \right) C_T + \frac{K_w'}{\{H^+\}} - \frac{\{H^+\}}{\gamma_{H^+}}. \quad (36)$$

The activity of an ion is simply the concentration of that ion (moles/L) multiplied by a dimensionless activity coefficient. Therefore,

$$\{H^+\} = \gamma_{H^+} [H^+], \quad (37)$$

where γ_{H^+} is the activity coefficient for H^+. The K' values in equation 36 are "mixed" equilibrium constants, defined as:

$$K_1' = \frac{\{H^+\} [HCO_3^-]}{[H_2CO_3^*]} = K_1 \frac{\gamma_{H_2CO_3^*}}{\gamma_{HCO_3^-}}, \quad (38)$$

$$K_2' = \frac{\{H^+\} [CO_3^{2-}]}{[HCO_3^-]} = K_2 \frac{\gamma_{HCO_3^-}}{\gamma_{CO_3^{2-}}}, \quad (39)$$

$$K_w' = \{H^+\} [OH^-] = \frac{K_w}{\gamma_{OH^-}}. \quad (40)$$

K_1, K_2, and K_w are the infinite-dilution equilibrium constants for the first and second dissociation reactions of carbonic acid and the dissociation reaction of water, respectively. These constants are known quantities; their values are easily calculated as a function of temperature. Activity coefficients for the ions are calculated with an extension of the Debye-Hückel law (see the user manual [Cole and Buchak, 1995]). Given values for C_T, *Alk*, the water temperature, and the dissolved solids concentration (needed to calculate activity coefficients), equation 36 can be solved iteratively for the hydrogen ion activity and, therefore, the pH ($pH = -\log \{H^+\}$).

In the USACE version of CE-QUAL-W2, alkalinity is assumed to be a conservative quantity. It is transported, dispersed, and affected by inputs and withdrawals, but it is not affected by chemical or biological reactions. Although this assumption is not necessarily limiting, alkalinity *is* known to be affected by some of the chemical and biological reactions included in the model. The USGS version of CE-QUAL-W2 was modified to allow alkalinity to be affected by nitrification, photosynthesis, and algal respiration. Hydrogen ions are produced when ammonium is nitrified:

$$NH_4^+ + 2O_2 \rightarrow NO_3^- + H_2O + 2H^+. \quad (41)$$

For every mole of ammonium ions consumed, the alkalinity will decrease by two equivalents. The effect of photosynthesis on alkalinity depends upon the form of nitrogen utilized by the algae. If nitrate is the nitrogen source, hydrogen ions are consumed according to equation 42 (Stumm and Morgan, 1981):

$$106CO_2 + 16NO_3^- + HPO_4^{2-} + 122H_2O + 18H^+ \rightarrow "Algae" + 138O_2, \quad (42)$$

and the alkalinity will increase by 18 equivalents for every 16 moles of nitrate consumed. If, however, ammonium is the nitrogen source for photosynthesis, then hydrogen ions are produced according to equation 43 (Stumm and Morgan, 1981):

$$106CO_2 + 16NH_4^+ + HPO_4^{2-} + 108H_2O \rightarrow "Algae" + 107O_2 + 14H^+, \quad (43)$$

and the alkalinity will decrease by 14 equivalents for every 16 moles of ammonium consumed. Algal respiration in this model is the reverse of equation 43; therefore, algal respiration will increase the alkalinity by 14 equivalents for every 16 moles of ammonium produced. These photosynthetic alkalinity adjustments have only a limited effect on the pH; the changes in C_T that accompany photosynthesis and respiration have the greatest effect on the pH. Nevertheless, these adjustments were included.

BOUNDARY CONDITIONS, REACTION RATES, AND FORCING FUNCTIONS

In order to simulate flow, temperature, and water quality in the Tualatin River, CE-QUAL-W2 requires many types of data. The model grid must be defined using bathymetric cross sections and longitudinal profiles of the river. Surface-water and ground-water sources to the river must be defined and measured. Withdrawals of water from the river must be located and measured or estimated. Meteorological data are needed to drive the heat budget and the growth of phytoplankton. Chemical and biological reaction rates must be measured or estimated. The water quality of each of the surface-water and ground-water inflows must be measured. These are the data that drive the simulations of water quality in the Tualatin River. This section describes these data.

River Bathymetry and the Model Grid

Possibly the most fundamental data used by a surface-water model are the bathymetric data used to create the numerical grid. This grid is just a simplified mathematical representation of the river bathymetry, designed to capture the basic channel characteristics and the volume of each river reach. It is imperative to create a correct representation of the volume of each river reach in order to accurately simulate the time required for a parcel of water to move through that reach. Accurate simulations of the travel time are required for this model application because the water quality of the Tualatin River is often determined by the dynamics of phytoplankton that are transported through the river system by its flow.

A numerical representation of the Tualatin River's channel from RM 38.4 (Rood Bridge Road) to RM 3.4 (Oswego diversion dam) was created from cross-sectional and midchannel depth measurements. Fifty-two cross sections were measured by USGS personnel between August 23 and October 19, 1990, concentrating on the reach between RMs 3.5 and 29. Most of the measurements were taken in mid-September of 1990. An additional 31 cross sections in the RM 3.5 to 27 reach were obtained from USA. The USA measurements were taken on September 14, 1986, and could be related to the USGS cross sections by accounting for differences in river stage. Using these cross-sectional data, a relation between the cross-sectional area and the midchannel depth was recognized. The simplest manifestation of this relation is the excellent correlation between the midchannel depth and the mean depth (fig. 10).

A continuous midchannel depth profile was collected by recording depths from a Lowrance sonar device while traveling the river from RM 3.4 to RM 36.6 in September of 1990. This longitudinal profile was used for two purposes. First, these data were instrumental in delineating the length and depth of several shallow reaches of the river. Shallow reaches can be important in enhancing or breaking down the vertical mixing of the river; these important features of the channel must be defined in the model grid. Second, the midchannel depth profile, in conjunction with the relation between it and the cross-sectional area, was used to infer cross-sectional information where cross sections were not measured.

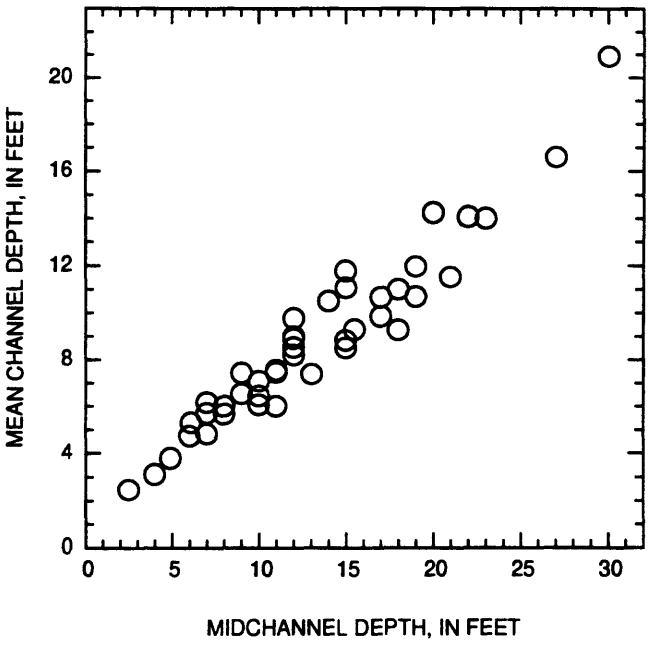

Figure 10. Relation of midchannel depth to mean depth in the Tualatin River. (The correlation coefficient is 0.96.)

Some bathymetric information was also obtained from a U.S. Army Corps of Engineers (1953) report.

CE-QUAL-W2 is a two-dimensional model, where the longitudinal dimension is along the direction of flow and the other dimension is in the vertical direction; lateral differences are not simulated. The model represents the channel bathymetry, therefore, with a two-dimensional grid of cells (fig. 11). In this grid, each individual layer height is constant from the upstream end of the grid to the downstream end. Different layers, however, need not have identical heights. The longitudinal dimension of the grid is made up of a series of segments, and segment lengths are not necessarily identical. Each segment of the grid is composed of a vertical stack of cells, where each cell has a height defined by the layer height, a length defined by the segment length, and a width unique to that cell. The cross section of an individual segment, therefore, is represented as a series of stacked rectangles, always increasing in width from bottom to top. The bottom of the channel is defined by a boundary cell with a width of zero. The measured cross-section data had to be manipulated so that the stacked-rectangle representation used by the model gave a reasonable approximation of the actual cross-sectional area (fig. 12).

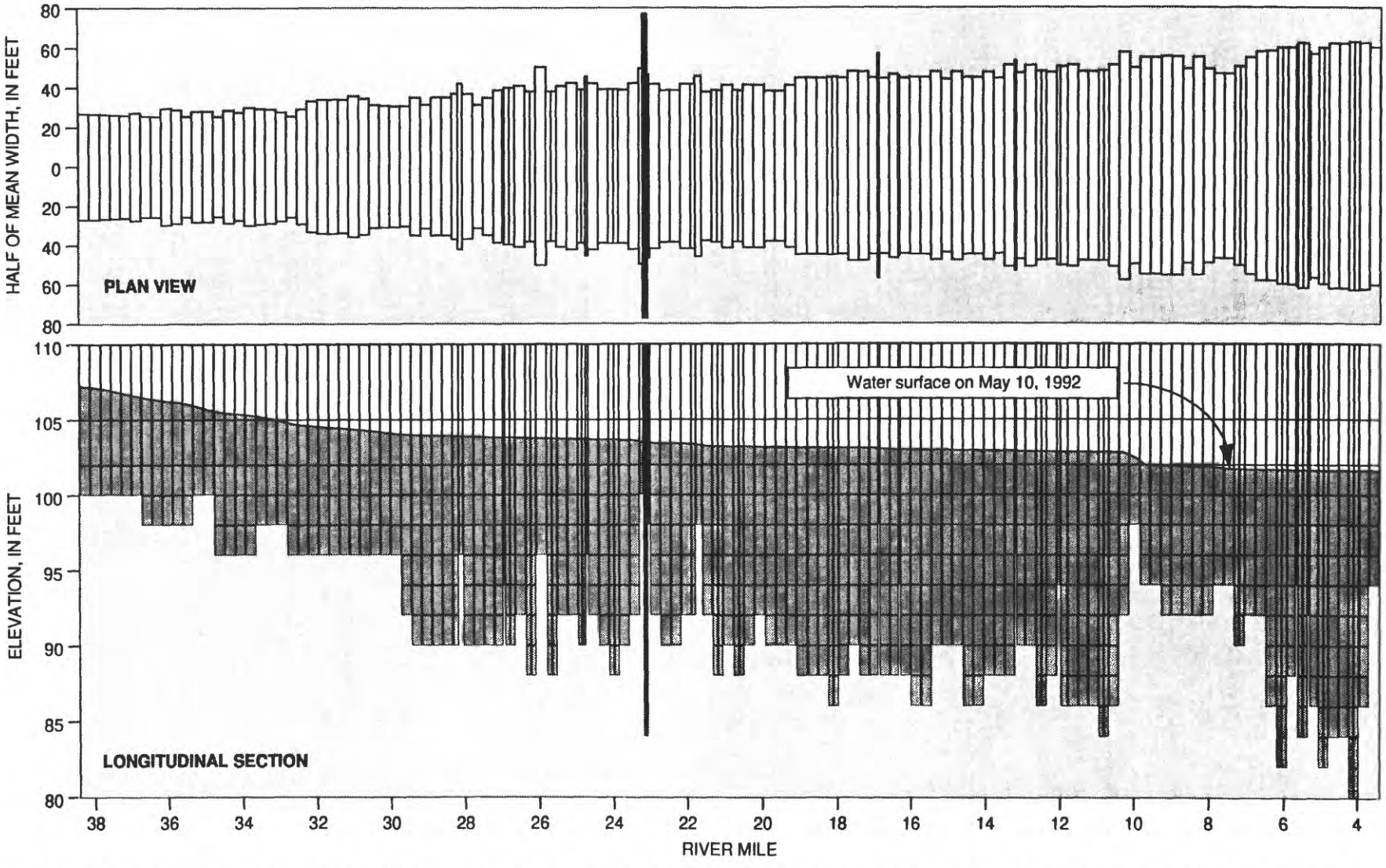

Figure 11. The two-dimensional grid used to represent the Tualatin River in CE-QUAL-W2. (Horizontal lines are layer boundaries; vertical lines are segment boundaries.)

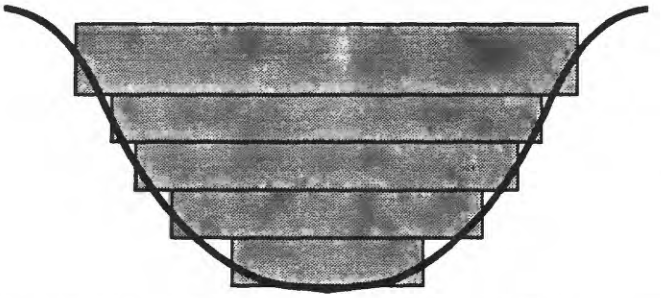

Figure 12. The stacked-rectangle representation of a cross section used in CE-QUAL-W2.

The numerical grid that represents the Tualatin River from RM 38.4 to RM 3.4 is composed of 155 segments and 16 layers. The choice of these grid dimensions was dictated mainly by the characteristic spatial scales of the river. During summertime low-flow periods, much of the main-stem Tualatin River from RM 30 to RM 3.4 is slow moving and placid. This reach has many of the characteristics of a lake; certain sites may stratify for weeks at a time. To capture this stratification and its associated water-quality consequences, it is necessary to discretize the grid vertically on a scale smaller than the thickness of the upper stratified layer, which is often 10 feet. In addition, light extinction in the Tualatin River is rapid. To capture differences in algal productivity and water quality with depth, a vertical discretization on the order of 2 feet is required. Most of the layers of the model grid, therefore, were chosen to be 2 feet in height. The length of most segments, set at 1,480 feet, was a compromise between the need to minimize longitudinal numerical dispersion and the need to minimize the time required to complete a simulation. The QUICKEST numerical solution method used by CE-QUAL-W2 expands the acceptable range of the Peclet number considerably (Leonard, 1979); these segment lengths were sufficiently short to avoid numerical instabilities. The lengths of a few shorter segments were specified according to the lengths of specific shallow or deep features of the channel. A model grid with more, shorter segments would give only slightly more accurate results, but would require more computer time to simulate. The cell lengths, heights, and widths that define the model grid for the Tualatin River are tabulated in Appendix B.

Throughout this report, references are made to several important locations along the main stem of the Tualatin River. Three important landmarks, for example, are RM 26.9 (Scholls Bridge), RM 16.2 (Elsner Road), and RM 5.5 (Stafford Road). These three are particularly important because many water-quality samples were collected at these sites for calibration purposes.

Discharge

A complete water budget for the main stem of the Tualatin River must include the major point sources (tributaries and wastewater-treatment plants [WWTPs]), nonpoint sources (small tributaries, seeps, tile drains, and ground water), irrigation withdrawals, surface-water diversions, precipitation, and evaporation in addition to the upstream and downstream boundary discharges. In the river reach from RM 38.4 (Rood Bridge) to RM 3.4 (Oswego diversion dam), 10tributaries were considered large enough to be explicitly included in the model. Both of the two large WWTPs discharge their effluent into this reach; these point sources are also included in the model as tributaries. One major diversion is present in the model reach; the Oswego canal is located at RM 6.7. Irrigation withdrawals are an important part of the water budget, and were distributed spatially at a number of locations in the model reach. A representation of the model reach is illustrated in figure 13, including the locations of all point sources and sinks.

Surface-Water Inflows

Gages continuously monitored the discharge at the upstream boundary of the model reach (RM 38.4) and at the Rock Creek and Durham WWTPs during the 1991 through 1993 period, and in one of the large tributaries (Fanno Creek) during 1992 and 1993. For Rock Creek (North) and the small tributaries that were not continuously monitored, intermittent discharge measurements were made by personnel from USGS and the Oregon Water Resources Department. These measurements were used to create gage height/discharge relations (rating tables), which in turn were used to estimate the discharge when only a gage height was recorded. Gage heights were noted whenever a water-quality sample was collected. For some of the small tributaries whose gage heights were read only intermittently, the discharge was sometimes estimated on the basis of the hydrographs of similar streams in the Tualatin River Basin or in neighboring drainage basins. All of the discharge data necessary to the model have been documented by Doyle and Caldwell (1996).

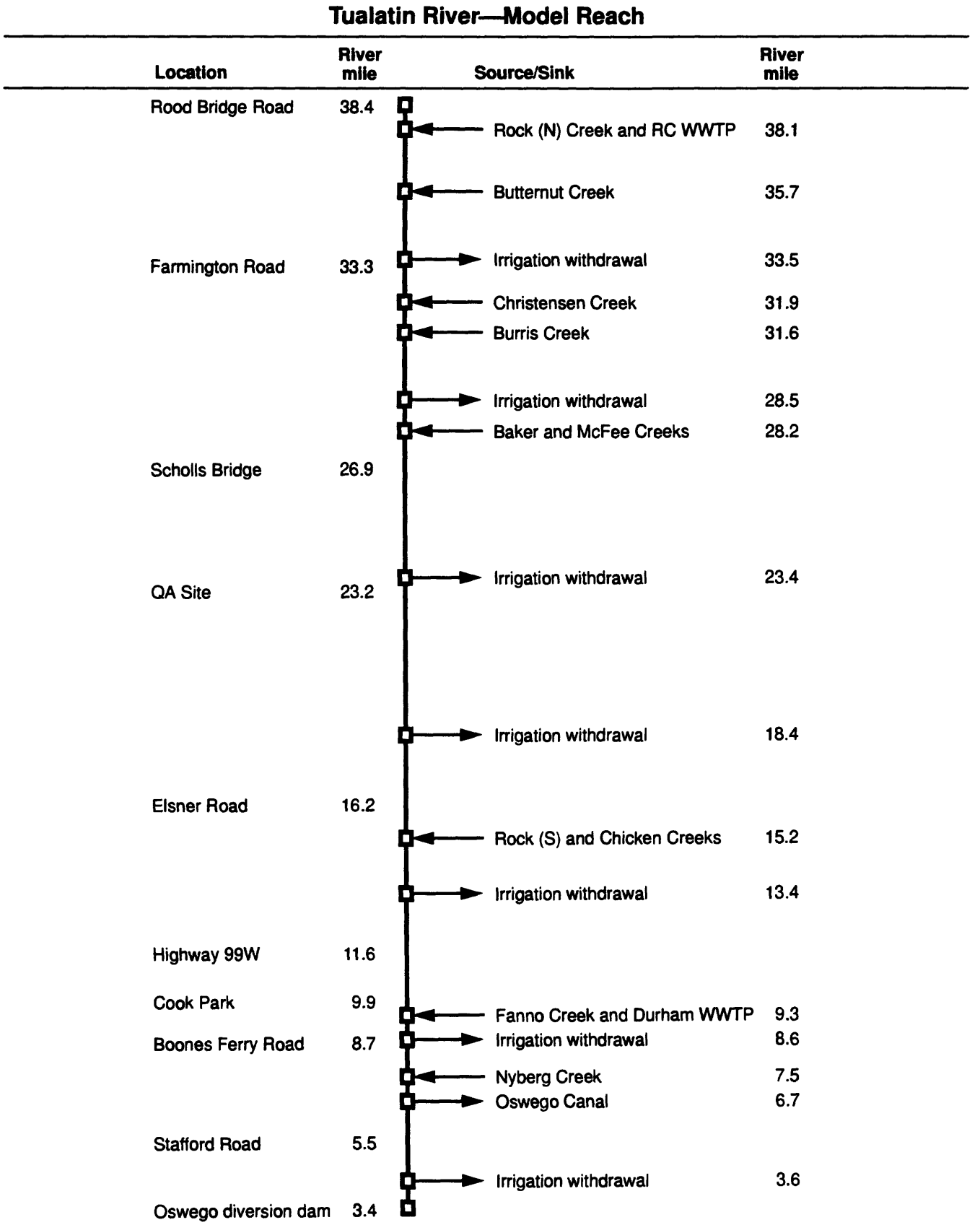

Figure 13. Schematic representation of the Tualatin River with the locations of tributaries, withdrawals, and sampling sites. (N, north; RC, Rock Creek; WWTP, wastewater-treatment plant; S, south; W, west)

Surface-Water Withdrawals

Irrigation withdrawals and one major diversion are important parts of the water budget of the Tualatin River. The Oswego canal diverts a large amount of water (about 60 ft^3/s) from the Tualatin at RM 6.7. Flow in the canal is continuously monitored; these data are used directly in the model. Accurate measurements of irrigation withdrawals as a function of location and time, however, were not available. These withdrawals, therefore, were estimated using known water rights and a measured relation between irrigation needs and meteorological conditions.

The probability that individual irrigators will exert their water right on a particular day depends upon whether water is needed, and that need is dependent upon the weather. One gaged withdrawal on the Tualatin River that illustrates this relation between need and the weather is the Spring Hill Pumping Plant operated by the Tualatin Valley Irrigation District (TVID) at RM 56.1. This pumping station feeds river water into a pipeline network that serves roughly 10,500 acres of agricultural land. Assuming that the water use per acre on the TVID network is similar to that of irrigators that withdraw their water directly from the river, an estimate of water withdrawal as a function of location and time can be generated using the acreages associated with known water rights. Water rights for Tualatin River water can be divided into two groups: TVID-permitted water rights and State water rights. During any one summer, not all of the State water rights may be used. For the purposes of this study, it was assumed that only 50 percent of the acreage served by State water rights was receiving Tualatin River water (Jerry Rodgers, Oregon Water Resources Department, oral commun., 1992). All of the TVID-permitted acres were assumed to be irrigated. For the sake of simplicity, the TVID and State acreages were divided into seven groups according to their location on the river (table 2). Over the May through October periods of 1991–93, the amount of water withdrawn from the river to irrigate those acres was estimated using the pumping-rate-per-acre statistics of the TVID pumping station. These withdrawals can amount to a significant loss of water from the river in the summer (fig. 14). Measured discharges for the Oswego canal and the Spring Hill Pumping Plant are documented by Doyle and Caldwell (1996).

Table 2. Irrigated acres used to estimate water withdrawals
[TVID, Tualatin Valley Irrigation District]

River reach (river miles)	Acres served by TVID permits	Estimated acres served by State water rights	Total irrigated acres (estimate)	Segment in grid where withdrawal is applied
38.4–33.3	743	589	1,332	19
33.3–28.3	828	587	1,415	37
28.3–23.3	955	442	1,397	63
23.3–18.2	407	370	777	87
18.2–13.2	320	176	496	108
13.2–8.4	0	168	168	129
8.4–3.4	0	85	85	154

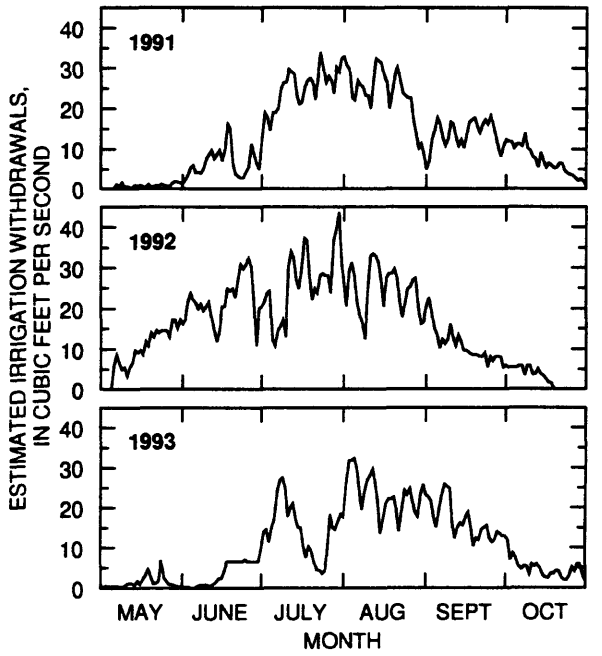

Figure 14. Estimated water withdrawals from the modeled reach of the Tualatin River for irrigation, May–October of 1991–93.

Downstream Outflow

Water leaves the model grid at the downstream boundary by flowing past the Oswego diversion dam at RM 3.4. The Oswego diversion dam is composed of three structures that transmit water: a broad, flat-crested, cement weir; a fish ladder; and a submerged "fish attractor" pipe located near the fish ladder. The hydraulic properties and physical dimensions of each of these structures, in conjunction with the water-surface elevation behind the dam, control the rate at which water flows past the dam. The dimensions and hydraulic properties of the fish ladder and the pipe are shown in table 3.

Table 3. Physical dimensions and hydraulic parameters of the fish ladder and the fish attractor pipe
[NGVD, National Geodetic Vertical Datum of 1929; —, dimensionless]

Structure	Parameter	Value	Units
Fish ladder	Elevation above NGVD of 1929	100.5	feet
	Width	6.0	feet
	Discharge coefficient	.62	—
Fish attractor pipe	Length	28.4	feet
	Diameter	2.5	feet
	Entrance loss coefficient	10	—
	Hazen-Williams friction coefficient	110	—

These values were measured either by USGS personnel or by members of Dr. Scott Wells' research group at Portland State University. The effective dimensions (elevation and width) and hydraulic characteristics (discharge coefficient) of the cement weir do not remain constant over the course of a summer.

The effective dimensions and hydraulic properties of the cement weir are periodically changed by employees of Lake Oswego Corporation in an attempt to regulate the water surface behind the dam. The water surface is elevated so that river water may be diverted into the Oswego canal (RM 6.7) without a pump. Regulation of the water surface behind the dam is achieved by placing "flashboards" on top of the cement weir. These "flashboards" are simply wooden boards, usually plywood in squares 4 feet wide, that are propped up to prevent water from flowing over part of the dam. If necessary, the entire width of the cement weir can be blocked with 47 of these "flashboards". The effective width of the cement weir, therefore, ranges from 0 to 188 feet. If the entire weir is blocked with "flashboards", water can flow over the top of any short "flashboards", if any are present. In this case, the broad-crested weir becomes a sharp-crested weir with a higher elevation and a restricted width. The base elevation of the cement weir is 100.5 feet above sea level. Changes in weir shape are manifested in the value of the weir coefficient. The hydraulic properties of the dam can also change if debris builds up behind it or on its crest. The time-varying dimensions and hydraulic characteristics of the cement weir are discussed in the *Calibration* section.

Nonpoint Inflows

CE-QUAL-W2 provides a mechanism to add water to the grid from a nonpoint (spatially distributed) source. In addition to providing a means of adding ground water to the river, this "distributed tributary" option can be used to account for the contributions of small, ungaged, point sources such as small tributaries, seeps, and tile drains. An exact quantification of the discharge from ungaged and nonpoint sources is, by definition, impossible. Estimates may be made, but such estimates usually prove to be inadequate. For example, it is known from measurements taken by USGS personnel that ground water discharges into the main stem of the Tualatin River during the low-flow summer months (Rounds and others, U.S. Geological Survey, unpub. data, 1993). These measurements of ground-water seepage showed slow, positive seepage amounting to roughly 2 ft^3/s in the model reach. The actual amount of ground-water discharge at a particular site, however, depends upon the hydraulic conductivity of the river bottom, a quantity that is spatially heterogeneous and poorly characterized. Even if the ground-water discharge were well characterized, the discharge of the many ungaged seeps, tile drains, and small tributaries would still be unknown, and would probably contribute much more water than the ground-water source. Therefore, the best method of estimating the total nonpoint contribution of water to the model reach is to simulate the discharge of the river without using a nonpoint source and compare that discharge to actual discharge measurements at the same site.

The best site to compare simulated and measured discharges to quantify the nonpoint source contribution is the downstream boundary of the model grid because it shows the effect of the distributed source on the entire model reach. The simulated flow past the Oswego diversion dam (RM 3.4) is easily compared to the continuously monitored discharge of the Tualatin River at RM 1.8 (West Linn). No significant tributaries or diversions are present on the river between RMs 3.4 and 1.8. This comparison of discharges and the resulting estimate of the nonpoint source of water to the model grid are discussed in the *Calibration* section. The measured discharge of the Tualatin River at RM 1.8 is documented by Doyle and Caldwell (1996).

The regional ground-water discharge for the entire model reach was assumed to be 2 ft^3/s, a rate that is consistent with a limited number of direct

measurements. If the total discharge from the distributed tributary was less than 2 ft^3/s at any time, then the entire amount was assumed to be regional ground water. If, on the other hand, the total discharge exceeded 2 ft^3/s at any time, then the balance of the water was assumed to come from a second source composed of small tributaries, seeps, and tile drains. Generally, the volume of nonpoint-source water decreased as the low-flow period progressed, but no clear seasonal functionality was apparent. The temperatures and water qualities of these two types of sources are discussed in the *Heat Flow* and *Water Quality* subsections of this *Boundary Conditions, Reaction Rates, and Forcing Functions* section.

Heat Flow

The source of the meteorological data and the methods used to estimate the light-extinction coefficients and the distributed-tributary temperature are discussed in this section.

Meteorology

Several meteorological parameters are required to drive the heat budget and the algal growth within CE-QUAL-W2. These parameters are (1) solar insolation, (2) air temperature, (3) dew-point temperature, (4) wind speed, (5) wind direction, (6) precipitation rate, and (7) precipitation temperature. Solar insolation data were collected hourly during the May through October months of 1991–93 using a Li-Cor LI-190SA quantum sensor mounted on top of one of the Durham WWTP buildings. This site is located near RM 9.3 and, therefore, provides insolation data that are fairly representative of the part of the model reach where most of the algal activity occurs. The raw data are documented by Doyle and Caldwell (1996). Daily values of dew-point temperature, wind speed, wind direction, rainfall amount, and minimum and maximum air temperature were obtained from the Agrimet weather station near Forest Grove, Oregon. This weather station, maintained by the TVID, is located on the valley floor and upstream of the model reach. These data are documented elsewhere (Doyle and Caldwell, 1996). Rainfall temperatures were estimated as the mean of the minimum and maximum air temperatures; almost any value, however, could have been used because the heat flux due to rainfall was insignificant in this summer period.

Quantum sensors measure solar insolation in terms of the number of photons in the 400 to 700 nm wavelength range that strike a unit horizontal area in a unit period of time. Light in this range of wavelengths is the energy source for photosynthesis and is called "photosynthetically active radiation" or PAR. Although a measurement of PAR is convenient when studying photosynthesis, the heat budget of the model requires solar insolation input from the entire spectrum of wavelengths, in units of energy rather than quanta. Morel and Smith (1974) studied the ratio of quanta to energy for PAR under a wide variety of solar angles and meteorological conditions; they found a mean quanta to energy ratio of 2.77×10^{18} quanta/sec/ Watt. The standard deviation of their measured ratio was only 0.58 percent, and no statistically significant differences in the ratio were found as a function of solar angle or cloud cover. The measured ratio of Morel and Smith (1974), therefore, was used to convert measurements of quanta flux into units of energy flux.

A relation between the solar energy flux in the 400 to 700 nm wavelength range and the corresponding energy flux of the entire solar spectrum (280 to 2800 nm) was obtained by comparing the response of a quantum sensor to that of a pyranometer. Side-by-side, hourly measurements of solar insolation by these two sensors (a Li-Cor LI-190SA quantum sensor and a Li-Cor LI-200SZ pyranometer) were obtained as part of another USGS study (Anderson and others, 1994). These data were measured at the Winston-Green WWTP on the South Umpqua River, Oregon, during 1991 and 1992. Using only the daytime measurements in the May through October periods, the following correlation was obtained:

$$E_{Full} = 2.342 E_{PAR} + 0.3 , \qquad (44)$$

where E_{Full} is the full-spectrum solar insolation in W/m^2 and E_{PAR} is the solar insolation in the 400 to 700 nm wavelength range, also in W/m^2. This correlation was performed with 2,185 data points and produced a correlation coefficient of 0.999. This relation was used to convert the hourly measurements of PAR at the Durham WWTP into hourly estimates of the full-spectrum energy flux.

CE-QUAL-W2 requires the air temperature in the heat transfer equations. Daily minimum and maximum air temperatures, however, were not sufficient. Because solar insolation data were available on an hourly basis, hourly air temperatures were estimated from the daily extremes. Assuming that the minimum and maximum air temperatures occurred at 5:30 a.m. and 3:30 p.m. each day, a simple sinusoidal curve was used to estimate hourly air temperatures (fig. 15).

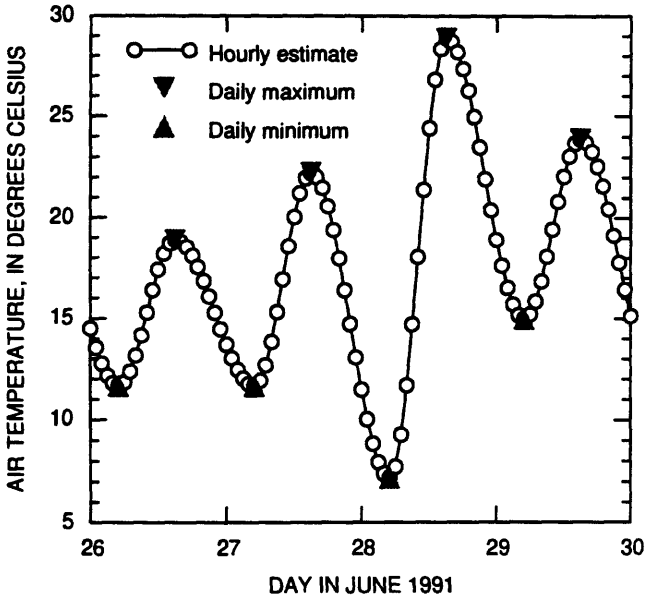

Figure 15. Example of the estimation of hourly air temperatures from a sinusoidal fit to daily minimum and maximum values.

Light Absorption

Vertical water-temperature variations are strongly affected by the absorption of solar energy. The conversion of light energy to heat energy is modeled with Beer's law (eq. 11), where the extinction coefficient is a function of the suspended solids and algal concentrations. The extinction coefficients associated with these constituents were estimated using a multiple linear regression of measured extinction coefficients against measured concentrations of total suspended solids (TSS) and chlorophyll-a. All data from RMs 26.9, 16.2, and 5.5 during 1991 and 1992 were combined in the regression. Algae and inorganic suspended solids are separate constituents in CE-QUAL-W2, but algal particles are included in measurements of TSS; therefore, biomass calculated from chlorophyll-a measurements was subtracted from TSS for the regression. The resulting regression model is:

$$\alpha_{tot} = \hat{\alpha}_{ss}\left(\Phi_{tss} - \frac{\sigma_{C:chla}}{\delta_C}\Phi_{chla}\right) + \hat{\alpha}_a\frac{\sigma_{C:chla}}{\delta_C}\Phi_{chla} + \hat{\alpha}_w, \quad (45)$$

where Φ_{tss} and Φ_{chla} are the measured concentrations of TSS and chlorophyll-a, $\sigma_{C:chla}$ is the ratio of carbon to chlorophyll-a in algal biomass (25 mg/mg), δ_C is the stoichiometric coefficient for carbon in organic matter (0.5 mg/mg), and the $\hat{\alpha}$ values are the statistical estimates of the extinction coefficients for suspended solids, algae, and water. The regression model produced an r^2 of 0.56, an $\hat{\alpha}_{ss}$ of 0.043 L/mg/m, an $\hat{\alpha}_a$ of 0.13 L/mg/m, and an $\hat{\alpha}_w$ of 1.002 m^{-1}. Extinction coefficients measured in the Tualatin River are typical of those measured in turbid, eutrophic lakes (Cole and Buchak, 1995).

A significant fraction of the incident solar radiation is absorbed at or near the surface of the river. That fraction, designated as β in equation 11, represents the light absorbed by organic material in the surface microlayer as well as much of the infrared and ultraviolet light that is easily absorbed by water. Light transmitted to greater depths is predominantly characterized by wavelengths in the 400 to 700 nm range. Literature values for β range from 0.4 to 0.75 (Eagleson, 1970). If only the 400 to 700 nm wavelength range of light were transmitted beyond the river surface, then β would be given by:

$$\beta \approx \frac{E_{Full} - E_{PAR}}{E_{Full}}. \quad (46)$$

Combining this result with equation 44, a value of 0.57 would be estimated for β. Because some infrared light is transmitted beyond the river surface, this estimate is probably too high, and β was chosen to be 0.53 for this application.

Nonpoint Inflows

The distributed tributary used in this application represents two sources of water to the Tualatin River. Regional ground water was assumed to provide a base flow of up to 2 ft^3/s; measurements of the temperature of that water showed a mean temperature of roughly 13.5°C. The balance of water in the distributed tributary was assumed to be due to ungaged tributaries, seeps, and tile drains. These sources are characterized by water temperatures that vary seasonally. On the basis of data from the small tributaries, the temperature of these sources was assumed to be 14°C on April 30 and October 27 and to vary sinusoidally in between, with a maximum temperature of 20°C. The temperature of the distributed tributary was calculated by combining the discharges from these two sources.

Water Quality

The Tualatin River and its tributaries have been sampled for various water-quality constituents

for many years, but a more extensive monitoring program was implemented in the spring of 1991 and continued through the fall of 1993. Sampling was concentrated during the 6-month period May 1 to October 31 of each year. A detailed description of the sampling methods and the analytical procedures used, and an electronic record of the data, has been published by Doyle and Caldwell (1996). Primary production data and phytoplankton and zooplankton abundances are also included in that report. For the purposes of this discussion, the data sets that provided boundary conditions, calibration data, and some of the parameters for the modelling effort are summarized in table 4.

Boundary Conditions

The upstream boundary and 10 tributaries that empty into the main stem were sampled approximately weekly for water-quality parameters (table 4). Several of the smaller tributaries were sampled less frequently or not at all in 1993 because the data from the previous 2 years indicated that their effect on overall budgets was negligible. WWTP effluent was sampled approximateLy twice weekly, with the exception of dissolved oxygen, which was measured daily.

Total phosphorus is not a compartment in CE-QUAL-W2; rather, it can be derived from the orthophosphate and organic-matter compartments in the model, using the appropriate stoichiometry. It was necessary, therefore, to establish a method for calculating the boundary conditions such that the total phosphorus entering the system was correct, according to the field measurements. In order to incorporate the total phosphorus data into the boundary conditions, the amount of detrital organic matter entering at the boundaries was calculated such that the total phosphorus at the boundaries matched the available data. This was done by calculating the phosphorus incorporated in algal biomass, and subtracting this and the orthophosphate concentration from the measured concentration of total phosphorus. The relationship between total phosphorus, chlorophyll-a, and orthophosphate measurements at the boundary is:

$$\Phi_{tot\text{-}P} = \delta_P\left(\Phi_{dt} + \frac{\sigma_{C:chla}}{\delta_C}\Phi_{chla}\right) + \Phi_P, \quad (47)$$

where $\Phi_{tot\text{-}P}$, Φ_{chla}, and Φ_P are the measured concentrations of total phosphorus, chlorophyll-a, and orthophosphate, respectively, and δ_P, δ_C, and $\sigma_{C:chla}$ are defined in table 5. Equation 47 was solved for the concentration of detrital organic matter at the boundary, Φ_{dt}. If the detrital organic-matter concentration calculated in this way was negative, it was set to zero.

Concentrations of water-quality parameters also had to be specified for the nonpoint-source input that accounts for ground water, ungaged tributaries, seeps and tile drains. This source is characterized by a single time-dependent concentration of each water-quality constituent in a manner analogous to that for a point source. The concentration and the discharge determine the total load of each constituent to the model reach; this load is then distributed evenly over the entire length of the model grid.

Because the nonpoint-source input accounts for both ground water and surface water, its concentration is determined by the mixing of two water types. The first water type is typical of ground water entering the system. Constituent concentrations in this water were set at 1.69 mg/L PO_4-P, 1.02 mg/L NH_3-N, 0 mg/L NO_3-N, 203 mg/L total dissolved solids, 4.3 mg/L chloride, and 0 mg/L dissolved oxygen. These concentrations were based on instream well data from RMs 36.8, 33.4, 27.0, and 20.8 obtained during the summer of 1993 (Doyle and Caldwell, 1996). The second water type, typical of surface water entering the system, was given concentrations of 0.10 mg/L PO_4-P, 0 mg/L NH_3-N, 0.1 mg/L NO_3-N, 181 mg/L total dissolved solids, 16.6 mg/L chloride, and dissolved oxygen at saturation, and is a composite of several of the smallest tributaries that were routinely sampled. The concentrations typifying small surface-water sources need not be very accurate because their small loads do not significantly affect the concentration in the receiving water. The concentrations typifying ground water are high enough, however, that the resultant load does contribute significantly to the nutrient budgets, particularly that of phosphorus. Most of the uncertainty in this groundwater load comes from uncertainty in the discharge, rather than the concentrations. Because the part of the nonpoint-source discharge attributed to ground water was known on the basis of seepage meter measurements (Rounds and others, U.S. Geological Survey, unpub. data, 1993) to be significant but highly variable, it was purposefully specified conservatively (never exceeding 2 ft^3/s, a small part of the total nonpoint-source discharge during most of the modeled period). Thus, by design, errors in the resultant load are more likely to underestimate than overestimate the contribution of the ground water to the nutrient budgets.

Table 4. Total number of samples collected, May–October of 1991–93, for water-quality constituents in the Tualatin River

[WWTP, wastewater-treatment plant; TKN, total Kjeldahl nitrogen; BOD, biochemical oxygen demand; —, no data; RM, river mile]

Constituent	River Mile																		
	38.4	38.1	38.1	36.8	35.7	31.9	31.6	28.2	28.2	26.9	23.2	16.2	15.2	15.2	11.6	9.3	9.3	8.7	7.5	5.5
	Rood Bridge	Rock Creek WWTP	Rock Creek (North)	Meriwether Golf Course	Butternut Creek [a]	Christensen Creek [b]	Burris Creek [b]	Baker Creek [b]	McFee Creek [b]	Scholls Bridge	QA site [b]	Elsner Road	Chicken Creek	Rock Creek (South) [b]	Highway 99W	Fanno Creek	Durham WWTP	Boones Ferry Road	Nyberg Creek [a]	Stafford Road
Chlorophyll-a	77	—	150	75	50	56	56	56	56	195	41	194	76	56	123	150	—	193	50	193
Phytoplankton abundances	—	—	—	—	—	—	—	—	—	38	—	49	—	—	—	—	—	—	—	54
Zooplankton abundances	—	—	—	—	—	—	—	—	—	37	—	40	—	—	—	—	—	—	—	43
Carbon uptake rate (assimilation number)	—	—	—	—	—	—	—	—	—	52	—	59	—	—	—	—	—	—	—	59
Water-column light intensity [d]	—	—	—	—	—	—	—	—	—	42	—	46	—	—	—	—	—	—	—	45
Algal settling velocities	—	—	—	—	—	—	—	—	—	—	—	59	—	—	—	—	—	—	—	61
Dissolved oxygen [e]	76	552	147	74	48	54	55	54	52	215	56	215	75	54	122	151	552	216	48	217
Total phosphorus	75	148	149	73	49	55	55	55	55	190	41	189	76	55	120	148	145	189	49	188
Soluble orthophosphate	77	151	153	75	50	56	56	55	56	195	42	194	77	56	124	151	148	194	50	194
Nitrate/nitrate	77	151	153	75	50	56	56	56	56	195	42	194	77	56	124	152	148	194	49	194
Ammonia	77	151	153	75	50	56	55	56	56	195	42	194	77	56	124	152	148	194	50	194
TKN	75	149	149	73	49	55	55	55	55	192	42	191	76	55	121	149	146	191	49	191
Total suspended solids	77	151	152	75	50	56	56	56	56	195	42	194	77	56	124	152	146	194	50	194
Total dissolved solids	77	151	150	75	50	56	56	56	56	195	42	194	77	56	124	150	146	194	50	194
Chloride	77	151	152	75	50	56	56	56	56	195	42	194	77	56	124	152	148	194	50	194
BOD [c]	—	(f)	71	—	—	—	—	—	—	49	—	25	—	—	—	71	(f)	—	—	56

[a] Data collected approximately weekly in 1991 and 1992; no data collected in 1993.

[b] Data collected approximately weekly in 1991 and 1992; data collected approximately monthly in 1993.

[c] Data collected at RM 26.9 and RM 5.5 in 1992 and 1993 only; at RM 16.2 in 1993 only.

[d] Data from 1991 and 1992 only; 1993 data collected but not used in this study.

[e] Sampling at RMs 26.9, 16.2, 11.6, 8.7, and 5.5 included a depth profile.

[f] Data available, but not used.

Table 5. Model parameters for the phytoplankton rate equation

[Type: l, from literature; c, calibration parameter; m, measured value. C, carbon; mg, milligrams; P, phosphorus; OM, organic matter; N, nitrogen; L, liter; W, Watts; m, meters; °C, degrees Celsius; m/day, meters per day]

Symbol	Description	Type	Value
K_{ag}	Maximum (light- and nutrient-saturated) algal growth rate at 20°C	c	4.5-6.0 day^{-1}
K_{am}	Maximum algal nonpredatory mortality rate	l	0.0 day^{-1}
K_{ae}	Maximum algal excretion rate	c	0.15 day^{-1}
K_{ar}	Maximum algal respiration rate	c	0.15 day^{-1}
$\sigma_{C:chla}$	Ratio of carbon to chlorophyll-a in algal biomass	m	25 mg C / mg chl-a
δ_C	Stoichiometric coefficient for carbon in OM (dry weight)	l	0.5 mg C / mg OM
δ_P	Stoichiometric coefficient of phosphorus in OM (dry weight)	l	0.011 mg P / mg OM
δ_N	Stoichiometric coefficient of nitrogen in OM (dry weight)	l	0.08 mg N / mg OM
h_N	Michaelis-Menten half-saturation constant for nitrogen limitation to algal growth	l	0.008 mg/L
h_P	Michaelis-Menten half-saturation constant for phosphorus limitation to algal growth	m	0.005 mg/L
I_S	Saturating light intensity for algal photosynthesis	m	177 W/m^2
α_w	Baseline light-extinction coefficient	m	1.002 m^{-1}
α_{ss}	Light extinction due to inorganic suspended solids	m	0.043 L/mg/m
α_a	Light extinction due to phytoplankton	m	0.13 L/mg/m
β	Fraction of incident light absorbed at water surface	m	0.53
ω_a	Algal settling velocity at 20°C	m	0.5 m/day
θ_a	Temperature-adjustment coefficient for algal processes	l	1.072

Initial Conditions

Initial conditions of water-quality compartments are not very important for this application because the model "self initializes" within one residence time, that is, the time for the boundary conditions at the upstream boundary to be transported through the model reach. The high spring flows that start the simulations each year guarantee that this will happen within a few days; therefore, the best means of initialization is to ignore the first few days of the simulation in each year.

The sediment compartment is an exception; initializing this compartment is important because it establishes the baseline SOD for the entire simulation. Measurements of SOD obtained from 1992 through 1994 were used to determine how the initialization should be done. The method used to obtain the SOD measurements is described by Caldwell and Doyle (1995) and by Rounds and Doyle (1997). These data are compiled in figure 16. The strategy of sampling at several locations, and both early and late in the season, was designed to capture any seasonal or spatial dependence in the SOD due to the growth and decline of large algal populations. There is no overall trend, although values at RM 5.5 do have a significantly higher median value than at the rest of the sites (Rounds and Doyle, 1997). This site is unusual, however, in that it is deeper than most other locations and bordered by shallow sills both upstream and downstream; therefore, the larger SOD rates observed at this site may not be representative of other locations in the model reach. Otherwise, no statistically significant seasonal or spatial dependence was found in these data; this result guided the approach to initializing the sediment compartment. It was concluded that the SOD in the Tualatin is determined primarily by a large accumulation of organic matter on the bottom of the river that decays slowly, is replenished somewhat by the settling of algal cells and detritus, and is not significantly depleted over a period of 6 months. A temporally consistent SOD is obtained in the model with a very slow decay rate such that only a small fraction of the organic matter in the sediments is depleted over the 6-month period of simulation. The sediment decay rate K_s was chosen such that approximately 10 percent of the sedimentary organic matter would be depleted in 6 months, or $K_s = 5 \times 10^{-4}$ day^{-1}. The initial sediment organic-matter content was then calculated using the equation:

$$O_{2\ demand} = K_s \delta_s \varphi_s^0, \qquad (48)$$

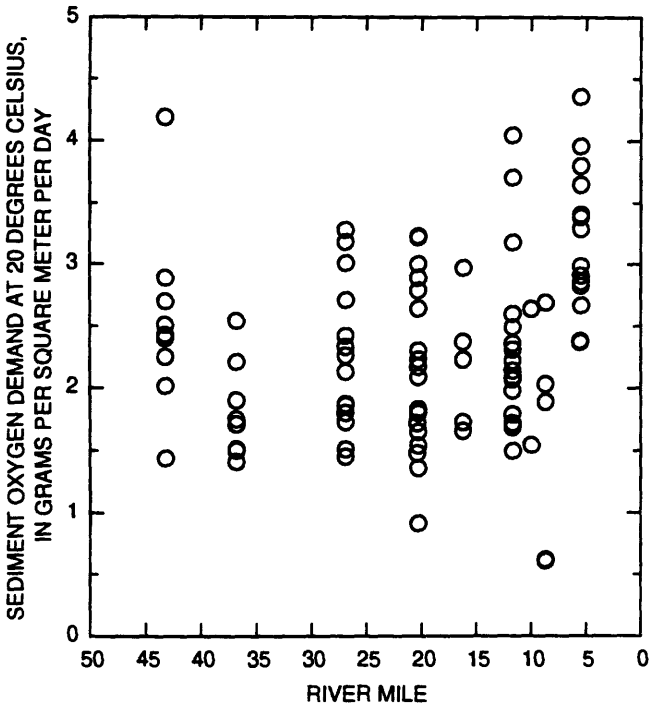

Figure 16. Sediment oxygen demand measured in the Tualatin River from 1992 through 1994, as a function of river mile.

where $O_{2\ demand}$ is the desired rate of SOD, φ_s^0 is the initial concentration of organic matter in the sediment (g/m^2), and δ_s is the oxygen stoichiometric coefficient for decay of sedimentary organic matter. The value of $O_{2\ demand}$ used was 1.8 g O_2/m^2/day. This value is somewhat lower than indicated by an appropriate statistic such as the median of all the data, which is 2.3 g O_2/m^2/day. A value on the low side was chosen as representative of the entire sediment surface area because the SOD measurements are representative of only the fraction of the sediment surface area soft enough to seat the measuring chambers. Some fraction of the bed sediment area is hard clay, into which the SOD chambers are not easily seated, and which probably exerts a lower oxygen demand. When averaged over the entire sediment surface area, therefore, the effective SOD should have a slightly lower value than indicated by the measurements.

Model Parameter Values

The model requires a set of input parameters to solve each of the rate equations presented in the *Algorithms* section. Each parameter must be measured either as part of the data collection effort, taken from the literature, or treated as a calibration parameter. Because the model requires many input parameters, it is not practical to treat all or even most of them as calibration parameters. The model parameters are summarized in tables 5–9, where each is designated as being calibrated (type "c"), measured (type "m") or taken from the literature (type "l"). The set of parameters that were treated as true calibration parameters and adjusted to give the best agreement between the modeled and observed concentrations was relatively small. These calibration parameters were the maximum algal growth rate (K_{ag}), the maximum algal excretion rate (K_{ae}), the maximum algal respiration rate (K_{ar}), the maximum zooplankton mortality rate (K_{zm}), the detrital settling velocity (ω_{dt}), and the fraction of sediment phosphorus that is unrecoverable (f_P). Experience simulating the Tualatin River with CE-QUAL-W2 indicated that these five parameters represent the minimum required degrees of freedom to calibrate the model for all of the water-quality constituents. In addition, the model is particularly sensitive to the values of these parameters, and each one governs an important step in the cycling of nutrients through the system. Calibrated values for the algae and zooplankton parameters were within literature ranges. These parameters are discussed in more detail in the *Calibration* section.

The remaining 38 water-quality parameters were assigned values and not varied as part of the calibration. Twelve of these were based on measurements made as part of the data collection effort. The literature, including other modeling applications, was relied on to provide values for the rest. Comprehensive lists of literature values provided by Bowie and others (1985) and the users manual for CE-QUAL-W2 (Cole and Buchak, 1995) were particularly useful. Estimates of a parameter in the literature often cover a large range, which casts some doubt on the reliability of any single value. Sensitivity results are not included in this discussion, but extensive experience with running the model and varying many parameters provided a basis for evaluating model sensitivity, and the uncertainty in the parameters taken from the literature is ameliorated somewhat by the fact that the model is, in general, not as sensitive to those parameters.

Table 5 summarizes the parameters required by the model to solve the rate equation for algal biomass, and the values used in the Tualatin River application. The model results are very sensitive to the choice of the maximum algal growth rate, and a single value for this parameter proved inadequate. Measurements of primary productivity were available, but these data do not constitute a direct measurement of K_{ag}.

Assimilation numbers (μg C/μg chl-a/hr) incorporate whatever environmental limitations to growth are present in the sample and, therefore, do not necessarily capture the theoretical maximum rate that is not limited by light or nutrients. They also depend directly on cellular composition, which is not concurrently measured and varies with species and cell size. Therefore, the primary productivity data were used as a rough guide to the probable seasonality in K_{ag}, and to set reasonable limits on its value, but K_{ag} was treated as a calibration parameter. Bowie and others (1985) report K_{ag} values from 0.6 to 5 day^{-1} for diatoms, which dominate the Tualatin River assemblage. The range of K_{ag} used in the Tualatin River simulations is 4.5 to 6 day^{-1}, which is at the high end of values reported in the literature, but well within the range indicated by the measured assimilation data and the measured cellular carbon:chlorophyll-a ratio. The seasonality of K_{ag} is discussed in detail in the *Calibration* section.

Nutrient limitation of the algal growth rate is determined by Michaelis-Menten kinetics as described in the *Model Description* section, which requires the specification of the half-saturation constants h_P and h_N. The half-saturation constant for nitrogen limitation h_N (0.008 mg/L) is within the range of literature values but does not play an important role in this application because nitrogen concentrations almost never reach limiting levels. The half-saturation constant for phosphorus limitation h_P (0.005 mg/L) is representative of values measured for the Tualatin River (U.S. Geological Survey, unpub. data, 1993).

In some models, the use of a Michaelis-Menten-type nutrient limitation based on extracellular nutrient concentrations has been replaced with a set of equations that decouples nutrient *uptake* from nutrient *assimilation* (Collins, 1980; Cunningham, 1996; Fernández and others, 1997). In these "variable stoichiometry" models, extracellular and intracellular concentrations of the nutrient are calculated separately. Nutrient uptake is faster than nutrient assimilation and is dependent on both external and internal nutrient concentrations, whereas the slower rate of assimilation is dependent only on internal nutrient concentrations.

The most important consequence of the decoupling of the uptake and growth processes is that "luxury" uptake is enabled; that is, the algae can take up a nutrient when it is in excess and store it for use at a later time when the same nutrient is in short supply. The practical effect of luxury uptake is to create a time lag between the apparent depletion of a nutrient and the effect of the depletion on growth, as nutrients are first depleted externally by the more rapid uptake step, and then depleted internally by the slower assimilation step. This time lag is most important when changes in the nutrient supply are "abrupt," and least important when changes in the nutrient supply are "gradual," where "abrupt" and "gradual" are measured relative to the time scale of algal growth.

DiToro and Connolly (1980) have shown formally that the Michaelis-Menten formulation closely approximates the variable stoichiometry formulation under conditions approaching steady state, that is, as long as the nutrient concentration is fairly steady over the time scale of algal growth. Because the variable stoichiometry formulation requires two more parameters than the Michaelis-Menten formulation in CE-QUAL-W2 in order to describe the additional assimilation step, its use should be carefully justified. Both formulations are in reality empirical descriptors of observed data, and the requirement of parsimony dictates that the best descriptor is that which provides an adequate description of the observations with the least number of unknown parameters.

In the Tualatin River application, the possibility of luxury uptake of nutrients in the upper river, to be used to supplement growth in the lower river, was considered. Changes in the nutrient supply to the algae as water moves downstream are gradual, however, and it is unlikely that the added complexity of the variable stoichiometry formulation is justified. The Michaelis-Menten formulation should provide an adequate description of the dependence of growth on nutrient concentration, provided the half-saturation constants are appropriate; therefore, the original formulation was retained.

The stoichiometry of the algal cells is determined by the parameters δ_C, δ_P, and δ_N. Of these, the carbon fraction of the cell is the least variable. The values given by Bowie and others (1985) for diatoms range from a low of 0.4 to a high of 0.53; values listed by Reynolds (1984) range from a minimum of 0.47 to a maximum of 0.56. The value of δ_C used in this application, 0.5, is in the middle of the reported range. Fractions of phosphorus and nitrogen are more variable. Bowie and others (1985) give ranges from 0.027 to 0.072 and from 0.004 to 0.02 for nitrogen and phosphorus in diatoms, respectively. Reynolds (1984) lists values from 0.033 to 0.104 for nitrogen and from 0.0003 to 0.029 for phosphorus. Although the values used in this application ($\delta_N = 0.08$ and $\delta_P = 0.011$) are

well within the documented range, they are at the high end. A minimum cell quota of these nutrients is required for the cell to be viable, but uptake of nutrients in excess of the immediate requirements for growth can result in a cell quota many times the minimum; the extremes that are possible in the cell quota are reflected in the wide range reported for the nutrient content of algal cells. The stoichiometric coefficients chosen for this application are typical, therefore, of cells that have been growing in an environment where nutrients are generally in excess of growth requirements. Aside from some ephemeral limitation by phosphorus at the surface of the water column, this is believed to be the case in the Tualatin River upstream of RM 5.5. Below RM 5.5, the model indicates that phosphorus limitation may be more severe, and perhaps cells synthesized under these conditions should be characterized by a lower value of δ_P. Model results between RMs 5.5 and 3.4 are speculative, however, because no observations are available for comparison.

The conversion between chlorophyll-a and biomass requires the specification of the carbon to chlorophyll-a ratio in the cells. CE-QUAL-W2 does not actually use this parameter, but it is required for the conversion between chlorophyll-a measurements made in the river and the dry weight biomass units used to describe the algae in the model (e.g., eq. 47). Literature estimates span a wide range. Values compiled by Bowie and others (1985) range from 10 to 112 for total phytoplankton and from 18 to 500 for diatoms. Using a δ_C of 0.5, estimates of $\sigma_{C:chla}$ can be calculated from the values of dry weight and chlorophyll-a per cell compiled by Reynolds (1984), giving a range from 12.5 to 91 for diatoms. The value used in this application, $\sigma_{C:chla} = 25$, is based on measurements made from Tualatin River samples (U.S. Geological Survey, unpub. data, 1993).

The loss rates due to nonpredatory mortality, excretion, and respiration were not measured directly. In some models, nonpredatory mortality losses are a function of bacterial populations or the physiological condition of the cells, but in this version of CE-QUAL-W2 the nonpredatory mortality term behaves exactly as does the respiration term. (This version of the code employs a van't Hoff (Q_{10}) temperature dependence for all reactions, whereas the USACE version employs a different temperature dependence for respiration and mortality, thus necessitating that the two be treated separately in that version.) For this reason, nothing is gained by treating mortality as a separate process, and the sum of the respiration and excretion terms should be interpreted to represent all of the losses not covered explicitly by the settling and grazing terms. This composite loss term depends on two rates, the maximum respiration rate K_{ar} and the maximum excretion rate K_{ae}, that are treated as calibration parameters. K_{ar} determines the rate at which nutrients incorporated into algal cells are cycled directly to the inorganic nutrient pool by respiration. K_{ae} determines the rate at which nutrients are sent to the dissolved organic-matter compartment by excretion, after which they are cycled to the nutrient pool by bacterially mediated decay. These two rates were calibrated such that the oxygen demand generated by respiration is generally between one and two times that generated by the bacterial decomposition of excreted organic matter; that is, the two pathways are comparable in terms of their effects on the dissolved oxygen. This choice is somewhat arbitrary, but reflects the belief that the dissolved organic-matter compartment should be large enough to support significant heterotrophic activity, but not large enough to exert more oxygen demand than respiration. The *sum* of the two rates, however, is the real calibration parameter, which is adjusted to achieve good agreement with observations. The rate of this composite loss term has an upper limit of 0.3 day^{-1} (K_{ar} and K_{ae} are both equal to 0.15 day^{-1}), or 5 percent of the maximum algal growth rate of 6 day^{-1} (6.7 percent when K_{ag} is at its minimum value, 4.5 day^{-1}). As a percentage of maximum primary productivity this represents the low end of estimates of total respiration.

The phytoplankton rate equation also requires several parameters that determine how the algal growth is affected by light intensity and how light intensity decreases with depth. Productivity vs. irradiance curves provided an estimate of the saturating light intensity for photosynthesis, by fitting the data to the hyperbolic tangent function of Jassby and Platt (1976) (see the *Model Description* section). The fitting parameters of this function are α, the slope of the light-saturation curve at low light intensities, and P_m^B, the light-saturated photosynthetic rate. The saturating light intensity can be written in terms of these two parameters as $I_s = 2.718\ P_m^B/\alpha$. The remaining light parameters determine the availability of PAR with depth in the water column. The extinction coefficients α_w, α_{ss}, and $t\alpha_a$, and the fraction of incident light adsorbed at the surface, β, are discussed previously see equation 45 on page 29.

Algal settling velocities were determined using the technique described by Bienfang and others (1982) in the laboratory at 20°C and in the presence of light (U.S. Geological Survey, unpub. data, 1993). The measurements of settling velocity varied a great deal, but without an obvious pattern. The entire data set (2 stations over 3 years) had a mean of 0.4 m/day and a standard deviation of 0.2 m/day. The value used in the calibration, ω_a = 0.5 m/day, was an early estimate based on the mean of only 1992 data, and is well within the range indicated by the entire data set.

The remaining parameter required for the algal rate equation is defined by the Q_{10} value for algal processes. The value used, $(Q_{10}^{0.1}) = \theta_a = 1.072$, represents a doubling of the growth rate for every 10°C increase in temperature and is a common choice for biological reactions. The range given by Reynolds (1984) for Q_{10} is between 2 and 2.3 for temperatures between 2 and 25°C.

No measurements of zooplankton parameters were available, so literature values were used for most of these parameters (table 6). Measurements of zooplankton abundances, however, were available. These data indicated that zooplankton biomass varied greatly over the three calibration seasons, reaching values an order of magnitude higher in 1991 than in 1992 or 1993. This difference can probably be attributed to increased planktivory by fish in the latter 2 years (U.S. Geological Survey, unpub. data, 1993). For this reason, the zooplankton predatory and nonpredatory mortality rate, K_{zm}, is left as a calibration parameter and is allowed to vary between years as described in the *Calibration* section.

For simplicity, the rest of the zooplankton parameters were taken from a modeling study of Lake Ontario by Scavia (1980). They are all within the ranges compiled by Bowie and others (1985), but the range for the grazing rate, K_{zg}, is particularly large. Cladocerans (*Daphnia sp.*) dominate the zooplankton assemblage in the lower river during the period in 1991 when grazing is an important loss term. The range of K_{zg} values compiled by Bowie and others (1985) for cladocerans is 0.045 to 13.8 day^{-1}; the range for total zooplankton is smaller, from 0.24 to 1.2 day^{-1}. Maximum growth rates, which are defined as the maximum grazing rate times the grazing efficiency, are also compiled by Bowie and others (1985). The range in maximum growth rate is from 0.35 to 0.74 day^{-1} for cladocerans, which compares favorably with the value $K_{zg}e_{zg}$ = 0.9 day^{-1} that is used in this application.

The rate of decay of labile organic material (table 7) is rapid because it represents the cycling of easily decomposed organic compounds. Cole and Buchak (1995) list values between 0.2 and 0.6 day^{-1} for several specific compounds; the value K_{lom} = 0.5 day^{-1} was a reasonable choice for dissolved organic matter comprised of many different compounds. The detritus decay rate, K_{dt} = 0.046 day^{-1}, is based on measurements of biochemical oxyden demand (BOD) rates from river samples at several times during 1991 and 1992 (Doyle and Caldwell, 1996). Decay rates were calculated using Lee's method (Velz, 1984). The range in decay constants calculated from the BOD data was not large. Since nitrogenous BOD contributed little to the overall BOD, it was reasonable to use the experimentally determined BOD decay rates to represent the decomposition rate of the detritus compartment in the model. Each of the reactions corresponding to the decay of organic matter has the same temperature-adjustment coefficient, θ = 1.065 (Thomann and Mueller, 1987).

Table 6. Model parameters for zooplankton rate equation
[Type: l, from literature; c, calibration parameter. mg/L, milligrams per liter]

Symbol	Description	Type	Value
K_{zg}	Maximum zooplankton grazing rate	l	1.8 day^{-1}
K_{zm}	Maximum zooplankton mortality rate	c	0.05–0.5 day^{-1}
K_{zr}	Maximum zooplankton respiration rate	l	0.1 day^{-1}
p_a	Preference for algae as food	l	1.0
p_{dt}	Preference for detritus as food	l	0.16
θ_z	Temperature-adjustment coefficient for zooplankton processes	l	1.072
e_{zg}	Efficiency of zooplankton grazing	l	0.5
μ_z	Threshold food concentration for zooplankton grazing	l	0.02 mg/L
h_{zg}	Half-saturation constant for zooplankton grazing	l	0.2 mg/L

Table 7. Model parameters for the detritus, labile organic matter, and bottom-sediment compartments
[Type: l, from literature; c, calibration parameter; m, measured value. g, grams; OM, organic matter; m^2, square meters; m/day, meters per day]

Symbol	Description	Type	Value
K_{lom}	Maximum labile decay rate	l	0.5 day^{-1}
K_{dt}	Maximum detritus decay rate	m	0.046 day^{-1}
K_s	Maximum sediment decay rate	m	0.0005 day^{-1}
θ_{lom}	Temperature-adjustment coefficient for labile decay	l	1.065
θ_{dt}	Temperature-adjustment coefficient for detritus decay	l	1.065
θ_s	Temperature-adjustment coefficient for sediment decay	l	1.065
φ_s^0	Initial concentration of sediment compartment	m	2570 g OM/m^2
ω_{dt}	Detrital settling velocity	c	0.0 m/day

Most of the parameters involved in the cycling of nutrients have already been discussed in the context of the rate equations for the organic-matter compartments, but three additional parameters are needed to complete the cycling of nitrogen and phosphorus (table 8). The nitrification rate is based on measurements of ammonia and nitrate at RMs 8.7 and 5.5 over the time period September 15 to 18, 1993, when the instream ammonia concentration was greater than 2 mg/L and the chlorophyll-a concentration was less than 10 µg/L. Eight samples were collected over a 2-day period at RM 8.7, and 11 samples were collected over a 3-day period at RM 5.5. An estimate of the travel time between these two sites (about 19 hours) was used to calculate the losses of ammonia to nitrification in this short reach of the river below the Durham WWTP, and the corresponding nitrification rate. The nitrification rate $K_{NH_3} = 0.023$ day^{-1} is an average of the resulting estimated rates. At this low rate, the oxygen demand created by nitrification is a very small factor in the overall dissolved oxygen budget. Nitrification can be important in an aerobic system if the concentrations of ammonia are high enough. In the Tualatin River, this is not usually the case in the summertime, although it was common before the WWTPs were upgraded. The temperature correction factor used, $\theta_{NH_3} = 1.047$, is typical of many biologically mediated reactions (Bowie and others, 1985).

Analysis of data collected after this model calibration was completed, for a period in the summer of 1995 when the Rock Creek WWTP was releasing abnormally large ammonia loads, indicated that a better estimate of the nitrification rate in the reach between RMs 38.1 and 16.2 was 0.11 day^{-1}. A change in the nitrification rate for the calibration conditions used in this study, however, would not translate to a significant change in the model results because the calibration conditions rarely included periods of any significant ammonia concentrations.

The final parameter required to complete the cycling of phosphorus is the fraction of phosphorus that is not released to the water column when organic matter in the sediments decays, f_P. This calibration parameter can have several different interpretations. Perhaps the most obvious is that it accounts for phosphorus that is sorbed to ferric oxyhydroxides or taken up by the sediment microbial population. This parameter is discussed in further detail in the *Calibration* section.

The remaining coefficients (table 9) specify the amount of oxygen produced by photosynthesis and

Table 8. Model parameters for the nutrient rate equations
[Type: m, measured value; l, from literature; c, calibration parameter. P, phosphorus]

Symbol	Description	Type	Value
K_{NH_3}	Maximum nitrification rate	m	0.023 day^{-1}
θ_{NH_3}	Temperature-adjustment coefficient for nitrification	l	1.047
f_P	Fraction of sediment P that is unrecoverable	c	0.9

Table 9. Oxygen stoichiometric coefficients
[Type: l, from literature. mg, milligrams; O, oxygen; N, nitrogen; OM, organic matter]

Symbol	Description	Type	Value
δ_{NH_3}	Oxygen stoichiometric coefficient for nitrification	l	4.33 mg O_2 / mg N
δ_{dt}	Oxygen stoichiometric coefficient for detritus decay	l	1.4 mg O_2 / mg OM
δ_s	Oxygen stoichiometric coefficient for bottom-sediment decay	l	1.4 mg O_2 / mg OM
δ_{lom}	Oxygen stoichiometric coefficient for dissolved OM decay	l	1.4 mg O_2 / mg OM
δ_{ag}	Oxygen stoichiometric coefficient for photosynthesis	l	1.4 mg O_2 / mg biomass
δ_{ar}	Oxygen stoichiometric coefficient for algal respiration	l	1.1 mg O_2 / mg biomass
δ_{zr}	Oxygen stoichiometric coefficient for zooplankton respiration	l	1.1 mg O_2 / mg biomass

consumed by the decay, respiration, and oxidation reactions previously discussed. Each of these stoichiometric coefficients was set at the value suggested by Cole and Buchak (1995), with the exception of δ_{NH_3}, which is reduced to 4.33 as suggested by Bowie and others (1985) from the value 4.57 that is indicated by the stoichiometry of the reactions.

CALIBRATION

The model was calibrated using data obtained during the May through October period of 1991, 1992, and 1993. These 3 summers had a wide range of hydrologic conditions, from dry in 1992 to wet in 1993. Because the water quality of the Tualatin River is closely coupled to its discharge, the summers of 1991–93 also had a wide range of water-quality conditions. The precipitation normally observed during May and June was absent in 1992, resulting in a lower-than-normal Tualatin River discharge during the early summer (table 10). Dry conditions persisted throughout the summer of 1992; daily mean flows were consistently lower than in the other 2 years. Characteristics of a wet year were observed in 1993, when high flows persisted until late June. The remaining year in this data set, 1991, was characterized by conditions between the other two; flows remained high until mid-June of 1991. The wide range of flow and water-quality conditions observed during the summers of 1991, 1992, and 1993 allows a very robust model of the Tualatin River to be created when all three of the May through October data sets are used for calibration. No part of these data sets was reserved for a separate verification. Because the model was calibrated with all available data, the resulting calibration parameters represent the best fit of the model to the entire range of observed conditions. Only two calibration parameters were allowed to vary seasonally or between years; therefore, the calibrated model is able to simulate a wide variety of conditions without a recalibration. Because the model can simulate a wide range of hydrologic and water-quality conditions with few, if any, changes to its calibration parameters, it also can be used predictively under a wide range of hypothetical conditions that are not too dissimilar from those of the calibration.

In this section, the calibration of CE-QUAL-W2 for the summers of 1991, 1992, and 1993 is presented. The model calibration is discussed in the same order it was performed: hydraulics, then water temperature, then water quality.

Hydraulics

Calibration of the water budget for the Tualatin River requires consideration of both the discharge of the river and its volume. These quantities are not independent, because a change in the water-surface elevation, and therefore the volume, of any part of the river will directly affect the discharge. This dependence is a complicating factor because the water-surface elevation of much of the modeled reach, during periods of low flow, is controlled mainly by the configuration of the Oswego diversion dam, situated at the downstream boundary of the model grid (RM 3.4). Therefore, when the dam configuration is static, the discharge of the reach near that dam is dominated by its upstream discharge and any intersecting boundary flows.

Table 10. Mean daily discharge in the Tualatin River at two sites, by month, for the summers of 1991–93
[ft^3/s, cubic feet per second]

Month	Tualatin River Discharge at river mile 33.3 (Farmington) (ft^3/s)			Tualatin River discharge at river mile 1.8 (West Linn) (ft^3/s)		
	1991	1992	1993	1991	1992	1993
May	636	374	1,041	751	444	1,280
June	302	160	558	366	147	686
July	189	152	222	237	118	229
August	181	138	161	156	90	145
September	171	127	218	141	112	202
October	180	151	199	189	142	173

When the dam configuration is changed, however, the discharge is determined in large part by the rate of change of the water-surface elevation behind the dam. Even if both the discharge and elevation are correctly simulated, an incorrect representation of the bathymetry will cause errors in simulated transport times. Calibration of the Tualatin River hydraulics, therefore, requires accurate bathymetric data, an account of the inputs and withdrawals of water to the RM 38.4 to RM 3.4 reach, travel-time data, and an accurate representation of the time-varying Oswego diversion dam configuration.

All of the withdrawals and all but one of the inputs of water to the Tualatin River between RM 38.4 (Rood Bridge) and RM 3.4 (the Oswego diversion dam) were either measured directly or estimated for the May through October period of 1991, 1992, and 1993. As described in the *Boundary Conditions, Reaction Rates, and Forcing Functions* section, and illustrated in figure 13, this model includes the surface-water inputs of two large tributaries (Rock [North] and Fanno Creeks), eight small tributaries (Butternut, Christensen, Burris, McFee, Baker, Chicken, Rock [South], and Nyberg Creeks), two WWTPs (Rock Creek and Durham), and the upstream boundary at RM 38.4. One major diversion (the Oswego canal at RM 6.7) is included; seven smaller withdrawals represent grouped estimates of irrigation demand. Measured precipitation rates are imposed via a time-varying boundary condition. Evaporation losses and the discharge at the downstream boundary are calculated within the model. The final piece of the water budget is a nonpoint source (the model's *distributed tributary*) that accounts for discharge from ground water, ungaged tributaries, seeps, and tile drains. The nature of the nonpoint source makes it impossible to measure directly; therefore, it was estimated by subtracting the simulated discharge of the river at the Oswego diversion dam (RM 3.4) from the measured discharge at the West Linn gage (RM 1.8). No significant sources or sinks of water are located between these two sites.

Defining the nonpoint discharge rate as the difference between the simulated (RM 3.4) and measured (RM 1.8) rates is probably the best way to balance the water budget; this method, however, generates two time-shift errors. The most obvious time shift is incurred because the measured flow is 1.6 miles and some number of hours downstream of the dam. The second time shift results from the fact that the total nonpoint discharge is calculated at the downstream boundary, but the model distributes the discharge evenly over the length of the entire modeled reach. Therefore, most of the water is added far upstream of the dam and its effect on the discharge at the dam is lagged by its travel time to the dam. If the nonpoint discharge rate varies over time, then a time lag will be observed when the distributed tributary is included in the model and the simulated (RM 3.4) and measured (RM 1.8) discharges are compared again. Fortunately, the errors incurred by these time shifts are generally small and acceptable.

Another inherent complexity in defining the nonpoint discharge, more important than the time shifts, derives from the fact that the simulated discharge past the Oswego diversion dam is a function of the dam's time-varying physical dimensions and hydraulic characteristics. These parameters vary because the water-surface elevation of the Tualatin River upstream of the dam is managed by

Lake Oswego Corporation personnel; in response to changes in flow conditions, the effective width and height of the 188-foot long cement weir of the Oswego diversion dam are controlled through the placement of flashboards on top of the weir. Although it was generally known how many flashboards were being used at any one time during 1991–93, that information was not enough to simulate sufficiently accurate water levels just upstream of the dam; therefore, the width and discharge coefficient of the broad cement weir were treated as calibration parameters. When flashboards are installed or removed, the discharge past the dam changes as water is either captured or released from storage. To minimize the inclusion of these dam-configuration-derived discharge variations in the estimate of the nonpoint discharge, two extra steps were included in the estimation process. First, the dimensions and hydraulic characteristics of the dam were calibrated initially so that the model roughly simulated the measured water-surface elevation upstream of the dam. Because the dam-configuration changes were included in the initial simulation, few of the resulting discharge variations were transferred into the nonpoint discharge estimate. Second, the nonpoint discharge rate determined by subtracting the simulated (RM 3.4) from the measured (RM 1.8) discharge was smoothed, eliminating still more of the dam-configuration and time-shift effects (fig. 17).

After the nonpoint source of water was estimated and included in the Tualatin River water budget, the physical dimensions and hydraulic characteristics of the Oswego diversion dam were recalibrated so that the model would properly simulate the measured water-surface elevation upstream of the dam. The dimensions and hydraulic parameters of the fish ladder and the submerged pipe remained constant (table 3). The effective width, elevation, and discharge coefficient of the broad cement weir, however, were

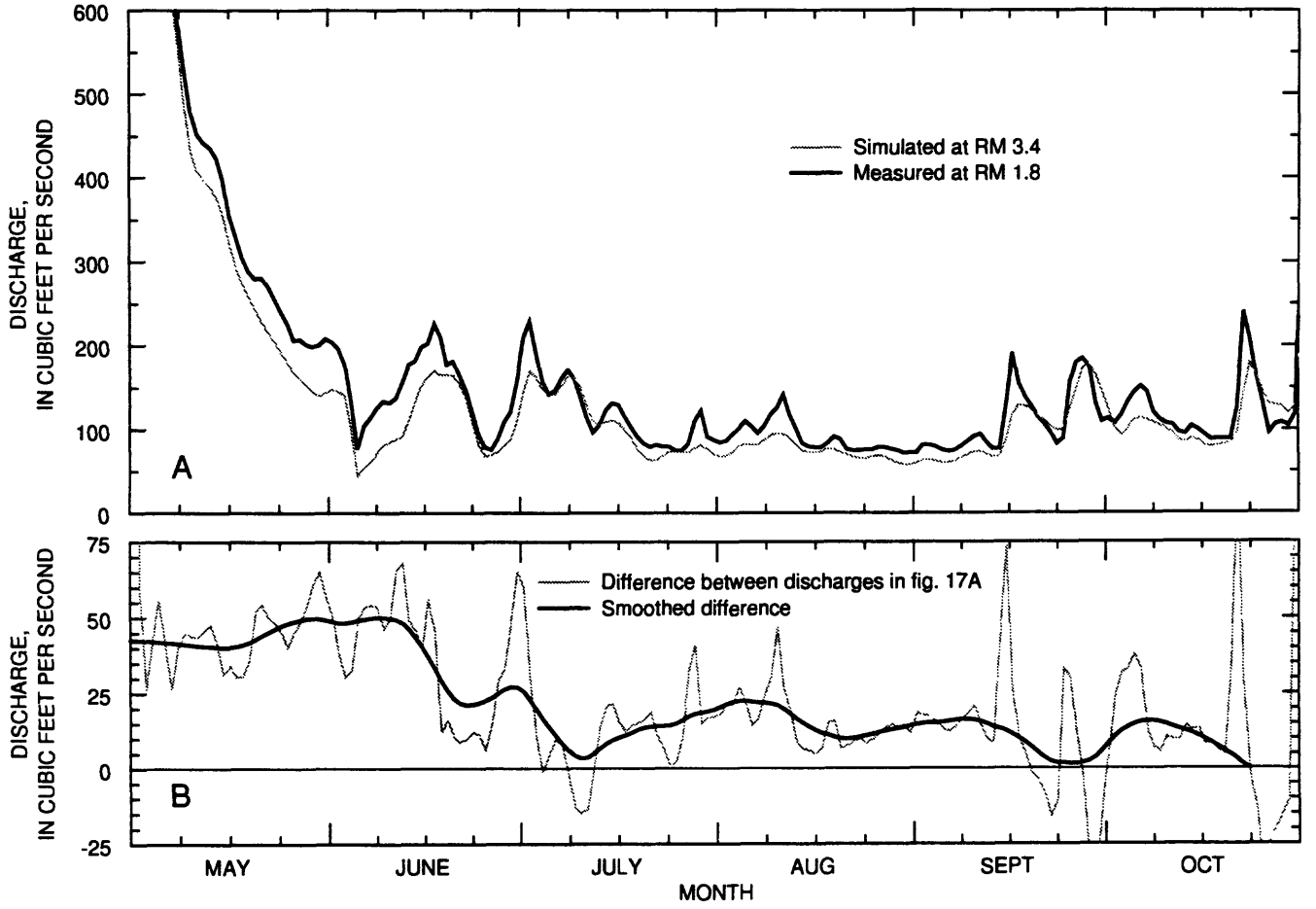

Figure 17. Estimation of the nonpoint discharge for 1992. (A) Comparison between measured and simulated downstream discharge before adding any nonpoint discharge and (B) the smoothed difference that is used as the nonpoint discharge estimate. (RM, river mile)

treated as calibration parameters. Even when detailed configuration notes were taken (in 1993), the observed width and theoretical discharge coefficient of the cement weir did not result in an acceptable simulation of the water-surface elevation upstream of the dam. Of course, the fish ladder and the cement weir are not perfect weirs. The equations that the model uses to simulate the discharge past these structures, therefore, cannot be expected to provide acceptable results without some calibration.

The elevation of the broad cement weir was held constant during calibration of the water-surface elevation upstream of the Oswego diversion dam. Dr. Scott Wells' research group at Portland State University measured that elevation to be 100.5 feet above sea level. The measured elevation was used at all times except for the period June 3 to October 25 of 1992, when the entire cement weir was blocked by flashboards. Several of the boards used in 1992 were only 10 inches high. Installing all of the boards, therefore, raised the base elevation to 101.3 feet above sea level.

Calibration of the discharge coefficient and the effective width of the broad cement weir was started by using all available information regarding the actual configuration of that structure. When flashboards were installed or removed, the effective width was decreased or increased, respectively. When debris accumulated on the structure, the discharge coefficient was decreased. Technically, specification of both the discharge coefficient and the effective width was unnecessary; their product was the real calibration parameter (eq. 3). Nevertheless, both parameters were specified because they each have a physical basis. In 1991, the calibrated width ranged between 2.8 and 188 feet; the discharge coefficient ranged from 0.60 to 1.15. In 1992, the ranges were 1.1 to 188 feet for the width and 0.60 to 1.15 for the discharge coefficient. The ranges in 1993 were 8.2 to 188 feet and 0.42 to 1.15 for the width and discharge coefficient, respectively.

The calibrated discharges and water-surface elevations compare favorably to the observed discharges and elevations (fig. 18 and fig. 19, respectively). When the flashboards were installed or removed all at once, the effect on the water-surface elevation was significant. In 1992, for example, all of the flashboards were raised on June 3, causing a marked increase in the elevation and a temporary decrease in the discharge. Similar effects were observed on July 23, 1991. The flashboards were installed a few at a time over a longer period in 1993; the resulting increase in elevation was less noticeable. When the flashboards were removed for repair and then reinstalled at the end of September of 1993, however, an abrupt decrease and subsequent increase in water-surface elevation occurred.

Although the calibrated water-surface elevation at RM 6.7 closely tracks the observed elevation, matching the water-surface elevation at that location does not guarantee an accurate simulation of the river volume. The model's bathymetric representation of the Tualatin River *should* be adequate because a large amount of bathymetric data was used in the creation of the model grid. Nevertheless, once the water budget had been balanced, the model's representation of the river volume was checked by testing its ability to simulate the time required for a water parcel to traverse a particular reach. These travel times are commonly measured with dye tracer tests; many such tests have been performed in the Tualatin River (Lee, 1995; Janice Miller, Unified Sewerage Agency of Washington County, written commun., 1995). Tracer tests were performed by USA in the 1980s; those tests measured travel times in many reaches from RM 55.3 to RM 5.5 under a wide range of flow conditions. The model is not calibrated for any year in the 1980s; however, these older travel times can be compared to simulated travel times for the 1991–93 period because the channel has not changed appreciably. Simulated travel times in 1991, 1992, and 1993 were found by modeling hypothetical dye clouds. The movements of thirty-five 10-minute injections of a tracer at the upstream boundary were tracked during the May through October period of each year. Travel times between certain stations were calculated by comparing the times at which the centroid of each tracer cloud passed those stations. Travel times are a strong function of the discharge in each reach.

A comparison of the simulated and measured travel times for various reaches of the Tualatin River shows that the model provides a realistic representation of the river volume. The 1980s tracer experiments relied on discharge measurements at established gages. The travel time between RM 26.9 (Scholls Bridge) and RM 16.2 (Elsner Road), therefore, was measured as a function of the average discharge at the nearest gage (RM 33.3, Farmington Road).

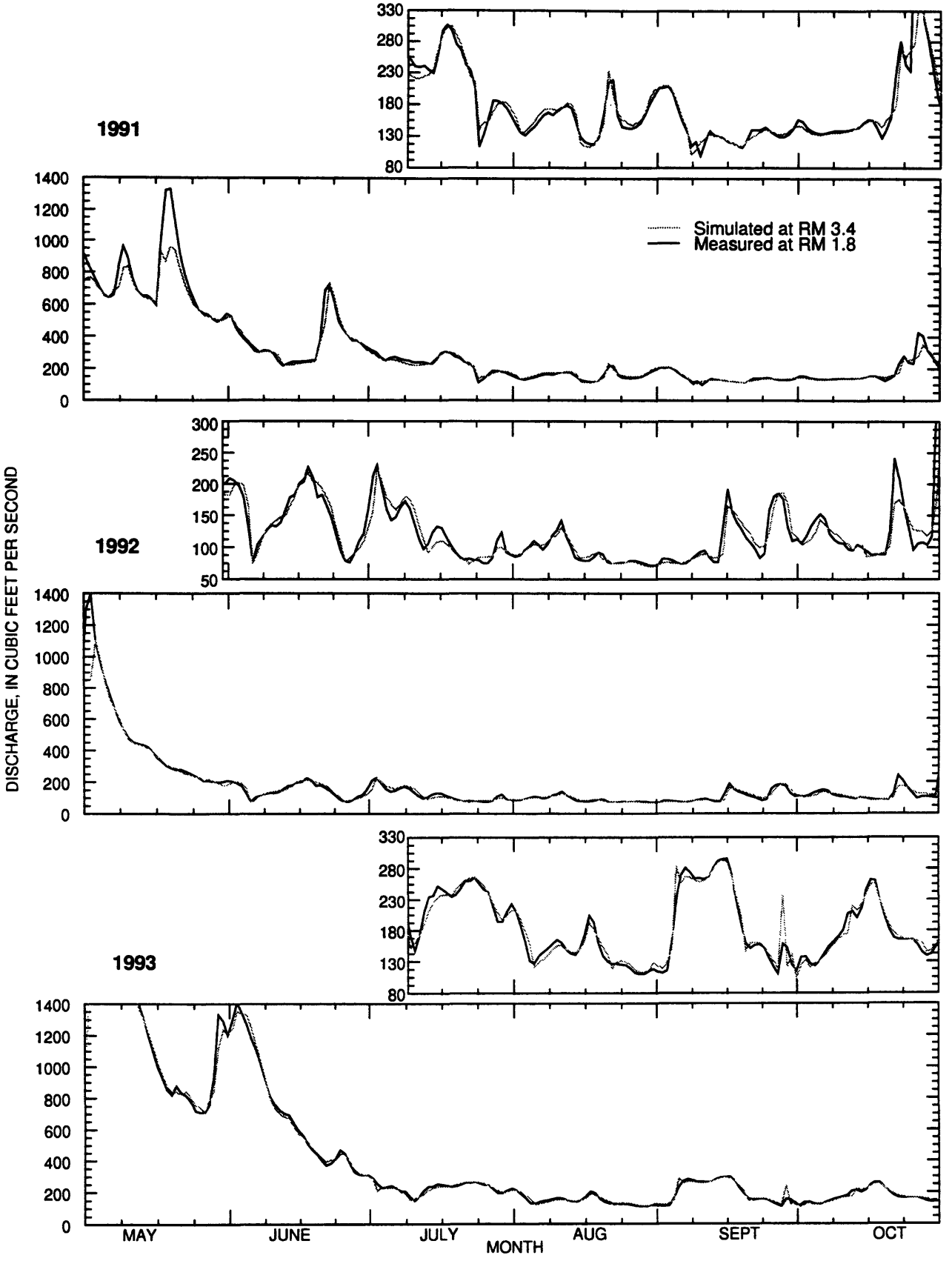

Figure 18. The calibrated Tualatin River discharge at river mile 3.4 (Oswego diversion dam) and the measured discharge at river mile 1.8 (West Linn) for May–October of 1991–93. (Smaller hydrograph is vertically exaggerated.)

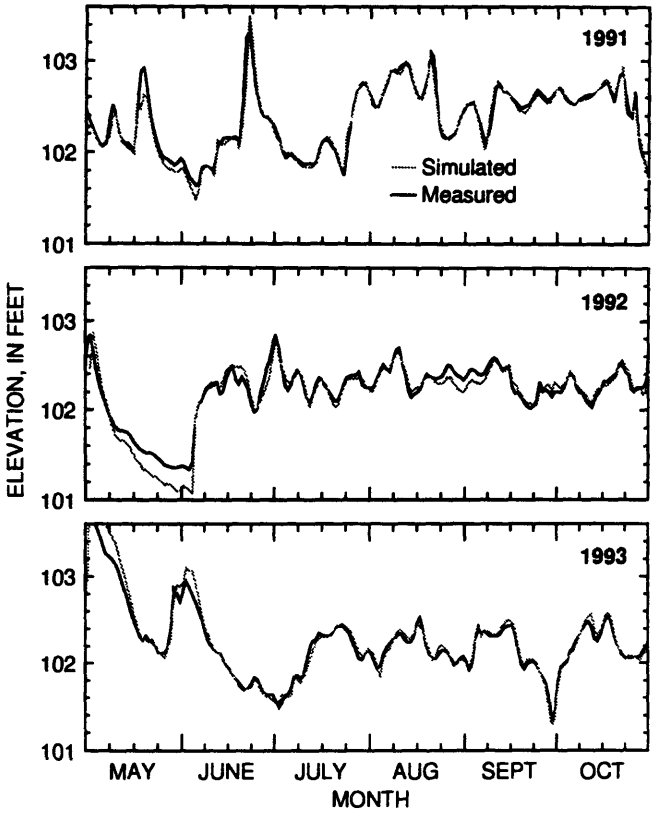

Figure 19. Calibrated and measured water-surface elevations of the Tualatin River at river mile 6.7 (Oswego canal) for May–October of 1991–93.

To compare the simulated and measured travel times for that reach, both were plotted as a function of the average discharge at RM 33.3 (fig. 20). The travel times compare favorably for this and other reaches. The fact that the travel times in figure 20 are plotted against a discharge measured outside of the reach of interest is a possible source of error, especially under changing hydrologic conditions. More of the variation in that graph, however, is due to the effect of different flashboard configurations at the Oswego diversion dam. Despite the fact that the dam is 12.8 miles downstream of Elsner Road, the dam's flashboard configuration still has an effect on the volume, and therefore the travel time, in the RM 26.9–16.2 reach. Two of the measured travel times, from August 1987 and September 1986, are slightly larger than their simulated counterparts because the river was generally maintained at a higher water-surface elevation in the 1980s than it was in the early 1990s.

Two other dye tracer experiments were conducted in the Tualatin River by USGS personnel in September of 1992 (Lee, 1995). The measured travel times from that study, limited to the upper part of the modeled reach, were simulated with a reasonable degree of accuracy by the model. In addition, data from those experiments were used to calibrate the longitudinal momentum-dispersion coefficient (eddy viscosity) and the longitudinal constituent-dispersion coefficient (eddy diffusivity). These parameters were set to 1.0 m^2/sec and 2.5 m^2/sec, respectively. Chloride measurements from 1991 through 1993 were also used to examine the model's ability to transport a conservative tracer. Indeed, the agreement between the simulated and observed chloride concentrations is excellent; a complete discussion is presented in the *Water Quality* calibration section on page 47.

In addition to the eddy viscosity, the hydraulics simulated by CE-QUAL-W2 are affected by shear stresses at the air/water and sediment/water interfaces. At the air/water interface, the effects of wind shear were found to be relatively unimportant in transporting water through the model grid, even though the riparian vegetation was assumed to decrease the measured wind speed by only 10 percent. At the sediment/water interface, a Manning's n, or roughness coefficient, of 0.03 was used throughout the grid. This value is consistent with measurements of n for slow, meandering rivers such as the Tualatin (Barnes, 1967; Arcement and Schneider, 1989). Experimentation with the model showed that changing the value of Manning's n had only a slight effect on the simulated surface slope and travel time in this river. Several physical characteristics of the Tualatin River such as surface slope and velocity change dramatically as the discharge decreases from a high value in May to a low value later in the summer season. Two short simulations were run to illustrate these changes. The first focused on a high-flow period in early May of 1992, the second on a low-flow period in late August of 1992. The water-surface elevation, discharge, and velocity for these two periods are compared as a function of river mile in figure 21. On May 10, 1992, the average simulated discharge within the model reach was approximately 430 ft^3/s; on August 22, 1992, that discharge was roughly 110 ft^3/s. The increases and decreases in discharge at specific locations were due to individual inputs and withdrawals. The largest changes in discharge were due to the two largest tributaries (RMs 38.1 and 9.3), the two WWTPs (RMs 38.1 and 9.3), and the Oswego canal diversion (RM 6.7). The simulated velocities reflect the variation in the river's cross-sectional area; higher velocities are required to transmit a given discharge through a smaller cross-sectional area.

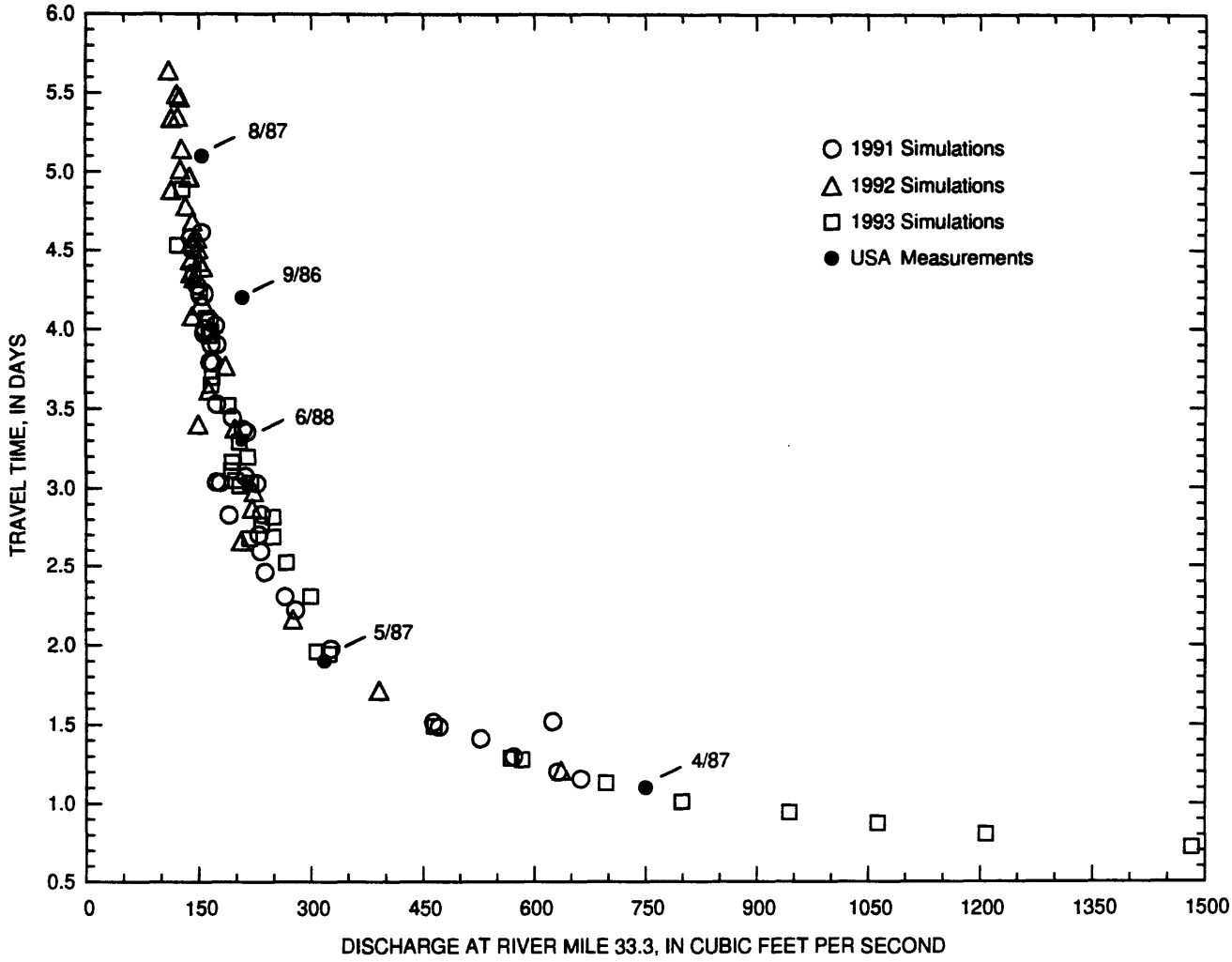

Figure 20. Simulated and measured travel times through the river mile 26.9 to river mile 16.2 reach of the Tualatin River. (USA, Unified Sewerage Agency of Washington County, Oregon)

The simulated water-surface elevations are also affected by geologic sills, such as the one at RM 10 (Cook Park). At that point, the river is shallow (about 4 feet deep) and the resulting flow constriction increases the water-surface elevation upstream during the high-flow period. No such constriction is present downstream of RM 10; as a result, the water-surface elevation decreases markedly just downstream of that point. During the low-flow period, however, the flashboards on the Oswego diversion dam (RM 3.4) are in place, backing up the river past RM 10 and all the way to RM 30.

The surface slope and velocity plots (fig. 21) illustrate both the effect of the dam's flashboards and the river's vulnerability to several water-quality problems. The Tualatin River is a slow-moving, low-gradient stream even when the discharge is higher than 400 ft^3/s. When the discharge decreases from 430 ft^3/s to 110 ft^3/s and the flashboards are raised, the mean surface slope from RM 30 to RM 3.4 decreases from 1.1 inches/mile to a very small 0.1 inch/mile. The mean velocity shows a corresponding decrease from 0.39 ft/s to 0.11 ft/s in that reach. Downstream of the Oswego canal (RM 6.7), the mean velocity for the low-flow period decreases to 0.04 ft/s. These low velocities result in long residence times; a parcel of water would require about 2 weeks to traverse the RM 30 to RM 3.4 reach under these low-flow conditions. A long residence time is one factor that contributes to excessive algal growth and the importance of SOD. Low velocities exacerbate those problems by slowing the transport of oxygen across the air/water interface. The physical characteristics of the Tualatin River (bathymetry, discharge, surface slope, and velocity) are among the most important factors in determining the river's water quality.

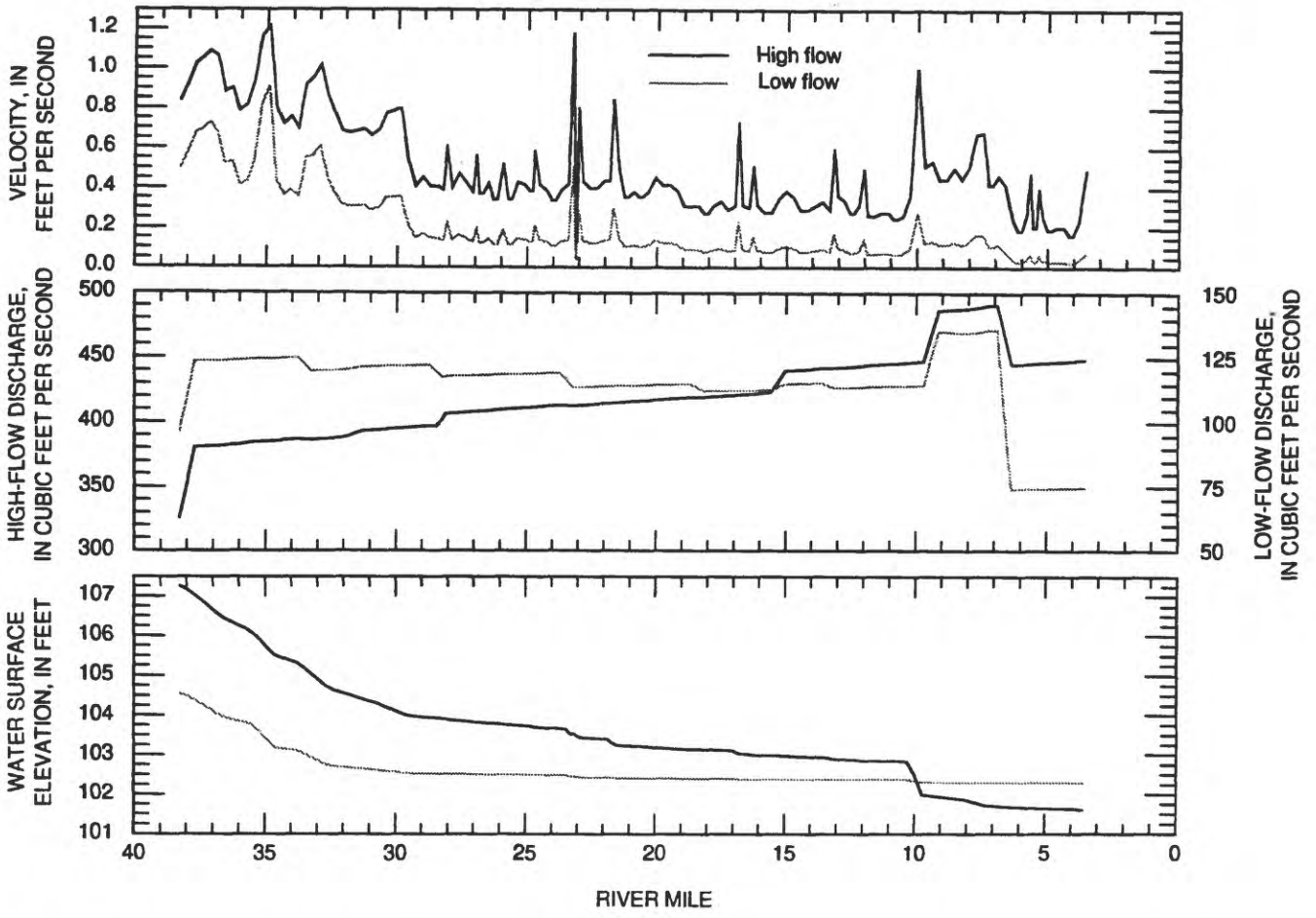

Figure 21. Simulated elevations, discharges, and velocities for one high-flow and one low-flow period in 1992. (Note that different axes are used for high flow and low flow in the discharge hydrograph.)

Water Temperature

In addition to hydraulic characteristics such as discharge and velocity, meteorological factors such as solar insolation and air temperature help to determine the water quality of the Tualatin River during the low-flow summer period. These factors influence many important processes. First, solar insolation is one of the most important forces driving photosynthetic activity. When coupled with warm water, sufficiently long travel times, and ample nutrients, several days of bright sunlight will produce a phytoplankton bloom. That bloom, and the crash that usually follows, will largely control the pH and will significantly affect the concentration of dissolved oxygen. Second, meteorological factors are important in determining the water temperature. That temperature, in turn, influences the rates of *all* of the chemical and biological reactions in the river. Although most of the reactions are weak functions of the water temperature, the effect is significant when assessed on a seasonal time scale. Water temperatures ranged from about 9°C to 26°C at RM 3.4 over the May through October period in 1991; an increase in water temperature from 9°C to 26°C would be accompanied by an increase in reaction rates of roughly a factor of three. Third, meteorological processes, coupled with river hydraulics, are responsible for the vertical thermal structure of the river. Certain reaches of the Tualatin River, especially between RM 6.5 and RM 3.4, tend to stratify during low-flow periods of warm, sunny weather. This stratification stabilizes the water column and allows vertical concentration gradients to develop for most of the modeled constituents. If the stratification is maintained for a sufficiently long period of time, the hypolimnion can be depleted completely of dissolved oxygen.

Calibration of the heat budget of the Tualatin River required the adjustment of only the shading coefficients. A wind-sheltering coefficient of 0.9 was used throughout, and was not found to be important to the heat budget in this application. All other parameters and boundary conditions necessary to the heat budget, such as the temperature of inflows and the solar insolation and air temperature, were either measured or estimated. Initial shading coefficients were estimated on the basis of the height of the riparian vegetation and the width of the river. Wider segments, therefore, received less shading than narrow segments with the same riparian cover, and the shading decreased from the upstream to the downstream boundary due to a gradual increase in river width. The shading coefficients were adjusted iteratively until the simulated water temperatures provided a good match for the observed data. The calibrated shading coefficients are tabulated in Appendix C.

Hourly measurements of water temperature at the Oswego diversion dam (RM 3.4), taken during each of the summers of interest, provide an excellent data set against which the simulated temperatures can be compared. Hourly values of the simulated water temperature at that location track the observed data fairly well (fig. 22), with a root mean square error of only 0.77°C; 98.8 percent of the simulated water temperatures fall within 2°C of the observed temperature, and 82 percent fall within 1°C. An error of 2°C in the simulated water temperature would produce only a 10 to 15 percent change in any reaction rate. During many time periods, such as May 20 to June 9 and August 13 to September 2 in 1992, the observed and simulated temperatures at RM 3.4 are in almost perfect agreement. Although any individual day's water temperature may not be simulated exactly, the general trends and the size of the diel variation are modeled very well.

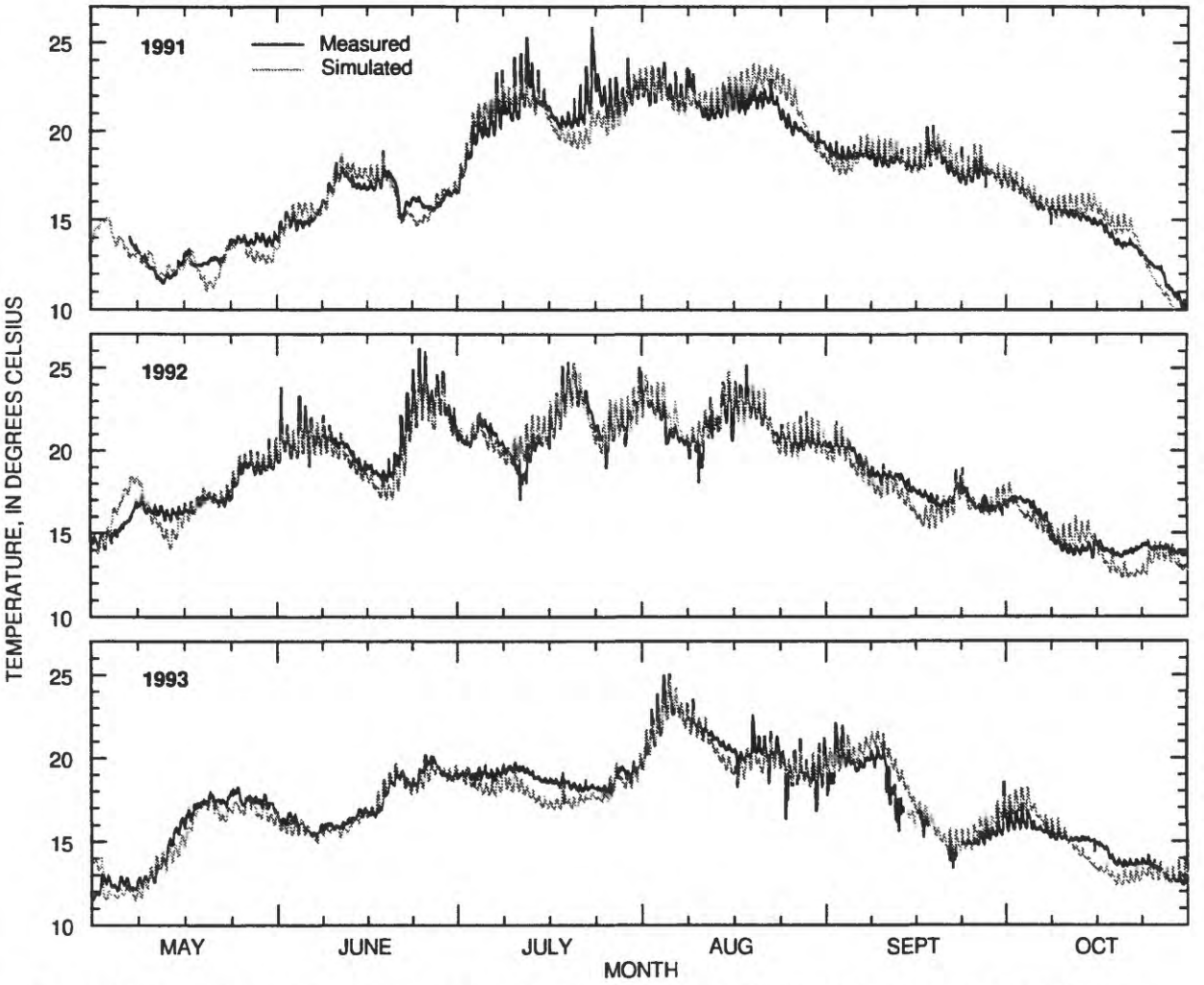

Figure 22. Simulated and observed hourly water temperatures for the Tualatin River at river mile 3.4 (Oswego diversion dam) for May–October of 1991–93.

This excellent agreement is obtained despite the fact that this model (1) has a shading algorithm that does not account for variations in shading due to time of day or segment orientation, (2) does not provide for heat conduction across the sediment/water interface, and (3) sometimes produces too much advective vertical mixing where the channel depth changes markedly, such as at the Oswego diversion dam (RM 3.4).

Vertical profiles of water temperature were measured at many locations within the model reach. These data were valuable in calibrating both the heat budget and the model parameters that control vertical dispersion. Vertical temperature gradients rarely persisted for more than a few days at RMs 16.2 and 11.5; thermal structure was almost never observed for more than one day at RMs 26.9 and 8.7. At RM 5.5 (Stafford Road), however, the Tualatin River often stratified for long periods of time. This stratification was the result of warm weather, a deep channel, and low velocities that resulted in a minimal amount of vertical dispersion. The vertical dispersion of heat is simulated in CE-QUAL-W2 as a function of horizontal shear stresses and vertical density gradients. Three input parameters can affect the calculation of the model's vertical dispersion coefficient: the minimum vertical eddy viscosity, and minimum and maximum limits for the vertical dispersion coefficient. (The current USACE version does not allow the user to input these values; they are set internal to the model.) If these parameters are set incorrectly, too much or too little vertical mixing will be simulated. After some investigation, these parameters were set at 1×10^{-7}, 1×10^{-6}, and 1 m^2/sec, respectively. The minimum values reflect physical limits imposed by the molecular properties of water; the maximum value is used only when a density inversion causes buoyancy-induced vertical mixing.

The model was able to reproduce the general lack of stratification observed at RMs 26.9, 16.2, 11.5, and 8.7 as well as the prolonged stratification events at RM 5.5. For example, the model simulated the observed depth-specific water temperatures at RM 16.2 and 5.5 fairly well for 1992 (fig. 23). Neither the simulated nor the observed data show much, if any, stratification at RM 16.2. In contrast, both the simulated and observed temperatures show significant vertical temperature gradients, sustained for weeks at a time, at RM 5.5. The simulated water temperatures at 1, 6, 12, and 15 feet match the observed data within 1°C most of the time, with a maximum discrepancy of about 2°C. The water temperature of the Tualatin River was simulated with sufficient accuracy to produce accurate variations in reaction rates. Vertical mixing, as measured by vertical variations in the water temperature, was also simulated with an acceptable degree of accuracy at each of the calibration sites.

Water Quality

Calibrating for a 6-month period during three different years requires the model to perform well under widely varied environmental conditions and over a continuous time period during which significant seasonal variations exist. There is an inherent compromise between (1) the ability to accurately reproduce the magnitude of fluctuations in water-quality constituents on a daily to weekly time scale, and (2) the ability to reproduce the timing of these fluctuations, but not necessarily their extreme values, over longer time scales and a broader range of environmental conditions. The decision was made in calibrating CE-QUAL-W2 to the Tualatin River data set that it is preferable to assure that the model perform adequately over a realistic range of conditions rather than simulate water-quality constituents with a great deal of accuracy for a short period of time over which environmental conditions are less variable. For this reason, most calibration parameters are constant for the entire 18 months of calibrated simulations. The set of parameters used represents the best description of the dominant processes in the river during the entire calibration period, but is not necessarily the optimal combination for a shorter subset of the calibration data. The above argument notwithstanding, it was necessary to acknowledge that two particular parameters were sufficiently sensitive to the model and varied greatly enough over the calibration period that it was reasonable to vary them in a simple and defensible manner. These two parameters were the light- and nutrient-saturated instantaneous algal growth rate, K_{ag}, which was varied seasonally within each year, and the zooplankton mortality rate, K_{zm}, which was varied from year to year. These two parameters are discussed with the chlorophyll-a calibration results.

A few comments are necessary concerning the overall confidence limits on the measured data that are presented in this and the following section. These data do not lend themselves to a rigorous statistical analysis for the fundamental reason that the measured value of any water-quality constituent in the river is not expected to be a random variable, as the greatest part of the variability in the measured quantity is due to temporally variable forcing functions upstream.

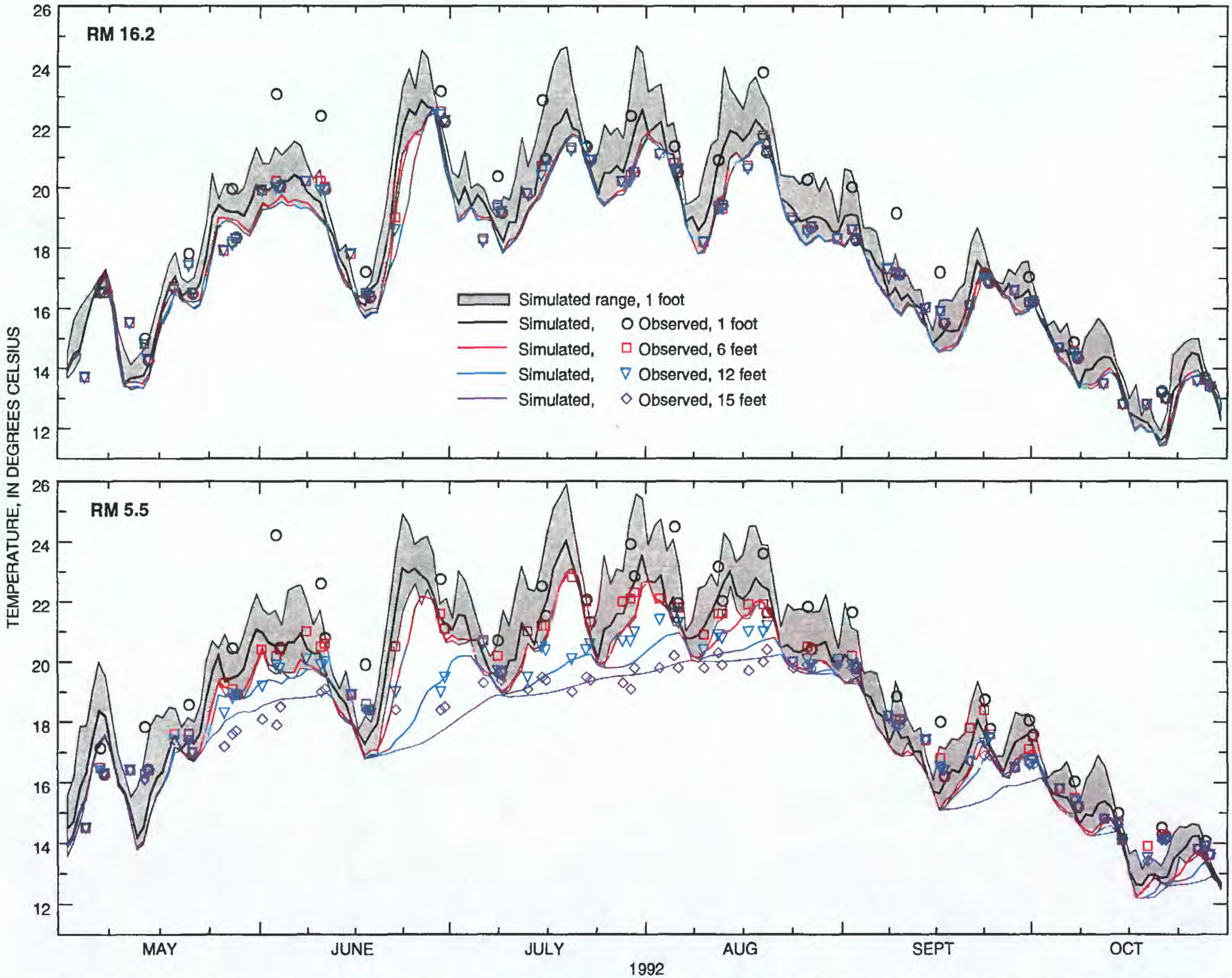

Figure 23. Simulated and observed water temperatures at several depths in the Tualatin River at river mile 16.2 (Elsner Road) and river mile 5.5 (Stafford Road), May–October of 1992. (RM, river mile)

On the other hand, errors in the analytical procedures used can be expected to be random, although they may contain a systematic component as well. Extensive quality assurance data were collected in conjunction with the field program in order to assess these errors. Systematic errors were found to be significant for ammonia in the concentration range 0.019 to 0.043 mg/L (median bias of +36 percent), total phosphorus in the concentration range 0.024 to 0.051 mg/L (median bias of +26 percent), and total Kjeldahl nitrogen (TKN) in the concentration range 0.019 to 0.078 (median bias of +134 to +257 percent). Analysis of blanks indicated that the systematic error in TKN was probably due to contamination. Fortunately, these systematic errors are not a concern in interpreting the model calibration results, because nutrient concentrations in the model reach are substantially higher than the ranges indicated.

The analysis of the random component of analytical error using replicate and laboratory reference samples indicated that accuracy and precision errors were comparable, being approximately ± 20 percent for TKN and total phosphorus, and approximately ± 10 percent for ammonia, nitrate-plus-nitrite, and orthophosphate. That is, in the concentration ranges of interest in this reach of the river, the majority of the reference samples were within ± 10 or 20 percent of the true value, and most of the replicate samples were within ± 10 or 20 percent of the mean of the replicates, depending on the nutrient measured. Thus it is reasonable to assume that the error in individual data points due to the analytical procedure is probably within 10 or 20 percent of the true value of the sample, depending on the nutrient measured; a similar level of accuracy was found for other parameters such as chlorophyll-a. This is a good guideline to use in interpreting the time series plots of data at a particular sampling site, with the caveat that this does not take into account any systematic or random error that occurs when temporal variability is mistakenly attributed to spatial variability as a result of the sampling strategy (aliasing).

Seasonal averages (May through October) are referred to frequently in the presentation of the calibration results. A formal propagation of errors states that the variance of the mean of a series of independent data points will equal the sum of the variances of each data point going into the mean, weighted by the point's contribution (Miller and Miller, 1988):

$$\sigma_{\bar{x}}^2 = \frac{1}{N}\sum_{i=1}^{N}\sigma_{x_i}^2. \qquad (49)$$

Assuming that the variance of each data point is approximately equal, the sum in the equation above can be approximated as $N\sigma_x^2$, where σ_x^2 is approximately equal to the variance of any data point, and the variance of the mean becomes $\sigma_{\bar{x}}^2 \approx \sigma_x^2$. A formal estimate of the variance of each data point is not available; nonetheless, it is reasonable to extrapolate the above result and conclude that the error in the seasonal averages should be the same order of magnitude as the error in the individual data points. Again, this refers only to the error due to the analytical procedure, and any errors due to aliasing are a separate issue. As an example, aliasing is discussed below in the context of the chloride results.

Chloride

The chloride data set provides an opportunity to evaluate how well the model describes the transport of a conservative tracer. This is an important test, because any difficulty the model has in simulating a conservative tracer will also apply to the other constituents in the model, but will be hard to separate from the effects of nonconservative processes. Chloride is a particularly good tracer to test the model because it can be measured with high accuracy; therefore, errors in individual data points do not significantly complicate the comparison to model results. The overall agreement between the modeled and observed time-varying concentration of chloride at RM 5.5 (fig. 24) is good. Accurately simulating a conservative quantity such as chloride requires both accurate measurements of its concentration at the boundaries *and* an accurate simulation of the amount and velocity of water in the river. The model was calibrated well for discharge, elevation, and travel time (see the *Hydraulics* section on page 38); the chloride calibration results reflect this. The fact that the model does a good job of simulating the transport of chloride through the system is further evidence that the hydraulics of the system should not be a major reason for disagreement between the model results and observations for any of the other constituents.

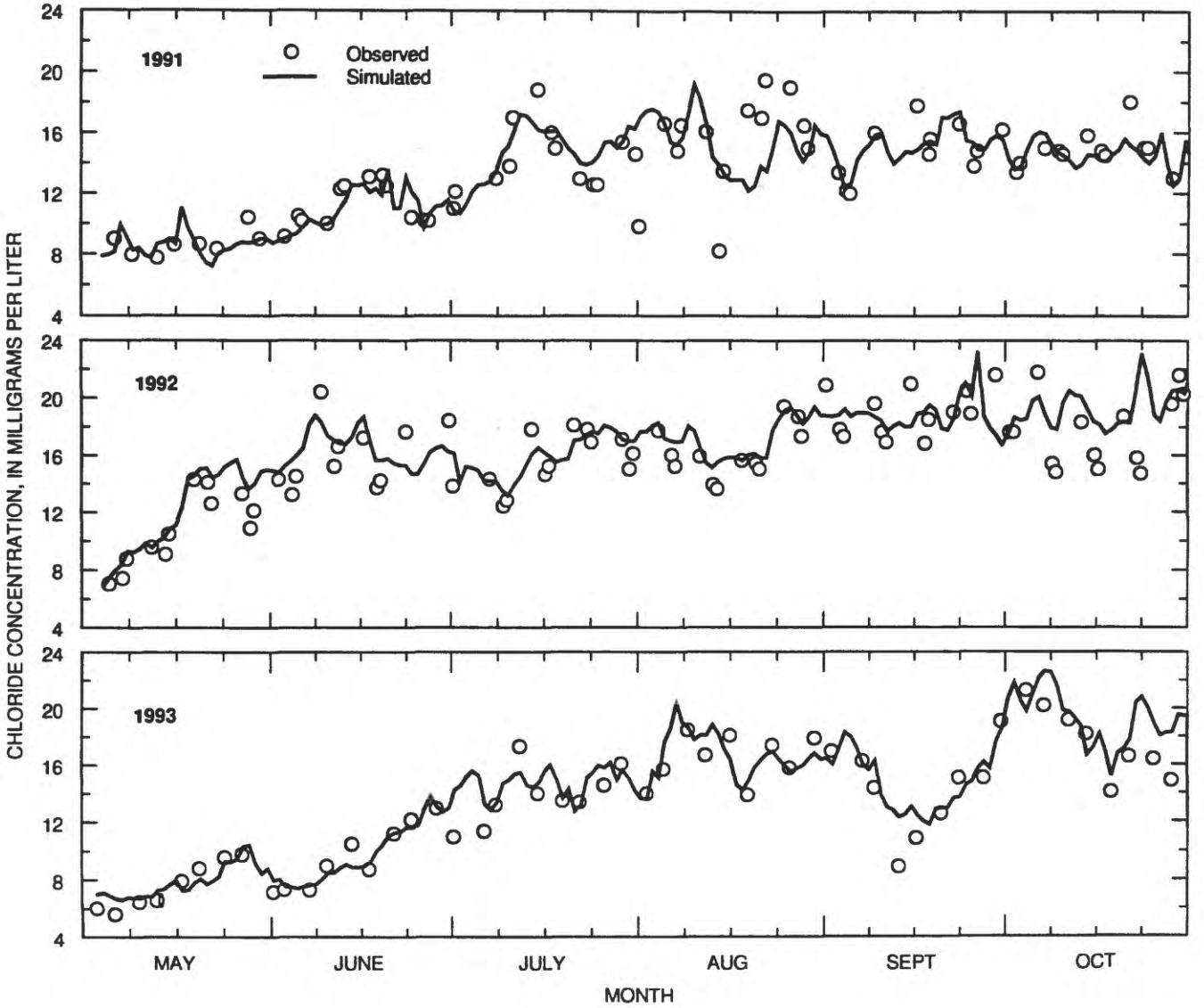

Figure 24. Measured chloride concentration compared with the simulated concentration in the Tualatin River at river mile 5.5 (Stafford), May–October of 1991–93.

In figure 25, the seasonally averaged (May through October) chloride data for each year are plotted against river mile. This figure again shows good agreement between modeled and observed data, but some interesting discrepancies appear. The dependence of the chloride observations on river mile shows distinctly the locations of the two WWTPs that discharge into the model reach. The Rock Creek WWTP, located at RM 38.1, causes an increase in the chloride concentration between the sampling stations at RM 38.4 and RM 36.8 in all 3 years. The chloride concentration then remains nearly constant until the next increase between sampling stations at RM 11.6 and RM 8.7, caused by discharge from the Durham WWTP at RM 9.3. In 1991 and 1992, the observed concentrations change little between RM 8.7 and RM 5.5, as there are no significant sources of chloride between these two stations, and the model data behave similarly. In 1993, however, the average concentration of chloride measured in the river increased between RM 8.7 and RM 5.5, while the model data remain nearly constant, consistent with the fact that there still was no significant source of chloride between these two stations. The stations at RM 8.7 and RM 5.5 provide a clear example of how the timing and location of sample collection can bias the resulting data.

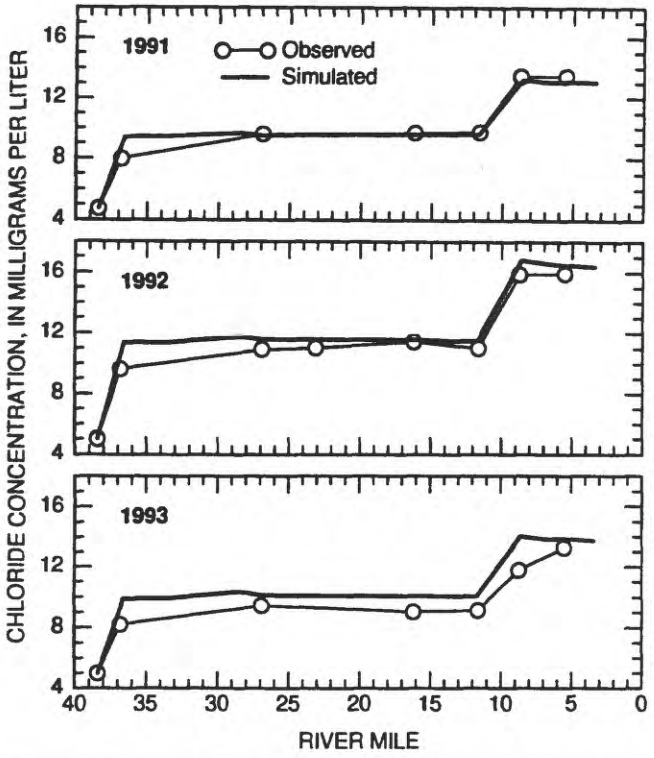

Figure 25. Comparison of the May–October mean of measured chloride concentration with the simulated concentration in the Tualatin River from river mile 38.4 to river mile 3.4, 1991–93.

The WWTP discharges have a daily cycle that is subject to aliasing, depending on the location of downstream sampling stations relative to the plants, in combination with the time of day that the downstream station is sampled. Data from a gage on the Rock Creek WWTP outfall from May through October of 1994 (fig. 26), for example, show that the median discharge from this plant is at a minimum between 4 and 6 a.m. and at a maximum near noon; the daily pattern in discharge from the Durham WWTP is similar, although the maximum discharge may be slightly smaller. If a water-quality constituent has a much higher concentration in the WWTP effluent than in the receiving water, as is the case with chloride, then the daily cycle in discharge from the plant will manifest itself downstream as a daily cycle in the concentration of the constituent in the river. The extremes in concentration travel downstream and appear at different sampling stations at different times of day; therefore the timing of sample collection becomes important, as it can bias the resulting data on either the high or low side.

The time of day that samples were taken downstream of the Durham WWTP affects the measured difference in concentration between RM 8.7 and RM 5.5, and explains the change in the seasonal averages from 1992 to 1993. In figure 27, the time of day that the sample was taken at RM 8.7 is plotted against the difference in concentration between the two stations (concentration at RM 8.7 minus the concentration at RM 5.5). The sample at RM 5.5 is nearly always taken within 1.5 hours of the sample at RM 8.7, so the difference in concentration is due almost entirely to spatial rather than temporal variability. Figure 27 shows clearly that, on average, analysis of samples taken in the morning yields higher concentrations at RM 5.5 than at RM 8.7, whereas the opposite is true of samples taken in the afternoon. It is also clear from this figure that the 1991 and 1992 data sets include morning *and* afternoon samples, whereas the 1993 data set includes only morning samples. Thus the differences in concentration between RMs 8.7 and 5.5 tend to cancel each other out in the seasonal average of the 1991 and 1992 data, whereas the seasonal average of the 1993 data shows a higher value at RM 5.5 than at RM 8.7.

The daily cycle in discharge from the WWTPs affects not only the relationship between consecutive downstream sampling stations, as described above, but also the comparison between the observed data and the modeled data at a single downstream station. The modeled data do not reproduce the daily cycle because boundary conditions for the WWTPs are based on daily averaged discharge. Therefore, a sampling bias may explain why the model consistently overestimates the difference in chloride concentration between the upstream boundary at RM 38.4 and the concentration at RM 36.8, which is downstream of the Rock Creek WWTP outfall (RM 38.1).

Model estimates of the travel time between the Rock Creek WWTP and RM 36.8 vary from about 1 hour during high-flow conditions to about 3 hours during low-flow conditions. Samples at RM 36.8 were taken in the morning, typically between 8 and 9 a.m., during all 3 calibration years. In this case, the samples taken from RM 36.8 between 8 and 9 a.m. would represent water that received discharges from the plant between 6 and 7 a.m. under high-flow conditions, or between 4 and 5 a.m. under low-flow conditions. Referring to figure 26, it is clear that discharges from the plant during either of these time windows is normally less than the average discharge over that day.

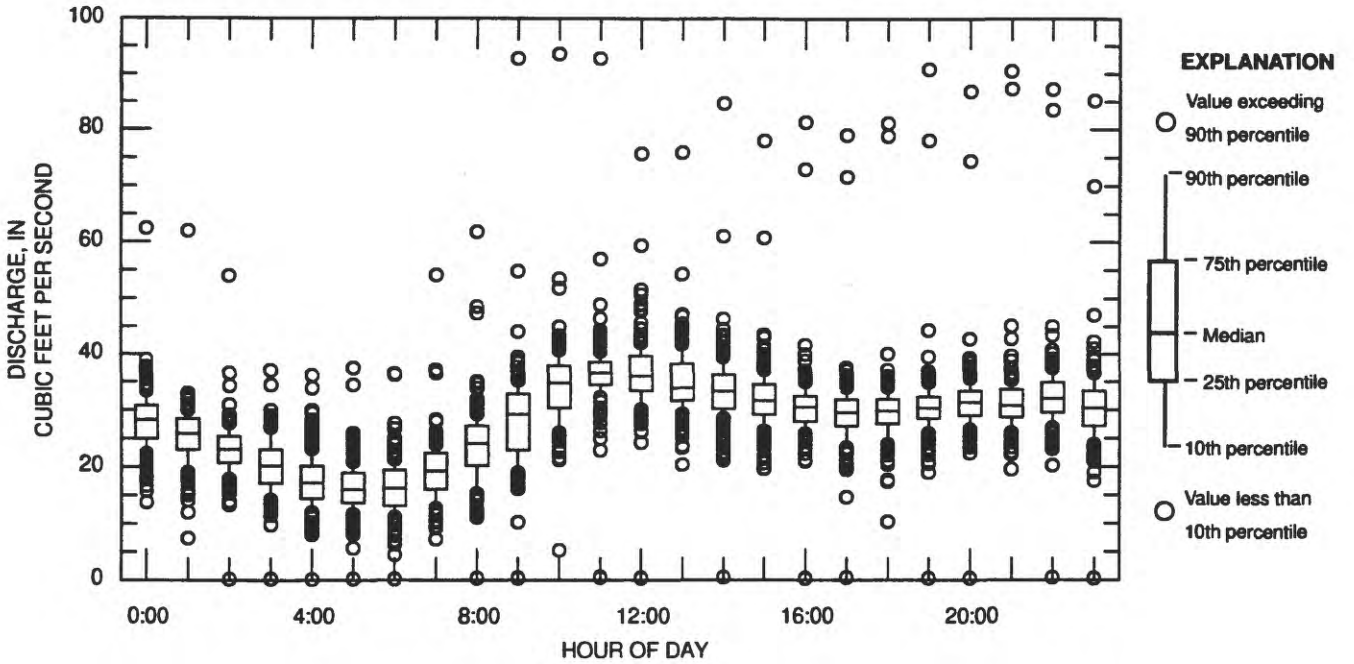

Figure 26. Rock Creek Wastewater-Treatment-Plant discharge as a function of the time of day, May–October of 1994.

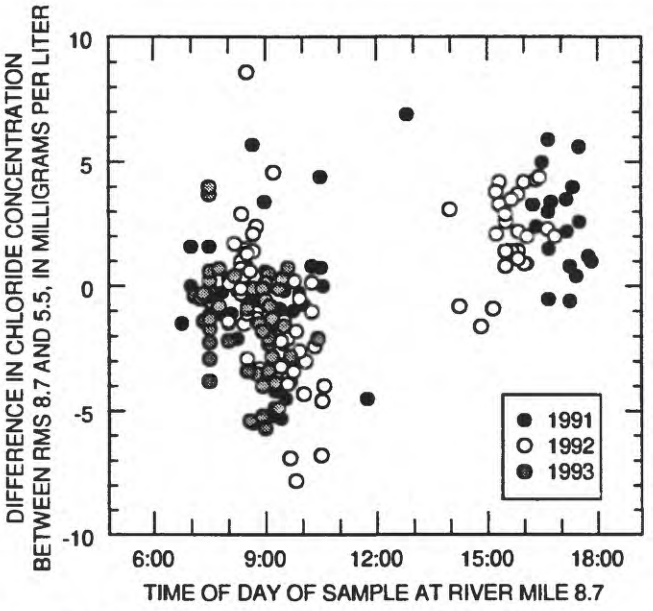

Figure 27. Difference in chloride concentration between river mile 8.7 and river mile 5.5 in the Tualatin River as a function of the time of day of the sample at river mile 8.7; data from May–October of 1991–93.(RM, river mile)

Since the model boundary conditions for the WWTP are daily averages, the model will generate higher downstream concentrations at RM 36.8 than those that were measured in the river between 8 and 9 a.m. A test of whether this explanation of the discrepancy at RM 36.8 is plausible was done by numerically "mixing" the water coming in at the upstream boundary with the only two significant inputs between RMs 38.4 and 36.8, the Rock Creek WWTP and the Rock Creek (North) tributary, ignoring the short travel time involved. This analysis indicated that if the daily averaged load to the river from the Rock Creek WWTP was based on a discharge that exceeded the actual discharge to the river in the 4 to 8 a.m. time period by an amount on the order of 10 ft^3/s (on a seasonally averaged basis), then this can explain the difference between the modeled and observed seasonally averaged concentration at RM 36.8. This amount of discharge is well within the daily discharge range measured at the plant.

The implications of the sampling strategy were discussed in some detail with regard to chloride because they undoubtedly affect the measurements of other constituents as well, but it is more difficult to detect sampling bias when other nonconservative processes are operating. The effect of sampling bias should be greatest when the WWTPs are an important source of a target constituent. Behavior analogous to that for chloride between RMs 8.7 and 5.5 was seen for total phosphorus, orthophosphate, TKN, and ammonia during 1991 and 1993, when the Durham WWTP had periodically high discharges of these nutrients. It is prudent to consider the possibility that sampling biases may have affected the measurements of these constituents. On the other hand, sampling biases should be minimal for constituents such as dissolved oxygen for which the processes operating within the river are much more important than point-source loads.

Phytoplankton and Zooplankton

Early in the calibration process it became clear that a single value of the maximum instantaneous algal growth rate, K_{ag}, was inadequate to capture the algal dynamics of the entire 6-month simulation period in each year. When K_{ag} was chosen such that the large blooms during the middle of the growing season were well-represented, the model consistently underestimated the size of the blooms at the beginning and end of the May through October period; a higher growth rate was clearly implicated for early and late-season blooms than for mid-season blooms. A reasonable explanation for this problem would be the occurrence of a seasonal succession in the phytoplankton assemblage. There are significant seasonal changes in environmental conditions in the Tualatin River that have been connected to shifts in the algal population dynamics and community structure in other natural systems. Residence time (McKnight and others, 1986), the onset of stratification (Pierson and others, 1992), and differential settling and grazing losses (Crumpton and Wetzel, 1982) have all been shown to precipitate a change in the species dominating the phytoplankton assemblage. The phytoplankton abundance data for the Tualatin River, however, show that one of several diatom species nearly always dominates the assemblage, and that there is no clear pattern of succession (Doyle and Caldwell, 1996).

A clear species succession is perhaps the highest in a hierarchy of ecological responses to a changing environment, but even in the absence of a clear shift of dominance from one species to another, the adaptation of individuals within the community to changing conditions can cause measurable physiological changes at the community level (Harris, 1980; Schubert and Forster, 1997). The primary productivity data indicate that this is probably the case in the Tualatin River because they show a discernible seasonal variation. The assimilation numbers from RMs 5.5, 16.2, and 26.9 are plotted together for all 3 years in figure 28. The curve on each graph is a polynomial fit to all the filled data points, and is provided only to identify the underlying pattern. Primary productivity tends to be highest early in the season, lowest during the middle of the season, and high again toward the end of the season. The pattern starts earliest in 1992, a dry year, when low summer discharge and significant algal growth began earlier than usual. The earliest data in each season (open symbols) indicate low productivity that does not fit the pattern, but these data were obtained before the

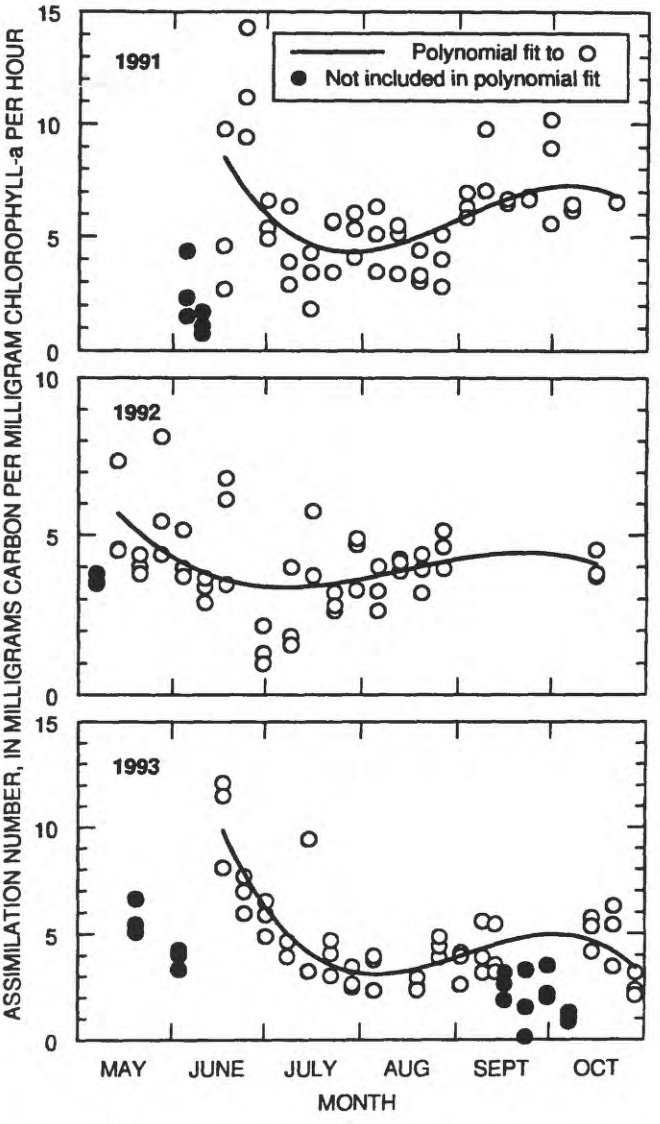

Figure 28. Measured assimilation number from three sites in the Tualatin River, May–October of 1991–93, with a polynomial fit to the data.

first big bloom in each year and probably represent a small population of cells not yet acclimated to favorable growing conditions. Several data points between September 12 and October 7 in 1993 are similarly low; these may be associated with a higher-than-normal release of water from Henry Hagg Lake that resulted in discharges of nearly 300 ft^3/s at RM 33.3 from September 1 to September 17 (fig. 29). The abrupt change in environmental conditions brought on by this surge of faster moving, colder water (for example, the predators were effectively flushed from the system) may have brought on the short-term dominance of a species normally present in small numbers and characterized by lower productivity per unit chlorophyll-a.

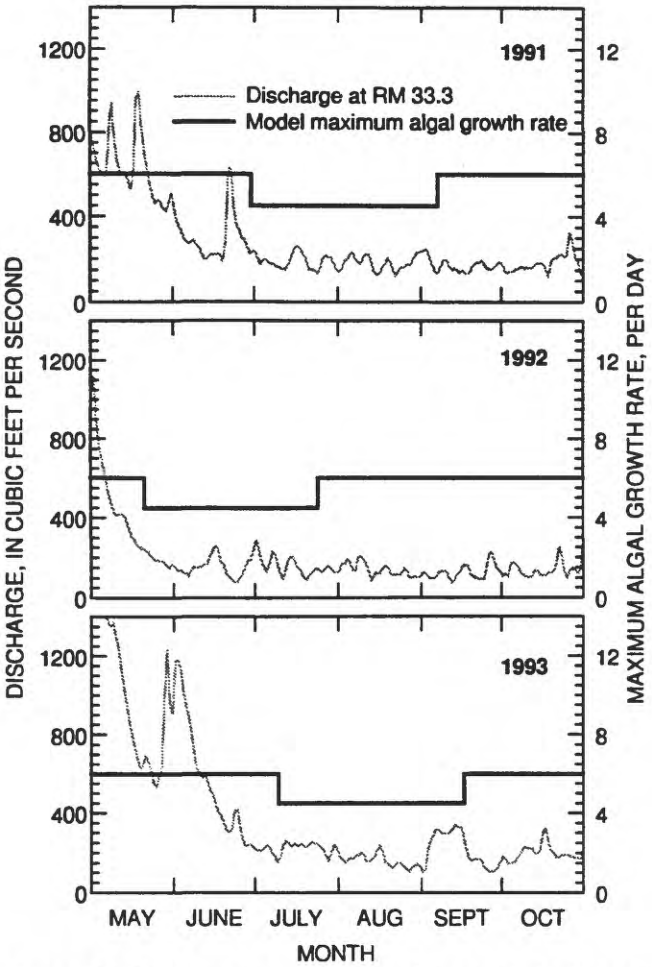

Figure 29. Maximum growth rate used in model simulations of the Tualatin River, with discharge at river mile 33.3, May–October of 1991–93. (RM, river mile)

The importance of these sorts of transient phenomena in altering species composition has been noted (Côté and Platt, 1983). The assimilation numbers are not a direct measurement of the growth rate K_{ag}, but do substantiate significant seasonality in the maximum algal growth rate. Therefore, the assimilation numbers were used as a guide in an iterative calibration procedure to arrive at a simple seasonality for K_{ag} that yielded greatly improved results.

This seasonality is shown in figure 29, where K_{ag} is plotted with the discharge at RM 33.3 in order to illustrate the relation between the two. A high growth rate early in the year while discharge is still high allows blooms to occur periodically even though the travel time in the river is short. The first change in K_{ag} is tied to the transition from high to low discharge, and occurs earliest in 1992 and latest in 1993. At this time, the early assemblage is shifted to an assemblage with a lower growth rate. The assimilation numbers indicated that the growth rate increased again later in the season, and the calibration confirmed that this increase was needed, but no specific environmental "trigger" was found. The seasonality in the calibrated growth rate is simple: K_{ag} is constant at 6 day^{-1} except for a 70-day period at the onset of low-flow conditions in each year, during which it is constant at 4.5 day^{-1}. The use of an early, mid-, and late-season value of K_{ag} retains a single set of input parameters that works well under a wide variety of environmental conditions while still imposing a significant physiological shift that the model algorithms cannot internally simulate.

Observed and simulated concentrations of chlorophyll-a, averaged over the entire season, are plotted against river mile in figure 30. In 1991 and 1992, both the model results and the observed data increase through the reach from the upstream boundary at RM 38.4 to RM 16.2. The observations show a slight decline in chlorophyll-a from RM 16.2 to RM 8.7, and then an increase in chlorophyll-a from RM 8.7 to RM 5.5, the last main-stem sampling station within the numerical grid. The modeled chlorophyll-a continues to increase from RM 16.2 to RM 11.6 before beginning to decline. Modeled chlorophyll-a increases again from RM 8.7 to RM 5.5, as do the observations. The model captures the basic trend in the seasonal average between each sampling station except at RMs 11.6 and 8.7. Through this reach the model simulates a large increase in chlorophyll-a, but concentrations in the river decrease instead. The last model reach from RM 5.5 to RM 3.4 cannot be compared with observations, but the drop in 1991 simulated values is due primarily to large grazing losses, which are discussed in the next paragraph. In 1993, observed chlorophyll-a increases from the upstream boundary to RM 11.6, declines slightly to RM 8.7, and then increases again as in the other 2 years. The model results capture all of the basic trends in the 1993 data, with the exception that between RM 11.6 and RM 8.7 model results increase very slightly instead of decreasing. In all 3 years, the model does a good job of simulating the seasonally averaged algal population from the upstream boundary to RM 16.2. The model's simulation of the time-dependent concentrations is also good (fig. 31). The increase and decrease of chlorophyll-a with successive blooms at RM 16.2 is captured by the model in all 3 years, even in 1992, which is characterized not so much by a succession of blooms as by an initial bloom followed by sustained high concentrations of chlorophyll-a through the rest of the season.

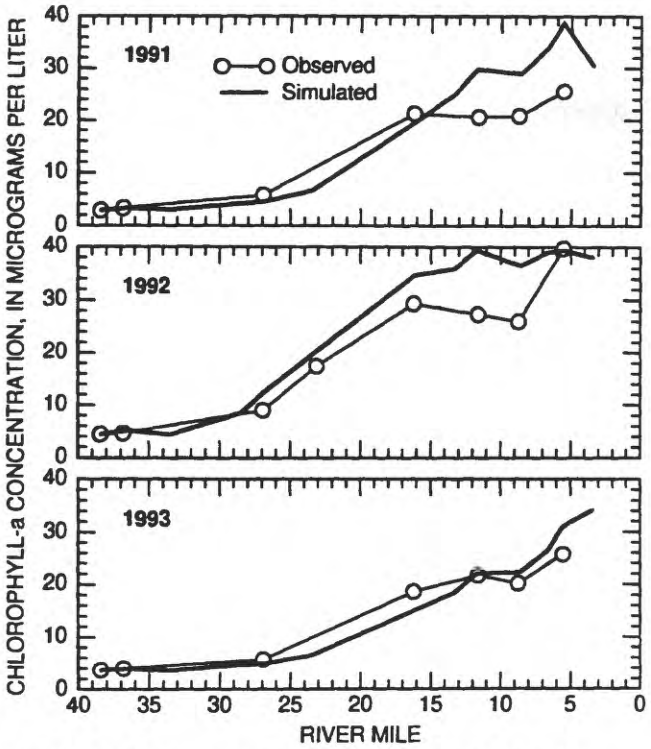

Figure 30. Comparison of the May–October mean of measured chlorophyll-a concentration with the simulated concentration in the Tualatin River from river mile 38.4 to river mile 3.4, 1991–93.

The performance of the model in the reach between RM 16.2 and RM 5.5 depends on whether the zooplankton biomass reaches the threshold (about 0.1 mg/L) required for grazing to become a significant loss process. The model does not capture some of the spatial and temporal intricacies of grazing, in large part because of the difficulty in modeling complex zooplankton population dynamics with a single rate constant for grazing, K_{zg}, and a single rate constant for mortality (predation), K_{zm}. The modeled and observed concentrations of zooplankton biomass at RM 5.5 are shown in figure 32. Observed zooplankton biomass concentrations were obtained from the zooplankton abundances (Doyle and Caldwell, 1996); these concentrations have strong seasonal and interannual variability. In order to simulate the very different maximum concentrations in biomass over the 3 years, it was necessary to acknowledge that different levels of fish predation probably occurred, and to incorporate this fact into the model by specifying a different value of K_{zm} for each year. The minimum value of K_{zm} used was 0.05 day^{-1} in 1991, when zooplankton biomass reached 1 mg/L for a midsummer period lasting several weeks. Much higher values of 0.4 and 0.2 day^{-1} were used in 1992 and 1993, respectively, when the maximum zooplankton biomass was much lower.

Varying K_{zm} interannually was judged a necessary compensation for the lack of explicit fish predation in the model, but varying zooplankton parameters seasonally would be contrary to the goal of minimizing the number of calibration parameters, and was not justified. Therefore, the simplification of a constant value of K_{zg} and K_{zm} for the entire 6-month simulation during each year was accepted, and manifests itself in two ways. First, the model cannot always capture the seasonal dynamics of the zooplankton population with a seasonally invariant K_{zg}, as can be clearly seen in early 1992 when the model zooplankton grow too slowly (fig. 32). Secondly, the model does not always correctly simulate the spatial dependence of grazing with a spatially invariant K_{zg}. In 1991, large grazing losses caused a precipitous decline in modeled chlorophyll-a from RM 5.5 to RM 3.4 (fig. 30), but did not significantly affect chlorophyll-a between RM 16.2 and RM 8.7.

A comparison of observed chlorophyll-a at RM 16.2 and RM 5.5, in combination with the observed zooplankton abundance data, points to a threshold of 0.1 mg/L of zooplankton biomass (at RM 5.5) for grazing to become an important loss process. This criterion delimits a large "grazing window" in 1991 from about July 19 to September 7, a smaller window in 1992 from about June 8 to July 8, and another in 1993 from about August 8 to September 7, although zooplankton concentrations in 1993 barely achieve the threshold level. The calibration results reflect the occurrence of these grazing windows, with good agreement between modeled and observed data outside of the windows and sometimes poor agreement within. In figure 33, the measured and modeled chlorophyll-a results are plotted against time at RM 5.5 for all 3 years, with the approximate grazing windows indicated. Two distinct blooms within the 1991 grazing window nearly disappeared from the observations of chlorophyll-a between RM 16.2 and RM 5.5. In the modeled data these two blooms continue to grow through this reach. Even though the model generates approximately the right amount of zooplankton biomass at RM 5.5 (fig. 32), and large grazing losses are modeled downstream of RM 5.5, grazing in the model does not affect the algae as far upstream as would be expected. Because the grazing rate is the same through the entire model reach, increasing K_{zg} to achieve the observed grazing losses between RM 16.2 and RM 5.5 results in unrealistically high grazing (and virtually no chlorophyll-a) between RM 5.5 and RM 3.4.

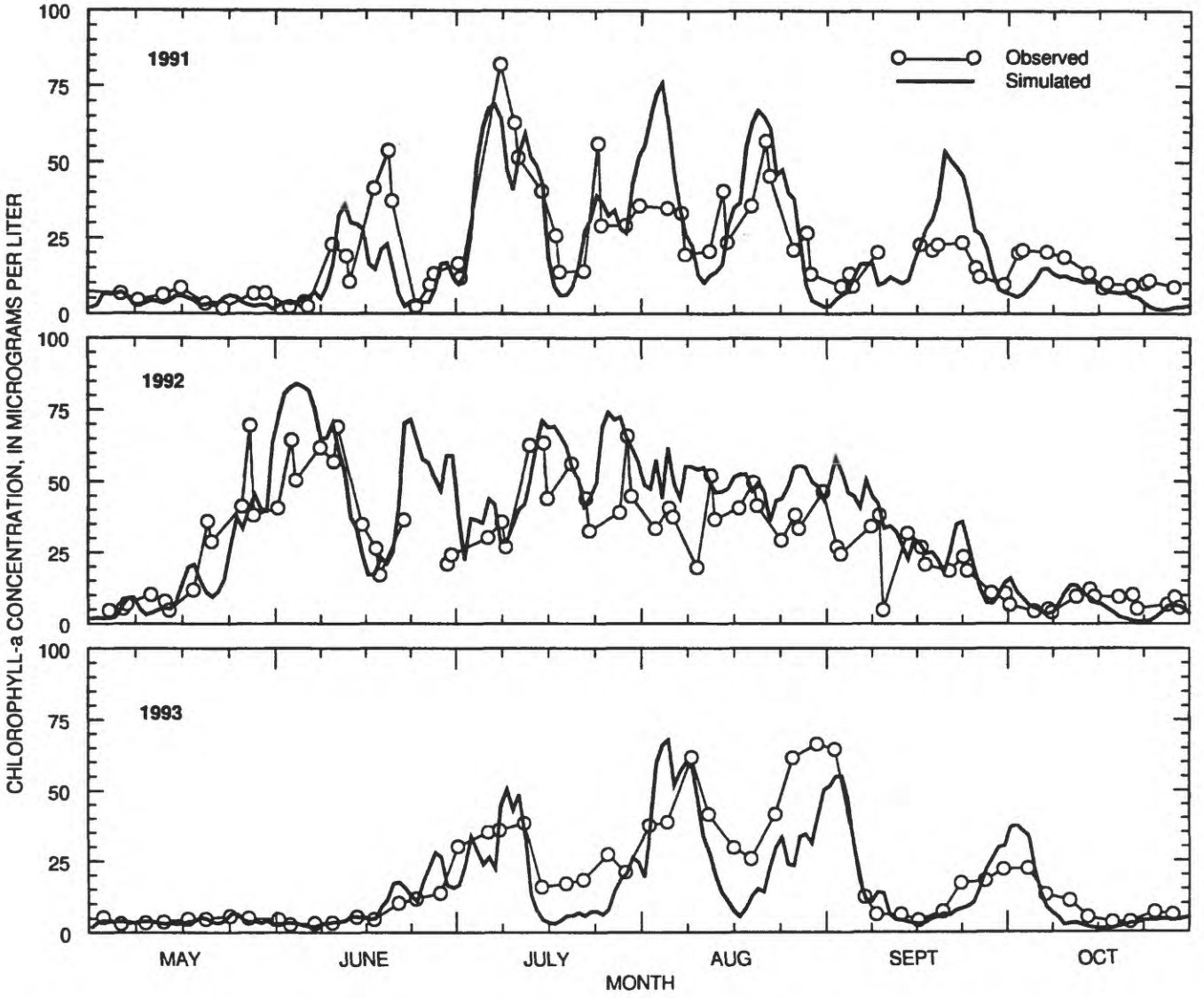

Figure 31. Measured chlorophyll-a concentration compared with the simulated concentration in the Tualatin River at river mile 16.2 (Elsner), May–October of 1991–93.

The modeling results, therefore, suggest that the grazing rate should be higher upstream (RM 16.2 and RM 5.5) than downstream (RM 5.5 and RM 3.4); it is plausible that there are downstream variations in zooplankton community structure (Urabe, 1990), with consequent variations in the grazing rate, but there are no data to confirm this. Fortunately, grazing is important for only a limited time period, even in 1991, when grazing has much more of an effect than in either 1992 or 1993. Large discrepancies in daily chlorophyll-a within the grazing window (fig. 33) are primarily responsible for the discrepancies in the seasonally averaged chlorophyll-a from RM 11.6 to RM 5.5 (fig. 30); outside of the grazing window, the model closely simulates the chlorophyll-a concentrations.

At the beginning of the 1992 season, the model zooplankton biomass grows too slowly and fails to reach the 0.1 mg/L threshold during the 1992 grazing window (fig. 32). As a result, the model also fails to capture the decline in chlorophyll-a beginning on June 5, the increase between June 15 and 18, and another decline beginning on June 23 (fig. 33). The agreement between modeled and observed chlorophyll-a is better outside of the grazing window, with the exception of the period between August 27 and September 16. Closer investigation of this time period shows that algal growth in the model is limited by low concentrations of phosphorus, but that growth in the observations is not phosphorus-limited to the same degree, if at all. Discrepancies in chlorophyll-a concentrations

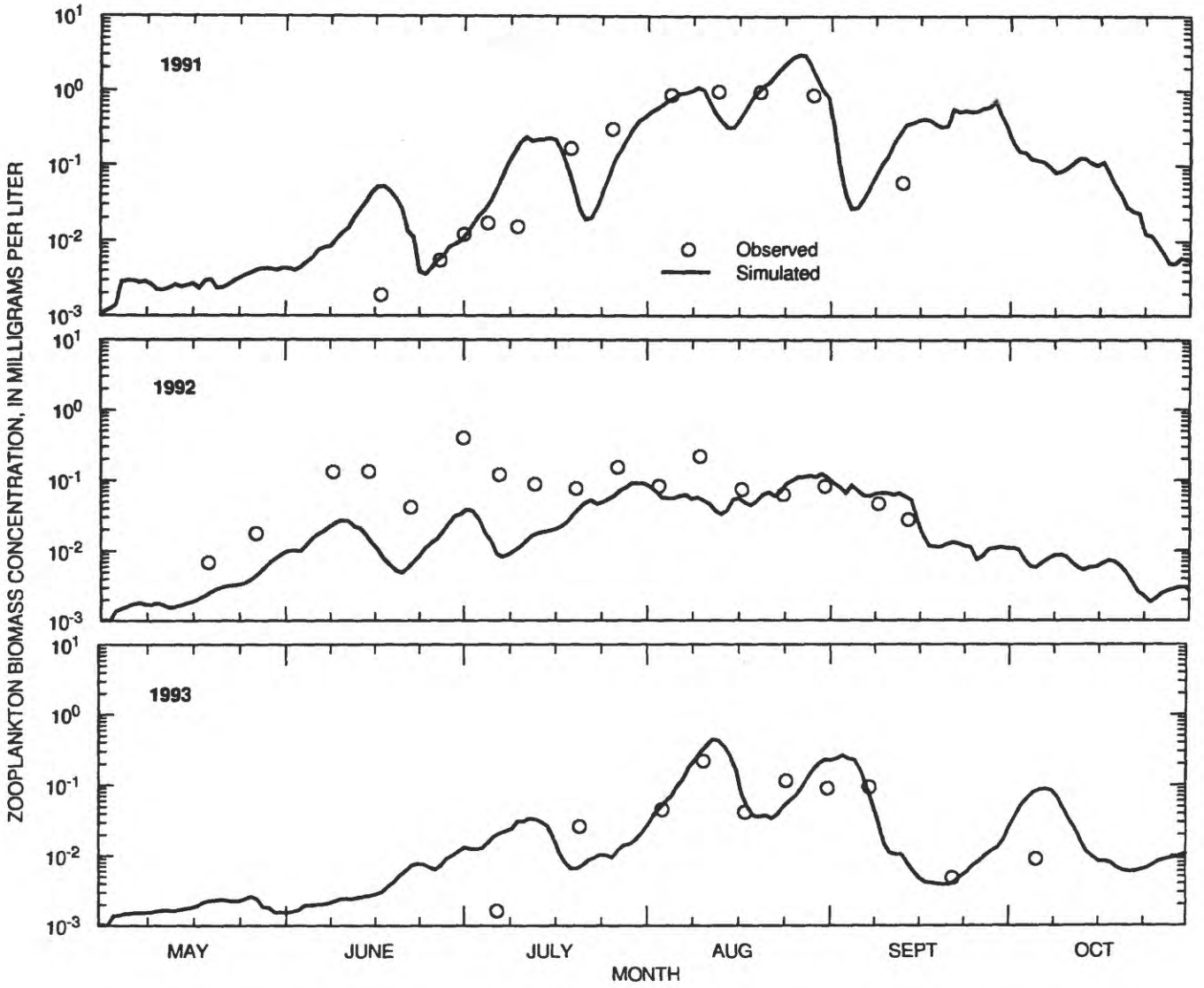

Figure 32. Measured zooplankton biomass concentration compared with the simulated concentration in the Tualatin River at river mile 5.5 (Stafford), May–October of 1991–93.

during this time period are directly attributable to discrepancies in the orthophosphate concentrations. This time period is discussed in more detail with the phosphorus calibration results.

Results from the calibration year 1993 are comparatively straightforward. Observed zooplankton biomass reaches but only barely exceeds the 0.1 mg/L threshold (fig. 32); therefore, zooplankton grazing is not an important factor during this season. The four distinct blooms apparent in both the observations and the model results at RM 16.2 (fig. 31) are still discernible at RM 5.5 (fig. 33). It is likely that zooplankton grazing is responsible for limiting the peaks of the second and third blooms by the time they reach RM 5.5, and that is why model chlorophyll-a levels are too high for these blooms at that location. In general, however, the model does a good job of depicting the sequence of blooms during this growing season.

Following the higher-than-normal release of water from Henry Hagg Lake in 1993 (September 1 to 17, fig. 18), which effectively flushed the phytoplankton from the river, the observed concentrations of chlorophyll-a recovered faster than the modeled concentrations (the bloom starts on September 22 in the observations and September 27 in the simulation). This is another indication, in addition to the change in primary productivity (fig. 28), that a significant shift in community structure followed this event. The rapid recovery of the algal population following this event, in spite of lower chlorophyll-a-normalized primary

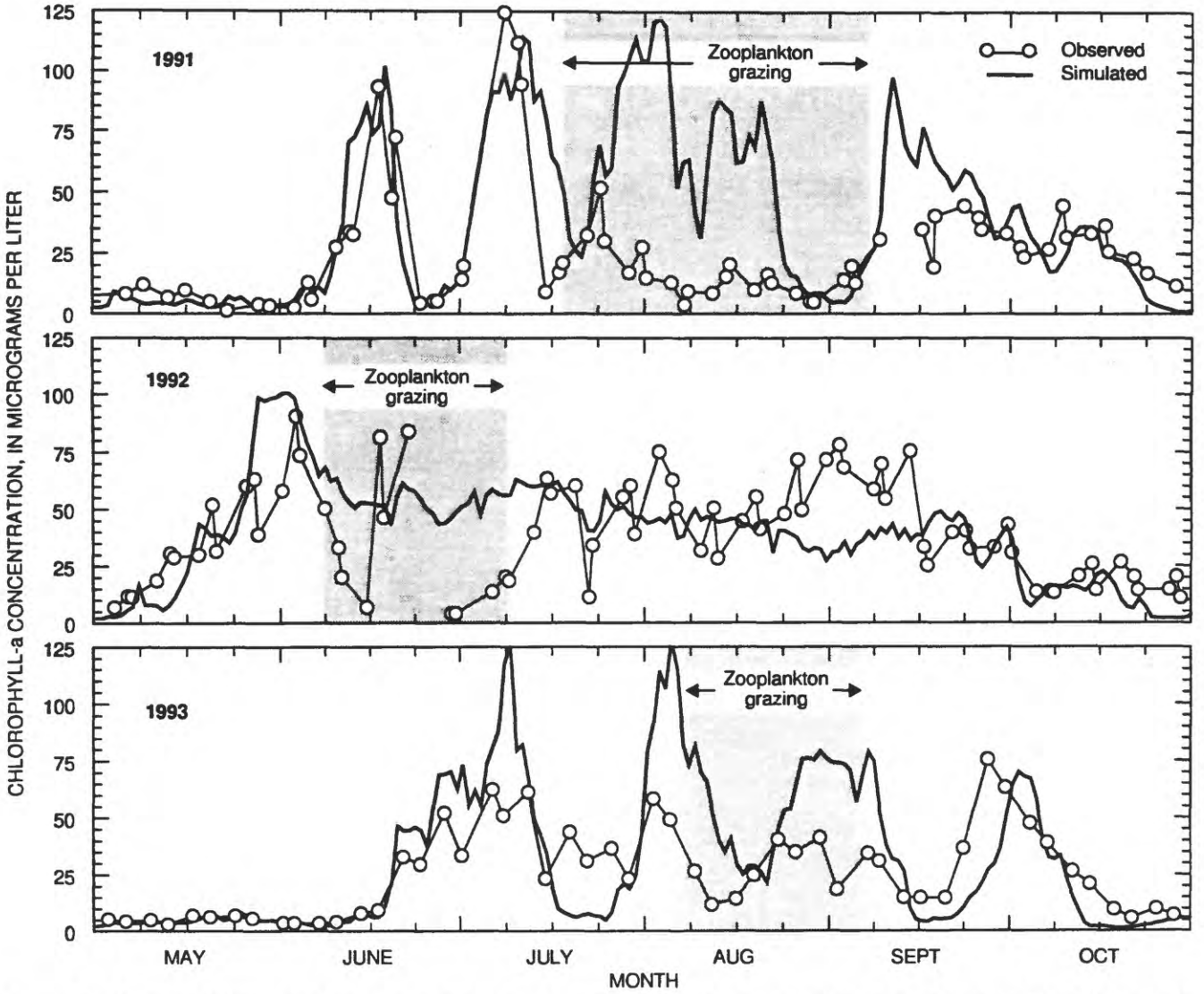

Figure 33. Measured chlorophyll-a concentration compared with the simulated concentration in the Tualatin River at river mile 5.5 (Stafford), May–October of 1991–93. (Shaded regions indicate time periods when measured zooplankton biomass concentration was greater than approximately 0.1 mg/L.)

productivity, suggests that the algal community has the capacity to adapt swiftly and to take advantage of a change in environmental conditions in a way that is not captured by the model algorithms. This particular time period serves as a reminder that much remains to be learned about the ecology of this river and that the modeling process often can provide an increased understanding of the system.

Following a water parcel downstream provides further insight into the sources and sinks that operate on the phytoplankton, and how the interaction of these processes ultimately results in a particular biomass concentration at the downstream boundary of the model grid. The model was used to track a water parcel through the model reach, starting from the upstream boundary on June 29 in 1991. Some inaccuracy is inherent to this exercise because horizontal and vertical mixing that normally would change the composition of the water parcel were not taken into account, but the inaccuracy should be tolerable since the purpose was to obtain approximate rates of gain or loss averaged over long stretches of the river. The water parcel reached RM 5.5 after about 7 days, at approximately the peak of the second algal bloom of 1991. The magnitude of the sources and sinks encountered along the way were calculated. The loading in pounds of algal C/day, averaged over six reaches, is plotted in figure 34 against the travel time from the upstream boundary. Little growth occurs through the first reach from RM 38.4 to RM 26.9 (about a day

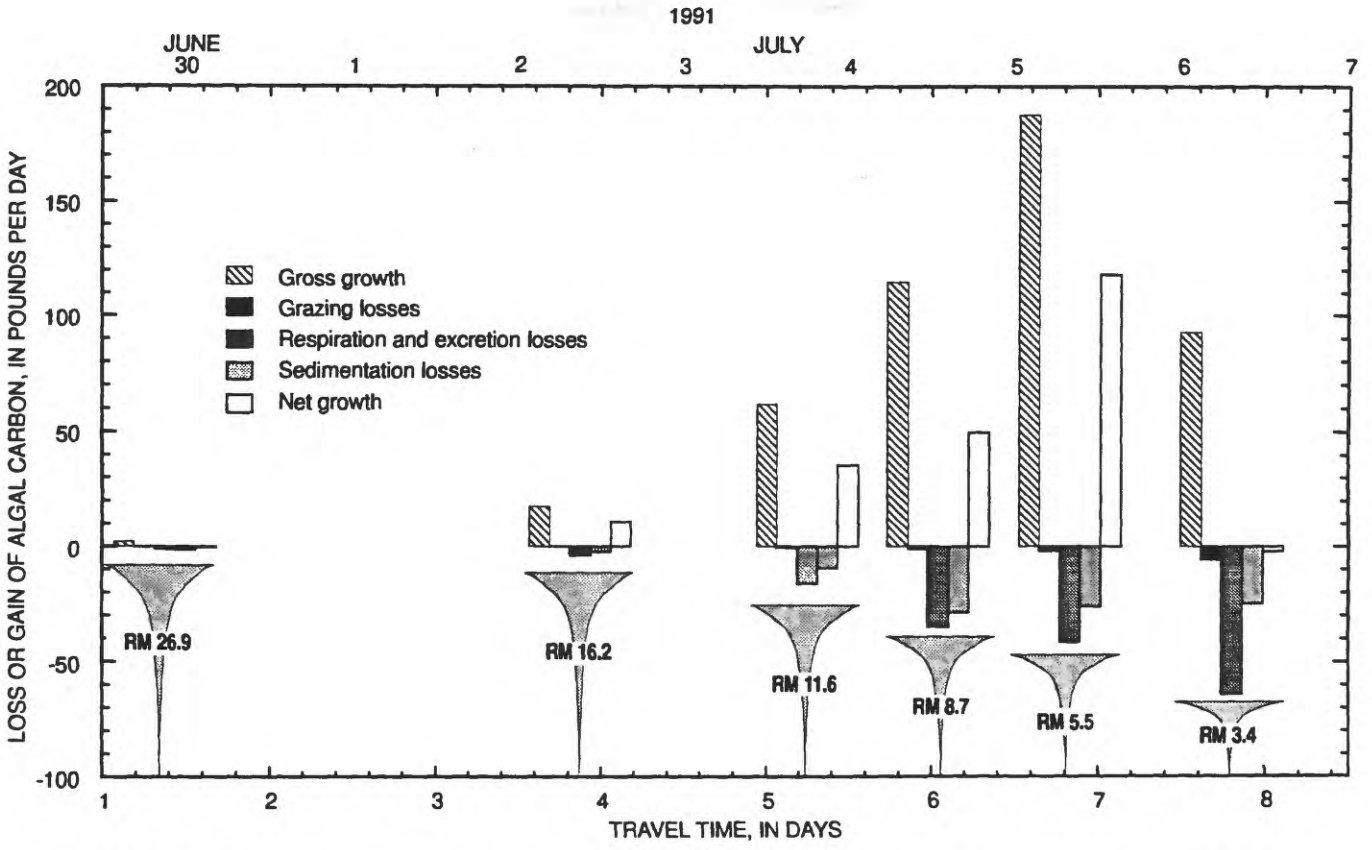

Figure 34. Simulated loss or gain of algal carbon through several reaches of the Tualatin River from river mile 38.4 to river mile 3.4 for a parcel of water released on June 29, 1991. (RM, river mile)

anda half of travel time); during this time the light conditions were not favorable for growth. Light conditions became favorable for growth around July 1, and remained so through July 9. Thus the algae in this parcel of water experienced positive net growth in the next reach between RM 26.9 and RM 16.2, with loss processes totaling about 39 percent of the gross growth; 59 percent of those losses were due to the combined processes of excretion and respiration, and 40 percent were due to sedimentation. Through the next three reaches, from RM 16.2 to RM 5.5, the algae experienced a dramatic increase in gross growth due to the combination of increased temperature, light, and a rapidly expanding population. Net growth is also positive and increases downstream. Total losses are 43, 57, and 37 percent of the gross growth through reaches 3, 4, and 5, respectively. As a percentage of the total losses, the contribution of sedimentation and respiration are fairly constant: 36, 44, and 38 percent for sedimentation, and 62, 54 and 59 percent for respiration in reaches 3, 4, and 5, respectively.

The final reach of the river included in the model grid, from RM 5.5 to RM 3.4, should be viewed with some caution since no observations of chlorophyll-a or nutrient concentrations were available at RM 3.4. It is believed, as stated above, that grazing losses in the model through this reach may be unrealistically high; however, the water parcel under consideration is not in the river during the 1991 grazing window. Grazing losses, therefore, are small—only about 6 percent of the total losses. During the grazing window, on the other hand, grazing losses can account for most of the total losses; a water parcel traveling through this reach from August 12 to August 14, for example, experiences total losses of 205 pounds of algal C/day, with grazing losses accounting for 59 percent of this total. Even without large grazing losses, and even though light conditions remain favorable, the algae in the water parcel experienced approximately zero net growth from RM 5.5 to RM 3.4. There is a significant increase in respiration losses, primarily because the deepest water in the river

is in this reach, and viable, respiring cells are distributed over the entire water column as they settle. The main reason that the algal population stabilizes through this reach, however, is a decrease in gross growth due to a limitation by low dissolved orthophosphate concentrations. The limiting concentrations in the model occur near the surface under stratified conditions, and would be difficult to establish from the observations, which are averaged over the upper 10 feet of the water column. It bears repeating that the model results in this last reach are somewhat speculative because there are no observations with which to compare near the downstream boundary of the grid.

Dissolved Oxygen

Dissolved oxygen is a nonconservative water-quality constituent; therefore, it is useful to precede the calibration results with a detailed description of the important sources and sinks of dissolved oxygen, as depicted by the model. The largest oxygen demands arising from bacterial metabolic activity are: allochthonous CBOD entering at the upstream boundary and tributaries (including the WWTPs) in the form of detrital organic matter; autochthonous CBOD produced within the model reach, primarily from the excretion of readily recycled organic material from viable cells; and SOD. Historically, instream nitrification of ammonia also was an important dissolved oxygen sink due to the large loads of ammonia discharged from the WWTPs. During this study period, however, the ammonia loads from the WWTPs were quite low (usually less than 100 pounds of ammonia-nitrogen per day), and ammonia nitrification was not an important DO sink. Such instream nitrification can be important at certain times of the year, particularly in late autumn (November) when ammonia wasteloads are higher (greater than 1000 pounds/day) and river discharge remains low (Kelly, 1996).

The rates of oxygen consumption by allochthonous CBOD, autochthonous CBOD, and SOD were calculated from the appropriate terms in the rate equation for dissolved oxygen during 1991, and the results at RM 5.5 are shown in figure 35. The seasonal average was also calculated at several points along the model reach and the results are shown in figure 36. Each type of demand dominates for short periods of time (days to weeks), but on a seasonally averaged basis the largest oxygen demand comes from the decay of the organic matter in the bed sediments. The SOD is also the most spatially and temporally consistent oxygen demand. The apparent variability in the volume-normalized SOD plotted in figure 36 is an artifact resulting from the geographic variations in the surface area to volume ratio of the model grid. When SOD is normalized to area rather than volume, it increases smoothly by about 25 percent from the upstream boundary to the downstream boundary, due mainly to the downstream increase in temperature. The variability in the time series of SOD at RM 5.5 (fig. 35) is also due to temperature effects on the rate of decay. The consistency in the SOD is by design, a result of the large accumulation of organic matter and the slow rate of decay that are inputs to the model (see the discussion in *Boundary Conditions, Reaction Rates, and Forcing Functions*). These inputs reflect the description of SOD that emerged from measurements made in the river at several stations and at different times of the year. One of the conclusions of that study was that the temperature-corrected SOD rate does not vary significantly over the summer season. As a result, the SOD primarily influences the concentration of dissolved oxygen on a seasonal, rather than daily or weekly, time scale.

Superimposed on the SOD is the allochthonous CBOD, which varies little through the model reach (fig. 36), but is characterized by strong temporal fluctuations that reflect the concentration of organic matter entering at the boundaries (fig. 35). Because the boundary conditions were determined by enforcing the total phosphorus constraint described in *Boundary Conditions, Reaction Rates, and Forcing Functions*, the fluctuations are, to a large extent, a manifestation of fluctuations in the total phosphorus concentration at the boundaries. The small increase at RM 9.3 in figure 36 is the result of large total phosphorus concentrations in the effluent from the Durham WWTP. Over most of the model reach, tributary loads and instream decomposition cause little change in the seasonally averaged allochthonous CBOD. The allochthonous CBOD is not allowed to settle in the model; it was found during the calibration that applying any significant settling velocity to the detrital organic matter entering at the upstream boundary quickly removed most of the CBOD in the shallow upper part of the model reach. This created difficulties in calibrating to the total phosphorus and nitrogen data, because significant amounts of these two nutrients were lost to the bed sediments between the upstream boundary and RM 26.9. Allowing this material to settle also resulted

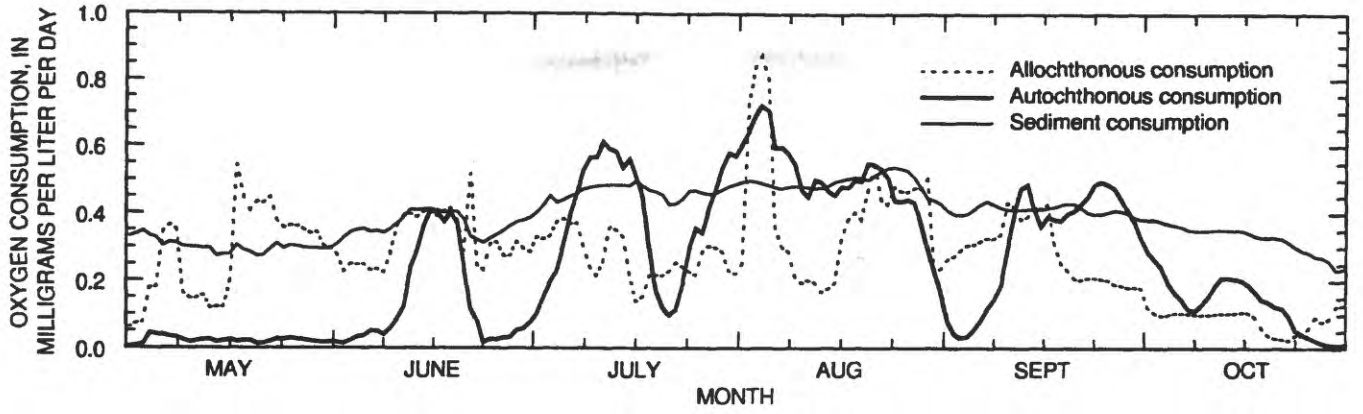

Figure 35. Simulated oxygen demands at river mile 5.5 (Stafford), May–October of 1991.

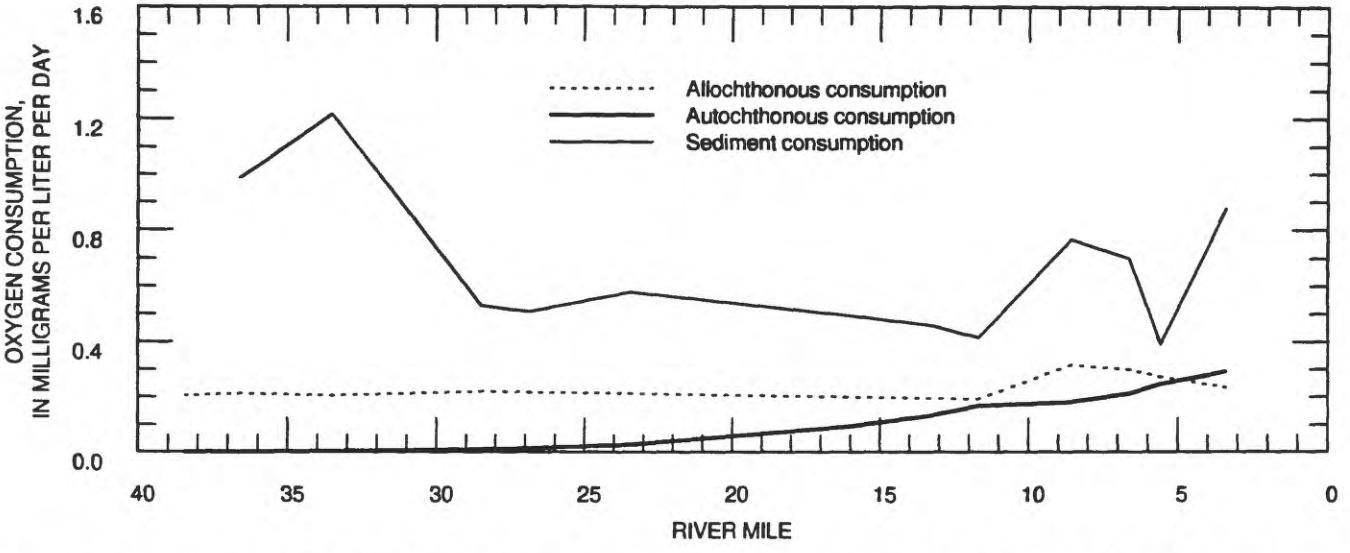

Figure 36. May–October mean of the simulated oxygen demands in the Tualatin River from river mile 38.4 to river mile 3.4, 1991.

in a relatively nonturbid water column through most of the model reach, which is in contrast to the fact that the lower Tualatin River has large concentrations of dissolved and suspended organic matter throughout its length. Therefore, the settling of allochthonous organic matter (ω_{dt}) was set to zero in the model in order to keep downstream concentrations of this constituent at a reasonable level. A large fraction of the organic material entering at the upstream boundary may be colloidal-sized particles such as organic macromolecules that do not settle, but it is likely that preventing the settling of the boundary detritus also compensates for unsimulated sources of organic material downstream, such as those directly from the riparian zone into the river.

The last important bacterially mediated component of the oxygen demand, the autochthonous CBOD, is significant only where algal growth occurs, primarily between RMs 16.2 and 3.4 (fig. 36). This CBOD is proportional to the phytoplankton biomass, and varies in time with the algal growth cycle (fig. 35). During algal blooms, this component of the CBOD dominates the other oxygen demands in the lower river miles.

Sources of DO include reaeration, point and nonpoint sources of water containing DO, and photosynthesis. Reaeration is not a particularly important source (or sink) for DO in the Tualatin River and is small compared to photosynthesis and inputs of oxygenated water. The slow rate of reaeration manifests

itself in the rather high degree of sub- and supersaturation of DO that is routinely observed. Inputs of oxygenated water can be important sources in some subreaches of the river, but only when those inputs are also important components of the water budget.

Downstream of RM 16.2, photosynthesis is by far the most important source of DO. Thriving algal cells under favorable light and nutrient conditions produce more dissolved oxygen through photosynthesis than they consume through the combined processes of respiration and the decay of excreted organic matter. Prolonged photosynthetic activity has another consequence, however; when it stops, respiration and the bacterial decay of cells continue to consume oxygen. Thus, a period of overcast weather that precipitates a "crash" of a large algal population can also precipitate a drop in dissolved oxygen. Photosynthetic production and the consumption of oxygen by respiration and autochthonous CBOD make the algae of primary importance in determining the dissolved oxygen concentration, particularly on the daily and weekly time scales that are typical of the algal growth cycle. It is not surprising, therefore, that the discussion of the dissolved oxygen calibration results is in large part parallel to the discussion of chlorophyll-a results. The same bloom cycle is apparent in the observations of chlorophyll-a at both RM 16.2 and RM 5.5 (figs. 31 and 33) and in the observations of dissolved oxygen (figs. 37 and 38). The daily range in dissolved oxygen computed by the model is indicated in figure 38 so that the noon value can be compared with the maximum and minimum for the day. In general, where the model overestimates the chlorophyll-a at the peaks of blooms, it overestimates the dissolved oxygen as well.

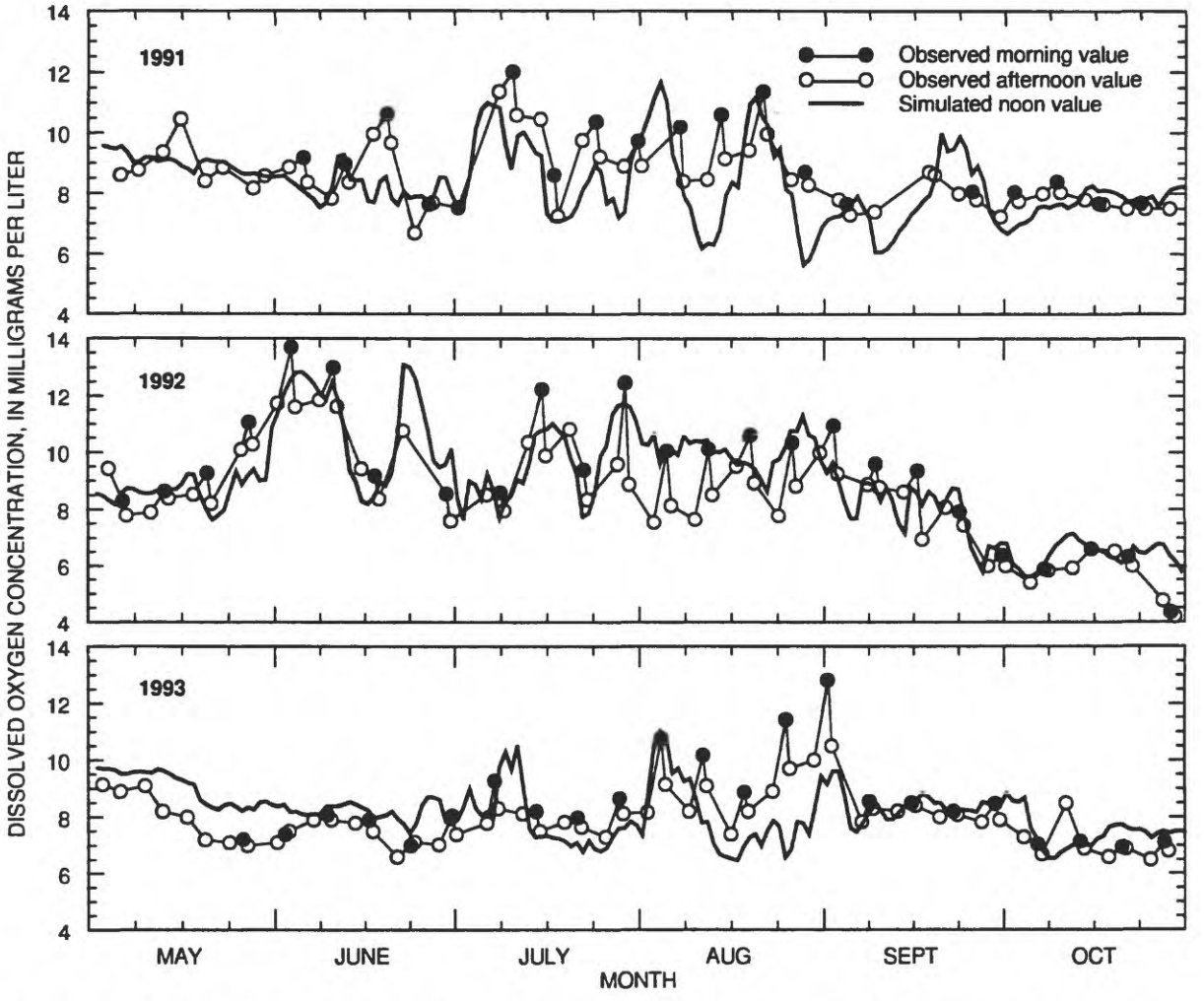

Figure 37. Comparison of observed dissolved oxygen concentration with the simulated concentration in the Tualatin River at river mile 16.2 (Elsner), May–October of 1991–93.

The converse is also true. A statistical analysis confirms that the difference between modeled and observed chlorophyll-a at RM 16.2 is significantly correlated ($p<.01$) with the difference between modeled and observed dissolved oxygen. The correlation coefficients are 0.59 for 1991 data, 0.50 for 1992 data, and 0.79 for 1993 data. Therefore, most of the discrepancy between the observed and modeled dissolved oxygen data can be attributed to the periodic failure of the model to accurately simulate the amount of algal biomass in the water column, especially at the peaks of blooms in the lower reaches of the river.

A calculation of the source and sink terms for dissolved oxygen for the same water parcel used to generate figure 34 underscores the relative importance of the various processes (fig. 39). The most consistent loss of dissolved oxygen is caused by SOD, which increases only slightly due to increasing temperature as the parcel moves downstream. The effects of allochthonous and autochthonous CBOD are combined in this plot, and the sum increases markedly as the parcel travels downstream. This combined CBOD, due in large part from the rapid decay of organic matter excreted from algal cells, becomes large enough to exceed the SOD in the lower river miles because the parcel encounters favorable growing conditions. The photosynthetic production of oxygen during this bloom period is prominent. Through the reach from RM 16.2 to the Oswego diversion dam (RM 3.4), the photosynthetic production of oxygen more than compensates for the various sinks, and the net effect is an increase in the DO concentration. Figure 39 also shows the relative importance of reaeration and the contribution of point and nonpoint sources.

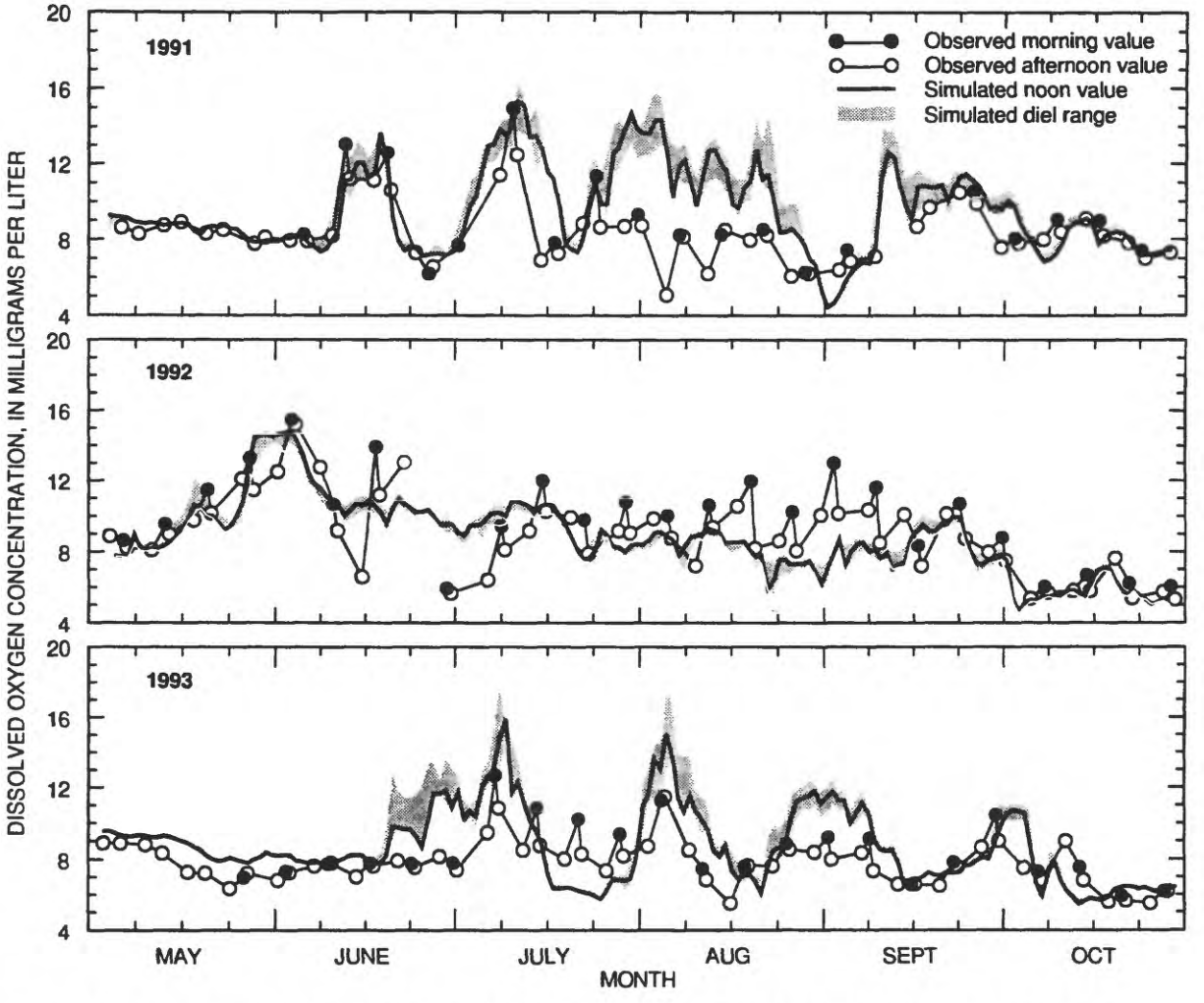

Figure 38. Comparison of observed dissolved oxygen concentration with the simulated concentration in the Tualatin River at river mile 5.5 (Stafford), May–October of 1991–93.

Reaeration is most effective in the reach from RM 38.4 to RM 26.9 where velocities are highest, but acts to decrease dissolved oxygen in the lower river miles, where photosynthetic production makes the water supersaturated with DO. Contributions of dissolved oxygen from small tributaries is generally small but positive from RM 26.9 to RM 16.2 and from RM 5.5 to RM 3.4. Contributions from the WWTPs dominate the point sources to the reach from RM 38.4 to RM 26.9 and from RM 16.2 to RM 5.5, and are significant inputs of dissolved oxygen to the river.

It is important to distinguish between the daily to weekly effect of algae on dissolved oxygen and their net *seasonal* effect. The algae clearly act to increase the dissolved oxygen concentration when they are growing and decrease it when they are in decline, but the magnitude of the increase or decrease is limited by residence time. The size of a bloom under continuously favorable light conditions is limited by the travel time between RM 16.2 and the Oswego diversion dam (RM 3.4), which usually does not exceed 9 days, even during low flows. Conversely, when light conditions become unfavorable for algal growth, the extent of oxygen depletion is also limited by travel time, since dead and respiring algal cells will eventually be advected out of the system. Dead algal cells that settle to the sediments continue to consume oxygen as they decay, but this does not significantly augment the high "background" SOD in the Tualatin River on short time scales. The *duration* of a bloom, however, is not limited by travel time, but only by the duration of favorable light, temperature, and nutrient conditions. Nutrient concentrations, by themselves, did not prevent the initiation of any phytoplankton blooms in this river during the study period. As a result, the effect of phytoplankton on the seasonal average of dissolved oxygen in the Tualatin River is largely a consequence of western Oregon's summer weather, which is characterized by favorable light conditions that often last for weeks at a time. The number of days that the algae are net producers of oxygen exceeds the number of days that they are net consumers; consequently, the seasonally averaged concentration of dissolved oxygen between RM 16.2 and the

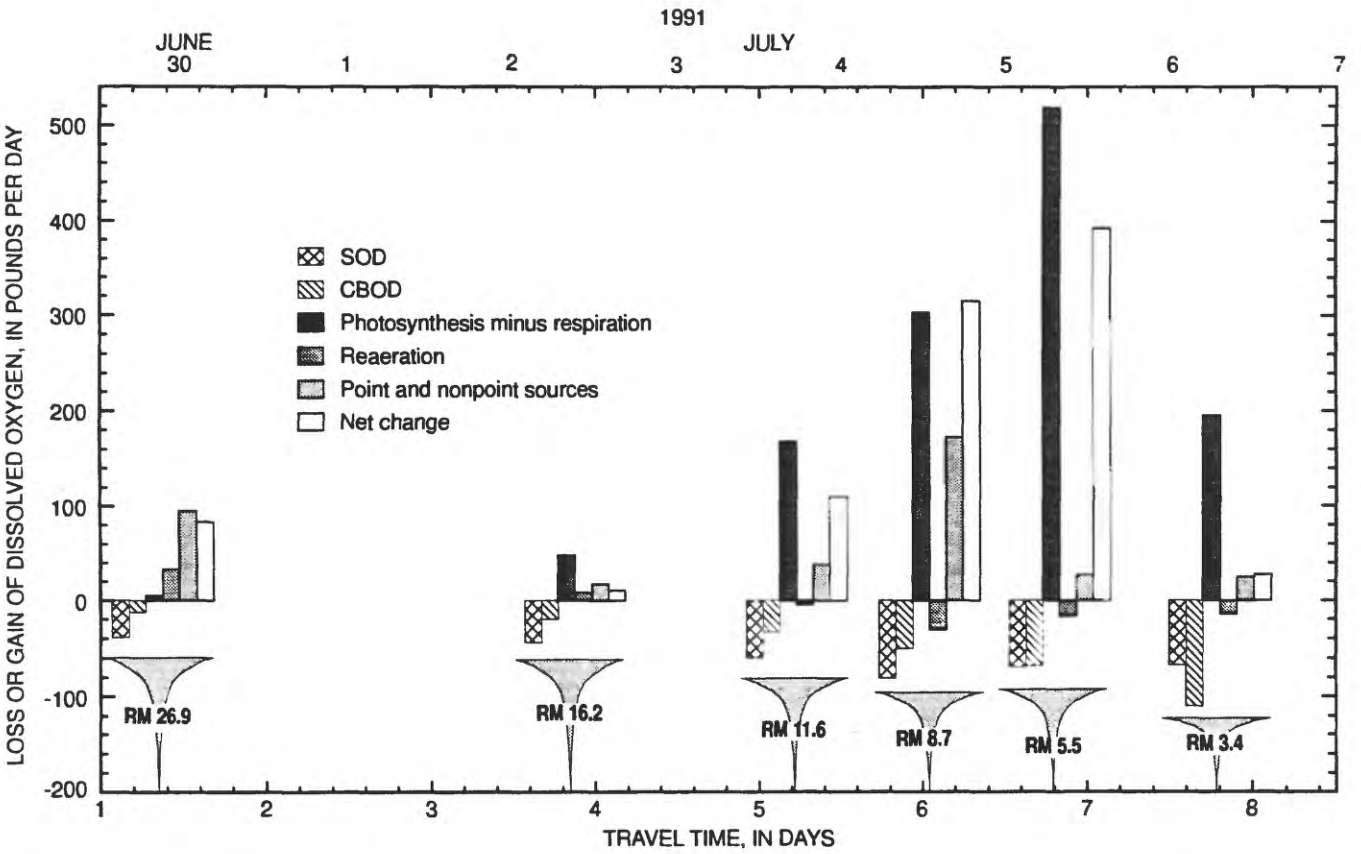

Figure 39. Simulated loss or gain of dissolved oxygen through several reaches of the Tualatin River from river mile 38.4 to river mile 3.4 for a parcel of water released on June 29, 1991. (RM, river mile)

Oswego diversion dam (RM 3.4) is increased over what it would be in the absence of primary production. A corollary is that if primary production were reduced, the SOD and allochthonous CBOD would remain largely unchanged, at least in the short term, and the seasonally averaged concentration of dissolved oxygen between RM 16.2 and the Oswego diversion dam would likely decrease. This is an important point to remember when interpreting management strategies for the river.

Phosphorus

Examination of the boundary inputs to the model reach shows that no source of phosphorus in the 1991 to 1993 summer periods can be singled out as vastly more important than any other. Averaged over the entire season, in 1991 and 1993, comparable fractions of the total input of phosphorus to the model reach came from the WWTPs and from the upstream boundary at RM 38.4 (table 11); the next biggest source was the tributaries, and the smallest, but still significant, source was nonpoint inputs. Much of the phosphorus in the tributaries, the upstream boundary, and the nonpoint sources originates from local and regional ground-water discharge that is rich in phosphorus (Rounds and others, U.S. Geological Survey, unpub. data, 1993). In 1992, when the WWTPs were generally operating at peak phosphorus-removal efficiency, the WWTPs became the smallest of the four sources, although still significant. The reduction in the proportion of phosphorus from the WWTPs in 1992 resulted in a reduction in the seasonally averaged concentration of total phosphorus in the model reach; however, the reduction was only significant downstream of the Durham WWTP at RM 9.3 (fig. 40). Each of these inputs of phosphorus is applied in the model as a time-dependent boundary condition. These boundary conditions, and the *net* transfer of phosphorus across the sediment/water interface, determine the total phosphorus concentration in the water column (fig. 40).

Table 11. Percentage of the total input of phosphorus to the model reach from various sources
[WWTPs, wastewater-treatment plants]

	Source			
Season	WWTPs	Upstream boundary	Tributaries	Nonpoint sources
1991	32	36	21	11
1992	8	48	25	19
1993	37	39	16	8

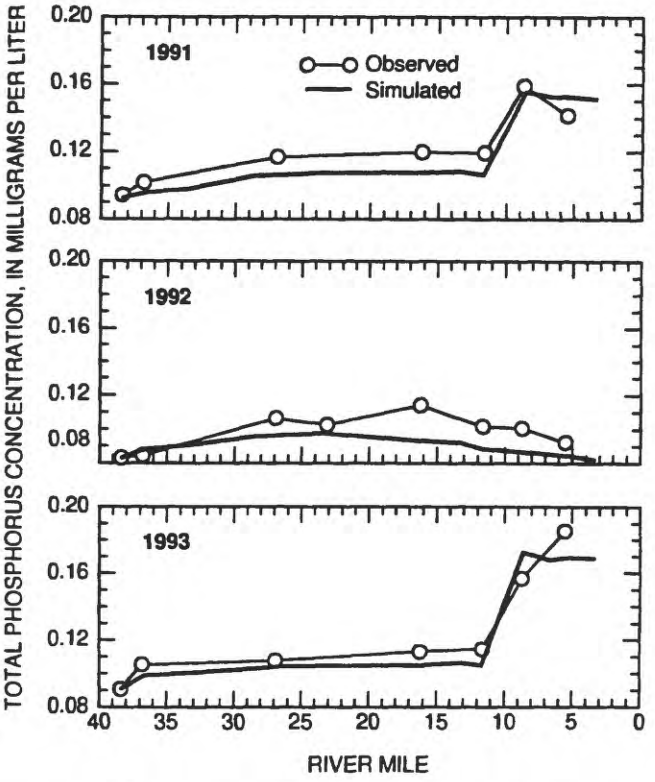

Figure 40. Comparison of the May–October mean of measured total phosphorus concentration with the simulated concentration in the Tualatin River from river mile 38.4 to river mile 3.4, 1991–93.

The net transfer across the sediment/water interface has three components: the nonpoint inputs, the release of phosphorus to the water column by decay of organic matter in the sediments, and sedimentation. The model simulation of these processes on a seasonally averaged basis is plotted as a function of river mile for 1991 in figure 41. In this figure, the total load of phosphorus from the sediments to the water column is separated into the contribution from the nonpoint source and the contribution proportional to sediment decay. The sedimentation load from the water column to the sediments is also shown. In principle, all three of these components of the net load are interdependent, but in this application that interdependence is minimal because (a) the sediment decay rate is nearly constant and therefore somewhat decoupled from the sedimentation rate, and (b) the algae are not severely phosphorus-limited, so nonpoint inputs of orthophosphate do not significantly affect the sedimentation rate.

Because the sedimentation of phosphorus is established by the settling velocity of algal cells and detritus, and because the nonpoint source of

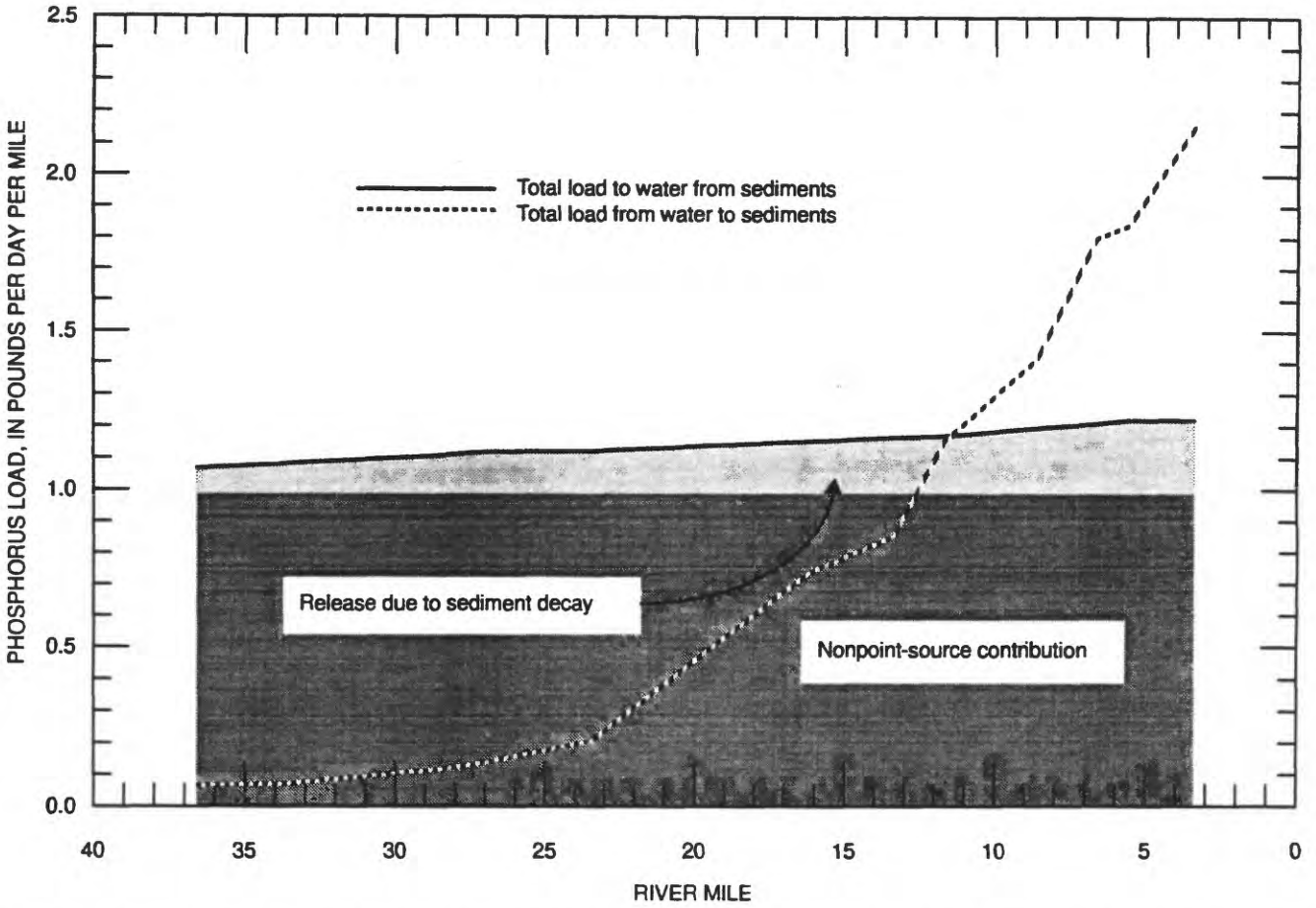

Figure 41. May–October mean of simulated phosphorus loads to the bed sediments from river mile 38.4 to river mile 3.4 in the Tualatin River, 1991.

phosphorus to the water column was defined as a boundary condition, 2 of the 3 components of the net transfer of phosphorus across the sediment/water interface are constrained by considerations other than a direct calibration with the phosphorus data. It was necessary, therefore, to calibrate the third component, the release of phosphorus from the sediments as a result of organic -matter decay, with the use of a parameter that would allow the *net* load of phosphorus from the sediments to be calculated correctly. This parameter, f_P, is the fraction of phosphorus stored in organic matter that is not released when that organic matter decays, and has more than one plausible interpretation. It could quantify the capacity of the oxidized surface of the bed sediments to retain phosphorus by adsorption to ferric oxyhydroxides or by incorporation into tissue of the microbial population. Alternatively, f_P could compensate for an overestimated nonpoint contribution of phosphorus; this remains a possibility even though the groundwater load to the river is believed to be specified conservatively (see *Boundary Conditions, Reaction Rates, and Forcing Functions*). It is also possible that the detrital material that makes up the greater part of the sediment organic matter is not as enriched in phosphorus as is the algal biomass (recall that the model uses a fixed stoichiometry for all organic matter). In this case, f_P adjusts for an overestimate of the amount of phosphorus incorporated into the sediment organic matter. The net transfer of phosphorus across the sediment/water interface can be calibrated correctly using f_P, but this net transfer in no way depends on knowing the appropriate interpretation of f_P. Similarly, the uncertainty in the meaning of f_P does not affect the interpretation of any management scenarios, because the release of phosphorus from the sediments is not subject to anthropogenic manipulation, regardless of the mechanisms involved.

The mechanistic interpretation of f_P is not the only, or even the greatest, uncertainty in accurately describing the transfer of phosphorus across the

sediment/water interface. In all likelihood, no *single* interpretation of f_P is correct because the bed sediments are highly heterogeneous. For example, measurements of ground-water seepage were sparse, but nonetheless clearly indicated that regional ground water, characterized by very high orthophosphate concentrations, discharges directly to the river (Rounds and others, U.S. Geological Survey, unpub. data, 1993). This ground water probably enters the river at localized areas where the river bottom intercepts a geologic stratum that is relatively transmissive. The localized discharge of high-phosphorus ground water implies that some of the sediments must be sorptively saturated with respect to phosphorus; on the other hand, nearby sediments may retain some of the phosphorus released as the organic matter in the sediments decays. This capacity of the sediments to retain phosphorus is usually attributed to adsorption of the phosphate ion by ferric oxyhydroxides in the oxidized surface layer of the sediments, implying that the ability of the sediments to limit the flux of phosphorus across the sediment/water interface is directly related to the number of available sorption sites (Jensen and others, 1992). It is clear that even if the *mechanisms* involved in the transfer of phosphorus across the sediment/water interface were better known, field measurements could not resolve the spatial variability of sediment characteristics on the scale of tens of meters. Therefore, some parameterization of this net transfer would probably be required for that reason alone.

Modeled total phosphorus concentrations are slightly lower, on a seasonally averaged basis, than those observed in the river (fig. 40). Modeled orthophosphate concentrations tend to be slightly higher on a seasonally averaged basis than those observed (fig. 42), although this discrepancy is limited to 1991 and 1993, and is weighted toward the downstream end of the model reach. Higher-than-observed model orthophosphate and lower-than-observed model total phosphorus concentrations are due to the choice of f_P. That parameter was chosen such that orthophosphate concentrations matched the observations closely, particularly in the upper part of the model reach where the algal population begins to grow. The increasing disparity between modeled and observed orthophosphate with distance downstream in 1991 and 1993 can be explained in large part by corresponding discrepancies in chlorophyll-a, as discussed below. The model does not account for all of the forms of phosphorus in the river, and the gap between modeled and observed total

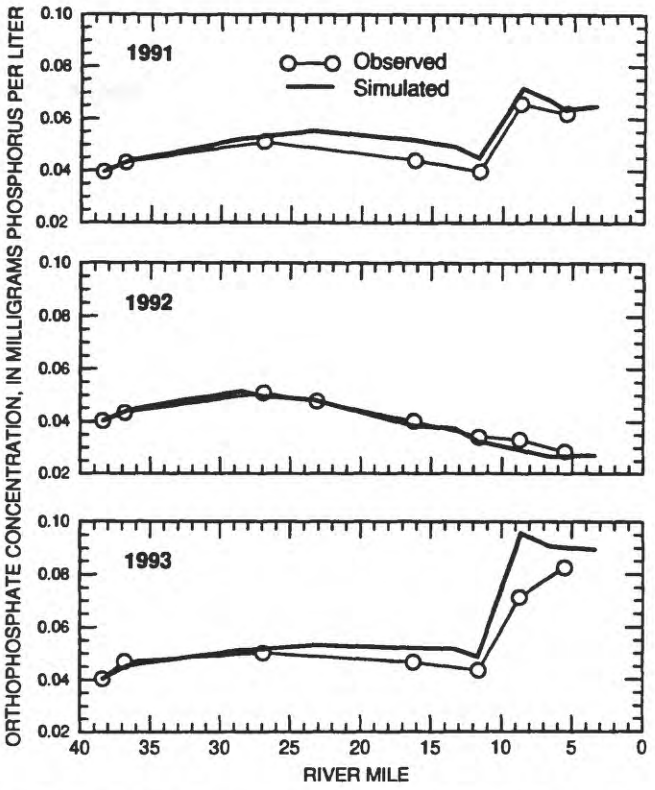

Figure 42. Comparison of the May–October mean of measured soluble orthophosphate concentration with the simulated concentration in the Tualatin River from river mile 38.4 to river mile 3.4, 1991–93.

phosphorus might be explained by the presence of a substantial colloidal fraction. On a seasonally averaged basis, this gap represents about 10 percent of the observed total phosphorus, which is similar in magnitude to measurements made in the Tualatin by Mayer (1995). The implications of a colloidal fraction depend on its bioavailability. A highly inert fraction implies an increase in total phosphorus with little or no effect on the cycling of orthophosphate. On the other hand, if the colloidal phosphorus is easily converted to a bioavailable form, then, to the extent that the algae are phosphorus-limited, that fraction would supply more nutrients for growth and the phytoplankton dynamics would change.

Through most of the model reach, the discrepancies between modeled and observed orthophosphate can be explained in large part by (1) the discrepancies between modeled and observed total phosphorus, and (2) the discrepancies between modeled and observed chlorophyll-a. The relation between these discrepancies can be quantified with the use of correlation analysis, the results of which are shown in table 12.

Table 12. Correlation coefficients between modeled minus observed values of orthophosphate, total phosphorus, and chlorophyll-a

[RM, river mile. *, four data points were removed from the observed data at RM 5.5 for 1992. Light shading indicates statistical significance at the 99 percent confidence level ($p<0.01$); dark shading indicates statistical significance at the 95 confidence level ($p<0.05$)]

Season	Δ{orthophosphate}, Δ{chlorophyll-a}		Δ{orthophosphate}, Δ{total phosphorus}		Δ{total phosphorus}, Δ{chlorophyll-a}	
	RM 16.2	RM 5.5	RM 16.2	RM 5.5	RM 16.2	RM 5.5
1991					-0.01	-0.18
1992				.28*	-.09	-.01*
1993				.11	-.01	.09

At RM 16.2, the difference between the modeled and observed orthophosphate concentration, denoted Δ{orthophosphate}, is negatively and significantly correlated with Δ{chlorophyll-a}, implying that there is some direct trade-off in the water column between the phosphorus contained in algal cells and that in the form of orthophosphate. At several times during all 3 years, an overestimate in chlorophyll-a at RM 16.2 (fig. 31) is correlated with an underestimate of orthophosphate (fig. 43). The correlation between these two quantities remains highly significant at RM 5.5. The correlation between Δ{total phosphorus} and Δ{chlorophyll-a}, however, is not significant at either RM 16.2 or RM 5.5; therefore, the interdependence between chlorophyll-a and orthophosphate does not affect the cycling of total phosphorus.

The other major contributor to the discrepancy between modeled and observed orthophosphate is the fact that the model did not simulate total phosphorus with complete accuracy, as evidenced by the positive and significant correlation between Δ{orthophosphate} and Δ{total phosphorus} at RM 16.2. This correlation breaks down somewhat at RM 5.5. The potential problem with aliasing in the observations downstream of the Durham WWTP has already been noted, and it is possible that such aliasing negatively affects the correlation between these two quantities at RM 5.5. Total phosphorus concentrations in the model are largely decoupled from algal growth, being determined by the upstream boundary condition, point inputs from tributaries and WWTPs, and the net load from or through the bottom sediments. Discrepancies between modeled and observed total phosphorus concentration (fig. 44) can largely be attributed to these factors and to the inherent error in the measured values (± 20 percent). Spikes in the observed total phosphorus concentration may be due to laboratory error or to an isolated and unmeasured input, such as might occur when a detention pond is drained.

The most uncertain phosphorus boundary condition is the nonpoint-source loading. It should be kept in mind that errors in this boundary condition, in particular in the contribution of regional ground water (which is high in phosphorus), can have a significant effect on the total phosphorus budget. This contribution was set at a maximum discharge of 2 ft^3/s in all 3 years and does not contain any seasonal or interannual variability. It is reasonable to assume that the regional ground-water discharge does not respond to short-term forcings. Therefore, large short-term fluctuations in the regional discharge are unlikely. Variability in the regional ground-water discharge is most likely to manifest itself on a seasonal or interannual basis; therefore, discrepancies between simulated and observed data on the scale of days to months are probably due to other factors.

The period between July 23 and September 1 in 1992 is notable because modeled total phosphorus concentrations are substantially lower than observed, and reach the lowest values of the entire 18 months of simulations (fig. 44). Modeled concentrations of orthophosphate (fig. 43) during this time are also lower than observed and are in the algal-growth-limiting range (recall that the Michaelis-Menten half-saturation constant for phosphorus was set at 0.005 mg/L). The lower-than-observed modeled phosphorus concentrations are clearly evident at RM 16.2, even though the effect of this phosphorus limitation on modeled algal growth is not evident until RM 5.5. This is the only time period during the entire 18 months of simulations when the model's difficulty in simulating algal growth correctly is directly attributable to an inaccuracy in simulated phosphorus concentrations.

The reason that the model underestimates phosphorus concentrations during this time period is not completely clear, but the fact that this time period was characterized by very low flows and prolonged sunny weather may be relevant. Stratification in the lower reach of the river was more severe than usual, and there were very high concentrations of total phosphorus and orthophosphate in an anoxic hypolimnion in

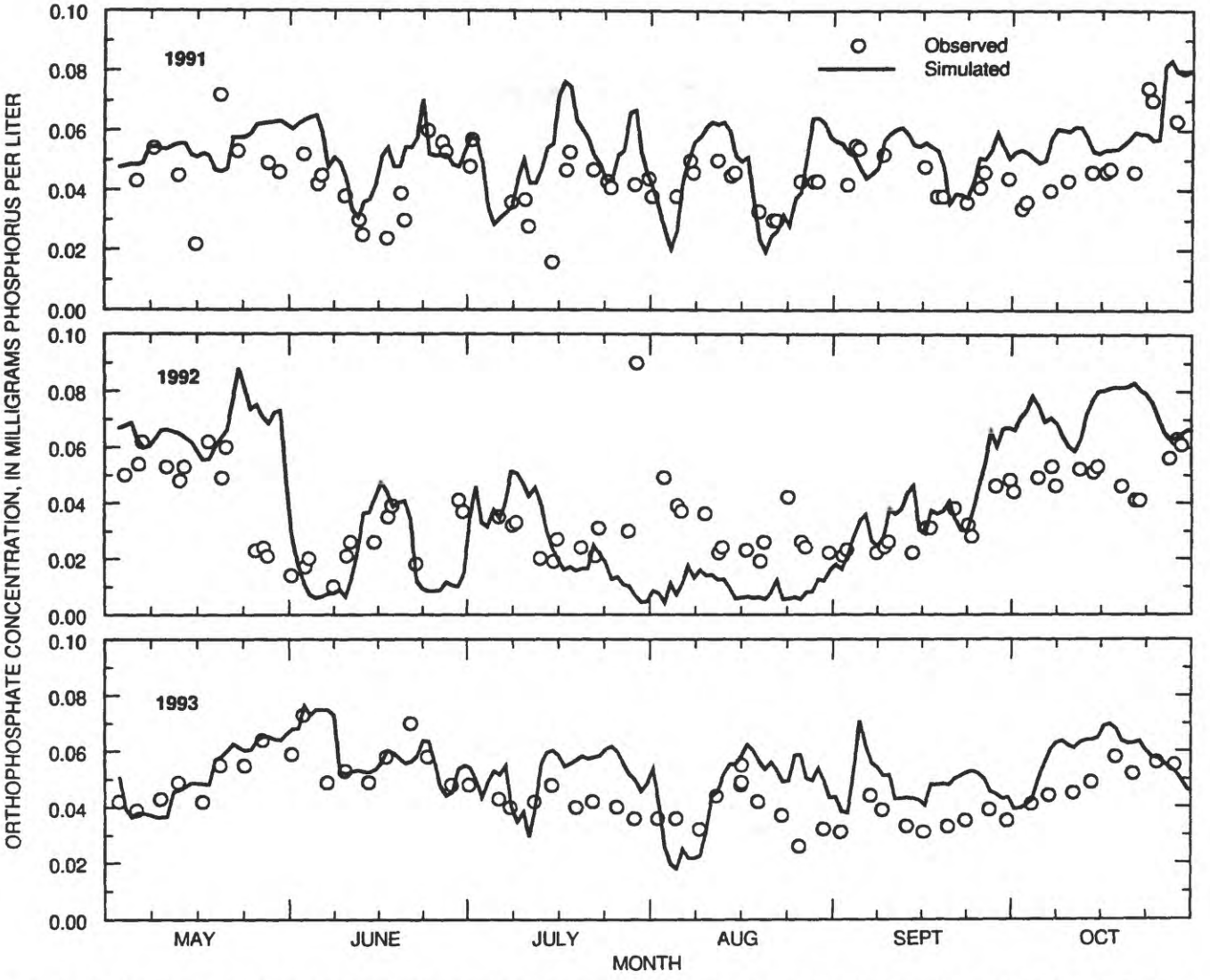

Figure 43. Measured soluble orthophosphate concentration compared with the simulated concentration in the Tualatin River at river mile 16.2 (Elsner), May–October of 1991–93.

several deep parts of the river. On July 20, for example, concentrations of total phosphorus and orthophosphate of 1.9 and 1.8 mg/L, respectively, were measured at RM 5.5 at a depth of 18 feet where there was no detectable dissolved oxygen (Doyle and Caldwell, 1996). At RM 4.0, concentrations of total phosphorus and orthophosphate were 1.6 and 0.3 mg/L, respectively, at a depth of 21 feet where there was no detectable dissolved oxygen; at a depth of 6 feet where dissolved oxygen was measured at 6.3 mg/L, the phosphorus concentrations were 0.04 and 0.01 mg/L, respectively.

These measurements reinforce the well-known fact that sustained reducing conditions at the sediment/water interface result in a release of phosphorus that was previously adsorbed onto an oxidized sediment surface layer. Except for some limited transient mixing that would continuously entrain some hypolimnetic phosphorus into the mixed surface layer, this phosphorus would remain trapped in the anoxic hypolimnion until the water column turns over, creating a strong vertical gradient in concentration. The observed temperature profile data confirm that the water column was stratified during this time at RM 5.5 and did not turn over completely for several weeks. The mechanism for sediment phosphorus release under anoxic conditions is not included in this application of CE-QUAL-W2, and its absence should create small discrepancies between simulated and observed phosphorus concentrations, but only downstream of those reaches that tend to stratify and produce significant regions of anoxic hypolimnetic water—between

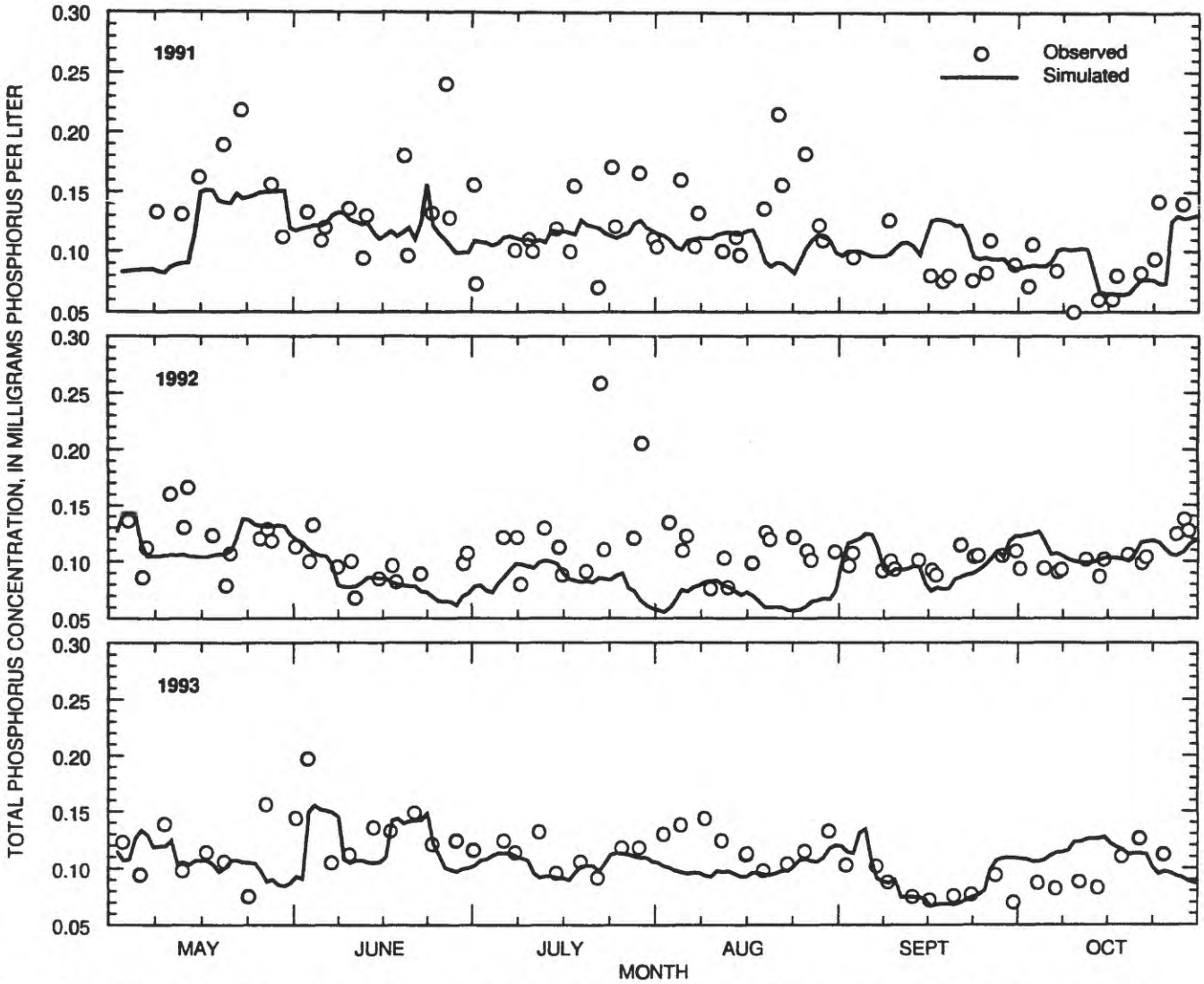

Figure 44. Measured total phosphorus concentration compared with the simulated concentration in the Tualatin River at river mile 16.2 (Elsner), May–October of 1991–93.

RMs 6.5 and 3.4, for the most part. The discrepancy between observed and simulated phosphorus concentrations, however, is apparent upstream of those reaches, even at RM 26.9 where the water column is shallower, any temperature gradients set up during the day are removed at night, and advectively isolated deep pools are not present. It is unlikely, therefore, that the hypolimnetic release of phosphorus is the mechanism responsible for the observed concentrations that are higher than modeled concentrations from July 23 to September 1, 1992.

If sediment phosphorus release under reducing conditions is to explain why modeled phosphorus concentrations are very low during this time period, then reducing conditions must be possible even in a shallow, unstratified water column. This may be possible if oxygen is rapidly depleted in a thin layer of water near the sediment/water interface and flows are so slow that the interface is only sporadically reoxygenated. Phosphorus released in this manner would mix more-or-less continuously with the rest of the water column, rather than be confined to a hypolimnion and released abruptly when the water column turned over. The warmer temperatures and lower flows of mid-1992 might provide conditions that enable this process to an extent not normally seen. Unaccounted-for losses in nitrate during this same time period provide additional evidence that reducing conditions are present, although denitrification does not necessarily have to occur in the sediments, as discussed below. Without further investigation of the sediment/water interface, however, this discussion remains speculative.

Nitrogen

Ammonia and nitrate-plus-nitrite nitrogen in the Tualatin River behave more like conservative substances than phosphorus, and are largely a reflection of the boundary inputs upstream (the main stem at RM 38.4 and the WWTPs at RMs 38.1 and 9.3). The combined total of ammonia and nitrate-plus-nitrite nitrogen in the river is well above concentrations that limit algal growth. Algal uptake does affect ammonia concentrations somewhat, but nitrate concentrations are large enough that algal uptake has little effect. In contrast to the phosphorus budget, a single source can be identified as dominant in the nitrogen budget. The primary sources of nitrogen to the model reach, averaged over the May through October season, are the WWTPs that account for well over half of the total input (table 13).

Table 13. Percentage of the total input of nitrogen to the model reach from various sources
[WWTPs, wastewater-treatment plants]

Season	Source			
	WWTPs	Upstream boundary	Tributaries	Nonpoint sources
1991	67	22.5	10	0.5
1992	79	14	6	1
1993	57	31.5	11	.5

The nitrogen inputs from the WWTPs result in abrupt concentration increases on plots of the seasonal averages of the various nitrogen constituents against river mile (figs. 45 and 46), but otherwise the spatial variation is minimal. Large inputs of ammonia from the Durham WWTP (RM 9.3) as a consequence of planned changes in operation are clearly evident in 1991 and 1993; in contrast, nitrification was able to remove nearly all the ammonia from the effluent in 1992. The effect of Rock Creek WWTP effluent (RM 38.1), which does not contribute greatly to ammonia-N in the river, can clearly be seen in the plots of nitrate-N (fig. 46). An abrupt increase in nitrate-N due to effluent from the Durham WWTP also can be seen at RM 9.3; this increase is larger in 1992 when more efficient nitrification in the WWTP converted ammonia-nitrogen to nitrate-nitrogen.

The time series of ammonia concentration at RM 5.5 (fig. 47) reflects primarily the load of ammonia from the Durham WWTP. Concentrations of ammonia downstream of the plant were much higher during most of 1991 and during August and September of 1993 than in 1992 due to interruptions in treatment at the plant.

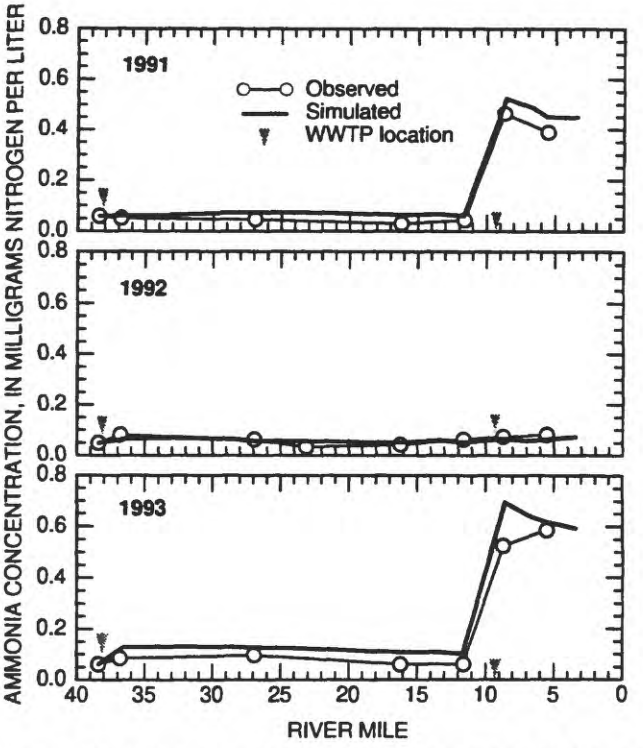

Figure 45. Comparison of the May–October mean of observed ammonia concentration with the simulated concentration in the Tualatin River from river mile 38.4 to river mile 3.4, 1991–93. (WWTP, wastewater-treatment plant)

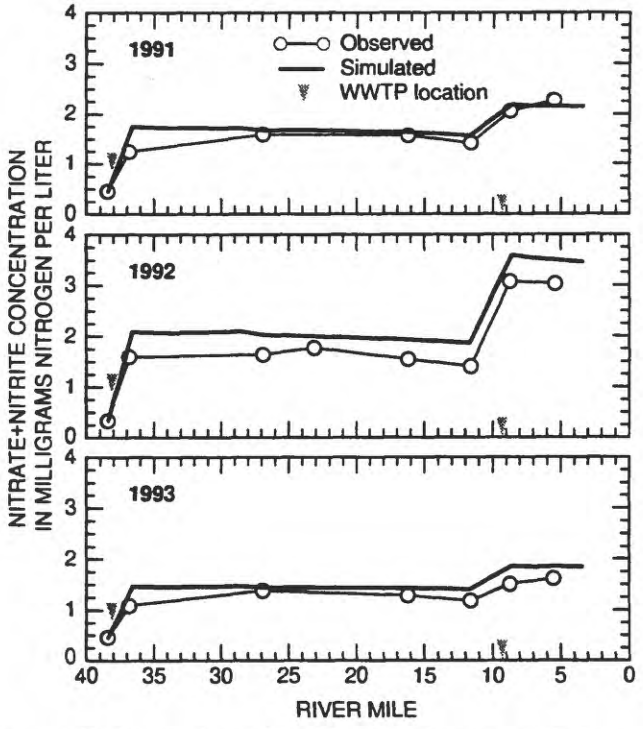

Figure 46. Comparison of the May–October mean of observed nitrate-plus-nitrite concentration with the simulated concentration in the Tualatin River from river mile 38.4 to river mile 3.4, 1991–93. (WWTP, wastewater-treatment plant)

The highest instream ammonia concentrations attained during 1991 and 1993, however, still did not result in significant nitrification in the river. Nitrification does become important, especially in the upper, shallower reach of the river, when concentrations comparable to those in September of 1993 are sustained long enough for a large population of nitrifying bacteria to develop, which can occur frequently in November (Kelly, 1996). Overall, the simulation of ammonia concentrations is good.

Nitrate concentrations (fig. 48) are the result of a combination of inputs, including the upstream boundary, the two WWTPs, and tributaries. Overall, the model does a good job of simulating the nitrate concentration, although for an extended period in 1992 and a shorter period in 1993, model concentrations are noticeably higher than observed concentrations. This is curious because the model generally does an excellent job of simulating conservative quantities, and nitrate, at the concentrations found in the Tualatin River, should be nearly conservative unless reducing conditions are encountered. Nonetheless, starting on July 23, 1992, modeled nitrate concentrations diverge from observed concentrations and are higher with such consistency that a sink of nitrate not included in the model is suggested. The period between July 23 and September 1, 1992, is particularly notable because during this time simulated phosphorus concentrations are low compared with observed values, as discussed previously. The nitrate data provide further evidence

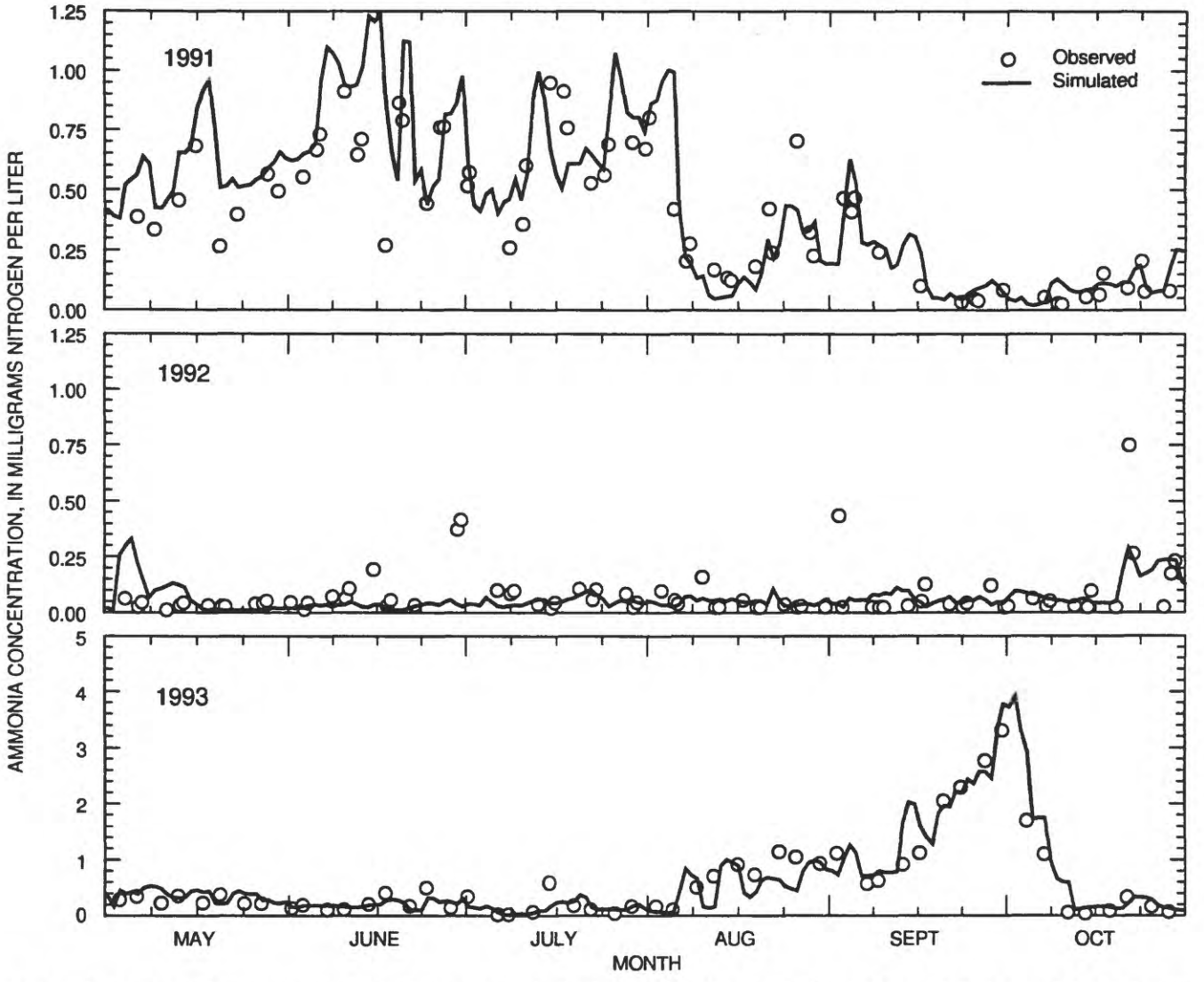

Figure 47. Measured ammonia concentration compared with the simulated concentration in the Tualatin River at river mile 5.5 (Stafford), May–October of 1991–93.

that reducing conditions may have been present at the sediment/water interface during this extremely warm, low-flow period, and that denitrification, a process not simulated by the model, may have occurred. The gap between simulated and observed nitrate concentration is apparent at RM 26.9, implying that significant denitrification must be occurring between the Rock Creek WWTP and that station.

The flux of nitrogen across the sediment/water interface through sedimentation and the decomposition of sediment organic matter is a much smaller percentage of the total nitrogen budget in comparison to phosphorus, for which these loadings play a major role. It was determined during the calibration process and from a review of the literature (Bowie and others, 1985), however, that the nitrogen released to the water column from the decay of sediment organic matter needed to be in the form of nitrate rather than ammonia. The amount of nitrogen entering the water column through this pathway is small relative to point sources. However, because water-column concentrations of ammonia are low, even small releases of ammonia from decaying organic matter resulted in modeled concentrations that were about twice as high as observed concentrations. Releasing the nitrogen from the sediments as nitrate solves this problem, but also implies the presence of nitrifying bacteria in the bed sediments, with a corresponding oxygen demand. This oxygen demand would be accounted for as a fraction of the measured SOD.

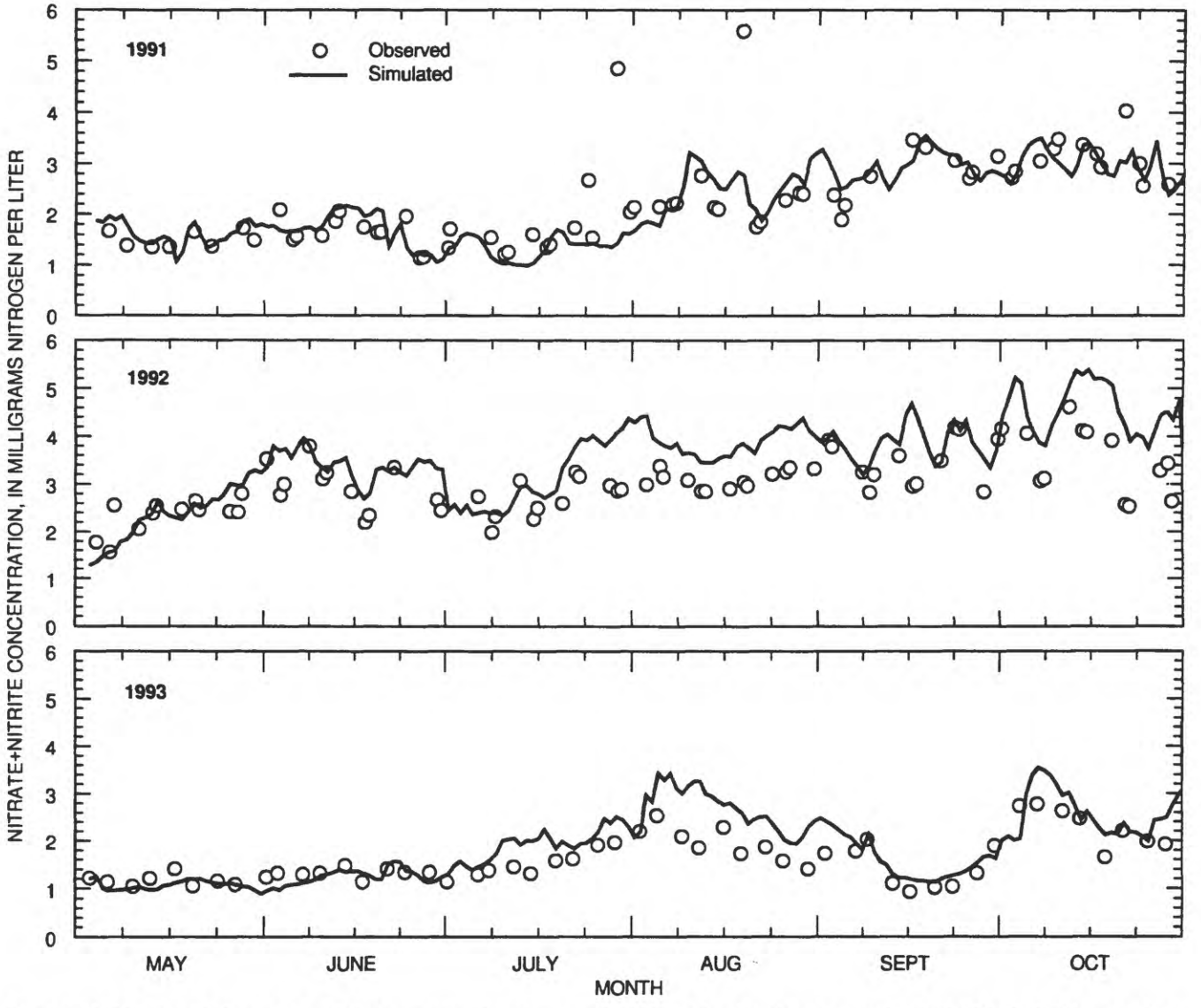

Figure 48. Measured nitrate-plus-nitrite concentration compared with the simulated concentration in the Tualatin River at river mile 5.5 (Stafford), May–October of 1991–93.

pH

The pH of the Tualatin River is a State of Oregon, regulated, water-quality parameter. To protect the health of resident fish populations, the State established a maximum-allowable-pH standard of 8.5 (and a lower limit of 6.5). Algal photosynthesis and respiration largely determine the pH of Tualatin River water from May through October. During warm, sunny days, photosynthetic activity extracts dissolved CO_2 from the water, causing an increase in pH. At night, algal respiration releases CO_2 to the water; as a result, the pH decreases. In 1991, 1992, and 1993, factors such as warm water, long travel times, and ample nutrients often resulted in large blooms of phytoplankton in the lower Tualatin River. The cycles of algal growth and respiration caused wide daily variations in the pH and a number of violations of the State pH standard (fig. 49). Because pH is an important parameter in this river, an attempt was made to include it in the water-quality model. Although the attempt was not entirely successful, the results are instructive.

As long as the pH of the Tualatin River is controlled by the chemistry of carbonic acid, it can be calculated easily from two of the other water-quality constituents simulated by CE-QUAL-W2: carbonate alkalinity and total inorganic carbon. These two constituents are transported with the flow and are affected by chemical and biological reactions (see the *Algorithms* section). In contrast, pH is neither

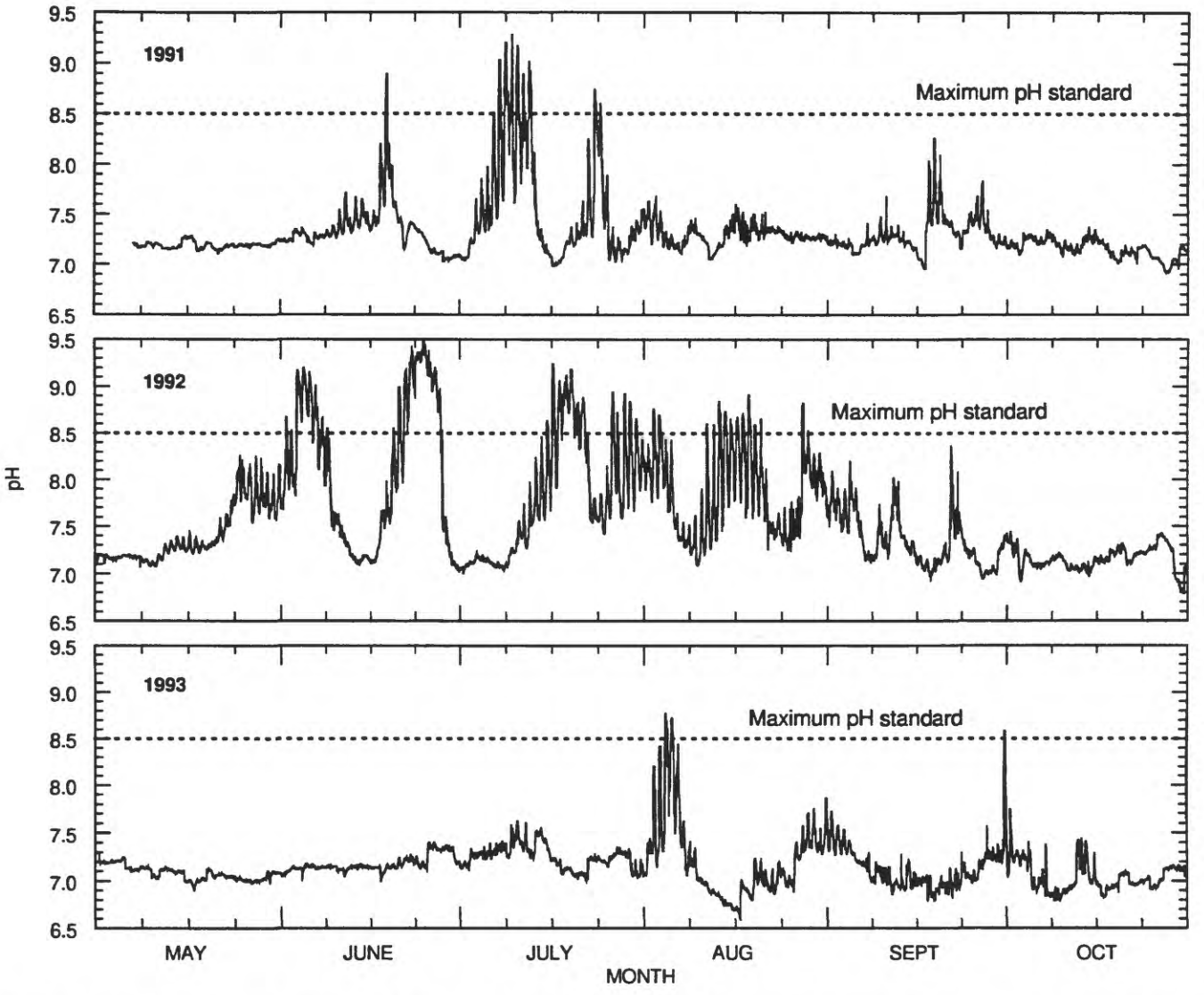

Figure 49. Hourly pH values observed in the Tualatin River at river mile 3.4 (Oswego diversion dam), May–October of 1991–93.

transported nor reacted; it is simply calculated using the concentrations of alkalinity and total inorganic carbon. The pH, alkalinity, and total inorganic-carbon constituents are not necessary to any other part of the model calibration. In this version of CE-QUAL-W2, the pH, alkalinity, and total inorganic-carbon constituents provide no feedback to the main suite of water-quality algorithms.

Measurements of carbonate alkalinity at the model boundaries were only available in the 1993 data set; therefore, pH could only be simulated for the May through October period of that year. Because total inorganic-carbon concentrations were not measured, estimates were calculated at the boundaries using equation 36 and the measured pH and alkalinity values. Assuming that this calculation provided reasonable estimates, Tualatin River water at RM 38.4 (Rood Bridge) was supersaturated with respect to CO_2, ranging from three to twenty-two times saturation.

Although the carbonate alkalinity in this model is affected by nitrification, photosynthesis, and respiration reactions, those perturbations are generally small. As a result, this constituent should behave like a conservative tracer, responding mainly to changes in the boundary conditions over time. Indeed, the model was able to simulate the transport of carbonate alkalinity relatively well (fig. 50). Neglecting the "high-flow" experiment from September 7 to 27 of 1993, for which only limited boundary condition data were available, the simulated alkalinities differ from their observed counterparts by less than 10 percent and often by less than 5 percent. Normally, such small errors would be more than acceptable. When the simulated alkalinity is used to calculate pH, however, greater accuracy may be required. An analysis of equation 36 reveals that the calculation of pH is dependent on, and sensitive to, the ratio of alkalinity (*Alk*) to total inorganic carbon (C_T). When that ratio is 1.0 and the concentrations of H^+ and OH^- are insignificant, the pH is 8.3 and almost all of the inorganic carbon is in the form of HCO_3^-. At that point, the pH is not well buffered. In fact, for values of *Alk* and C_T typically found in the Tualatin River, equation 36 simulates little buffering in the pH range from 7.5 to 9.1. Under these conditions, and if the ratio of *Alk* to C_T is near 1.0, a 5 percent error in either the simulated alkalinity or the simulated inorganic-carbon concentration would cause an error of almost a full unit in the simulated pH. Accurately simulating pH values in the range 7.5 to 9.1, therefore, is difficult and requires a very accurate simulation of the carbonate alkalinity and the inorganic carbon constituents.

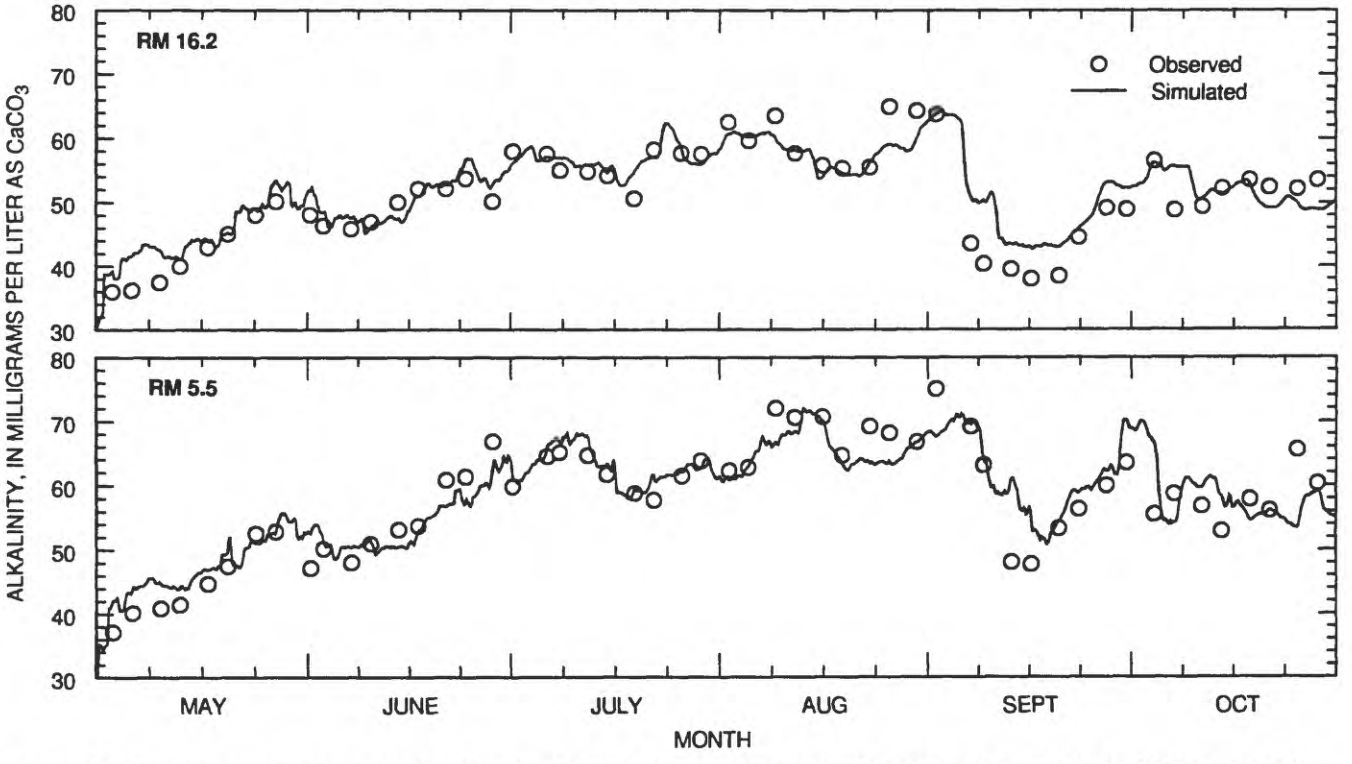

Figure 50. Ten-foot averaged values of carbonate alkalinity observed in the Tualatin River at river mile 16.2 (Elsner Road) and river mile 5.5 (Stafford Road) compared with simulated 10-foot averaged values, May–October of 1993.

Changes in the pH of Tualatin River water are driven mainly by changes in the total inorganic-carbon concentration, which, in turn, are determined by variable boundary conditions and the cycles of algal photosynthesis and respiration. The pH cannot be modeled accurately, therefore, unless the phytoplankton population is also modeled accurately. The goal of the model calibration, however, was not to simulate each algal bloom to a high degree of accuracy. Rather, the goal was to capture the dynamics of the processes that control water quality without sacrificing the constancy of model parameters and, therefore, the ability to extrapolate the calibration beyond the conditions of an individual algal bloom. Consistent with that goal, the calibrated model was able to capture the general dynamics of algal growth and water quality in the Tualatin River while varying only two of the calibration parameters. The compromise inherent to this approach was that many of the individual algal blooms would not be modeled exactly. As a result, the simulated pH values also would not be expected to match the measured values exactly. Indeed, although the simulated pH values generally rise, fall, and show daily variations when they should, they do not match the observed values at RMs 16.2 and 5.5 closely enough to be predictive (fig. 51). Too often, the simulated pH values predict a violation of the State standard when none was observed. If the goal of the modeling work had been to exactly simulate each individual algal bloom, then the simulated pH values for those time periods would have been more accurate. The calibration parameters for each bloom, however, would apply only to a very limited set of conditions, making the model less useful as a predictive tool.

The discrepancies between the simulated and observed pH values are due almost entirely to similar discrepancies between the simulated and observed chlorophyll-a concentrations. At RM 16.2, for example, while the simulated and observed pH values match fairly well, the periods of time in which the model simulates pHs that are too low are the same periods when the model simulates too little algae (fig. 31). When the model simulates the algae accurately at that site, the simulated pH values are excellent. At RM 5.5, the simulated pH values for June 19 to July 14, August 8 to 13, and August 23 to September 7 are generally too high, resulting from simulated algal populations that are too large (fig. 33). In addition, measured pH values at that site are slightly higher than the simulated values for July 14 to 29, resulting from simulated algal populations that are too small.

At the Oswego diversion dam (RM 3.4), the continuous monitor of pH and DO shows that the pH of Tualatin River water is determined largely by (a) algal photosynthesis and respiration, and (b) the chemistry of carbonic acid. Because reaeration in the slow-moving Tualatin River is slow, the DO concentration acts as a good surrogate for algal activity. A plot of the pH against the DO concentration, therefore, illustrates the influence of algal activity (fig. 52). That plot shows a very close relation between pH and DO and, therefore, between pH and algal activity. Both the observed and simulated data have an inflection in the pH/DO curve at a pH of about 8.0 to 8.3. This inflection is obvious in the graph of the simulated data, and still readily discernible in the graph of the measured data. The presence of an inflection point in that pH range is characteristic of the dissociation reactions of carbonic acid. Essentially, the plot of pH against DO mimics a titration curve for HCO_3^-. The simulated data show the inflection because the chemistry of carbonic acid was imposed by the model. The fact that the measured data show an inflection means that carbonic acid is important in determining the pH of Tualatin River water. The inflection observed in the measured relation is less pronounced than its simulated counterpart probably because the pH of the natural system is also influenced by other acids and bases. Natural waters are buffered to some extent by a wide variety of humic and fulvic acids that are not included in the model simulations. Including that sort of buffering in the model would be exceedingly difficult, due to the nonuniform structure and activity of these substances. The effect of these other acids on the pH, however, is small relative to the effects of photosynthesis, respiration, and the reactions of carbonic acid.

MODEL APPLICATIONS

A primary goal of this application of CE-QUAL-W2 to the Tualatin River has been to create a calibrated model that can be used to determine the probable efficacy of hypothetical scenarios quickly and inexpensively. The modeled results of several possible scenarios are discussed in this section. The results presented illustrate some important concepts, and they demonstrate the potential for the model to address other management questions as they arise.

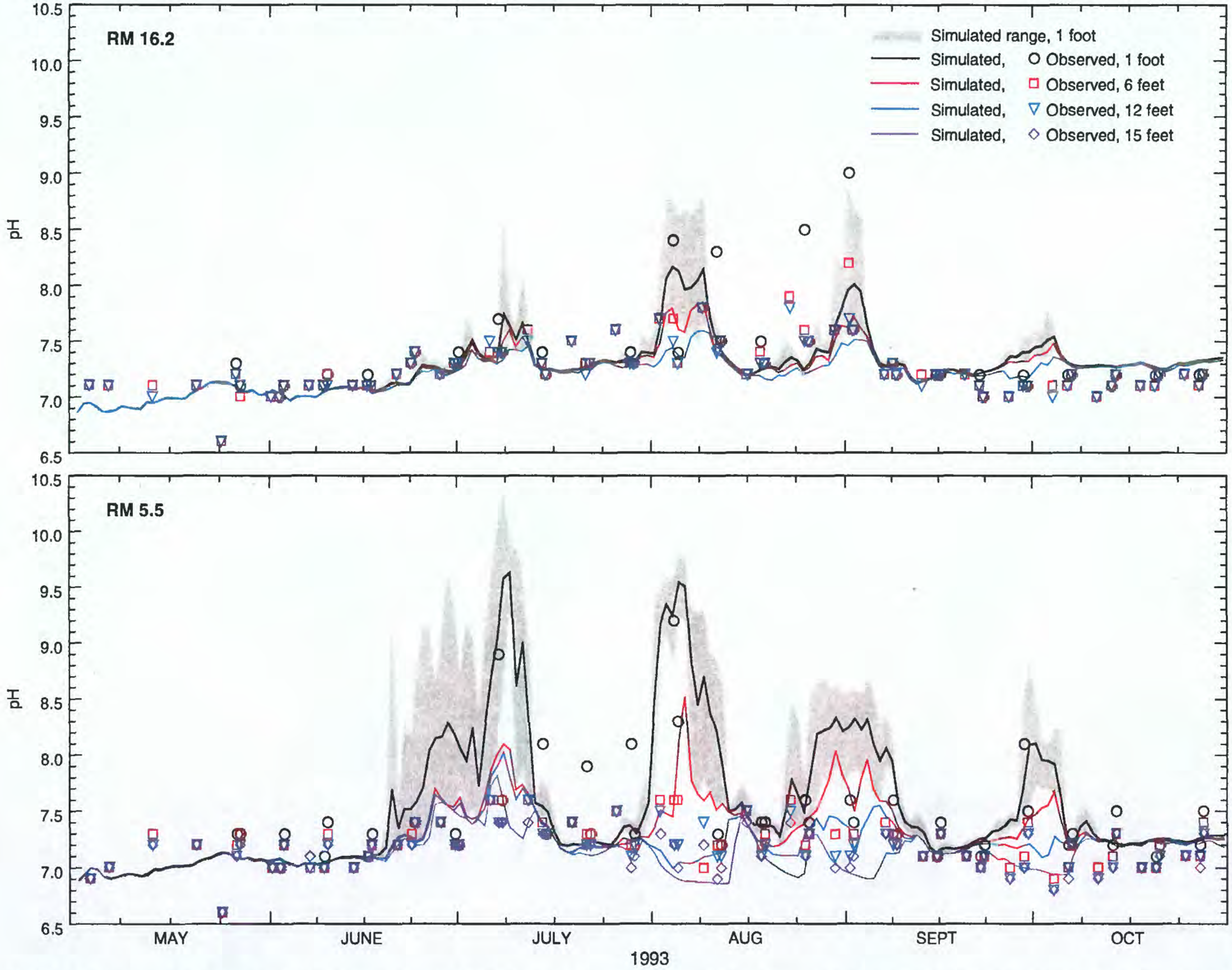

Figure 51. Simulated and observed pH at several depths in the Tualatin River at river mile 16.2 (Elsner) and river mile 5.5 (Stafford Road), May–October of 1992. (RM, river mile)

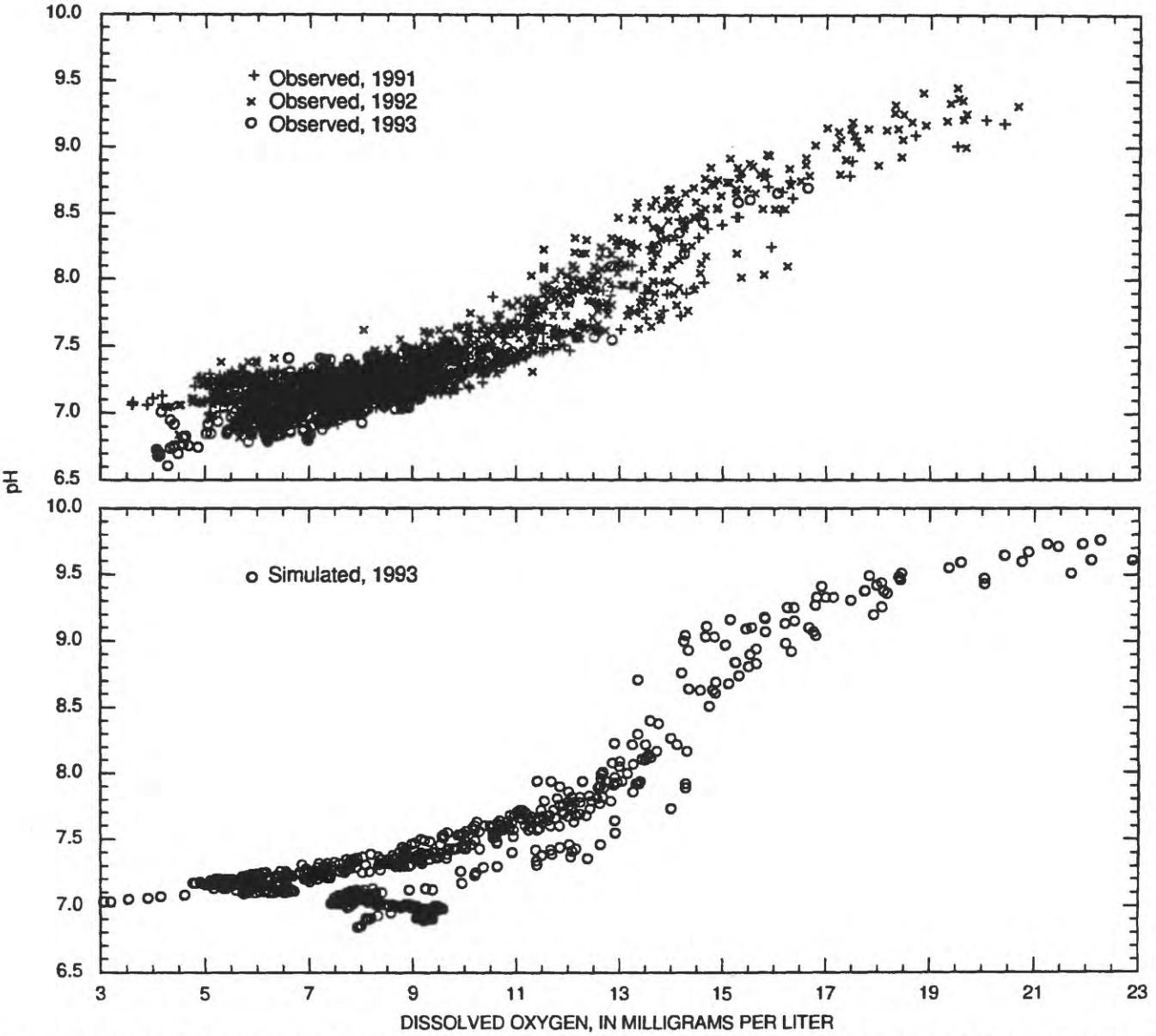

Figure 52. Relation of near-surface dissolved oxygen concentration to pH for the Tualatin River at the U.S. Geological Survey monitor at river mile 3.4 (Oswego diversion dam): observed (May–October of 1991–93) and simulated (May–October of 1993).

The testing of hypothetical management scenarios requires that the model be applied in a prognostic mode and, by definition, that it be applied under conditions to which it has not been explicitly calibrated. In this application, two decisions were made in an attempt to assure that the calibration parameters would remain valid under the new, hypothetical conditions. The first was that as few parameters as possible would be varied over the 18 months of calibrated simulations, so that the final set of parameters would be robust and broadly applicable (see the discussion in the *Calibration* section). The second decision was that hypothetical scenarios would be tested by using the same forcing functions and boundary data used in the calibration, with minor changes as required for the scenario being tested. In other words, the scenarios answer the question "What would the river have looked like if this management option had been implemented in 1991 (or 1992 or 1993)?" In this way, it can be ensured that the environmental conditions (including hydrology, meteorology, and water quality) of the hypothetical scenarios are small deviations from those under which the model was calibrated, and that the calibration parameters remain valid. Each scenario was tested using all three (1991–93) calibration seasons in order to simulate its effect for a wide range in hydrologic conditions.

The strategy of testing the hypothetical scenarios by reusing the calibration data sets has the further advantage that the performance of the model has already been determined by a comparison with the observations. The accuracy of the hypothetical scenarios depends in large part on the accuracy of the calibration runs; for those time periods and river reaches that the calibration runs were more (or less) accurate, the hypothetical scenarios should also be more (or less) accurate. The calibration indicated, for example, that the model performs best through the reach of the river from the upstream boundary to RM 16.2. Results from RM 16.2 to RM 5.5 are sometimes very good, but not as consistently good as they are through the upstream reach. The results from RM 5.5 to the Oswego diversion dam at RM 3.4 need to be interpreted carefully because there were no calibration data for some constituents at the downstream boundary. The biggest temporal consideration to emerge from the calibration is that the model performance was seen to degrade somewhat at RM 5.5 when grazing was an important loss process for phytoplankton.

Most of the scenarios are designed to reduce algal growth, either by reducing the length of time the algae are in the river (the travel time) or by making environmental conditions less favorable for growth. There are two reasons for the focus on reducing algal growth. The first is that the algae are a "nuisance" factor, and the second is the presumption that a reduction in algal growth will result in improved water quality. Algae in this river affect water quality primarily through their influence on dissolved oxygen and pH. For the reasons stated previously, however, pH was not modeled with sufficient accuracy to warrant its inclusion in the hypothetical scenarios. Therefore, dissolved oxygen is the primary indicator of water quality considered in this discussion.

The various hypothetical scenarios are summarized in table 14. A reduction in travel time is accomplished either by flow augmentation (scenarios 2a and 2b), or by lowering the surface elevation at the Oswego diversion dam (scenarios 4a and 4b). Environmental conditions are made less favorable for algal growth by lowering the water temperature (scenarios 5a and 5b), or by reducing nutrient concentrations (scenarios 1a, 1b, 6a, and 7). Two scenarios employ a combination of flow augmentation and reduced nutrient concentrations (scenarios 3a and 3b). Four of the scenarios listed in table 14 are not necessarily management scenarios, but they provide useful comparisons. Scenario 6b simulates the potential effect of population growth in the Tualatin River Basin, scenario 8 simulates the effect of reducing the SOD by one-half, and scenarios 9a and 9b provide an idea of what benefit has already been gained as a result of the implementation of advanced phosphorus removal and ammonia nitrification in the WWTPs.

It is instructive to look at the results of all of the scenarios together before discussing them individually. In figure 53, the difference in monthly mean dissolved oxygen concentration between 11 of the hypothetical management scenarios and the calibration simulation is plotted against the same difference in monthly mean chlorophyll-a concentration at RM 16.2. Throughout this discussion, the calibration simulation provides the base case against which each hypothetical simulation is compared, because it is the *changes* induced by the hypothetical scenario that are of interest, not how well the model simulates the observed data. The latter has already been discussed in the *Calibration* section. A positive difference indicates that the quantity increased in the hypothetical scenario relative to the calibration. One data point is plotted for each month of simulated results, or 18 points for each scenario. Scenarios 6a and 7 are not included because they do not plot significantly away from the origin. Scenario 8 (not a management scenario) is included in the figure because it provides a useful comparison.

Using the model parameter values as described previously, the simulated change in monthly mean dissolved oxygen for most of the scenarios is positively correlated with the change in monthly mean chlorophyll-a, illustrating that the presumed connection between reduced algal growth and increased dissolved oxygen does not appear in the monthly mean data. The data for most of the scenarios tend to fall along a positively sloping line that is offset some distance below the origin, with the result that the greatest increases in monthly mean dissolved oxygen produced by a given scenario tend to be associated with the *smallest* decreases in monthly mean chlorophyll-a. Therefore, the maximum increase in dissolved oxygen achieved by any given scenario (on a monthly basis) has less to do with changes in algal growth than with other aspects of that scenario that affect dissolved oxygen.

Table 14. Hypothetical scenarios tested by this application of CE-QUAL-W2

[TMDL, total maximum daily load; CBOD, carbonaceous biochemical oxygen demand; RM, river mile; ft^3/s, cubic feet per second; °C, degrees Celsius; WWTP(s), wastewater-treatment plant(s); SOD, sediment oxygen demand]

Scenario	Title	Description
1a	Tributary phosphorus reduction	Total phosphorus in all tributaries and the upstream boundary decreased to TMDL levels by preferentially removing detrital phosphorus. Removal of organic phosphorus also reduces CBOD inputs.
1b		Total phosphorus in all tributaries and the upstream boundary decreased to TMDL levels by preferentially removing ortho-phosphate.
2a	Flow augmentation	Discharge at RM 38.4 not allowed to drop below 150 ft^3/s.
2b		Discharge at RM 38.4 not allowed to drop below 200 ft^3/s.
3a	Tributary phosphorus reduction with flow augmentation	Total phosphorus in all tributaries and the upstream boundary decreased to TMDL levels by preferentially removing detrital phosphorus, and discharge at RM 38.4 not allowed to drop below 150 ft^3/s. Removal of organic phosphorus also reduces CBOD inputs.
3b		Total phosphorus in all tributaries and the upstream boundary decreased to TMDL levels by preferentially removing ortho-phosphate, and discharge at RM 38.4 not allowed to drop below 150 ft^3/s.
4a	Oswego diversion dam (RM 3.4) modifications	No flashboards installed at the Oswego diversion dam.
4b		Base elevation of the Oswego diversion dam lowered by 4 ft.
5a	Stream temperature reductions	Temperature of all tributaries and the upstream boundary reduced by 2°C.
5b		Temperature of all tributaries and the upstream boundary reduced by 5°C.
6a	Optimal WWTP operations	Durham and Rock Creek WWTPs operating at peak efficiency, based on 1992 performance.
6b		Durham and Rock Creek WWTPs operating at peak efficiency, based on 1992 performance, and treatment plant effluent discharge doubled.
7	Denitrification in the WWTPs	State-of-the-art nitrification/denitrification implemented at the Durham and Rock Creek WWTPs.
8	Reduction in SOD	Sediment oxygen demand reduced by one-half.
9a	WWTP operations prior to nutrient removal	Effluent nutrient concentrations set at typical 1988 levels; an instream nitrification rate of 0.023 day^{-1} used.
9b		Effluent nutrient concentrations set at typical 1988 levels; instream nitrification rates of 0.219 day^{-1} (RMs 38.4 to 30) and 0.055 day^{-1}(RMs 30 to 3.4) used.

This result may seem counterintuitive in light of the numerous eutrophication studies that might suggest otherwise, but it is consistent with Tualatin River data when one considers how the effects of each scenario are manifested. For example, the flow augmentation and reduced dam elevation scenarios (2a,b and 4a,b) reduce the travel time in the river, thereby reducing the amount of DO removed by SOD and CBOD, and somewhat increase the reaeration. The scenarios that involve removal of detrital phosphorus at the boundaries (1a and 3a) result in greatly reduced allochthonous CBOD and, therefore, greatly reduced oxygen consumption by water-column decay processes. Most of the increase in DO associated with scenarios 1a and 3a results from reduced CBOD rather than from reduced algal growth. The scenarios that reduce temperature (5a and 5b) increase dissolved oxygen primarily by decreasing the reaction rates of decay in the water column and sediments and secondarily by increasing its solubility.

The largest increases in mean DO during any month are produced by scenarios 1a, 2b, 3a, 4a, 5b, and 8, with relatively small changes in the monthly mean chlorophyll-a concentration. On the other hand, the largest decreases in chlorophyll-a are produced by scenarios 1b, 2b, and 3b, and all produce relatively large decreases in DO. Scenarios 1b and 3b demonstrate that algal growth (during blooms) can be effectively limited by reducing the supply of nutrients, but these scenarios have a small offset to the right of the origin and, therefore, the least positive effect on DO. Scenario 8, the nonmanagement scenario in which SOD is reduced by half, demonstrates the importance of sediment organic-matter decay in determining DO concentrations. This scenario generates the largest monthly mean increases in DO with very little change in algal growth.

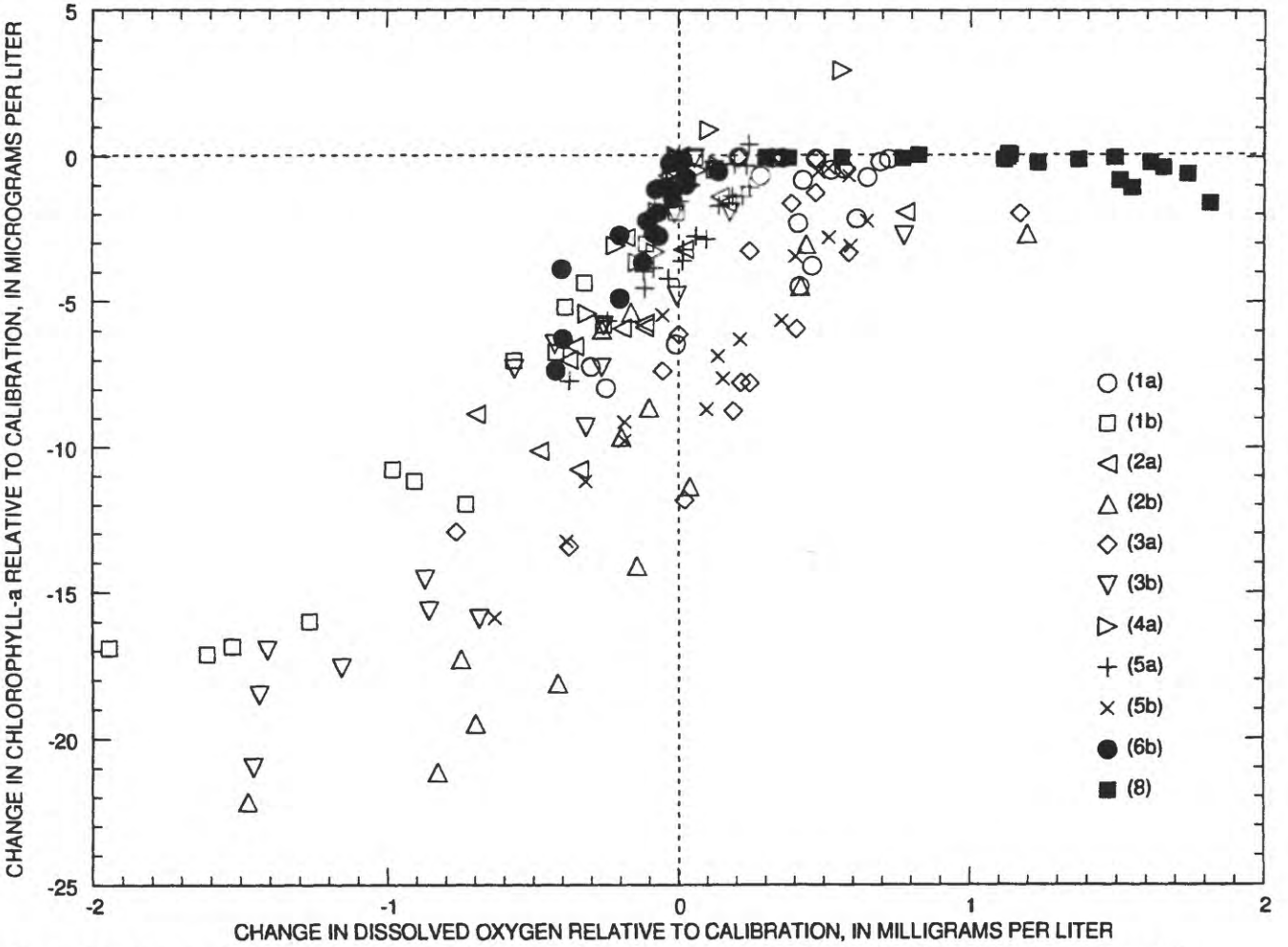

Figure 53. Relation of the monthly means of the differences between various management scenarios and the model calibration for chlorophyll-a and dissolved oxygen at river mile 16.2 (Elsner). (Eighteen monthly means are included: May–October of 1991–93.)

Monthly means are not necessarily good indicators of the extent and frequency of the minima in dissolved oxygen concentration, or of overall ecological health. A better indicator, perhaps, is the frequency of violation of the State of Oregon minimum dissolved oxygen standard for waters designated as cool-water aquatic resources, which is the designation for the modeled reach of the Tualatin River. Prior to July of 1996, the minimum DO standard was 6.0 mg/L. After July of 1996, however, the standard was modified such that any instantaneous measurement of DO must be greater than 4.0 mg/L, the 7-day mean of daily minima must be greater than 5.0 mg/L, and the 30-day mean must be greater than 6.5 mg/L (Oregon Department of Environmental Quality, 1997). Neither the 7-day mean minimum nor the 30-day mean allow credit for supersaturation conditions; if such conditions occur, then the concentration at saturation is used. The modified standard also states that when insufficient data are available to calculate these statistics, the dissolved oxygen concentration should never be less than 6.5 mg/L. Hourly dissolved oxygen concentrations from the calibration simulation and all of the hypothetical scenarios were compared to this modified DO standard for two sites in the model reach (tables 15 and 16). The scenarios that resulted in more than a 20 percent decrease in chlorophyll-a, when averaged over a 6-month season, are shaded in the tables to provide a simultaneous measure of how effectively each scenario reduces algal growth.

Data in tables 15 and 16 show that the scenarios that are most effective at reducing the number of occurrences of below-standard DO are not necessarily the same scenarios that are most effective at reducing algal growth. Scenario 1a is effective in reducing the number of occurrences of below-standard DO (because CBOD is reduced), but does not appreciably reduce algal growth. On the other hand, scenarios 1b and 3b effectively reduce algal growth but do not appreciably reduce the occurrences of below-standard DO.

Table 15. Percentage of time that simulated 10-foot vertically averaged dissolved oxygen concentrations at river mile 16.2 (Elsner) on the main-stem Tualatin River violated the State of Oregon minimum dissolved oxygen standard

[DO, dissolved oxygen; <, less than; mg/L, milligrams per liter. No credit is given for supersaturation in the calculation of DO statistics. Percentages are based on simulated hourly data. Shaded cells indicate that the 6-month average of the chlorophyll-a concentration was decreased by at least 20 percent, as compared to the calibration simulation. Simulation 4b is not included because 4b was run only for the reach downstream of river mile 10]

	Tiered standard									Alternate standard					
	Hourly DO < 4.0 mg/L (percent)			7-day mean minimum < 5.0 mg/L (percent)			30-day mean < 6.5 mg/L (percent)			Hourly DO < 6.5 mg/L (percent)			Hourly DO < 6.5 mg/L (days)		
Simulation number	1991	1992	1993	1991	1992	1993	1991	1992	1993	1991	1992	1993	1991	1992	1993
Calibration	0	0	0	0	0	0	0	2.8	0	4.5	11	1.2	13	26	7
1a	0	0	0	0	0	0	0	0	0	.7	.6	0	5	4	0
1b	0	0	0	0	0	0	0	6.8	0	6.1	13	2.0	18	32	9
2a	0	0	0	0	0	0	0	0	0	4.1	2.2	0	12	7	0
2b	0	0	0	0	0	0	0	0	0	1.1	0	0	4	0	0
3a	0	0	0	0	0	0	0	0	0	0	0.2	0	1	2	0
3b	0	0	0	0	0	0	0	0	0	5.3	3.9	0	15	11	1
4a	0	0	0	0	0	0	0	0	0	4.8	7.6	.9	13	19	3
5a	0	0	0	0	0	0	0	0	0	3.2	6.3	.4	11	17	4
5b	0	0	0	0	0	0	0	0	0	1.1	2.5	.3	4	9	2
6a	0	0	0	0	0	0	0	2.8	0	4.1	11	1.0	13	26	5
6b	0	0	0	0	0	0	0	0	0	3.7	8.1	.7	11	21	3
7	0	0	0	0	0	0	0	2.8	0	4.4	11	1.1	13	26	7
8	0	0	0	0	0	0	0	0	0	0	0	0	0	0	0
9a	2.2	16	.6	17	26	13	40	24	36	38	33	39	85	72	87
9b	20	28	16	43	34	43	57	30	70	58	48	57	125	97	113

Flow augmentation (scenario 2b) seems to be effective at both reducing algal growth and reducing the number of occurrences of below-standard DO concentrations; the decrease in residence time not only decreases the algal population, but decreases the effect of the CBOD and the SOD. These results are similar to those for monthly mean concentrations: most scenarios affect the DO minima more through their effect on other consumption processes, such as CBOD and SOD, rather than through a reduction in algal growth. The importance of other oxygen demands in determining the DO concentration and the number of below-standard occurrences is further demonstrated by scenario 8, which is included in the tables for comparison purposes. This scenario all but eliminates violations of the State DO standard in all 3 years, but results in almost no change in algal growth.

Many of the important conclusions drawn from the hypothetical management scenarios discussed below can be demonstrated by looking first at the comparison of two scenarios (1a and 3b) with the base case. Scenarios 1a and 3b were chosen because 1a achieves the maximum *overall* increase in DO concentration, and 3b achieves the maximum *overall* decrease in chlorophyll-a. Both of these assessments were made by simply taking average values over the entire 6-month season, and comparing with the average value for the calibration. A plot of chlorophyll-a at RM 16.2 (fig. 54) shows that the combination of flow augmentation with a significant reduction in orthophosphate (scenario 3b) can very effectively limit the size of algal blooms, often by as much as 50 percent. A comparison of figure 54 with figure 55 shows that the reduction in algal growth in scenario 3b manifests itself primarily as a much lower oxygen concentration during algal blooms. There is little evidence of the expected increase in oxygen concentration during algal crashes, probably because of their short duration and because the background oxygen demands are so high that they dominate oxygen consumption even during algal crashes.

Table 16. Percentage of time that simulated 10-foot vertically averaged dissolved oxygen concentrations at river mile 5.5 (Stafford) on the main-stem Tualatin River violated the State of Oregon minimum dissolved oxygen standard

[DO, dissolved oxygen; <, less than; mg/L, milligrams per liter. No credit is given for supersaturation in the calculation of DO statistics. Percentages are based on simulated hourly data. Shaded cells indicate that the 6-month average of the chlorophyll-a concentration was decreased by at least 20 percent, as compared to the calibration simulation]

	Tiered standard									Alternate standard					
	Hourly DO < 4.0 mg/L (percent)			7-day mean minimum < 5.0 mg/L (percent)			30-day mean < 6.5 mg/L (percent)			Hourly DO < 6.5 mg/L (percent)			Hourly DO < 6.5 mg/L (days)		
Simulation number	1991	1992	1993	1991	1992	1993	1991	1992	1993	1991	1992	1993	1991	1992	1993
Calibration	0	0	0	0	0	0	0	6.0	0	3.4	15	17	8	33	40
1a	0	0	0	0	0	0	0	0	0	2.3	9.4	1.5	5	23	5
1b	0	0	0	1.7	2.3	0	0	32	.5	6.9	35	19	19	78	48
2a	0	0	0	.6	0	0	0	5.7	0	3.8	13	16	9	30	43
2b	0	0	0	0	0	0	0	0	0	4.8	7.3	10	14	16	32
3a	0	0	0	0	0	0	0	0	0	2.5	3.7	2.0	5	12	6
3b	0	0	0	1.1	0	0	0	6.6	2.5	5.7	13	17	14	40	48
4a	0	0	0	0	0	0	0	5.5	0	3.8	14	12	9	30	36
4b	0	0	0	0	0	0	0	0	0	2.0	3.4	0	5	15	0
5a	0	0	0	0	0	0	0	7.2	0	3.7	15	10	10	32	30
5b	0	0	0	0	0	0	0	7.6	0	3.4	16	6.9	9	35	22
6a	0	0	0	0	0	0	0	6.2	0	3.0	15	14	7	33	32
6b	0	0	0	0	0	0	0	4.7	0	3.1	14	6.0	6	28	17
7	0	0	0	0	.6	0	0	6.2	0	3.4	15	15	8	33	38
8	0	0	0	0	0	0	0	0	0	.8	.2	0	2	1	0
9a	5.4	18	8.9	17	19	23	8.0	19	16	26	23	35	60	49	70
9b	18	21	26	23	26	36	32	21	63	35	31	42	76	66	80

The only time period when scenario 3b significantly increases DO concentration is October of 1992, when the flow augmentation decreases the time of travel enough that oxygen consumption by CBOD and SOD is reduced substantially. Therefore, the management strategy that most effectively reduces algal growth is not the same strategy that generates the greatest overall increase in dissolved oxygen concentration.

The phosphorus reduction scenario in which detrital phosphorus is removed preferentially (scenario 1a) is most effective at increasing dissolved oxygen because of the reduced concentration of allochthonous CBOD. This scenario also reduces orthophosphate somewhat because phosphorus release from the decomposition of detrital organic matter is reduced, but the ability of this scenario to limit algal growth is minimal, except at the peak of very large blooms. Algal growth is affected by this scenario somewhat more in 1992 because simulated phosphorus concentrations during the midsummer months are very low to begin with, so the phosphorus limitation to algal growth enhances the effect of the small reduction in orthophosphate. The effect of scenario 1a on dissolved oxygen is primarily a relatively constant positive offset (fig. 55), due to a reduction in the background oxygen demand from the decay of allochthonous CBOD. The comparison of scenarios 1a and 3b demonstrates that the role of the algae in determining the dissolved oxygen concentration is primarily one of production rather than consumption; therefore, a reduction in

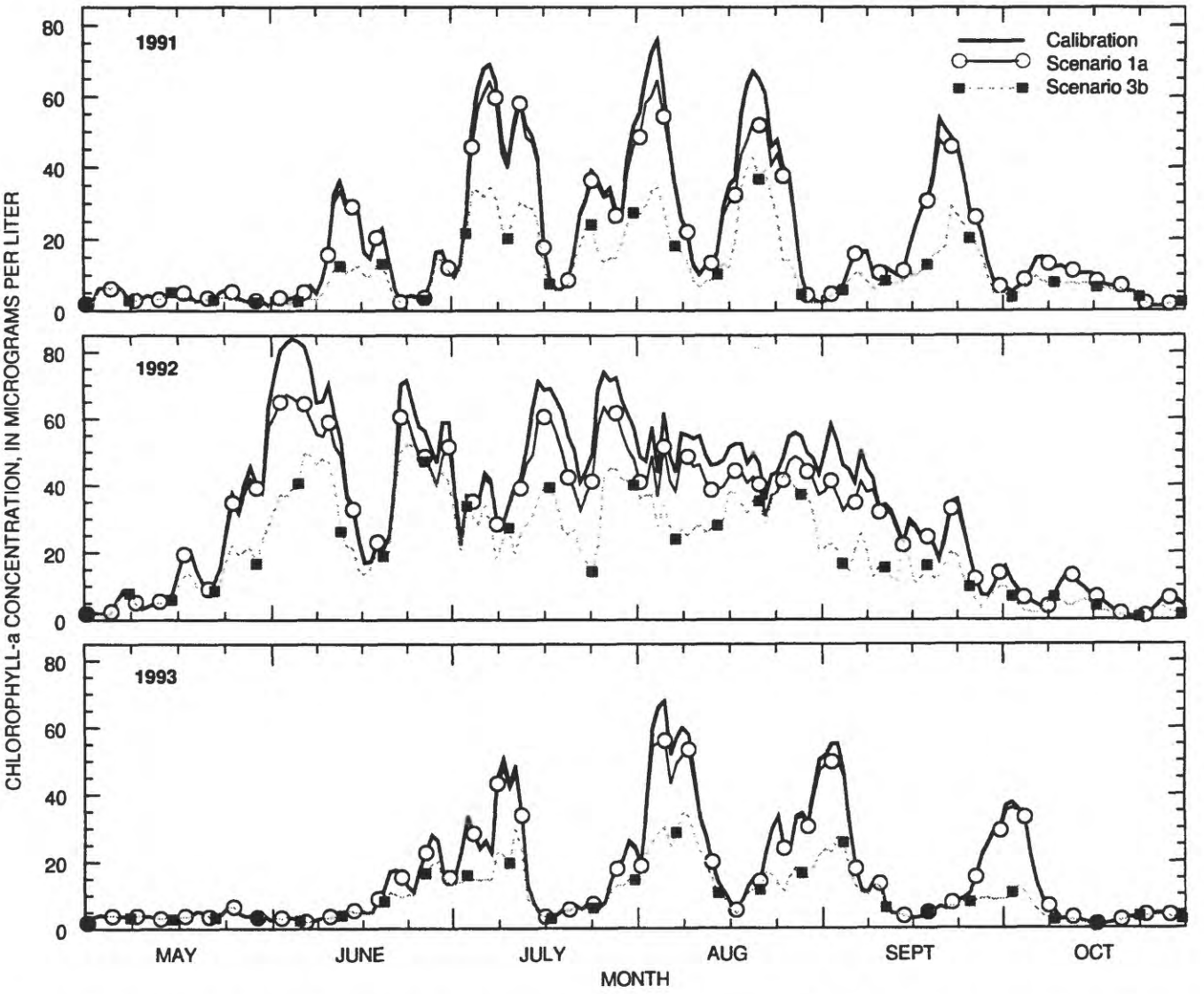

Figure 54. Calibrated chlorophyll-a concentration at river mile 16.2 (Elsner) compared with simulated concentrations under scenarios 1a and 3b.

algal growth generally reduces rather than increases dissolved oxygen concentrations. This is not altogether bad, as a reduction in the size of an algal bloom will also decrease the diel variation in DO and pH during that bloom; such variations can cause stress to aquatic organisms. A reduced but more stable DO concentration may be better for aquatic life than a higher but more erratic level. The most effective way to increase overall dissolved oxygen concentrations, however, is to reduce the high background demand for oxygen. The other management strategies discussed below share some of the effects of these two scenarios.

In order to quantitatively summarize each of the hypothetical simulations in a concise manner, a table of bimonthly means of the relevant parameters was constructed for each scenario. The 2-month periods are intended to roughly capture a seasonal pattern in the summer cycle. The first 2 months, May and June, are generally characterized by higher discharge and smaller algal blooms than the July–August period, when low summer flows have been established, the weather is generally favorable for algal growth, and the size of algal blooms is the largest of the year. The September–October period is commonly an important period in terms of water quality because discharge remains low through this period, but light conditions become less favorable for the algae. Very low oxygen concentrations typically are observed during this period because low flows and high temperatures result in continued strong oxygen demand from CBOD

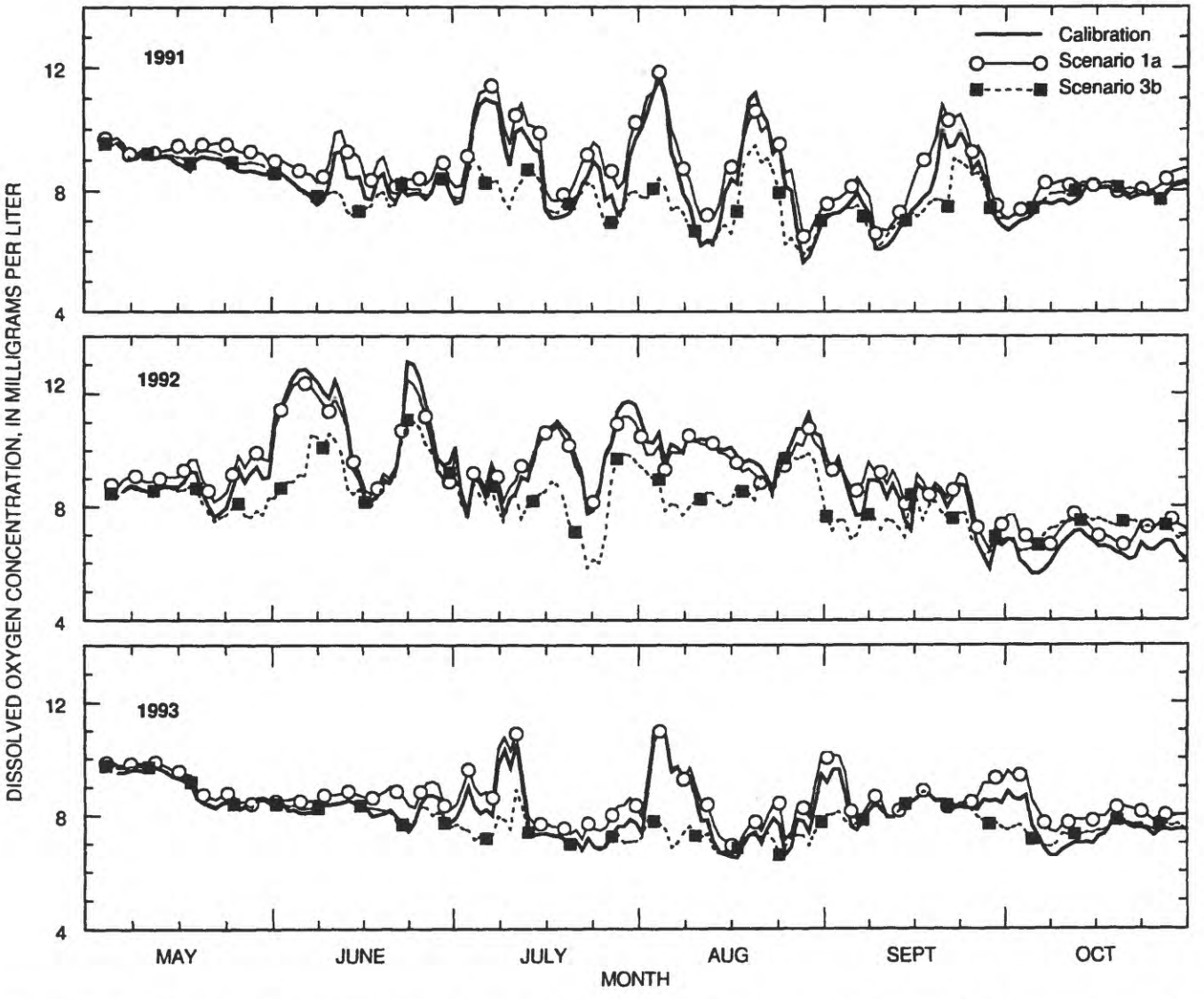

Figure 55. Calibrated dissolved oxygen concentration at river mile 16.2 (Elsner) compared with simulated concentrations under scenarios 1a and 3b.

decay and SOD, but photosynthetic production of oxygen slows considerably. A very dry year presents an exception to this rough characterization of the bimonthly periods; in 1992, the May–June period behaves much like the July–August period because summer low flows were established earlier than normal. On each table, the bimonthly means for the model calibration run are also included. This is the base case against which the changes induced by the hypothetical scenarios are compared.

Statistics at both RM 16.2 and RM 5.5 are included in each table. The calibration results established that the model performs consistently well from the upstream boundary to RM 16.2 (see the discussion in the *Calibration* section). Because algal growth is well established at this river mile, this station makes a good point of reference when comparing simulations. The results are sometimes very good from RM 16.2 to RM 5.5, but not as consistently good as upstream of RM 16.2, primarily because of occasionally important grazing activity. Interpreting the summary statistics for the hypothetical scenarios at RM 5.5 is sometimes difficult because some of the tested strategies generate slightly *increased* algal growth at that site, in particular during the July–August period of 1991 and 1992. The scenarios that decrease the travel time in the river (especially 2a, 2b, 4a, and 4b) occasionally result in increased algal populations at RM 5.5 because the algal population tends to peak before grazing losses cause it to decline. Depending on how important the grazing losses are, the amount of phytoplankton at the end of the reach can be quite sensitive to the travel time.

This sensitivity is illustrated with schematic growth curves for phytoplankton and zooplankton in figure 56. Shortening the travel time from τ_2 to τ_1, for example, results in an increased algal population at the lower boundary because τ_1 is closer to the peak in algal biomass concentration. Although the curves in figure 56 are only qualitative, this effect of a decreased travel time on the phytoplankton and zooplankton populations may manifest itself in the hypothetical scenarios when grazing losses are important. The scenarios that decrease the temperature of the water (5a and 5b) also show occasionally enhanced algal growth because the rates of growth in both zooplankton and algae are slowed, and the effect is analogous to shortening the travel time.

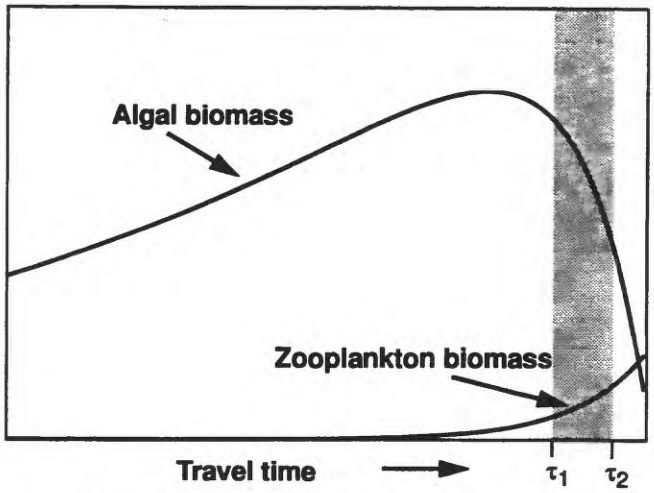

Figure 56. The interaction of algal and zooplankton biomass as a function of travel time through the river reach. (The shaded region indicates a region of relatively large change in algal biomass with a relatively small change in the travel time.)

Each of the hypothetical scenarios is discussed briefly below, with a description of the modifications to the boundary conditions needed to simulate the scenario and the important points to be gleaned from the results. The reader is advised that the results of the hypothetical simulations are best suited to qualitative rather than quantitative interpretation. The model can be used to determine whether a particular process has a negligible, secondary, or primary effect on a water-quality constituent, but it is not appropriate to use the model to distinguish between, for example, a 10 percent and a 20 percent reduction in a given water-quality constituent on a given day.

Tributary Phosphorus Reduction

In these scenarios, the total phosphorus entering the river at the upstream boundary and each tributary (not including the WWTPs) was reduced to the level of the regulated total maximum daily load (TMDL). The TMDL criteria are 0.07 mg/L total phosphorus for the three largest tributaries and 0.05 mg/L total phosphorus at RM 38.4 (Oregon Department of Environmental Quality, 1997). The small tributaries do not have TMDLs, but were assigned concentrations of 0.07 mg/L for these scenarios. The reduction in

total phosphorus was achieved in two ways. In the first case (scenario 1a), the phosphorus exceeding the TMDL was first removed from the detrital phosphorus compartment. If that compartment was depleted entirely, then the orthophosphate compartment was tapped for the remaining amount. This scenario amounts to a reduction primarily in allochthonous CBOD in order to achieve the phosphorus TMDL levels; a secondary decrease in orthophosphate occurs because less orthophosphate is released through CBOD decay. Scenario 1a was discussed previously in this section because it was found to achieve the greatest increase in the seasonally averaged DO concentration (although not necessarily the greatest increase over a shorter period of time). In the second case (scenario 1b), the process is reversed—the phosphorus is removed first from the orthophosphate compartment and then, if necessary, from the detrital phosphorus compartment. This scenario relies primarily on a reduction in orthophosphate and generally requires little reduction in allochthonous CBOD to achieve TMDL levels at the boundaries. Both scenarios result in less orthophosphate in the water column, although scenario 1b reduces orthophosphate much more than does scenario 1a (rows 3 and 4, 27 and 28 in table 17).

The summary statistics for these two scenarios are found in table 17, and their intercomparison is straightforward. While both scenarios reduce algal growth, preferentially removing orthophosphate (scenario 1b) to achieve TMDL levels reduces growth more than preferentially removing detrital phosphorus (scenario 1a) at both RM 16.2 and RM 5.5 (compare row 15 with row 16 and row 39 with row 40 in table 17). Scenario 1a, however, results in a consistently higher bimonthly averaged DO concentration than scenario 1b (0.31 to 1.62 mg/L), and for most of the 2-month time periods scenario 1a results in a higher bimonthly averaged DO concentration than the calibration run (-0.16 to 0.52 mg/L). On the other hand, the bimonthly averaged DO concentrations from scenario 1b are almost always lower than in the calibration run (-1.78 to 0.03 mg/L) because of reduced photosynthetic production (compare rows 19, 21 and 22, and rows 43, 45, and 46 in table 17).

Flow Augmentation

For the flow augmentation scenarios (2a and 2b), a minimum discharge at the upstream boundary (RM 38.4) was maintained at 150 ft^3/s in scenario 2a and at 200 ft^3/s in scenario 2b. The additional water required was assumed to come from Henry Hagg Lake and have the same quality, except for temperature, as the water sampled at RM 58.8 (Dilley), just downstream of the outflow from the lake. Most water-quality parameters should be nearly conservative from RM 58.8 to RM 38.4, but the heat content will certainly change. Therefore, the additional water was assumed to have the same temperature as the base flow at the upstream boundary. The amount of water required to carry out this scenario, particularly in the case of maintaining a minimum flow of 200 ft^3/s, makes this level of flow augmentation almost impossible to achieve in most years without another large water supply, as USA has rights to only 12,618 acre-feet of water in Henry Hagg Lake (table 18).

The summary statistics for scenarios 2a and 2b are compiled in table 19. Flow augmentation to maintain 200 ft^3/s at RM 38.4 (scenario 2b) is often more effective in limiting algal growth at RM 16.2 than is the scenario (1b) that reduces orthophosphate to TMDL levels. Flow augmentation to maintain 150 ft^3/s at RM 38.4 (scenario 2a), while it limits algal growth somewhat as far as RM 16.2, is not as effective at limiting algal growth as is scenario 1b (compare rows 2 and 3 in table 19 with row 16 in table 17). Chlorophyll-a decreases consistently at RM 16.2 with greater flow augmentation, but the consequences for DO concentration are mixed (rows 5 and 6 in table 19); sometimes DO increases because the reduced travel time reduces oxygen consumption by SOD and CBOD, and sometimes DO decreases due to reduced photosynthetic production. In any event, the changes in DO are relatively small, generally less than 0.8 mg/L.

During two July–August periods (1991 and 1992), chlorophyll-a is simulated to increase slightly at RM 5.5 with some degree of flow augmentation (rows 8 and 9 in table 19). This is due to the effect described earlier in this section in which a reduced travel time can cause the algal growth curve to end closer to the peak in concentration (fig. 56). The changes in DO at RM 5.5 are generally not great, but during two periods in 1992, when flows in the river were very low (July–August and September–October), both levels of flow augmentation resulted in an increase in DO at RM 5.5 (rows 11 and 12).

Table 17. Summary statistics for the phosphorus reduction scenarios

[mg/L, milligrams per liter; P, phosphorus; µg/L; micrograms per liter. Mean concentrations for each constituent were derived from simulated, daily, 10-foot-average concentrations at noon. Concentrations given for the calibration simulation are the model's best representation of observed conditions in the summers of 1991, 1992, and 1993. The other runs superimpose combinations of phosphorus removal and flow augmentation on top of the calibrated conditions of 1991, 1992, and 1993. Scenario 2a maintained a minimum flow of 150 ft^3/s at Rood Bridge (river mile 38.4). In scenario 1a, total phosphorus concentrations were reduced to their target total maximum daily load (TMDL) concentrations by removing detrital phosphorus first. In scenario 1b, the TMDL levels were achieved by removing orthophosphate first. The other two scenarios, 3a and 3b, removed phosphorus as in 1a and 1b while augmenting the flow as in 2a. Shaded cells highlight concentrations that would be in violation of a TMDL criteria, the dissolved oxygen standard, or the chlorophyll-a action level]

Site	Parameter	Scenario	1991			1992			1993			Row
			May June	July August	September October	May June	July August	September October	May June	July August	September October	
River mile 16.2 (Elsner)	Ortho-phosphate (mg/L as P)	Calibration	0.051	0.048	0.056	0.042	0.018	0.055	0.055	0.048	0.053	1
		2a	.051	.050	.054	.044	.020	.047	.055	.049	.052	2
		1a	.042	.035	.046	.031	.013	.042	.047	.039	.044	3
		1b	.015	.022	.030	.014	.010	.025	.017	.022	.027	4
		3a	.042	.038	.045	.033	.015	.038	.047	.040	.044	5
		3b	.015	.023	.031	.016	.011	.024	.017	.022	.027	6
	Total phosphorus (mg/L as P)	Calibration	.115	.110	.098	.100	.076	.104	.113	.102	.100	7
		2a	.115	.107	.091	.096	.075	.089	.113	.100	.094	8
		1a	.055	.063	.063	.057	.051	.061	.060	.066	.064	9
		1b	.056	.065	.064	.059	.055	.063	.060	.067	.065	10
		3a	.055	.063	.063	.058	.053	.060	.060	.065	.063	11
		3b	.056	.065	.063	.059	.056	.061	.060	.067	.064	12
	Chlorophyll-a (µg/L)	Calibration	8.4	36.7	13.9	35.5	50.4	18.3	6.7	25.9	12.9	13
		2a	8.4	29.9	10.3	29.8	44.7	12.0	6.7	22.6	8.4	14
		1a	8.1	33.4	13.6	31.2	43.6	16.4	6.6	24.5	12.5	15
		1b	5.3	22.7	10.1	24.6	33.4	12.1	5.7	17.0	9.2	16
		3a	8.2	28.4	10.2	27.5	40.0	11.5	6.6	21.4	8.2	17
		3b	5.3	20.1	8.4	23.2	31.5	9.1	5.7	15.0	6.9	18
	Dissolved oxygen (mg/L)	Calibration	8.56	8.62	7.74	9.79	9.85	7.21	8.61	7.99	7.92	19
		2a	8.57	8.26	7.77	9.36	9.68	7.44	8.61	7.91	7.83	20
		1a	9.03	9.14	8.22	9.88	9.69	7.81	8.95	8.46	8.41	21

Table 17. Summary statistics for the phosphorus reduction scenarios—Continued

Site	Parameter	Scenario	1991 May June	1991 July August	1991 September October	1992 May June	1992 July August	1992 September October	1993 May June	1993 July August	1993 September October	Row
River mile 16.2 (Elsner)—Continued	Dissolved oxygen (mg/L)	1b	8.50	7.63	7.51	8.84	8.07	6.74	8.64	7.22	7.70	22
		3a	9.03	8.84	8.14	9.54	9.63	7.82	8.95	8.33	8.22	23
		3b	8.50	7.62	7.68	8.86	8.41	7.27	8.64	7.27	7.79	24
River mile 5.5 (Stafford)	Ortho-phosphate (mg/L as P)	Calibration	0.081	0.058	0.051	0.028	0.009	0.043	0.101	0.112	0.058	25
		2a	.081	.055	.052	.029	.007	.041	.101	.111	.059	26
		1a	.072	.050	.042	.021	.006	.032	.092	.104	.050	27
		1b	.051	.049	.035	.010	.006	.023	.067	.098	.039	28
		3a	.072	.048	.044	.021	.005	.033	.092	.104	.051	29
		3b	.051	.046	.036	.010	.005	.023	.067	.097	.040	30
	Total phosphorus (mg/L as P)	Calibration	.166	.174	.117	.094	.066	.094	.169	.199	.140	31
		2a	.166	.168	.112	.092	.065	.087	.169	.195	.134	32
		1a	.107	.133	.086	.053	.043	.059	.116	.166	.109	33
		1b	.108	.140	.089	.057	.050	.063	.116	.170	.110	34
		3a	.107	.130	.085	.055	.046	.061	.116	.163	.105	35
		3b	.108	.134	.087	.057	.051	.062	.116	.166	.106	36
	Chlorophyll-a (µg/L)	Calibration	17.4	65.7	33.2	46.7	47.5	24.7	13.8	52.9	26.1	37
		2a	17.4	69.6	30.0	44.8	49.8	21.0	13.9	50.1	21.4	38
		1a	15.5	60.8	31.7	37.8	38.2	21.4	13.3	48.1	23.5	39
		1b	9.4	45.6	23.0	29.5	33.8	17.5	9.0	34.9	19.4	40
		3a	15.5	62.9	27.9	38.2	41.4	18.7	13.4	45.6	20.2	41
		3b	9.4	47.4	21.5	30.0	35.9	16.3	9.0	33.1	16.2	42
	Dissolved oxygen (mg/L)	Calibration	8.69	11.08	8.64	10.47	8.75	6.97	8.74	9.49	7.73	43
		2a	8.69	11.07	8.34	10.27	9.29	7.21	8.75	9.25	7.44	44
		1a	9.18	11.10	9.02	10.21	8.33	7.43	9.17	9.71	8.09	45
		1b	8.24	8.82	7.59	8.77	6.92	6.20	8.49	7.67	7.16	46
		3a	9.17	11.05	8.67	10.21	8.90	7.53	9.18	9.50	7.89	47
		3b	8.24	8.93	7.60	8.95	7.64	6.84	8.49	7.61	7.05	48

Table 18. Total amount of water (in acre-feet) required to maintain a minimum discharge at river mile 38.4 (May–October)
[These numbers include the Unified Sewerage Agency's actual flow augmentation for these low-flow seasons; ft^3/s, cubic feet per second]

Minimum discharge (ft^3/s)	Volume of water required in each year (acre-feet)		
	1991	1992	1993
150	16,800	24,600	11,800
200	27,500	40,300	20,800

Tributary Phosphorus Reduction with Flow Augmentation

These scenarios are a combination of scenario 2a, in which a minimum discharge of 150 ft^3/s was maintained at RM 38.4, and scenarios 1a and 1b, in which all boundary phosphorus (except the WWTPs) was reduced to TMDL levels. Flow augmentation that maintains 150 ft^3/s at RM 38.4 was used because it is more realistically attainable than that used in scenario 2b (minimum of 200 ft^3/s at RM 38.4). In scenario 3a, phosphorus was preferentially removed from the detrital phosphorus compartment, as in 1a; in scenario 3b, phosphorus was preferentially removed from the orthophosphate compartment, as in 1b. Scenario 3b was discussed earlier in this section because it produces the greatest overall reduction in algal growth. The summary statistics for these scenarios are included with the summary statistics for scenarios 1a and 1b in table 17. The results from scenario 2a are repeated in table 17 for reference.

The combination of orthophosphate reduction and flow augmentation in scenario 3b results in a greater reduction in algal growth than either of these scenarios (1b, 2a) produces alone at RM 16.2 (compare rows 14, 16, and 18 in table 17). Scenario 3a results in consistently higher chlorophyll-a (0.9 to 8.5 µg/L) and consistently higher DO (0.31 to 1.22 mg/L) than 3b at RM 16.2. Because this scenario contains elements of both 1a and 2a, the changes in DO at RM 5.5 relative to the calibration are mixed. Sometimes the reduction in chlorophyll-a results in lower DO because of lower photosynthetic production (compare rows 41 and 37); sometimes (notably May–June of 1991 and 1993) the reduction in CBOD causes DO to be increased relative to the calibration (compare rows 47 and 43). At RM 5.5, the reduced travel time sometimes results in increased algal growth in scenario 3b compared to an orthophosphate limitation without flow augmentation (scenario 1b), for the same reason that flow augmentation alone (scenario 2a) sometimes results in increased algal growth compared to the base case (compare rows 40 and 42).

Oswego Diversion Dam Modifications

In scenarios 4a and 4b, a decrease in travel time was achieved without requiring additional water from Henry Hagg Lake by lowering the water-surface elevation at the downstream end of the model reach. The elevation at the Oswego diversion dam was lowered in two phases. In the first phase (scenario 4a), it was assumed that none of the flashboards were put in place. The water then discharges over the full length of the broad cement weir, and the water-surface elevation of the pool is decreased by about 1.5 to 2 feet. In the second phase (scenario 4b), it was assumed that the entire weir structure was lowered by 4 feet and no flashboards were used, resulting in a water-surface reduction of about 5 to 5.5 feet. To accomplish this second phase, it was necessary to fix a new upstream boundary and generate new boundary conditions at RM 9.9 (Cook Park). When the Oswego diversion dam was lowered by 4 feet in the second phase, RM 9.9 became a shallow riffle that controlled the elevation upstream, in effect decoupling the reach of the river upstream of RM 9.9 from the reach downstream. Therefore, scenario 4b was simulated for a smaller grid covering only RMs 9.9 to 3.4, under the assumption that conditions upstream of RM 9.9 were unchanged from scenario 4a. This assumption was tested by incrementally lowering the dam elevation below the base elevation, and it was found that discharge and concentrations at RM 9.9 were unchanged from those in scenario 4a.

The effect of these scenarios on chlorophyll-a and dissolved oxygen at RM 16.2 is small, if noticeable at all (lines 2 and 4 in table 20; note that the results at RM 16.2 are the same for scenario 4a and 4b). At RM 5.5, the results can be most easily compared with the results of the flow augmentation scenario, to which it is most closely related. In general, the flow augmentation scenario, even at a floor of 150 ft^3/s (scenario 2a) effects more of a reduction in algal growth than does lowering the elevation at the Oswego diversion dam by removing all of the flashboards as in scenario 4a (compare row 8 in table 19 with row 6 in table 20).

Table 19. Summary statistics for the flow augmentation scenarios

[µg/L, micrograms per liter; mg/L, milligrams per liter. Mean concentrations for each constituent were derived from simulated, daily, 10-foot-average concentrations at noon. Concentrations given for the calibration simulation are the model's best representation of observed conditions in the summers of 1991, 1992, and 1993. Scenarios 2a and 2b simulate the effect of augmenting the discharge in the river with water having the same quality as that found in the Tualatin River at Dilley (river mile 58.8). These conditions were superimposed on the calibrated conditions of 1991, 1992, and 1993. These simulations maintained a minimum flow of either 150 ft^3/s (cubic feet per second) (2a) or 200 ft^3/s (2b) at the upstream boundary (river mile 38.4). Shaded cells highlight concentrations that would be in violation of a total maximum daily load criteria, the dissolved oxygen standard, or the chlorophyll-a action level]

Site	Parameter	Scenario	1991			1992			1993			Row
			May June	July August	September October	May June	July August	September October	May June	July August	September October	
River mile 16.2 (Elsner)	Chlorophyll-a (µg/L)	Calibration	8.4	36.7	13.9	35.5	50.4	18.3	6.7	25.9	12.9	1
		2a	8.4	29.9	10.3	29.8	44.7	12.0	6.7	22.6	8.4	2
		2b	7.7	18.3	6.8	21.6	35.1	8.0	6.6	16.1	6.4	3
	Dissolved oxygen (mg/L)	Calibration	8.56	8.62	7.74	9.79	9.85	7.21	8.61	7.99	7.92	4
		2a	8.57	8.26	7.77	9.36	9.68	7.44	8.61	7.91	7.83	5
		2b	8.55	7.90	7.98	8.93	9.33	7.62	8.61	7.84	8.08	6
River mile 5.5 (Stafford)	Chlorophyll-a (µg/L)	Calibration	17.4	65.7	33.2	46.7	47.5	24.7	13.8	52.9	26.1	7
		2a	17.4	69.6	30.0	44.8	49.8	21.0	13.9	50.1	21.4	8
		2b	16.1	62.6	20.6	38.1	49.3	16.5	13.9	40.4	15.5	9
	Dissolved oxygen (mg/L)	Calibration	8.69	11.08	8.64	10.47	8.75	6.97	8.74	9.49	7.73	10
		2a	8.69	11.07	8.34	10.27	9.29	7.21	8.75	9.25	7.44	11
		2b	8.60	10.28	7.92	9.74	9.57	7.30	8.75	8.69	7.44	12

Table 20. Summary statistics for the Oswego diversion dam (river mile 3.4) modification scenarios

[µg/L, micrograms per liter; mg/L, milligrams per liter. Mean concentrations for each constituent were derived from simulated, daily, 10-foot-average concentrations at noon. Concentrations given for the calibration simulation are the model's best representation of observed conditions in the summers of 1991, 1992, and 1993. Scenarios 4a and 4b superimpose changes in the Oswego diversion dam configuration on top of the calibrated conditions of 1991, 1992, and 1993. In scenario 4a, no flashboards are installed at any time. In scenario 4b, no flashboards are used and the entire dam is lowered by 4 feet. Shaded cells highlight concentrations that would be in violation of a total maximum daily load criteria, the dissolved oxygen standard, or the chlorophyll-a action level]

Site	Parameter	Scenario	1991			1992			1993			Row
			May June	July August	September October	May June	July August	September October	May June	July August	September October	
River mile 16.2 (Elsner)	Chlorophyll-a (µg/L)	Calibration	8.4	36.7	13.9	35.5	50.4	18.3	6.7	25.9	12.9	1
		4a	8.1	32.4	11.7	36.0	50.3	17.1	6.6	24.6	12.2	2
	Dissolved oxygen (mg/L)	Calibration	8.56	8.62	7.74	9.79	9.85	7.21	8.61	7.99	7.92	3
		4a	8.55	8.36	7.69	9.83	10.09	7.24	8.61	7.95	7.94	4
River mile 5.5 (Stafford)	Chlorophyll-a (µg/L)	Calibration	17.4	65.7	33.2	46.7	47.5	24.7	13.8	52.9	26.1	5
		4a	16.8	76.1	30.8	47.5	52.4	26.5	13.7	54.0	25.8	6
		4b	13.6	61.2	29.5	44.9	53.8	27.5	13.1	44.6	23.7	7
	Dissolved oxygen (mg/L)	Calibration	8.69	11.08	8.64	10.47	8.75	6.97	8.74	9.49	7.73	8
		4a	8.69	11.80	8.42	10.58	9.60	7.38	8.74	9.78	7.89	9
		4b	8.72	10.16	8.65	10.14	9.51	8.04	8.83	9.12	8.27	10

In contrast, scenario 4a results in bimonthly average DO concentrations at RM 5.5 that generally exceed those in scenario 2a by -0.01 to 0.73 mg/L (compare row 9 in table 20 with row 11 in table 19). If the dam is lowered by an additional 4 ft (4a to 4b), then additional reductions of as much as 15 μg/L of chlorophyll-a are sometimes achieved at RM 5.5, with concomitant losses of as much as 1.6 mg/L of DO (compare row 6 with 7 and 9 with 10 in table 20). During the sensitive September–October period, however, lowering the dam by 4 feet generates higher DO concentrations (0.31 to 0.83 mg/L) at RM 5.5 than produced by either of the flow augmentation scenarios (compare row 10 in table 20 with rows 11 and 12 in table 19).

Stream Temperature Reductions

In the stream temperature reduction scenarios (5a and 5b), the temperature of all tributary boundaries (not including the WWTPs) and the upstream boundary (RM 38.4) was decreased by 2°C (scenario 5a) and 5°C (scenario 5b). Experimentation with variations on this scenario demonstrated that reductions in temperature for tributaries downstream of RM 38.4 made little difference in the main-stem temperature. In order to create significant reductions in the main-stem temperature, the temperature of the water entering the system at the upstream boundary had to be lowered. Even when this was done, a 5°C reduction at RM 38.4 amounted to only about a 1°C decrease at RM 5.5 from July to October, and a 2 to 3°C decrease in May and June (rows 10 and 12, table 21).

The summary statistics for these scenarios show that algal growth is consistently reduced (by 11 to 40 percent) at RM 16.2 when the stream temperature is reduced (rows 5 and 6, table 21). This is generally true also at RM 5.5, although during the July–August period in 1991 and 1992 algal growth is shown to actually increase slightly; this is probably due to a slowing of growth in both the algae and the zooplankton that serves to shift the population backward along the growth curve shown in figure 56. In general, the DO concentration increases in the bimonthly means as water temperature decreases (lines 8, 9, 17 and 18 in table 21).

Scenarios 5b and 1a make an interesting comparison (figs. 55 and 57). The temperature reduction scenarios reduce the rate of decay of organic matter in the sediments and the water column, and sometimes increase the DO more than does a reduction in CBOD—during May, for example. During a rapid succession of algal blooms, such as the July–August period of 1991, the reduced stream temperature moderates the "peaks" and "valleys" of the DO by reducing photosynthetic production during blooms and reducing consumption of DO during subsequent crashes of the algal population. The bimonthly mean of DO during this period, however, decreases in scenario 5b as compared to the calibration because the number of phytoplankton bloom days is greater than the number of crash days. On the other hand, scenario 1a tends to increase DO at both the high and low points in chlorophyll-a concentrations, so that DO is usually higher when compared to the temperature reduction scenarios (compare rows 8 and 9 in table 21 with row 21 in table 17).

Optimal Wastewater-Treatment-Plant Operations

For scenarios 6a and 6b, ceilings were placed on ammonia, orthophosphate, and total phosphorus concentrations in the WWTP effluent. These ceilings were based on an examination of the effluent concentrations when the WWTPs were operating at peak efficiency during selected periods of 1992. For scenario 6a, the concentration of ammonia was capped at 0.3 mg/L as N, and any ammonia over this amount was added to the nitrate concentration under the assumption that nitrification was converting ammonia to nitrate. The orthophosphate concentration was capped at 0.03 mg/L as P and the total phosphorus concentration at 0.07 mg/L as P. Any phosphorus in excess of these concentrations was assumed to be removed entirely from the effluent by the treatment process. For scenario 6b, it was assumed that the WWTPs were operating at the same efficiency, but that the amount of WWTP discharge was doubled. This scenario was designed to simulate the effect of population growth in the basin.

The summary statistics in table 22 show that operating the plants at peak efficiency has very little effect (less than 0.003 mg/L) on the concentrations of orthophosphate and total phosphorus at RM 16.2 (compare row 2 with 1 and 5 with 4 in table 22), mainly because the Rock Creek WWTP was already operating near peak phosphorus removal efficiency during this time period.

Table 21. Summary statistics for the stream temperature reduction scenarios

[°C, degrees Celsius; µg/L, micrograms per liter; mg/L, milligrams per liter. Mean temperatures and concentrations were derived from simulated, daily, 10-foot-averages at noon. Temperatures and concentrations given for the calibration simulation are the model's best representation of observed conditions in the summers of 1991, 1992, and 1993. Scenarios 5a and 5b simulate the effect of decreasing the water temperature of all tributary and upstream sources to the main stem by 2°C and 5°C, respectively. Shaded cells highlight concentrations that would be in violation of a total maximum daily load criteria, the dissolved oxygen standard, or the chlorophyll-a action level]

Site	Parameter	Scenario	1991			1992			1993			Row
			May June	July August	September October	May June	July August	September October	May June	July August	September October	
River mile 16.2 (Elsner)	Temperature (°C)	Calibration	13.97	19.78	15.07	17.79	19.95	14.93	15.25	18.34	14.76	1
		5a	12.73	19.13	14.37	17.02	19.46	14.39	13.90	17.66	14.00	2
		5b	10.87	18.17	13.34	15.91	18.67	13.58	11.88	16.62	12.87	3
	Chlorophyll-a (µg/L)	Calibration	8.4	36.7	13.9	35.5	50.4	18.3	6.7	25.9	12.9	4
		5a	6.8	30.0	11.2	33.1	48.4	15.8	5.7	22.1	10.8	5
		5b	5.3	22.1	8.3	29.4	44.7	12.7	4.7	17.2	8.2	6
	Dissolved oxygen (mg/L)	Calibration	8.56	8.62	7.74	9.79	9.85	7.21	8.61	7.99	7.92	7
		5a	8.73	8.32	7.82	9.80	9.91	7.28	8.78	7.95	8.06	8
		5b	9.04	8.12	8.05	9.83	9.94	7.45	9.05	7.97	8.32	9
River mile 5.5 (Stafford)	Temperature (°C)	Calibration	14.33	20.94	16.07	18.31	20.93	15.57	15.73	18.99	15.84	10
		5a	13.32	20.52	15.69	17.76	20.64	15.26	14.60	18.59	15.41	11
		5b	11.80	19.92	15.09	16.91	20.25	14.80	12.91	17.87	14.72	12
	Chlorophyll-a (µg/L)	Calibration	17.4	65.7	33.2	46.7	47.5	24.7	13.8	52.9	26.1	13
		5a	14.4	68.5	30.8	44.7	48.8	23.4	11.3	48.7	24.1	14
		5b	10.5	69.2	26.2	41.2	50.3	21.5	8.2	41.3	20.9	15
	Dissolved oxygen (mg/L)	Calibration	8.69	11.08	8.64	10.47	8.75	6.97	8.74	9.49	7.73	16
		5a	8.72	11.13	8.47	10.44	9.01	6.96	8.79	9.25	7.77	17
		5b	8.82	11.08	8.24	10.35	9.33	7.02	8.90	8.81	7.84	18

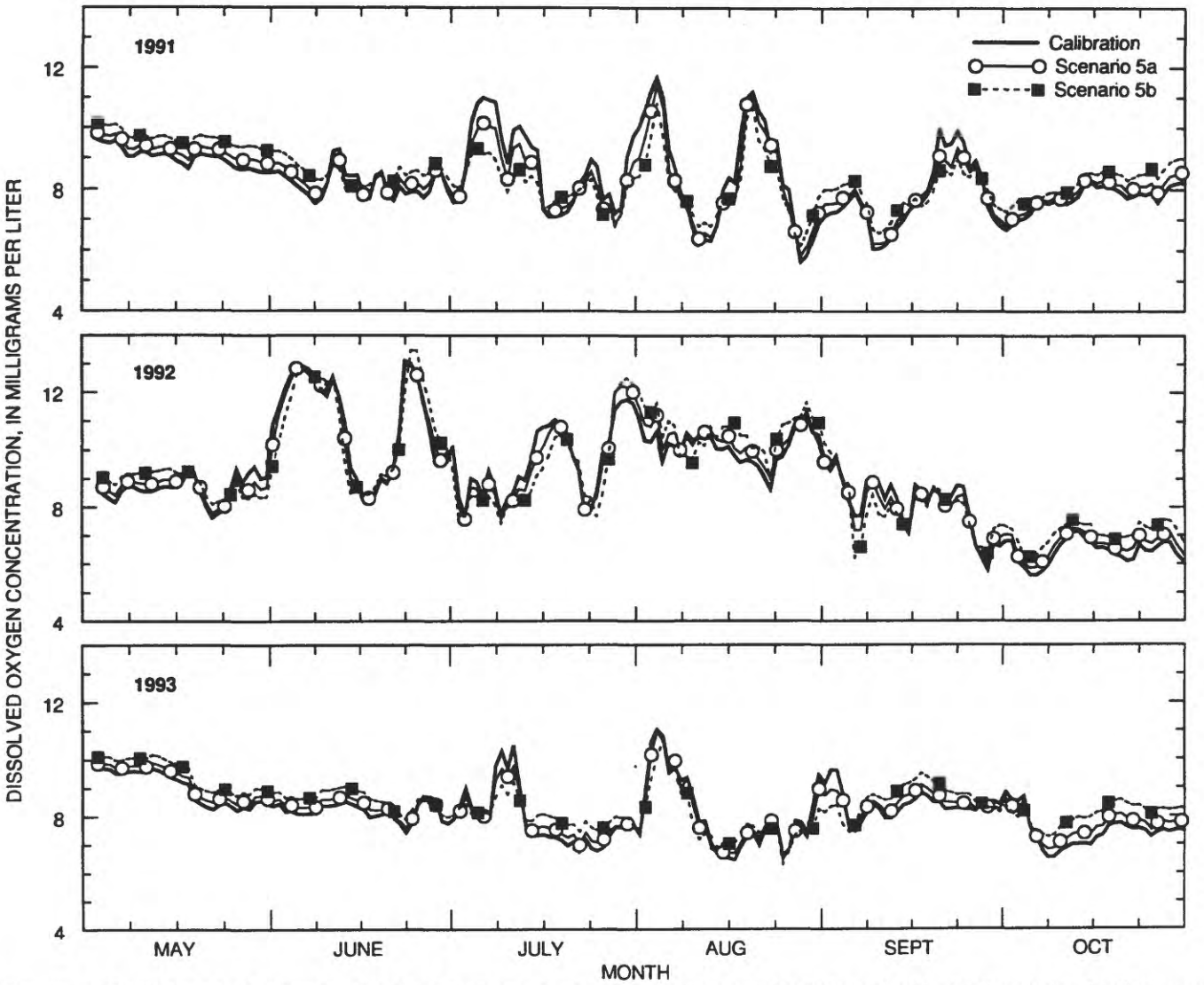

Figure 57. Comparison of calibrated dissolved oxygen concentration at river mile 16.2 (Elsner) with simulated dissolved oxygen concentrations from two temperature reduction scenarios.

The fractional decrease in ammonia concentrations is sometimes large (0 to 49 percent), especially in 1993 (compare row 8 with 7), but ammonia concentrations were already less than 0.1 mg/L, so even a 50 percent reduction is not particularly significant. It is not surprising, therefore, that the changes in simulated chlorophyll-a and DO concentrations are negligible (compare row 11 with 10 and 14 with 13 in table 22). Both the peak efficiency (6a) and peak efficiency with growth (6b) scenarios simulate total phosphorus concentrations at RM 16.2 that remain out of compliance with the total phosphorus TMDL criteria. The very slight reduction in total phosphorus concentration between scenario 6a and 6b at RM 16.2 (compare row 5 with 6 in table 22) indicates that effluent concentrations of total phosphorus are generally lower than the receiving water concentrations, thus when the effluent is doubled the total phosphorus in the river is diluted slightly. A slight reduction in the algal population (-5 to -16 percent) is also simulated at RM 16.2 when the effluent is doubled, which can be attributed to an effect similar to a small amount of flow augmentation. The effluent from the Rock Creek WWTP averaged about 20 ft^3/s through the July–August period during all 3 years, so a doubled effluent discharge would augment the flow through the model reach by an additional 20 ft^3/s.

At RM 5.5, downstream of the Durham WWTP, the effect of operating the plant at peak efficiency on the algae is noticeable during 1991 and 1993, producing reductions in chlorophyll-a of 25 and 18 percent, respectively, in midsummer.

Table 22. Summary statistics for the peak efficiency and population growth scenarios

[milligrams per liter; P, phosphorus; N, nitrogen; µg/L, micrograms per liter. Mean concentrations for each constituent were derived from simulated, daily, 10-foot-average concentrations at noon. Concentrations given for the calibration simulation are the model's best representation of observed conditions in the summers of 1991, 1992, and 1993. Scenarios 6a and 6b superimpose two hypothetical changes in the operation of the wastewater-treatment plants on top of the calibrated conditions of 1991, 1992, and 1993. In the Peak Efficiency scenario (6a), both the Rock Creek and Durham Wastewater-Treatment Plants are operated at peak efficiency, defined with maximum effluent concentrations of orthophosphate, total phosphorus, and ammonia nitrogen of 0.03, 0.07, and 0.3 mg/L, respectively. In the Population Growth scenario (6b), the wastewater-treatment plants are operated at peak efficiency and their discharge is doubled. Shaded cells highlight concentrations that would be in violation of a total maximum daily load criteria, the dissolved oxygen standard, or the chlorophyll-a action level]

Site	Parameter	Scenario	1991			1992			1993			Row
			May June	July August	September October	May June	July August	September October	May June	July August	September October	
River mile 16.2 (Elsner)	Ortho-phosphate (mg/L as P)	Calibration	0.051	0.048	0.056	0.042	0.018	0.055	0.055	0.048	0.053	1
		6a	.051	.048	.056	.042	.018	.055	.054	.048	.052	2
		6b	.049	.048	.052	.041	.018	.049	.053	.046	.049	3
	Total phosphorus (mg/L as P)	Calibration	.115	.110	.098	.100	.076	.104	.113	.102	.100	4
		6a	.115	.110	.097	.100	.076	.104	.110	.100	.098	5
		6b	.110	.104	.090	.095	.073	.096	.108	.097	.092	6
	Ammonia (mg/L as N)	Calibration	.095	.035	.064	.064	.028	.061	.184	.055	.086	7
		6a	.090	.035	.061	.052	.028	.061	.094	.041	.059	8
		6b	.091	.034	.061	.055	.025	.059	.101	.051	.068	9
	Chlorophyll-a (µg/L)	Calibration	8.4	36.7	13.9	35.5	50.4	18.3	6.7	25.9	12.9	10
		6a	8.3	36.6	13.9	35.6	50.1	18.2	6.7	25.9	12.9	11
		6b	7.3	30.6	12.2	32.2	46.7	17.3	6.1	22.7	11.3	12
	Dissolved oxygen (mg/L)	Calibration	8.56	8.62	7.74	9.79	9.85	7.21	8.61	7.99	7.92	13
		6a	8.56	8.62	7.75	9.80	9.82	7.20	8.63	8.04	7.96	14
		6b	8.51	8.32	7.72	9.49	9.61	7.27	8.61	7.88	7.88	15
River mile 5.5 (Stafford)	Ortho-phosphate (mg/L as P)	Calibration	.081	.058	.051	.028	.009	.043	.101	.112	.058	16
		6a	.047	.022	.039	.028	.008	.043	.050	.031	.045	17
		6b	.045	.022	.036	.027	.006	.037	.050	.031	.042	18
	Total phosphorus (mg/L as P)	Calibration	.166	.174	.117	.094	.066	.094	.169	.199	.140	19
		6a	.116	.098	.091	.094	.065	.093	.113	.093	.095	20
		6b	.110	.093	.084	.089	.062	.086	.110	.090	.090	21
	Ammonia (mg/L as N)	Calibration	.710	.490	.150	.054	.051	.089	.287	.346	1.236	22
		6a	.097	.044	.053	.042	.046	.066	.090	.045	.072	23
		6b	.104	.044	.059	.041	.036	.067	.101	.054	.084	24
	Chlorophyll-a (µg/L)	Calibration	17.4	65.7	33.2	46.7	47.5	24.7	13.8	52.9	26.1	25
		6a	15.5	49.5	30.6	46.7	47.6	24.6	13.7	43.2	23.7	26
		6b	13.7	50.4	27.9	41.6	46.4	23.3	12.1	38.7	21.0	27
	Dissolved oxygen (mg/L)	Calibration	8.69	11.08	8.64	10.47	8.75	6.97	8.74	9.49	7.73	28
		6a	8.63	10.37	8.60	10.47	8.78	6.97	8.78	9.04	8.02	29
		6b	8.54	10.12	8.45	10.11	9.06	7.27	8.70	8.76	7.94	30

Orthophosphate and ammonia concentrations are reduced by an average of 45 and 82 percent, respectively, in those seasons (compare row 17 with 16 and 23 with 22 in table 22), and as a result chlorophyll-a concentrations are reduced by up to 25 percent, especially during the July–August period when the largest blooms occur (compare row 26 with 25). In 1992, the WWTPs were already operating at peak efficiency. The effect of doubling the effluent discharge on top of peak operating efficiency is to further limit algal growth by roughly an additional 10 percent during 1991 and 1993, probably due to the flow augmentation effect (compare rows 25, 26, and 27 in table 22). The slight increase in chlorophyll-a during July–August of 1991 is due to bringing the travel time closer to the time of peak algal concentration (fig. 56). Dissolved oxygen bimonthly means in 1991 and 1993 generally decrease (by as much as 0.71 mg/L) with these decreases in chlorophyll-a; an increase in the DO for September–October of 1993 (row 29, table 22) can be attributed to a decrease in instream nitrification corresponding to instream ammonia concentration reductions by more than 1 order of magnitude (compare row 23 with 22, table 22). Generally, and as stated previously, instream nitrification does not play a large role in this system during the summer months since advanced ammonia and phosphorus removal was implemented at the WWTPs. However, the September–October concentrations in 1993 downstream of the Durham WWTP are the highest of the 18 months of simulations, and high enough that instream nitrification plays a noticeable but still minor role in determining DO concentrations.

Denitrification in the Wastewater-Treatment Plants

In scenario 7, it was assumed that state-of-the-art nitrification and denitrification was implemented in the WWTPs. This type of nitrogen removal can be expected to decrease effluent nitrate concentrations to about 2 mg/L as N (Mike Duvendack, CH2M-Hill, oral commun., 1994). Nitrification was assumed to be complete under these conditions, so the ammonia effluent concentration was set to 0 mg/L as N. In order to simulate a "worst-case" scenario, the nitrogen half-saturation constant for algal growth was set at 0.025 mg/L, which is considerably higher than the value of 0.008 mg/L used in all other scenarios and the calibration. The purpose of this simulation was to determine if WWTP nitrification/denitrification could result in instream nitrogen concentrations low enough to limit algal growth.

The summary statistics are compiled in table 23. Reductions in nitrate concentrations were significant (0.25 to 3.38 mg/L as N); reductions in ammonia concentrations were not as consistent, but the concentrations were routinely reduced below 0.08 mg/L as N. Occasionally, at very low ammonia concentrations, this WWTP denitrification scenario simulated a small increase in ammonia concentration (up to 0.022 mg/L as N) over the calibration, particularly at RM 16.2 (row 2 in table 23). This occurs because the half-saturation constant used in this simulation decreases the algal preference for ammonia at very low ammonia concentrations (see eq. 30), and therefore the algae take up relatively more nitrate in this simulation than in the calibration. The chlorophyll-a and dissolved oxygen statistics show less than a 3 percent change between the calibration and the denitrification scenario. In short, this scenario shows that the background concentrations of nitrate in this river are high enough that even if very efficient denitrification (down to 2 mg/L of NO_3-N) were implemented at the WWTPs, nitrogen cannot be made to limit algal growth without taking other measures.

Reduction in Sediment Oxygen Demand

In scenario 8, the sediment compartment was initialized such that the resultant SOD was one-half of that used in the calibration runs. This scenario is not a particularly feasible management scenario because management strategies that keep soil and organic matter out of the river may not be expected to achieve such a reduction. This scenario does, however, demonstrate the importance of SOD in the Tualatin River, and it is useful for comparison purposes. The summary statistics are presented in table 24. This scenario results in almost no change (0 to 6 percent) in the concentrations of orthophosphate, total phosphorus, or chlorophyll-a. Bimonthly mean concentrations of total phosphorus that are out of compliance with the TMDL criteria in the calibration remain so in this scenario. The increases in DO produced by this scenario, however, are the largest achieved by any of these scenarios (0.43 to 2.42 mg/L), especially during the sensitive September–October period (row 16 in table 24).

Table 23. Summary statistics for the wastewater-treatment-plant denitrification scenario

[mg/L, milligrams per liter; N, nitrogen; µg/L, micrograms per liter. Mean concentrations for each constituent were derived from simulated, daily, 10-foot-average concentrations at noon. Concentrations given for the calibration simulation are the model's best representation of observed conditions in the summers of 1991, 1992, and 1993. Scenario 7 simulates the effect of installing denitrification capabilities at the Rock Creek and Durham wastewater-treatment plants. Effluent concentrations of ammonia and nitrate were assumed to be 0.0 and 2.0 mg/L as nitrogen, respectively. These conditions were imposed on top of the calibrated conditions of 1991, 1992, and 1993. An algal half-saturation constant for nitrogen of 0.025 mg/L was used in scenario 7. Shaded cells highlight concentrations that would be in violation of a total daily maximum load criteria, the dissolved oxygen standard, or the chlorophyll-a action level]

Site	Parameter	Scenario	1991			1992			1993			Row
			May June	July August	September October	May June	July August	September October	May June	July August	September October	
River mile 16.2 (Elsner)	Ammonia (mg/L as N)	Calibration	0.095	0.035	0.064	0.064	0.028	0.061	0.184	0.055	0.086	1
		7	.091	.048	.069	.062	.048	.069	.090	.051	.057	2
	Nitrate (mg/L as N)	Calibration	1.60	1.55	1.76	1.52	1.80	2.48	1.05	1.67	1.56	3
		7	.83	.66	.64	.70	.56	.61	.80	.69	.60	4
	Chlorophyll-a (µg/L)	Calibration	8.4	36.7	13.9	35.5	50.4	18.3	6.7	25.9	12.9	5
		7	8.4	36.7	14.0	35.7	50.7	18.3	6.7	26.0	13.0	6
	Dissolved oxygen (mg/L)	Calibration	8.56	8.62	7.74	9.79	9.85	7.21	8.61	7.99	7.92	7
		7	8.56	8.62	7.74	9.79	9.87	7.21	8.62	8.01	7.93	8
River mile 5.5 (Stafford)	Ammonia (mg/L as N)	Calibration	.710	.490	.150	.054	.051	.089	.287	.346	1.236	9
		7	.090	.066	.062	.054	.073	.077	.082	.057	.075	10
	Nitrate (mg/L as N)	Calibration	1.59	1.91	2.96	2.82	3.50	4.20	1.13	2.29	2.10	11
		7	.87	.57	.75	.73	.75	.82	.82	.72	.75	12
	Chlorophyll-a (µg/L)	Calibration	17.4	65.7	33.2	46.7	47.5	24.7	13.8	52.9	26.1	13
		7	17.4	65.6	33.3	46.7	47.4	24.7	13.8	52.6	26.2	14
	Dissolved oxygen (mg/L)	Calibration	8.69	11.08	8.64	10.47	8.75	6.97	8.74	9.49	7.73	15
		7	8.73	11.15	8.65	10.47	8.78	6.97	8.76	9.52	7.94	16

Table 24. Summary statistics for the sediment oxygen demand reduction scenario.

[mg/L, milligrams per liter; P, phosphorus; µg/L, micrograms per liter. Mean concentrations for each constituent were derived from simulated, daily, 10-foot-average concentrations at noon. Concentrations given for the calibration simulation are the model's best representation of observed conditions in the summers of 1991, 1992, and 1993. Scenario 8 simulates the effect of cutting the initial sediment oxygen demand rate in half while maintaining all other rates and parameters from the calibration simulations of 1991, 1992, and 1993. Shaded cells highlight concentrations that would be in violation of a total maximum daily load criteria, the dissolved oxygen standard, or the chlorophyll-a action level]

Site	Parameter	Scenario	1991			1992			1993			Row
			May June	July August	September October	May June	July August	September October	May June	July August	September October	
River mile 16.2 (Elsner)	Ortho-phosphate (mg/L as P)	Calibration	0.051	0.048	0.056	0.042	0.018	0.055	0.055	0.048	0.053	1
		8	.051	.047	.055	.041	.017	.054	.054	.047	.052	2
	Total phosphorus (mg/L as P)	Calibration	.115	.110	.098	.100	.076	.104	.113	.102	.100	3
		8	.115	.109	.096	.098	.075	.102	.112	.101	.099	4
	Chlorophyll-a (µg/L)	Calibration	8.4	36.7	13.9	35.5	50.4	18.3	6.7	25.9	12.9	5
		8	8.3	36.2	13.9	35.0	49.3	18.1	6.7	25.7	13.0	6
	Dissolved oxygen (mg/L)	Calibration	8.56	8.62	7.74	9.79	9.85	7.21	8.61	7.99	7.92	7
		8	9.14	10.00	8.99	10.97	11.63	8.79	9.04	9.35	9.05	8
River mile 5.5 (Stafford)	Ortho-phosphate (mg/L as P)	Calibration	.081	.058	.051	.028	.009	.043	.101	.112	.058	9
		8	.081	.058	.049	.027	.008	.042	.100	.110	.057	10
	Total phosphorus (mg/L as P)	Calibration	.166	.174	.117	.094	.066	.094	.169	.199	.140	11
		8	.165	.173	.115	.093	.064	.092	.169	.196	.139	12
	Chlorophyll-a (µg/L)	Calibration	17.4	65.7	33.2	46.7	47.5	24.7	13.8	52.9	26.1	13
		8	17.3	61.6	32.3	45.9	44.9	24.0	13.8	52.0	25.4	14
	Dissolved oxygen (mg/L)	Calibration	8.69	11.08	8.64	10.47	8.75	6.97	8.74	9.49	7.73	15
		8	9.43	12.78	10.33	11.90	11.17	9.06	9.31	11.24	9.25	16

This scenario complements those that reduce allochthonous CBOD (scenarios 1a and 3a); taken together, these scenarios demonstrate that most of the oxygen demand in the Tualatin River comes from the decay of allochthonous organic matter in the water column and the decay of organic matter in the bed sediments.

Wastewater-Treatment-Plant Operations Prior to Nutrient Removal

Scenarios 9a and 9b are included to demonstrate that biological nutrient removal (nitrogen and phosphorus) and two-stage alum addition for further phosphorus removal at the WWTPs has had a significant effect on the size of the algal blooms and on the DO concentration in the Tualatin River. Concentrations of total phosphorus, orthophosphate, ammonia and nitrate for this scenario were based on typical 1988 summer effluent concentrations, as indicated in table 25. For scenario 9a, the same nitrification rate was used as in the calibration simulations (0.023 day^{-1}). For scenario 9b, the nitrification rate was substantially increased, under the supposition that if ammonia concentrations were historically at much higher levels for the entire summer, then a large population of nitrifying bacteria would build up in the river and nitrification would proceed at a faster rate than was measured in 1993. The nitrification rate used was based on a modeling study of a 2-week period in November 1992, when large loads of ammonia were discharged into the river (Kelly, 1996). Nitrification rates of 0.22 day^{-1} in the upper river (RMs 38.4 to 30) and 0.055 day^{-1} in the lower river (RMs 30 to 3.4) were derived from that modeling study, and those rates were used in scenario 9b.

Table 25. Typical effluent concentrations during the summer of 1988 for two wastewater-treatment plants on the Tualatin River
[WWTP, wastewater-treament plant; P, phosphorus; N, nitrogen]

Parameter	Rock Creek WWTP	Durham WWTP
Total Phosphorus	2.1 mg/L as P	3.6 mg/L as P
Orthophosphate	1.6 mg/L as P	3.0 mg/L as P
Ammonia	23.3 mg/L as N	12.5 mg/L as N
Nitrate	2.6 mg/L as N	4.8 mg/L as N

As mentioned previously in the *Boundary Conditions, Reaction Rates, and Forcing Functions* section, an instream nitrification rate of 0.11 d^{-1} for the reach from RM 38.1 to 16.2 was determined from data collected in 1995, after the model calibration was completed. Scenario 9b should be closer to the expected results with this new nitrification rate.

Both scenarios 9a and 9b simulate much larger algal blooms than those observed with the calibration data. The most extreme case is provided by 1992, when the July–August mean chlorophyll-a concentration is simulated at 3 times and 5 times the observed values at RM 16.2 and RM 5.5, respectively (compare rows 14 and 15 with 13, rows 32 and 33 with 31, and rows 50 and 51 with 49 in table 26). Nutrient concentrations are greatly increased in these scenarios. Orthophosphate concentrations increase by a factor of 3 to 40, with the biggest fractional increases at RM 5.5 (row 38, July–August 1992). Ammonia concentrations increase by a factor of 5 to 80, with the biggest fractional increases at RM 26.9 (row 8, July–August 1992). Such greatly increased concentrations may well violate the assumption that scenario conditions are small deviations from the calibration conditions, and that the calibration parameters remain valid. Therefore, these results must be interpreted with the appropriate caution. Nonetheless, there is some evidence that historical levels of chlorophyll-a were indeed a great deal higher than they have been since the WWTPs were upgraded. During 1987, for example, which was a very low-flow year and comparable to 1992, algal blooms produced near-surface chlorophyll-a concentrations of up to 400 µg/L at RM 16.2 and almost 250 µg/L at RM 5.5. Those conditions were accompanied by measured dissolved oxygen concentrations in excess of 20 mg/L, which is comparable to these model results. These results and the 1987 data both suggest that if light and temperature conditions were favorable, travel times were long, and grazing losses were small, algal blooms could grow much larger historically than they do under the same conditions today. Similarly, if the upgrades had not been made at the WWTPs, the potential for producing enormous phytoplankton blooms today, with concomitant DO problems due to algal bloom/crash cycles, would be very high. Clearly, contemporary nutrient load reductions have had a significant, positive effect on water quality in the Tualatin River.

Scenarios 9a and 9b also demonstrate the historical importance of nitrification. Simulated concentrations of ammonia in these scenarios are out

Table 26. Summary statistics for the wastewater-treatment-plant operations prior to nutrient-removal scenarios

[mg/L, milligrams per liter; P, phosphorus; N, nitrogen; µg/L, micrograms per liter. Mean concentrations for each constituent were derived from simulated, daily, 10-foot-average concentrations at noon. Concentrations given for the calibration simulation are the model's best representation of observed conditions in the summers of 1991, 1992, and 1993. Scenarios 9a and 9b simulate the effect of imposing wastewater-treatment-plant loads of nitrate, ammonia, orthophosphate and total phosphorus similar to those observed in 1988 on top of the calibrated conditions of 1991, 1992, and 1993. Scenario 9a used a nitrification rate of 0.023 d^{-1}, while scenario 9b used two, higher nitrification rates (0.22 d^{-1}, river mile 38.4–30; 0.055 d^{-1}, river mile 30–3.4) to represent the buildup of a large community of nitrifying bacteria in the river. Shaded cells highlight concentrations that would be in violation of a total maximum daily load criteria, the dissolved oxygen standard, or the chlorophyll-a action level]

Site	Parameter	Scenario	1991			1992			1993			Row
			May June	July August	September October	May June	July August	September October	May June	July August	September October	
River mile 26.9 (Scholls)	Ortho-phosphate (mg/L as P)	Calibration	0.049	0.058	0.053	0.054	0.040	0.054	0.053	0.053	0.049	1
		9a	.149	.232	.247	.230	.271	.308	.119	.247	.236	2
		9b	.149	.232	.247	.230	.272	.308	.119	.247	.236	3
	Total phosphorus (mg/L as P)	Calibration	.115	.109	.094	.100	.089	.100	.113	.102	.096	4
		9a	.244	.333	.343	.324	.383	.424	.196	.345	.335	5
		9b	.244	.333	.343	.324	.383	.424	.196	.345	.335	6
	Ammonia (mg/L as N)	Calibration	.093	.054	.076	.081	.038	.056	.189	.093	.097	7
		9a	1.519	2.497	2.794	2.497	3.181	3.580	1.042	2.777	2.695	8
		9b	1.369	2.087	2.354	2.069	2.561	2.928	.948	2.329	2.313	9
	Nitrate (mg/L as N)	Calibration	1.61	1.67	1.76	1.64	1.99	2.45	1.07	1.71	1.53	10
		9a	.88	.87	.75	.96	.94	.79	.85	.86	.70	11
		9b	1.03	1.28	1.19	1.39	1.56	1.44	.94	1.31	1.08	12
	Chlorophyll-a (µg/L)	Calibration	3.8	5.9	3.9	11.6	19.4	6.2	3.9	6.7	4.2	13
		9a	3.8	5.8	3.8	12.0	20.1	6.1	3.9	6.7	4.1	14
		9b	3.8	5.8	3.8	12.0	20.1	6.1	3.9	6.7	4.1	15
	Dissolved oxygen (mg/L)	Calibration	8.99	8.00	8.54	8.68	8.55	8.14	8.94	8.10	8.71	16
		9a	8.78	7.34	7.85	8.05	7.58	7.14	8.83	7.45	8.15	17
		9b	8.30	6.15	6.57	6.88	5.88	5.37	8.51	6.17	7.04	18
River mile 16.2 (Elsner)	Ortho-phosphate (mg/L as P)	Calibration	.051	.048	.056	.042	.018	.055	.055	.048	.053	19
		9a	.147	.210	.247	.179	.166	.308	.115	.229	.240	20
		9b	.147	.210	.247	.179	.167	.308	.115	.229	.240	21
	Total phosphorus (mg/L as P)	Calibration	.115	.110	.098	.100	.076	.104	.113	.102	.100	22
		9a	.236	.313	.334	.293	.333	.417	.187	.326	.331	23
		9b	.236	.313	.334	.293	.333	.417	.187	.326	.331	24

Table 26. Summary statistics for the wastewater-treatment-plant operations prior to nutrient-removal scenarios—Continued

Site	Parameter	Scenario	1991			1992			1993			Row
			May June	July August	September October	May June	July August	September October	May June	July August	September October	
River mile 16.2 (Elsner)—Continued	Ammonia (mg/L as N)	Calibration	.095	.035	.064	.064	.028	.061	.184	.055	.086	25
		9a	1.384	1.989	2.480	1.788	1.994	3.169	.929	2.309	2.463	26
		9b	1.196	1.465	1.891	1.306	1.242	2.295	.819	1.740	1.929	27
	Nitrate (mg/L as N)	Calibration	1.60	1.55	1.76	1.52	1.80	2.48	1.05	1.67	1.56	28
		9a	.95	1.11	1.03	1.16	1.35	1.24	.87	1.13	.96	29
		9b	1.14	1.63	1.62	1.64	2.10	2.11	.98	1.70	1.50	30
	Chlorophyll-a (µg/L)	Calibration	8.4	36.7	13.9	35.5	50.4	18.3	6.7	25.9	12.9	31
		9a	8.5	40.8	13.9	67.5	143.8	22.9	6.7	31.7	13.5	32
		9b	8.5	41.5	14.0	66.9	143.6	23.2	6.7	31.7	13.5	33
	Dissolved oxygen (mg/L)	Calibration	8.56	8.62	7.74	9.79	9.85	7.21	8.61	7.99	7.92	34
		9a	8.05	7.15	5.78	11.10	16.13	4.56	8.35	6.66	6.26	35
		9b	7.48	5.83	4.21	9.83	14.33	2.49	8.01	5.18	4.84	36
River mile 5.5 (Stafford)	Ortho-phosphate (mg/L as P)	Calibration	.081	.058	.051	.028	.009	.043	.101	.112	.058	37
		9a	.279	.374	.491	.358	.351	.579	.205	.470	.503	38
		9b	.279	.373	.490	.357	.350	.576	.205	.469	.502	39
	Total Phosphorus (mg/L as P)	Calibration	.166	.174	.117	.094	.066	.094	.169	.199	.140	40
		9a	.399	.566	.638	.532	.625	.748	.300	.637	.647	41
		9b	.399	.566	.638	.532	.624	.747	.300	.637	.646	42
	Ammonia (mg/L as N)	Calibration	.710	.490	.150	.054	.051	.089	.287	.346	1.236	43
		9a	1.700	1.937	2.928	1.933	1.802	3.450	1.165	2.635	3.005	44
		9b	1.503	1.457	2.251	1.522	1.213	2.616	1.050	2.069	2.403	45
	Nitrate (mg/L as N)	Calibration	1.59	1.91	2.96	2.82	3.50	4.20	1.13	2.29	2.10	46
		9a	1.20	1.64	1.74	1.57	2.09	2.11	1.03	1.76	1.64	47
		9b	1.40	2.12	2.41	1.98	2.68	2.91	1.14	2.32	2.24	48
	Chlorophyll-a (µg/L)	Calibration	17.4	65.7	33.2	46.7	47.5	24.7	13.8	52.9	26.1	49
		9a	20.0	115.2	46.2	109.3	250.1	55.1	14.4	78.2	36.2	50
		9b	20.0	119.9	49.1	108.7	250.6	55.9	14.4	78.8	37.1	51
	Dissolved Oxygen (mg/L)	Calibration	8.69	11.08	8.64	10.47	8.75	6.97	8.74	9.49	7.73	52
		9a	8.22	13.93	6.76	14.05	24.22	6.24	8.44	9.44	6.34	53
		9b	7.66	12.86	5.28	13.01	22.72	4.94	8.11	8.06	4.85	54

of compliance with the ammonia TMDL criteria throughout most of the model reach. At the higher rate of nitrification (scenario 9b), out-of-compliance dissolved oxygen concentrations are also generated throughout the model reach. Nitrification, like each of the other oxygen demands, removes more oxygen from the water when travel times are long. Therefore, the decreases in DO are greatest during the low-flow periods (July–August and September–October, table 26), and particularly during 1992 when flows were lower than in 1991 or 1993.

SUMMARY

The two-dimensional, laterally averaged water-quality model CE-QUAL-W2 proved to be a useful tool for developing and understanding water-quality issues in the Tualatin River. With modifications to a few algorithms, the simulation of the water budget, heat budget, and water-quality constituents calibrated well to observed data. Future improvements to the model, such as the inclusion of a more predictive sediments compartment, algorithms to trigger seasonal variations in algal growth, and refinements in the phytoplankton/zooplankton interactions, will further enhance its usefulness.

Phytoplankton growth is a primary factor determining the quality of water in the Tualatin River. Observed data indicate that the timing and extent of an algal bloom is overwhelmingly dependent on the travel time in the river, the temperature of the water, and the incident solar radiation. Therefore, the water budget was carefully balanced in order to ensure that travel times would be accurate. Good insolation and air temperature data provided the forcing functions for the heat budget, and shading coefficients provided a means of calibration. As a result, the model was able to simulate water temperature and the degree of thermal stratification reliably. An accurate water budget and heat budget, and good insolation data allowed the model to simulate the cycle of algal growth with acceptable accuracy. The calibration philosophy limited this accuracy somewhat; the goal of the calibration was to define a set of model parameters that would provide the best overall calibration to 18 months of data while varying parameters only as absolutely necessary. Thus accuracy in day-to-day fluctuations was secondary to accuracy in depicting the overall cycle of algal growth for the entire May–October season in each of three hydrologically distinct calibration years.

The phytoplankton play a fundamental role in determining the dissolved oxygen concentration and the pH in the water column, two primary quantities defining water quality in the Tualatin River. Because the pH is highly sensitive to the rate of photosynthetic assimilation of carbon, small errors in simulated algal biomass translate to large errors in the predicted pH. The accuracy in algal biomass required to adequately model the pH was incompatible with the goal of varying the calibration parameters as little as possible; therefore, pH calculations were not included in the simulation of the hypothetical scenarios. Dissolved oxygen, however, was simulated with acceptable accuracy, and the model was able to provide some insight into the relative magnitude of the influence of various factors on the dissolved oxygen concentration. That the production of dissolved oxygen is dominated by algal photosynthesis is apparent in the dissolved oxygen and chlorophyll-a observations, which parallel each other through each bloom cycle. The model clearly reproduced that result. The primary sources of oxygen demand are not as obvious in the observations, but the model results indicate that oxygen depletion is dominated by high background demands due to sediment oxygen demand and allochthonous carbonaceous biochemical oxygen demand. The phytoplankton play an oxygen-consumption role through respiration and the production of autochthonous carbonaceous biochemical oxygen demand, but oxygen consumption is dominated by the decay of organic matter that originated as terrestrial detritus, except for short periods of time following an algal crash. Reaeration in this system is so slow that it is ineffectual in compensating for either excessive production or consumption of oxygen.

Phosphorus was a motivating constituent for this study because it was assumed that reducing the high phosphorus levels in the Tualatin would limit algal growth and other associated water-quality problems. The model calibration indicated that phosphorus is not currently the primary factor limiting growth except for short periods of time near the surface of the water column. Applying hypothetical boundary conditions to the model indicated that substantial decreases in phosphorus concentration would significantly limit the size of algal blooms, but whether such decreases are achievable remains to be answered. There are high concentrations of background phosphorus in this

system, in particular, high concentrations that do not originate at the wastewater-treatment plants, the most readily defined point sources. Field work has shown that ground water high in phosphorus enters the river and its tributaries. The model results confirm that large amounts of phosphorus must be entering the water column from or through the bottom sediments, although it is difficult to establish exactly what fraction is from ground water and what fraction is recycled from the sediments in proportion to the high and ubiquitous sediment oxygen demand. In either case, it is probably wise to take into account the difficulty of controlling these phosphorus releases from the sediments when setting regulatory limits on the phosphorus concentration in the water column.

The model was also used to explore several different management options. These options were based on the premise that curtailing algal growth, either by reducing travel time or by decreasing nutrient concentrations, will lead to improvements in water quality. The model results indicate, however, that the goals of reducing algal growth *and* increasing dissolved oxygen concentrations are not mutually dependent and, in fact, are to some extent incompatible. The modeling effort clearly demonstrates the overwhelming importance of background oxygen demands, both in the water column and at the surface of the bed sediments, in defining the "baseline" dissolved oxygen concentration. The activity of the algae is superimposed on this baseline, and because the algae are more important as producers of oxygen than as consumers, severe reductions in algal growth tend to result in reduced production during the blooms, without significant reductions in consumption at other times. It should be noted, however, that a remarkable improvement in dissolved oxygen concentrations did not result from any of the management alternatives tested. The most significant increases in dissolved oxygen concentration that resulted from these management scenarios occurred during the sensitive late September and October period when flows remained low and algal activity had nearly ceased. During October, a monthly mean increase of 1 mg/L or more at river mile 16.2 or river mile 5.5 occurred only in 1992 and only for a scenario that required a great deal of flow augmentation or a scenario that required somewhat less flow augmentation, in combination with a significant reduction in the detrital phosphorus (and thus a reduction in carbonaceous biochemical oxygen demand) entering at the boundaries.

This emphasis on dissolved oxygen is not intended to imply that dissolved oxygen is the only measure of water quality. In particular, excursions of high pH are also of concern in the Tualatin River, and those high pH values are clearly associated with large algal blooms. Therefore, the goals of reducing algal growth and reducing the number of pH violations are, to a large extent, mutually dependent.

Addressing the problem of improving water quality in the Tualatin River, assuming that the aesthetic considerations are secondary, requires a shift in the current paradigm governing its management. Based on the model results and the available data, the focus on algal growth is somewhat misplaced. Some limitation on the magnitude of algal blooms may indeed be the best strategy for limiting very high pH excursions, but limiting the size of blooms does not guarantee that the lowest dissolved oxygen concentrations, which currently reach values that are believed to be detrimental to fish and other biota, will increase. In addition, limiting algal growth via decreased phosphorus concentrations may not be easily attainable given the high background loads of phosphorus. If the goal is to improve dissolved oxygen conditions, the focus is better placed on some means of decreasing the background oxygen demands; specifically, those demands that continue to operate whether phytoplankton are photosynthesizing or not. Those demands include decay processes in the water column and in the sediments. The background demands can be reduced either by reducing the travel time or by reducing the amount of organic material available for decay; this discussion has not considered the feasibility of accomplishing either of these reductions. Model simulations indicate that the greatest improvement in dissolved oxygen might be achieved with a combination of these two approaches.

REFERENCES CITED

Ambrose, R.B., Wool, T.A., Connolly, J.P., and Schanz, R.W., 1988, WASP4—A hydrodynamic and water quality model—Model theory, user's manual, and programmer's guide: U.S. Environmental Protection Agency, EPA/600/3–87/039.

Anderson, C.W., Tanner, D.Q., and Lee, D.B., 1994, Water-quality data for the South Umpqua River Basin, Oregon, 1990–92: U.S. Geological Survey Open-File Report 94–40, 156 p.

Arcement, G.J., Jr., and Schneider, V.R., 1989, Guide for selecting Manning's roughness coefficients for natural channels and flood plains: U.S. Geological Survey Water-Supply Paper 2339, 38 p.

Barnes, H.H., Jr., 1967, Roughness characteristics of natural channels: U.S. Geological Survey Water-Supply Paper 1849, 213 p.

Bennett, J.P., and Rathbun, R.E., 1972, Reaeration in open-channel flow: U.S. Geological Survey Professional Paper 737, p. 58.

Bienfang, P.K., Harrison, P.J., and Qarmby, L.M., 1982, Sinking rate response to depletion of nitrate, phosphate, and silicate in four marine diatoms: Marine Biology, v. 67, p. 295–302.

Bowie, G.L., Mills, W.B., Porcella, D.B., Campbell, C.L., Pagenkopf, J.R., Rupp, G.L., Johnson, K.M., Chan, P.W.H., Gherini, S.A., and Chamberlin, C.E., 1985, Rates, constants, and kinetics formulations in surface water quality modeling: U.S. Environmental Protection Agency, EPA/600/3–85/040, 455 p.

Caldwell, J.M., and Doyle, M.C., 1995, Sediment oxygen demand in the lower Willamette River, Oregon, 1994: U.S. Geological Survey Water-Resources Investigations Report 95–4196, 14 p.

Cole, T.M., and Buchak, E.M., 1995, CE-QUAL-W2: A two-dimensional, laterally averaged, hydrodynamic and water quality model, version 2.0: U.S. Army Corps of Engineers Instruction Report EL–95–1 [variously paged].

Collins, C.D., 1980, Formulation and validation of a mathematical model of phytoplankton growth: Ecology, v. 61(3), p. 639–649.

Côté, B., and Platt, T., 1983, Day-to-day variations in the spring-summer photosynthetic parameters of coastal marine phytoplankton: Limnology and Oceanography, v. 28(2), p. 320–344.

Crumpton, W.G., and Wetzel, R.G., 1982, Effects of differential growth and mortality in the seasonal succession of phytoplankton populations in Lawrence Lake, Michigan: Ecology, v. 63(6), p. 1729–1739.

Cunningham, A., 1996, Accounting for nutrient processing time in mathematical models of phytoplankton growth: Limnology and Oceanography, v. 41(4), p. 779–783.

DiToro, D.M., and Connolly, J.P., 1980, Mathematical models of water quality in large lakes—Part 2—Lake Erie: U.S. Environmental Protection Agency Ecological Research Series, EPA–600/3–80–065.

Doyle, M.C., and Caldwell, J.M., 1996, Water-quality, streamflow, and meteorological data for the Tualatin River Basin, Oregon, 1991–93: U.S. Geological Survey Open-File Report 96–173, 49 p., 1 CD-ROM.

Eagleson, P.S., 1970, Dynamic Hydrology: New York, McGraw-Hill, p. 41.

Edinger, J.E., and Buchak, E.M., 1975, A hydrodynamic, two-dimensional reservoir model—The computational basis: Cincinnati, Ohio, prepared for U.S. Army Engineer Division, Ohio River.

Fernández, J.A., Clavero, V., Villalobos, J.A., and Niell, F.X., 1997, A nonlinear model of phosphorus flux in the phytoplankton of a temperate eutrophic reservoir: Hydrobiologia, v. 344, p. 205–214.

Harris, G.P., 1980, Temporal and spatial scales in phytoplankton ecology—Mechanisms, methods, models, and management: Canadian Journal of Fisheries and Aquatic Science, v. 37, p. 877–900.

Jassby, A.D., and Platt, T., 1976, Mathematical formulation of the relationship between photosynthesis and light for phytoplankton: Limnology and Oceanography, v. 21(4), p. 540–547.

Jensen, H.S., Kristensen, P., Jeppesen, E., and Skytthe, A., 1992, Iron:phosphorus ratio in surface sediment as an indicator of phosphate release from aerobic sediments in shallow lakes: Hydrobiologia, v. 235/236, p. 731–743.

Kelly, V.J., 1996, Dissolved oxygen in the Tualatin River, Oregon, during winter flow conditions, 1991 and 1992: U.S. Geological Survey Open-File Report 95–451, 74 p.

Lee, K.K., 1995, Stream velocity and dispersion characteristics determined by dye-tracer studies on selected stream reaches in the Willamette River Basin, Oregon: U.S. Geological Survey Water-Resources Investigations Report 95–4078, 39 p.

Leonard, B.P., 1979, A stable and accurate convective modelling procedure based on quadratic upstream interpolation: Computer Methods in Applied Mechanics and Engineering, v. 19, p. 59–98.

Mayer, T.D., 1995, Interactions of phosphorus and colloidal iron oxides in model solutions and natural waters: Beaverton, Oregon, Oregon Graduate Institute of Science & Engineering, Ph.D. thesis, 112 p.

McCutcheon, S.C., and French, R.H., 1989, Water quality modeling—Volume I—Transport and surface exchange in rivers: Boca Raton, Florida, CRC Press, p. 218.

McKnight, D., Brenner, M., Smith, R., and Baron, J., 1986, Seasonal changes in phytoplankton populations and related chemical and physical characteristics in lakes in Loch Vale, Rocky Mountain National Park, Colorado: U.S. Geological Survey Water-Resources Investigations Report 86–4101, 64 p.

Miller, J.C., and Miller, J.N., 1988, Statistics for analytical chemistry (2d ed.): Chichester, England, Ellis Horwood Limited, p. 227.

Morel, A., and Smith, R.C., 1974, Relation between total quanta and total energy for aquatic photosynthesis: Limnology and Oceanography, v. 19(4), p. 591.

Oregon Department of Environmental Quality, 1997, Oregon Administrative Rules: Dissolved oxygen in Tualatin River, OAR 340–041–0445(2aE); pH in Tualatin River, OAR 340–041–0445(2dB); nuisance phytoplankton growth, OAR 340–041–0150(1b); TMDLs for Tualatin River, OAR 340–041–0470(9).

Pankow, J.F., 1991, Aquatic chemistry concepts: Chelsea, Michigan, Lewis Publishers, 673 p.

Pierson, D.C., Pettersson, K., and Istvanovics, V., 1992, Temporal changes in biomass specific photosynthesis during the summer—Regulation by environmental factors and the importance of phytoplankton succession: Hydrobiologia, v. 243/244, p. 119–135.

Press, W.H., Flannery, B.P., Teukolsky, S.A., and Vetterling, W.T., 1989, Numerical recipes—The art of scientific computing (Fortran version): New York, Cambridge University Press, p.113.

Reynolds, C.S., 1984, The ecology of freshwater phytoplankton: New York, Cambridge University Press, 384 p.

Rounds, S.A., and Doyle, M.C., 1997, Sediment oxygen demand in the Tualatin River Basin, Oregon, 1992–96: U.S. Geological Survey Water-Resources Investigations Report 97–4103, 19 p.

Scavia, D., 1980, An ecological model of Lake Ontario: Ecological Modelling, v. 8, p. 49–78.

Schubert, H., and Forster, R.M., 1997, Sources of variability in the factors used for modeling primary productivity in eutrophic waters: Hydrobiologia, v. 349, p. 75–85.

Smith, R.A., 1980, The theoretical basis for estimating phytoplankton production and specific growth rate from chlorophyll, light and temperature data: Ecological Modeling, v. 10, p. 243–264.

Steele, J.H., 1962, Environmental control of photosynthesis in the sea: Limnology and Oceanography, v. 7, p. 137–150.

Streeter, V.L., and Wylie, E.B., 1985, Fluid mechanics (8th ed.): New York, McGraw-Hill, 586 p.

Stumm, W., and Morgan, J.J., 1981, Aquatic chemistry: New York, John Wiley & Sons, 780 p.

Thomann, R.V., and Mueller, J.A., 1987, Principles of surface water quality modeling and control: New York, Harper & Row, 644 p.

Thornton, K.W., and Lessem, A.S., 1978, A temperature algorithm for modifying biological rates: Trans. Am. Fish. Soc., v. 107(2), p. 284–287.

Urabe, J., 1990, Stable horizontal variation in the zooplankton community structure of a reservoir maintained by predation and competition: Limnology and Oceanography, v. 35(8), p. 1703–1717.

Unified Sewerage Agency, 1997, Tualatin River flow management technical committee—1996 annual report: Hillsboro, Oregon [variously paged].

U.S. Army Corps of Engineers, 1953, Review of survey report on Tualatin River, Oregon—Appendix C—Public hearings: Portland, Oregon [variously paged].

Velz, C.J., 1984, Applied stream sanitation (2d ed.): New York, John Wiley and Sons, Inc., 800 p.

APPENDIXES

APPENDIX A— MAJOR MODIFICATIONS TO CE-QUAL-W2

The model used in this study is a modification of version 2.0 (May, 1989) of the U.S. Army Corps of Engineers (USACE) model CE-QUAL-W2. This appendix briefly describes each of the major modifications that were made to the program. Before the modifications are discussed, however, it is important to recognize that water-quality modeling is a rapidly developing field. The best water-quality models are continually improved, incorporating the latest research results and the most efficient algorithms. Indeed, during the course of this study, the USACE continued to develop CE-QUAL-W2; version 2.0 is no longer current. The modelers at the USACE recognize that each application of the model may require code modifications to incorporate new algorithms or to add new capabilities. Version 2.0 of the code was written with the expressed purpose of making it easy to modify. During this study, U.S. Geological Survey (USGS) personnel were in frequent contact with USACE personnel. As a result, many code modifications and bug fixes were shared, to the benefit of both the USGS and USACE versions of the model.

The modifications to this version of the model were made for a variety of reasons. Several changes were necessary to tailor the hydraulic and water-quality algorithms to the Tualatin River. A few modifications were made to incorporate algorithms or details that were added by the USACE in a later version. Some changes were needed to fix errors in the code. Other changes were necessary to add capabilities that were important to this application. In general, only the major modifications are mentioned here. Many minor modifications were made to the code, but they do not merit discussion because of their minimal impact. Modifications that relate to the model grid are discussed first, followed by changes to the hydraulics, the heat budget and then the water-quality algorithms.

The version of CE-QUAL-W2 that was the starting point for this work, although labeled "version 2.0," was actually a modification of version 2.0 obtained from Dr. Scott Wells at Portland State University. Dr. Wells and his research group had started to implement some important changes to the code. Some changes were complete, others were completed by USGS personnel. The important changes made by Dr. Wells and his research group are included in this list. Throughout the following discussion, this code obtained from Dr. Wells, the starting point for the USGS modeling work, is referred to as the "parent version." The existence of errors in the parent version in no way implies that the current USACE version of the model still contains those errors. No attempt is made here to assess the current USACE version of the model.

Model Grid

A Cross Section of Stacked Rectangles

The mathematical representation of the channel cross section in the parent version was not consistent throughout the program. In some algorithms, the cross section was treated as if it were composed of a set of stacked rectangles; in other algorithms, it was treated as a set of stacked trapezoids. Although each representation has its advantages, a cross section composed of rectangles is easier to implement. Many changes were made throughout the program to consistently implement the "stacked rectangle" representation of the channel cross section.

Nonuniform Segment Lengths

CE-QUAL-W2 uses a two-dimensional grid in which the layers, or rows, of the grid can have different heights; however, the height is constant within a layer. Similarly, each segment, or column, of the grid can have a unique length, but that length is constant within a segment. The ability of the model to operate with segments of different lengths was not completely implemented in the parent version. Modifications were made to complete the implementation of this important feature of the model.

One-Dimensional Reaches

The parent version of CE-QUAL-W2 restricted the grid such that each segment had to contain at least two layers that were actively transporting water. In other words, the entire river had to be deep enough to be modeled in two dimensions at all times. To make the model more flexible, code was added to allow the existence of segments that contain only one *active* layer. This is a change that was partially implemented by Dr. Wells and his research group; USGS personnel completed the modification.

Water-Surface Location

The parent version of the model did not properly account for a variety of variables whenever the water-surface slope of the river extended over more than two layers of the model grid. Modifications were made to allow the water-surface slope to extend over a large number of layers, limited only by the number of layers in the grid.

Hydraulics

Discharge Over the Oswego Diversion Dam

An algorithm that calculates the discharge over two types of weirs and through a pipe was added to the parent version by Dr. Scott Wells and his research group at

Portland State University. This subroutine is used by the model to calculate the discharge of the Tualatin River at the Oswego diversion dam (river mile 3.4, the downstream boundary of this modeling work) as a function of the water-surface elevation just upstream of that structure. The flow at the downstream boundary, therefore, is calculated internally by the model rather than imposed externally. The specific algorithms used in this subroutine are discussed in the Algorithms section of this report. A few modifications were made to the original algorithms to allow the dimensions and hydraulic characteristics of the weirs to vary over time.

Distributed Tributaries

Distributed tributaries in the USACE version of the model are an alternate mechanism of simulating precipitation as well as inputs from nonpoint sources. In this application, precipitation was specified explicitly, and the nonpoint sources, including ground water, were simulated through a modification of the distributed tributaries algorithm. The algorithms in the parent version that distributed the nonpoint source of water among the various cells of the grid, however, had two inherent problems. First, although the intent of the algorithm was to distribute the input among the segments of the grid as a function of segment surface area, the surface area was not calculated correctly for a river whose water surface elevation extends over more than one layer of the grid. Second, all of the water from this nonpoint source was placed into the grid at the river surface. If the nonpoint source is dominated by bank seeps, tile drains, and ungaged tributaries, then perhaps the water should be added at the top of the water column. For these types of sources, however, a distribution of the flow as a function of segment surface area seems inappropriate; bank length would be a better predictor. If, on the other hand, ground water is the dominant nonpoint source, then a surface-area normalization is appropriate, but the source should be distributed over the entire water column rather than simply placed at the top.

Many types of nonpoint water sources are important in the Tualatin River water budget. Bank seeps, tile drains, ungaged tributaries, and ground water all contribute a significant amount of water to the river, depending *upon* the time of year. The rate of ground-water discharge is often small, but it transports a significant load of nutrients. The algorithms that distribute the nonpoint sources were modified to (a) allocate those sources to the segments as a function of segment length and (b) distribute each segment's nonpoint discharge to the layers of that segment as a function of sediment surface area. These algorithms represent a compromise that seems appropriate for the Tualatin application. Normalization to bank length rather than sediment surface area recognizes that a significant fraction of the nonpoint source is not due to ground water. For those periods of time when the nonpoint source is mostly ground-water discharge, a normalization to bank length results in a higher ground-water discharge rate in the upper, narrower part of the grid, which is consistent with the actual measurements of ground-water discharge. The distribution of the nonpoint source to all layers within a segment reflects the importance of the ground-water source.

Horizontal Pressure Gradient

The hydraulic section of CE-QUAL-W2 calculates the water-surface elevation of each segment first, followed by the horizontal and then the vertical velocities. Some terms in the water-surface elevation equation, however, depend *upon* the magnitude of the horizontal velocities. The horizontal velocities, in turn, depend in part *upon* the water-surface slope. This interdependence can create mass-balance problems if it is not properly handled. In theory, the best solution is to iterate through the calculation of elevations and velocities until an acceptable level of error is reached. Although the user manual (Cole and Buchak, 1995) indicates that this level can be achieved in about four iterations, those iterations consume valuable computer time, and the iterative approach was not implemented in the USACE version. Alternate approaches can avoid the computational costs of iteration while still avoiding mass-balance problems and unacceptable amounts of numerical error. The parent version contained an altogether unacceptable method of handling the elevation/velocity interdependence that was a remnant from an older USACE version; it did not circumvent the mass-balance problem, and will not be discussed here. The USACE changed its approach in later versions of the model, using a vertical integration technique that adjusts the horizontal velocities and forces compliance with continuity.

The solution implemented in the USGS version recognizes that the mass-balance error was the result of an inconsistency in the use of the horizontal pressure gradient term in the hydraulic equations. The horizontal pressure gradient term of the laterally averaged horizontal momentum equation is:

$$-\frac{1}{\rho}\frac{\partial BP}{\partial x}, \qquad (1A)$$

where ρ is the water density, B is the river width, P is pressure, and x is the horizontal dimension. CE-QUAL-W2 splits the pressure gradient into two components:

$$\frac{\partial P}{\partial x} = -\rho_\eta g\frac{\partial \eta}{\partial x} + g\int_\eta^z \frac{\partial \rho}{\partial x}dz, \qquad (2A)$$

where ρ_η is the water density at the surface, g is the gravitational constant, η is the water-surface elevation referenced to a specified datum, and z is the vertical dimension.

The first term embodies the water-surface slope and is called the barotropic gradient. The second term represents the horizontal density gradient and is called the baroclinic gradient. The calculation of both the water-surface elevations and the horizontal velocities depend *upon* this horizontal pressure gradient. The problem in the parent version is that the baroclinic gradient was first used to find the elevations, then recalculated before it was used to find the horizontal velocities. This recalculation of the baroclinic gradient results in horizontal velocities that are inconsistent with the calculated water-surface elevations.

Changes were made in the USGS version of the model to ensure that both the barotropic and baroclinic gradients were used consistently throughout the hydraulic section of the program. The baroclinic gradient was not recalculated before being used in the determination of the horizontal velocities. These changes result in a consistent set of water-surface elevations and horizontal velocities because they are determined from the same set of forcing functions. Continuity is preserved; no mass-balance problems are created.

Manning's Equation

The frictional shear stress imposed at the sides and bottom of the channel was represented in the parent version with Chezy's formula. Chezy's coefficient is known to be a function of the roughness and hydraulic radius of the channel. Manning's equation makes use of that functionality, but the resulting equation has only one, simple, well-defined parameter: Manning's n (a roughness coefficient). Changes were made in the parent version by Dr. Scott Wells and his research group to implement Manning's approach rather than Chezy's. Further refinements in that implementation were made by USGS personnel. The *Algorithms* section discusses this modification in somewhat greater detail.

Heat Budget

Heat Balance

Similar to the volume balance that was present in the parent version of the model, code was added to keep track of the overall heat budget of the river. This heat-balance code is simply used to check that the model preserves continuity with respect to heat. This addition to the program does not use a significant amount of computational time, and yet provides information that is very valuable.

Light Penetration

The parent version of the model erroneously calculated the downward energy flux of light from one model layer to the next. As shortwave light penetrates the water column, its energy is absorbed and converted to heat. This process is modeled with Beer's law, where the extinction coefficient is a function of both the suspended solids and phytoplankton concentrations. Because these concentrations vary from the top to the bottom of the water column, the extinction coefficient will also vary. The parent version did not properly apply vertical changes in the extinction coefficient at each layer boundary. Modifications were made to the program to explicitly calculate (a) the energy flux at the top of a layer, (b) the rate of light absorption within that layer, and (c) the resulting energy flux at the bottom of that layer. By keeping track of the energy flux at each layer boundary, the effects of a vertically varying extinction coefficient are properly incorporated into the heat budget.

Shading

Compared to most lakes and reservoirs, the Tualatin River is relatively narrow. As a result, riparian vegetation can cast a significant shadow over the water surface of the river. During the calibration of the heat budget for the Tualatin River application, the need for a shading algorithm quickly became apparent. A simple shading mechanism, therefore, was added to the model. Each segment was given a shading coefficient, representing the fraction of solar insolation prevented from reaching the water surface. The shading coefficients were also given a seasonal dependence to represent the effects of deciduous vegetation. The shading algorithms are discussed in the *Algorithms* section.

Transport Scheme

The parent version of the model did not contain a current version of the QUICKEST (Leonard, 1979) transport scheme. Modifications were made to upgrade this transport algorithm, making the implementation similar to that used by a later USACE version of the model.

Water Quality

Algal Preference for Ammonia Nitrogen

In the parent version, phytoplankton were not given a preference for ammonia over nitrate as a source of nitrogen. Such a preference exists, however, and modifications were made to incorporate such an algorithm into CE-QUAL-W2. The form of the ammonia preference algorithm was taken from the hydrodynamic and water-quality model WASP4 (Ambrose and others, 1988). The *Algorithms* section discusses this algorithm in more detail.

Algal Light-Limitation Function

Algal photosynthesis, as modeled by CE-QUAL-W2, can be limited by either a lack of nutrients (phosphorus or

nitrogen) or a lack of light. The function used to describe the relation between the algal growth rate and the amount of available light was changed in the USGS version of the model. The parent version used a light limitation function developed by Smith (1980) and Steele (1962); that function includes photoinhibition at high light intensities as well as light extinction with depth. The instantaneous growth-rate multiplier given by the Smith/Steele function, averaged from depth z_1 to depth z_2, is:

$$\frac{e}{\alpha_{tot}(z_2 - z_1)}\left(e^{\frac{I_1}{I_s}e^{-\alpha_{tot}(z_2 - z_1)}} - e^{\frac{I_1}{I_s}} \right), \qquad (3A)$$

where e is the irrational number 2.71828, α_{tot} is the total extinction coefficient, I_1 is the solar energy flux (light intensity) at depth z_1, and I_s is the saturating light intensity of the algae.

The light limitation function used in this application is based *upon* the light-saturation curve proposed by Jassby and Platt (1976). Although this function does not model photoinhibition, it is widely accepted as one of the best formulations available. The instantaneous growth-rate multiplier given by the Jassby and Platt function, averaged from depth z_1 to depth z_2, is:

$$\frac{1}{(z_2 - z_1)} \int_0^{(z_2 - z_1)} \tanh\left(\frac{eI_1}{I_s} e^{-\alpha_{tot} z} \right) dz. \qquad (4A)$$

The presence of the hyperbolic tangent function precludes an analytical integration, but a numerical integration is simple. A subroutine that integrates this function using Simpson's Rule was adapted from Press and others (1989).

Mass Balance

Similar to the heat balance that was added to the parent version of the model, code was added to keep track of the overall mass budget of each water-quality constituent. This mass-balance code is simply used to check that the model preserves continuity with respect to each constituent. This addition to the program does not use a significant amount of computational time, and yet provides information that is very valuable.

Nonconservative Alkalinity

The parent version of the model assumed carbonate alkalinity to be a conservative quantity. In this version, a subroutine was added to allow the alkalinity to be affected by nitrification, photosynthesis, and algal respiration. For more details, see the *Algorithms* section.

Phosphorus Retention by Sediments

As the organic matter in the river sediment decomposes, oxygen from the overlying water is consumed, and carbon, nitrogen, and phosphorus are released to that water. In the Tualatin River application, it was necessary to prevent a fraction of the phosphorus from recycling into the water column. Therefore, the phosphorus subroutine was modified such that a fraction f_P of the phosphorus normally released via sediment decomposition is retained by the sediments. This phosphorus retention may be the result of one or more different processes. Phosphorus is readily adsorbed by ferric oxyhydroxide solids in oxidized surface sediments; some losses to adsorption, therefore, are expected. It is also reasonable to expect that much of the phosphorus liberated from the organic matter via decomposition will be scavenged and incorporated by the resident microbial community. Furthermore, the C:N:P ratio of sediment organic-matter changes as that material ages. Within CE-QUAL-W2, however, the C:N:P ratio of all of the organic matter constituents, living or not, is restricted to one constant number. This modification, then, could be viewed as a mechanism that compensates for the existence of sedimentary organic matter that is naturally low in phosphorus.

Reaeration

The exchange of oxygen and carbon dioxide across the air/water interface in the parent version was assumed to be a function of wind speed. That algorithm may be accurate for a large lake, but is not appropriate for many riverine systems. For the Tualatin River application, the reaeration algorithm was changed to one developed for rivers by Bennett and Rathbun (1972). That algorithm models the air/water exchange of gases as a function of the average velocity and depth of each segment; it is discussed in greater detail in the *Algorithms* section.

Sediment

In the parent version, the sediment constituent had units of grams of organic matter per cubic meter of river water. That is a counterintuitive convention, because the sediments interact with the overlying water through a specific surface area. That convention has some unfortunate attributes, such as the generation of more sediment oxygen demand in a deep segment than in a shallow segment that has the same width and sediment organic-matter content. The code was changed to give the sediment constituent units of grams of organic matter per unit sediment surface area. This approach greatly simplifies the initialization of the sediment constituent, because its units now are similar to those for sediment oxygen demand (grams oxygen consumed per unit sediment surface area per time).

Two Nitrification Rates

The parent version supports the use of only one nitrification rate. That rate, except for a water-temperature adjustment, is spatially and temporally constant. The nitrification rate in riverine systems, however, can be expected to vary both spatially and temporally. Nitrifying bacteria require a substrate for attachment and are generally found in shallow, rocky river reaches. Although they can be important in deeper reaches, as long as sufficient suspended material is available as a substrate, these bacteria generally will find more suitable habitat in the upper, shallower reaches of the Tualatin model grid. Nitrifying bacteria also grow slowly and significant populations will only develop in the presence of sufficiently high ammonia concentrations. The overall rate of nitrification, therefore, would be expected to vary temporally if ammonia loads in the river also vary.

The temporal variability of nitrification is difficult to simulate, but the spatial variability of that rate can be implemented easily. For the Tualatin River application, an additional nitrification rate was introduced such that it was applied to the upper part of the model grid, and the original nitrification rate was applied to the rest of the grid. The boundary was chosen at a point where the shallow reach ends and the deeper, more reservoir-like reach begins. The original behavior of the model can still be achieved by equating the two nitrification rates. The calibration runs used only one nitrification rate because the ammonia concentrations were usually low. This code modification was necessary, however, to implement one of the hypothetical simulations in which high loads of ammonia were input to the river.

Temperature Dependence of Reactions

The rates of most of the chemical and biological reactions simulated by CE-QUAL-W2 are temperature dependent. This dependence is modeled through the use of a rate-multiplier function. In the parent version of the model, a very flexible function was applied such that the multiplier (a) was low, or zero, at cold water temperatures, (b) increased to a value near one at the optimum temperature for the reaction, and (c) decreased to a low, or zero, value at high temperatures (Thornton and Lessem, 1978). The exact inflections of the function were controlled by a set of four input parameters for each reaction. Rather than use this function, however, changes were made to the program so that each of the chemical and biological reactions use the classical van't Hoff equation as a temperature-rate multiplier. The van't Hoff function specifies the multiplier as:

$$\gamma = Q_{10}^{(T-20)/10} = \theta^{(T-20)}, \qquad (5A)$$

where Q_{10} is a factor near 2, and T is the water temperature in degrees Celsius. Because this multiplier is an unbounded exponential, the rates of reaction specified to the model are the rates at 20°C rather than the maximum reaction rates. Although many biological reaction rates might be expected to decrease at very high temperatures, it was felt that the van't Hoff relation would provide more accurate results for the range of water temperatures encountered in this application. In addition, this approach requires only one input parameter rather than the four used by the original formulation. Each chemical or biological reaction modeled by CE-QUAL-W2 was given a value for θ.

Temperature Dependence of Settling

Several settling velocities are specified in CE-QUAL-W2 to simulate the downward transport of suspended solids, detritus, and algae due to gravity. The parent version kept these velocities constant. The USGS version was modified to add a temperature dependence to the settling velocities. This algorithm is based *upon* Stokes' law of settling, and employs the known variation of the viscosity of water with temperature. With a 10°C increase in temperature, the settling velocity can increase by as much as 30 percent. This dependence is implemented as:

$$\omega = \frac{2gr^2(\rho_p - \rho_w)}{9\mu_w}, \qquad (6A)$$

where ω is the settling velocity, g is the acceleration due to gravity, ρ_p is the particle density, ρ_w is the water density, r is the particle radius, and μ_w is the viscosity of the water. Because $r^2(\rho_p - \rho_w)$ is approximately constant with temperature compared to μ_w, a good approximation to the temperature correction is:

$$\omega_T = \omega_{20°}\frac{\mu_{w,\,20°}}{\mu_{w,\,T}}. \qquad (7A)$$

Although the settling velocity does vary significantly with temperature, this modification normally will not have a significant effect on the model simulations.

Variable Algal Growth Rate

Because the parent version of CE-QUAL-W2 represented all phytoplankton with a single compartment and a seasonally constant algal growth rate, seasonal variations in the algal growth rate (or estimates of the effects of algal succession) could not be simulated. In the Tualatin River application, the system is simulated over long (6-month) periods of time. Over the length of an entire summer, the algal community adapts to changes in the flow, light, and temperature conditions by changing its growth rate without a classic succession of different species; these growth rate changes are quite important. In an attempt to simulate that seasonality, changes were made to implement a seasonally variable algal growth rate for the

single algal compartment. The time-varying algal growth rate at 20°C is simply input from a file, like many other model parameters.

Zooplankton

The decision regarding where to truncate the food web is always a difficult one. In this application, reasonably good data for zooplankton were available; therefore, the food web was truncated above that level. The basic water-quality algorithms for modeling zooplankton had already been added to the parent version by Dr. Wells and his research group at Portland State University. USGS personnel simply made a few minor modifications. The zooplankton algorithms are discussed in more detail in the *Algorithms* section.

APPENDIX B

Table B1. Lengths, widths, and depths of the cells in the model grid

[Segments 1 and 155 are boundary segments. Layers 1 and 16 are boundary layers. Cells in boundary segments or layers have zero widths. The river bottom is marked by cells with zero widths. To illustrate the change in elevation of the river bottom with river mile, cells with widths of zero are shaded. Elevations of each layer, noted in the header, are relative to the National Geodetic Vertical Datum of 1929]

				Width of cell (feet)													
Segment number	Upstream river mile	Down-stream river mile	Length (feet)	Layer 2 120–110 feet	Layer 3 110–105 feet	Layer 4 105–102 feet	Layer 5 102–100 feet	Layer 6 100–98 feet	Layer 7 98–96 feet	Layer 8 96–94 feet	Layer 9 94–92 feet	Layer 10 92–90 feet	Layer 11 90–88 feet	Layer 12 88–86 feet	Layer 13 86–84 feet	Layer 14 84–82 feet	Layer 15 82–80 feet
2	38.40	38.12	1,478	110	75	60	20	0	0	0	0	0	0	0	0	0	0
3	38.12	37.84	1,478	110	75	60	20	0	0	0	0	0	0	0	0	0	0
4	37.84	37.56	1,478	110	75	60	20	0	0	0	0	0	0	0	0	0	0
5	37.56	37.28	1,478	110	75	60	20	0	0	0	0	0	0	0	0	0	0
6	37.28	37.00	1,478	110	75	60	20	0	0	0	0	0	0	0	0	0	0
7	37.00	36.72	1,478	120	75	60	30	0	0	0	0	0	0	0	0	0	0
8	36.72	36.44	1,478	120	85	70	40	10	0	0	0	0	0	0	0	0	0
9	36.44	36.16	1,478	120	85	70	40	10	0	0	0	0	0	0	0	0	0
10	36.16	35.88	1,478	130	85	70	50	35	0	0	0	0	0	0	0	0	0
11	35.88	35.60	1,478	130	85	70	50	30	0	0	0	0	0	0	0	0	0
12	35.60	35.32	1,478	130	85	70	40	15	0	0	0	0	0	0	0	0	0
13	35.32	35.04	1,478	140	90	70	20	0	0	0	0	0	0	0	0	0	0
14	35.04	34.76	1,478	140	100	70	20	0	0	0	0	0	0	0	0	0	0
15	34.76	34.48	1,478	140	100	80	55	30	10	0	0	0	0	0	0	0	0
16	34.48	34.20	1,478	150	110	80	60	40	25	0	0	0	0	0	0	0	0
17	34.20	33.92	1,478	150	110	80	60	35	20	0	0	0	0	0	0	0	0
18	33.92	33.64	1,478	150	110	90	60	45	20	0	0	0	0	0	0	0	0
19	33.64	33.36	1,478	160	110	90	50	15	0	0	0	0	0	0	0	0	0
20	33.36	33.08	1,478	170	120	90	45	20	0	0	0	0	0	0	0	0	0
21	33.08	32.80	1,478	170	120	90	40	20	0	0	0	0	0	0	0	0	0
22	32.80	32.52	1,478	170	120	90	60	30	10	0	0	0	0	0	0	0	0
23	32.52	32.24	1,478	170	130	90	67	45	20	0	0	0	0	0	0	0	0
24	32.24	31.96	1,478	170	130	100	75	50	30	0	0	0	0	0	0	0	0
25	31.96	31.68	1,478	170	130	100	83	50	30	0	0	0	0	0	0	0	0
26	31.68	31.40	1,478	170	130	100	83	50	30	0	0	0	0	0	0	0	0
27	31.40	31.12	1,478	170	130	100	83	50	30	0	0	0	0	0	0	0	0
28	31.12	30.84	1,478	170	130	100	86	64	30	0	0	0	0	0	0	0	0
29	30.84	30.56	1,478	170	130	100	86	64	20	0	0	0	0	0	0	0	0

Table B1. Lengths, widths, and depths of the cells in the model grid—Continued

Segment number	Upstream river mile	Down-stream river mile	Length (feet)	Width of cell (feet)													
				Layer 2	Layer 3	Layer 4	Layer 5	Layer 6	Layer 7	Layer 8	Layer 9	Layer 10	Layer 11	Layer 12	Layer 13	Layer 14	Layer 15
				120–110 feet	110–105 feet	105–102 feet	102–100 feet	100–98 feet	98–96 feet	96–94 feet	94–92 feet	92–90 feet	90–88 feet	88–86 feet	86–84 feet	84–82 feet	82–80 feet
30	30.56	30.28	1,478	180	140	100	75	49	20	0	0	0	0	0	0	0	0
31	30.28	30.00	1,478	180	140	100	75	49	20	0	0	0	0	0	0	0	0
32	30.00	29.72	1,478	200	140	100	74	49	20	0	0	0	0	0	0	0	0
33	29.72	29.44	1,478	200	140	110	93	75	57	20	10	0	0	0	0	0	0
34	29.44	29.16	1,478	220	140	110	97	85	71	58	46	20	0	0	0	0	0
35	29.16	28.88	1,478	220	140	110	96	81	68	54	20	10	0	0	0	0	0
36	28.88	28.60	1,478	220	140	110	97	85	72	58	47	20	0	0	0	0	0
37	28.60	28.32	1,478	220	140	110	97	85	72	58	47	20	0	0	0	0	0
38	28.32	28.16	820	220	140	110	98	89	75	62	52	30	0	0	0	0	0
39	28.16	28.04	658	220	140	110	92	75	59	0	0	0	0	0	0	0	0
40	28.04	27.76	1,478	220	140	110	98	87	75	63	52	30	0	0	0	0	0
41	27.76	27.48	1,478	220	140	110	96	81	68	54	20	10	0	0	0	0	0
42	27.48	27.20	1,478	220	140	110	97	85	72	58	47	20	0	0	0	0	0
43	27.20	26.97	1,216	250	150	110	99	88	78	67	56	45	0	0	0	0	0
44	26.97	26.92	262	250	150	110	92	79	62	26	0	0	0	0	0	0	0
45	26.92	26.78	739	280	160	120	105	89	79	66	56	46	0	0	0	0	0
46	26.78	26.64	739	280	160	120	105	89	79	66	56	46	0	0	0	0	0
47	26.64	26.36	1,478	280	160	120	105	89	74	59	46	0	0	0	0	0	0
48	26.36	26.22	739	280	160	120	108	96	85	73	61	49	20	0	0	0	0
49	26.22	26.08	739	280	160	120	108	96	85	73	61	49	20	0	0	0	0
50	26.08	25.80	1,478	280	160	120	107	94	82	0	0	0	0	0	0	0	0
51	25.80	25.66	739	280	160	120	108	96	85	73	61	49	20	0	0	0	0
52	25.66	25.52	739	280	160	120	108	96	85	73	61	49	20	0	0	0	0
53	25.52	25.24	1,478	280	160	120	105	89	74	59	46	0	0	0	0	0	0
54	25.24	24.96	1,478	280	160	120	106	92	78	64	50	0	0	0	0	0	0
55	24.96	24.85	559	280	160	120	106	92	78	64	50	39	0	0	0	0	0
56	24.85	24.75	559	280	160	120	106	92	78	64	50	39	0	0	0	0	0
57	24.75	24.68	361	280	160	120	105	82	59	0	0	0	0	0	0	0	0
58	24.68	24.40	1,478	280	160	120	106	92	78	64	50	0	0	0	0	0	0
59	24.40	24.12	1,478	280	160	120	107	94	82	69	56	22	0	0	0	0	0
60	24.12	23.98	739	280	160	120	109	98	87	76	65	54	22	0	0	0	0
61	23.98	23.84	739	280	160	120	109	98	87	76	65	54	22	0	0	0	0

Table B1. Lengths, widths, and depths of the cells in the model grid—Continued

Segment number	Upstream river mile	Down-stream river mile	Length (feet)	Width of cell (feet)													
				Layer 2	Layer 3	Layer 4	Layer 5	Layer 6	Layer 7	Layer 8	Layer 9	Layer 10	Layer 11	Layer 12	Layer 13	Layer 14	Layer 15
				120–110 feet	110–105 feet	105–102 feet	102–100 feet	100–98 feet	98–96 feet	96–94 feet	94–92 feet	92–90 feet	90–88 feet	88–86 feet	86–84 feet	84–82 feet	82–80 feet
62	23.84	23.56	1,478	280	160	120	107	94	82	69	56	22	0	0	0	0	0
63	23.56	23.28	1,478	280	160	120	106	92	78	64	50	0	0	0	0	0	0
64	23.28	23.18	525	279	161	121	82	0	0	0	0	0	0	0	0	0	0
65	23.18	23.12	312	459	328	230	213	197	180	164	148	131	115	98	82	0	0
66	23.12	23.06	312	459	328	230	213	197	180	164	148	131	115	98	82	0	0
67	23.06	23.00	330	279	161	121	98	66	0	0	0	0	0	0	0	0	0
68	23.00	22.72	1,478	280	160	120	106	92	78	64	50	0	0	0	0	0	0
69	22.72	22.44	1,478	280	160	120	107	94	82	69	56	22	0	0	0	0	0
70	22.44	22.16	1,478	280	160	120	107	94	82	69	56	22	0	0	0	0	0
71	22.16	21.88	1,478	280	160	120	106	92	78	64	50	0	0	0	0	0	0
72	21.88	21.76	625	280	160	120	105	92	79	66	49	0	0	0	0	0	0
73	21.76	21.60	853	280	160	120	98	66	0	0	0	0	0	0	0	0	0
74	21.60	21.32	1,478	280	160	120	105	89	74	59	22	0	0	0	0	0	0
75	21.32	21.18	739	280	160	120	109	98	87	76	65	54	22	0	0	0	0
76	21.18	21.04	739	280	160	120	109	98	87	76	65	54	22	0	0	0	0
77	21.04	20.76	1,478	280	160	120	108	96	85	73	61	49	0	0	0	0	0
78	20.76	20.62	739	280	160	120	109	98	87	76	65	54	22	0	0	0	0
79	20.62	20.48	739	280	160	120	109	98	87	76	65	54	22	0	0	0	0
80	20.48	20.20	1,478	280	160	120	108	96	85	73	61	49	0	0	0	0	0
81	20.20	19.92	1,478	280	160	120	106	92	78	64	50	0	0	0	0	0	0
82	19.92	19.64	1,478	280	160	120	107	94	82	69	56	22	0	0	0	0	0
83	19.64	19.36	1,478	280	160	120	107	94	82	69	56	22	0	0	0	0	0
84	19.36	19.08	1,478	300	170	130	116	102	88	75	61	23	0	0	0	0	0
85	19.08	18.80	1,478	320	180	140	127	114	102	89	76	63	25	0	0	0	0
86	18.80	18.52	1,478	320	180	140	127	114	102	89	76	63	25	0	0	0	0
87	18.52	18.24	1,478	320	180	140	127	114	102	89	76	63	25	0	0	0	0
88	18.24	18.10	739	320	180	140	129	118	106	95	84	73	62	25	0	0	0
89	18.10	17.96	739	320	180	140	129	118	106	95	84	73	62	25	0	0	0
90	17.96	17.68	1,478	320	180	140	127	114	102	89	76	63	25	0	0	0	0
91	17.68	17.40	1,478	320	180	140	126	112	99	85	71	57	0	0	0	0	0
92	17.40	17.12	1,478	320	180	140	128	116	104	92	80	68	56	0	0	0	0
93	17.12	16.88	1,282	320	180	140	128	115	102	89	75	62	26	0	0	0	0

Table B1. Lengths, widths, and depths of the cells in the model grid—Continued

Segment number	Upstream river mile	Down-stream river mile	Length (feet)	Width of cell (feet)														
				Layer 2	Layer 3	Layer 4	Layer 5	Layer 6	Layer 7	Layer 8	Layer 9	Layer 10	Layer 11	Layer 12	Layer 13	Layer 14	Layer 15
				120–110 feet	110–105 feet	105–102 feet	102–100 feet	100–98 feet	98–96 feet	96–94 feet	94–92 feet	92–90 feet	90–88 feet	88–86 feet	86–84 feet	84–82 feet	82–80 feet
94	16.88	16.84	197	320	180	140	115	98	0	0	0	0	0	0	0	0	0
95	16.84	16.56	1,478	320	180	140	127	114	102	89	76	63	25	0	0	0	0
96	16.56	16.32	1,282	320	180	140	127	114	102	89	76	63	56	0	0	0	0
97	16.32	16.28	197	320	180	140	118	105	82	33	0	0	0	0	0	0	0
98	16.28	16.00	1,478	320	180	140	127	114	102	89	76	63	25	0	0	0	0
99	16.00	15.72	1,478	320	180	140	129	118	106	95	84	73	62	25	0	0	0
100	15.72	15.44	1,478	320	180	140	129	118	106	95	84	73	62	25	0	0	0
101	15.44	15.16	1,478	320	180	140	126	112	99	85	71	57	0	0	0	0	0
102	15.16	14.88	1,478	320	180	140	125	110	95	80	65	25	0	0	0	0	0
103	14.88	14.60	1,478	320	180	140	126	112	99	85	71	57	0	0	0	0	0
104	14.60	14.32	1,478	320	180	140	129	118	106	95	84	73	62	25	0	0	0
105	14.32	14.04	1,478	320	180	140	129	118	106	95	84	73	62	25	0	0	0
106	14.04	13.76	1,478	320	180	140	128	116	104	92	80	68	56	0	0	0	0
107	13.76	13.48	1,478	320	180	140	127	114	102	89	76	63	25	0	0	0	0
108	13.48	13.20	1,478	350	190	150	137	124	112	99	86	73	60	0	0	0	0
109	13.20	13.16	197	350	190	150	125	98	75	0	0	0	0	0	0	0	0
110	13.16	12.92	1,282	350	190	150	132	115	98	80	63	52	0	0	0	0	0
111	12.92	12.64	1,478	350	190	150	135	120	106	91	76	61	0	0	0	0	0
112	12.64	12.50	739	350	190	150	138	126	114	102	90	78	66	27	0	0	0
113	12.50	12.36	739	350	190	150	138	126	114	102	90	78	66	27	0	0	0
114	12.36	12.08	1,478	350	190	150	136	123	109	95	81	68	27	0	0	0	0
115	12.08	11.99	459	350	190	150	131	112	85	52	0	0	0	0	0	0	0
116	11.99	11.80	1,019	350	190	150	141	128	118	105	92	79	66	52	0	0	0
117	11.80	11.52	1,478	350	190	150	139	127	116	105	94	82	71	60	0	0	0
118	11.52	11.24	1,478	350	190	150	138	126	114	102	90	78	66	27	0	0	0
119	11.24	10.96	1,478	350	190	150	138	126	114	102	90	78	66	27	0	0	0
120	10.96	10.82	739	350	190	150	139	129	118	107	97	86	75	65	27	0	0
121	10.82	10.68	739	350	190	150	139	129	118	107	97	86	75	65	27	0	0
122	10.68	10.40	1,478	360	200	160	147	134	122	109	96	83	70	29	0	0	0
123	10.40	10.12	1,478	400	220	170	150	130	111	91	71	0	0	0	0	0	0
124	10.12	9.84	1,478	400	220	170	160	20	0	0	0	0	0	0	0	0	0
125	9.84	9.56	1,478	400	220	170	146	122	97	73	0	0	0	0	0	0	0

Table B1. Lengths, widths, and depths of the cells in the model grid—Continued

Segment number	Upstream river mile	Downstream river mile	Length (feet)	Width of cell (feet)													
				Layer 2	Layer 3	Layer 4	Layer 5	Layer 6	Layer 7	Layer 8	Layer 9	Layer 10	Layer 11	Layer 12	Layer 13	Layer 14	Layer 15
				120–110 feet	110–105 feet	105–102 feet	102–100 feet	100–98 feet	98–96 feet	96–94 feet	94–92 feet	92–90 feet	90–88 feet	88–86 feet	86–84 feet	84–82 feet	82–80 feet
126	9.56	9.28	1,478	400	220	170	146	122	97	73	0	0	0	0	0	0	0
127	9.28	9.00	1,478	400	220	170	150	130	111	91	71	0	0	0	0	0	0
128	9.00	8.72	1,478	400	220	170	150	130	111	91	71	0	0	0	0	0	0
129	8.72	8.44	1,478	400	220	170	148	126	105	83	31	0	0	0	0	0	0
130	8.44	8.16	1,478	400	220	170	150	130	111	91	71	0	0	0	0	0	0
131	8.16	7.88	1,478	400	220	170	148	126	105	83	31	0	0	0	0	0	0
132	7.88	7.60	1,478	400	220	170	143	116	88	31	0	0	0	0	0	0	0
133	7.60	7.32	1,478	400	220	170	143	116	89	31	0	0	0	0	0	0	0
134	7.32	7.18	739	400	220	170	152	134	116	98	79	30	0	0	0	0	0
135	7.18	7.04	739	400	220	170	152	134	116	98	79	30	0	0	0	0	0
136	7.04	6.76	1,478	400	220	170	150	130	111	91	71	0	0	0	0	0	0
137	6.76	6.48	1,478	400	230	180	159	138	117	96	75	0	0	0	0	0	0
138	6.48	6.20	1,478	400	240	190	175	160	144	129	114	99	84	34	0	0	0
139	6.20	6.06	739	400	240	190	178	166	154	142	130	118	106	94	82	35	0
140	6.06	5.92	739	400	240	190	178	166	154	142	130	118	106	94	82	35	0
141	5.92	5.69	1,216	400	240	190	173	155	138	120	103	86	72	0	0	0	0
142	5.69	5.64	262	400	240	190	171	144	112	69	0	0	0	0	0	0	0
143	5.64	5.50	739	400	240	190	177	164	151	138	125	112	99	86	73	0	0
144	5.50	5.36	739	400	240	190	177	164	151	138	125	112	99	86	73	0	0
145	5.36	5.31	262	400	240	190	167	131	115	98	72	0	0	0	0	0	0
146	5.31	5.08	1,216	400	240	190	174	158	142	126	110	94	78	33	0	0	0
147	5.08	4.94	739	400	240	190	178	166	154	142	130	118	106	94	82	35	0
148	4.94	4.80	739	400	240	190	178	166	154	142	130	118	106	94	82	35	0
149	4.80	4.52	1,478	400	240	190	177	164	151	138	125	112	99	86	73	0	0
150	4.52	4.24	1,478	400	240	190	177	164	151	138	125	112	99	86	73	0	0
151	4.24	4.10	739	400	240	190	179	169	158	148	137	127	116	105	95	84	74
152	4.10	3.96	739	400	240	190	179	169	158	148	137	127	116	105	95	84	74
153	3.96	3.68	1,478	500	240	190	176	161	147	133	119	104	90	76	0	0	0
154	3.68	3.40	1,478	500	240	190	163	136	109	82	0	0	0	0	0	0	0

APPENDIX C

Table C1. Shading factors and orientations for segments of the model grid

[Shading factors represent the fraction of river surface shaded by riparian vegetation. Segment orientations are defined in degrees, where zero degrees means that the river is flowing from the north to the south. Segment numbers 1 and 155 are boundary segments and therefore are not included]

Segment number	Upstream river mile	Downstream river mile	Shading factor	Orientation (degrees)	Segment number	Upstream river mile	Downstream river mile	Shading factor	Orientation (degrees)
2	38.40	38.12	0.47	260	45	26.92	26.78	.37	290
3	38.12	37.84	.47	290	46	26.78	26.64	0.37	290
4	37.84	37.56	.47	20	47	26.64	26.36	.37	310
5	37.56	37.28	.47	290	48	26.36	26.22	.37	290
6	37.28	37.00	.47	70	49	26.22	26.08	.37	290
7	37.00	36.72	.47	350	50	26.08	25.80	.37	220
8	36.72	36.44	.44	210	51	25.80	25.66	.37	280
9	36.44	36.16	.44	330	52	25.66	25.52	.37	280
10	36.16	35.88	.44	350	53	25.52	25.24	.37	310
11	35.88	35.60	.44	340	54	25.24	24.96	.37	340
12	35.60	35.32	.44	20	55	24.96	24.85	.37	320
13	35.32	35.04	.43	140	56	24.85	24.75	.37	320
14	35.04	34.76	.40	60	57	24.75	24.68	.37	320
15	34.76	34.48	.40	0	58	24.68	24.40	.37	90
16	34.48	34.20	.39	350	59	24.40	24.12	.37	90
17	34.20	33.92	.39	20	60	24.12	23.98	.37	10
18	33.92	33.64	.39	10	61	23.98	23.84	.37	10
19	33.64	33.36	.39	35	62	23.84	23.56	.37	340
20	33.36	33.08	.39	35	63	23.56	23.28	.37	270
21	33.08	32.80	.39	30	64	23.28	23.18	.37	240
22	32.80	32.52	.39	0	65	23.18	23.12	.26	240
23	32.52	32.24	.39	340	66	23.12	23.06	.26	240
24	32.24	31.96	.39	70	67	23.06	23.00	.37	240
25	31.96	31.68	.39	320	68	23.00	22.72	.37	90
26	31.68	31.40	.39	210	69	22.72	22.44	.37	225
27	31.40	31.12	.39	280	70	22.44	22.16	.37	260
28	31.12	30.84	.39	350	71	22.16	21.88	.37	350
29	30.84	30.56	.39	320	72	21.88	21.76	.37	235
30	30.56	30.28	.39	320	73	21.76	21.60	.37	235
31	30.28	30.00	.39	320	74	21.60	21.32	.37	235
32	30.00	29.72	.39	350	75	21.32	21.18	.37	220
33	29.72	29.44	.39	70	76	21.18	21.04	.37	220
34	29.44	29.16	.39	20	77	21.04	20.76	.37	220
35	29.16	28.88	.39	300	78	20.76	20.62	.37	250
36	28.88	28.60	.39	290	79	20.62	20.48	.37	250
37	28.60	28.32	.39	290	80	20.48	20.20	.37	270
38	28.32	28.16	.39	270	81	20.20	19.92	.37	0
39	28.16	28.04	.39	270	82	19.92	19.64	.37	315
40	28.04	27.76	.39	120	83	19.64	19.36	.37	280
41	27.76	27.48	.39	180	84	19.36	19.08	.36	30
42	27.48	27.20	.39	230	85	19.08	18.80	.34	40
43	27.20	26.97	.39	290	86	18.80	18.52	.34	70
44	26.97	26.92	.39	290	87	18.52	18.24	.34	320

Table C1. Shading factors and orientations for segments of the model grid—Continued

Segment number	Upstream river mile	Downstream river mile	Shading factor	Orientation (degrees)	Segment number	Upstream river mile	Downstream river mile	Shading factor	Orientation (degrees)
88	18.24	18.10	.34	270	122	10.68	10.40	.32	275
89	18.10	17.96	.34	270	123	10.40	10.12	.31	330
90	17.96	17.68	0.34	10	124	10.12	9.84	.31	260
91	17.68	17.40	.34	100	125	9.84	9.56	.31	315
92	17.40	17.12	.34	20	126	9.56	9.28	.31	280
93	17.12	16.88	.34	300	127	9.28	9.00	.31	345
94	16.88	16.84	.34	300	128	9.00	8.72	.31	315
95	16.84	16.56	.34	220	129	8.72	8.44	.31	280
96	16.56	16.32	.34	275	130	8.44	8.16	.31	240
97	16.32	16.28	.34	275	131	8.16	7.88	.31	290
98	16.28	16.00	.34	260	132	7.88	7.60	.31	290
99	16.00	15.72	.34	270	133	7.60	7.32	.31	290
100	15.72	15.44	.34	280	134	7.32	7.18	.31	280
101	15.44	15.16	.34	300	135	7.18	7.04	0.31	280
102	15.16	14.88	.34	190	136	7.04	6.76	.31	280
103	14.88	14.60	.34	110	137	6.76	6.48	.31	275
104	14.60	14.32	.34	180	138	6.48	6.20	.30	260
105	14.32	14.04	.34	60	139	6.20	6.06	.30	300
106	14.04	13.76	.34	210	140	6.06	5.92	.30	300
107	13.76	13.48	.34	270	141	5.92	5.69	.30	270
108	13.48	13.20	.33	280	142	5.69	5.64	.30	270
109	13.20	13.16	.33	290	143	5.64	5.50	.30	300
110	13.16	12.92	.33	290	144	5.50	5.36	.30	300
111	12.92	12.64	.33	320	145	5.36	5.31	.30	0
112	12.64	12.50	.33	290	146	5.31	5.08	.30	0
113	12.50	12.36	.33	290	147	5.08	4.94	.30	330
114	12.36	12.08	.33	270	148	4.94	4.80	.30	330
115	12.08	11.99	.33	200	149	4.80	4.52	.30	310
116	11.99	11.80	.33	200	150	4.52	4.24	.30	315
117	11.80	11.52	.33	250	151	4.24	4.10	.30	330
118	11.52	11.24	.33	240	152	4.10	3.96	.30	330
119	11.24	10.96	.33	250	153	3.96	3.68	.30	35
120	10.96	10.82	.33	260	154	3.68	3.40	.30	340
121	10.82	10.68	.33	260					